

**THE RHEOLOGY OF
CARBON BLACK DISPERSIONS.**

A thesis submitted to Cardiff University
in candidature for the degree of
Doctor of Philosophy

Claire L. Barrie
(June 2004)

UMI Number: U583942

All rights reserved

INFORMATION TO ALL USERS

The quality of this reproduction is dependent upon the quality of the copy submitted.

In the unlikely event that the author did not send a complete manuscript and there are missing pages, these will be noted. Also, if material had to be removed, a note will indicate the deletion.



UMI U583942

Published by ProQuest LLC 2013. Copyright in the Dissertation held by the Author.
Microform Edition © ProQuest LLC.

All rights reserved. This work is protected against
unauthorized copying under Title 17, United States Code.



ProQuest LLC
789 East Eisenhower Parkway
P.O. Box 1346
Ann Arbor, MI 48106-1346

DECLARATION


This work has not previously been accepted in substance for any degree and is not concurrently submitted in candidature for any degree.

Signed  (candidate)

Date 4/6/04

STATEMENT 1


This thesis is the result of my own investigations, except where otherwise stated. Other sources are acknowledged by footnotes giving explicit references.

Signed  (candidate)

Date 4/6/04

STATEMENT 2

I hereby give consent for my thesis, if accepted, to be available for photocopying and for inter-library loan, and for the title and summary to be made available to outside organisations.

Signed  (candidate)

Date 4/6/04

SUMMARY

The interaction of carbon black with an acrylic resin in aqueous solution has been investigated by rheology. Two carbon blacks Raven L and Raven M, with similar particle size and surface characteristics but quite different particle morphologies, have been examined. In the absence of polymer, stable aqueous dispersions could not be obtained. Stable dispersions could be obtained however upon addition of polymer to a level corresponding to a ratio of 50mg of polymer per 13m^2 (± 1) of surface area (i.e.15wt% particles). These stable dispersions exhibit flow typical of concentrated dispersions - Newtonian behaviour up to some apparent "yield" or critical value. Above which shear thinning is observed. This critical stress increases with increasing polymer concentration. At low polymer concentrations, the dispersions are predominantly viscous at low shear stresses. The phase angle decreases significantly over a narrow shear stress range and the rheology tends to more elastic behaviour. At higher shear stresses, the dependence on particle morphology is weak.

Furthermore, increasing the pH of the aqueous dispersions has little effect, but changing the adsorbent does alter the rheology somewhat. In addition to Raven L and Raven M, other carbon blacks were also investigated in which the surface chemistry had been modified by ozonolysis.

In addition to aqueous systems, a selection of oil based systems have also been investigated. Here, four carbon blacks were used with a bitumen binder: the low-medium structured fine particle (Raven L), the medium-high structured fine particle (Raven M), a low-medium structured coarse particle (N772) and a medium-high structured coarse particle (N660). For these systems, the rheology and the dispersion colour properties have been investigated. Finally, a rheology study on the effect of bimodal dispersions was undertaken.

**TO MY FAMILY AND
FRIENDS**

ACKNOWLEDGEMENTS

I would like to express my gratitude to a great number of people who have all been, however much they have contributed, an essential part of the past four years. In particular I wish to thank:

Cardiff University and my PhD supervisor, Dr Peter C. Griffiths for his continuous support, encouragement and guidance.

Columbian Chemicals Company for my sponsorship and my industrial supervisor, Dr Richard J. Abbott for all of his help and his friendship. All of the employees at the ECL laboratory in Avonmouth are also greatly thanked.

Special thanks go to all the people who I have worked with in the lab past and present, it's been an adventure; Dr Alison Paul (for her endless help, our "tea and toast" breaks and her ice-cream stress remedy), Dr Jason "skinny boy" Davies (for his ability to make me smile), Dr Angie Winnington (you're a "star"), Dr Angela Cheung (one of the nicest people I'll ever meet), Natasha Hirst (little miss politics!), Sarah Waters (you'll get there girl!), Rob, Zeena, Champa, Tess and Eak. I would also like to thank Dr Christian Tipples (will you ever leave Cardiff Uni?) and last but my no means least, my best mate Anna Attwood, we've been through a lot...most of it, I'd do all over again!

Finally, I would like to thank all of my family especially my mum, my dad, Samantha and my "lil sis" Gemma (mims).....it can't have been easy putting up with me! Many thanks to Callam and Nikki for keeping me amused (like kids do) and lastly, to Martin (need I say more!).

I would also like to thank all of my friends, in addition to those already mentioned.....I love you all, Cheers!

CONTENTS

DECLARATION	ii
SUMMARY	iii
ACKNOWLEDGEMENTS	v
CHAPTER 1: INTRODUCTION	1
REFERENCES:	26
CHAPTER 2: COLLOIDAL DISPERSIONS	33
2.1: POLYMERS	33
2.1.1: Description	33
2.1.2: Relative molecular mass, molar mass and molecular weight	33
2.1.3: Composition	35
2.1.4: Polymer structure	36
2.1.5: Polymer architecture	36
2.1.6: Polymers in solution	38
2.1.7: Polymer solution thermodynamics	39
2.1.8: Polymer-solvent interactions	40
2.1.9: Flory-Huggins theory	40
2.1.10: Solvent quality	41
2.1.11: Size and shape	41
2.2: COLLOIDS	43
2.2.1: Classification of a colloid	43
2.2.2: Preparation of colloidal dispersions	43
2.2.3: Colloidal motion	44
2.2.4: Stabilisation of a colloid	44
2.2.5: Steric stabilisation	45
2.2.6: Factors that influence steric stabilisation	45

2.2.7:	Electrostatic stabilisation	46
2.2.8:	Factors that influence electrostatic repulsion	47
2.2.9:	Colloidal forces	49
2.2.10:	Driving force for adsorption	49
2.2.11:	Kinetics of polymer adsorption	50
2.2.12:	Methods of adsorption	50
2.2.13:	Polymer segment-surface interactions	51
2.2.14:	Surface characteristics that affect adsorption	52
2.2.15:	Adsorption and the properties of polymers in solution	53
2.2.16:	Measurement of adsorbed amount	53
2.2.17:	Volume fraction profiles	55
2.2.18:	Polymer coated particle interactions	56

REFERENCES:		60
-------------	--	----

CHAPTER 3: MATERIALS		62
-----------------------------	--	----

3.1:	CARBON BLACK	62
3.1.1:	Introduction	62
3.1.2:	Microstructure of carbon black	63
3.1.3:	Manufacture of carbon black	63
3.1.4:	Formation of carbon black	64
3.1.5:	Important properties of carbon black	64
3.1.6:	The use of fractal geometry	68
3.1.7:	The influence of carbon black properties on applications performance	69
3.1.8:	Carbon black grades that were studied	70
3.2:	COLLOIDAL SILICA	73
3.3:	ADSORBANTS	75
3.3.1:	Acrylic resins	75
3.3.2:	Poly(ethylene oxide), PEO	77
3.3.3:	PEG / PPG / PEG block copolymer	77

3.3.4:	The oil medium	78
3.4:	SAMPLE PREPARATION	78
3.4.1:	Aqueous dispersions of carbon black and J61	78
3.4.2:	Oil dispersions of carbon black	79
3.4.3:	Carbon black in oil for colour measurements	79
3.5:	EQUIPMENT	80
3.5.1:	Rheology	80
3.5.2:	Small-angle neutron scattering studies	80
3.5.3:	High-resolution ultrasonic measurements	80
3.5.4:	Colour measurements	81

REFERENCES:		83
--------------------	--	----

CHAPTER 4: RHEOLOGY		84
----------------------------	--	----

4.1:	INTRODUCTION TO RHEOLOGY	84
4.1.1:	Definition	84
4.1.2:	Uses of rheology	84
4.1.3:	Solids and Liquids	84
4.1.4:	Shear stress, shear rate and viscosity	84
4.2:	SOLIDS AND LIQUIDS	87
4.2.1:	Classification of materials	87
4.2.2:	Linearity and non-linearity	89
4.2.3:	Yield stress	92
4.2.4:	Deborah number	93
4.2.5:	The Péclet number	93
4.3:	MEASUREMENTS	95
4.3.1:	Measurement of viscoelasticity	95
4.3.2:	How to measure the viscosity of a solution	99
4.3.3:	Rotational rheometer	101
4.3.4:	Selection of appropriate measuring system	104
4.3.5:	How do we obtain the shear stress and the shear rate?	105
4.4:	ANALYSIS OF RESULTS	106

4.4.1:	Flow curves and flow models	106
4.4.2:	Factors that affect the rheology of a material	108
4.4.3:	Time effects-thixotropy	110
4.5:	COMMON RHEOLOGICAL PROBLEMS	110
4.5.1:	Turbulent flow	110
4.5.2:	Wall slip	111
REFERENCES:		114

CHAPTER 5: OTHER TECHNIQUES 115

5.1:	COLOUR MEASUREMENTS	115
5.1.1:	What is colour?	115
5.1.2:	Chromatic colours	115
5.1.3:	Electronic excitations	116
5.1.4:	Beer-Lambert law	117
5.1.5:	Measurement of colour	117
5.1.6:	Colour applications of carbon black	119
5.2:	ULTRASONIC SPECTROSCOPY	120
5.2.1:	Introduction	120
5.2.2:	Uses of ultrasonic spectroscopy	120
5.2.3:	Ultrasonic attenuation and ultrasonic velocity	121
5.2.4:	Methods for obtaining the attenuation and velocity	122
5.2.5:	Principles of ultrasonic spectroscopy	123
5.2.6:	Interpretation of ultrasonic results	124
5.2.7:	Comparison with rheology measurements	124
REFERENCES:		126

CHAPTER 6: RESULTS AND DISCUSSION

-AQUEOUS DISPERSIONS 127

6.1:	Reproducibility	127
------	-----------------	-----

6.2:	Particle characterisation	131
6.3:	Rheology-the effect of polymeric binder concentration	136
6.4:	Rheology-Polymeric binder in solution	139
6.5:	Rheology-Dilution experiments	141
6.6:	Oscillatory rheology	143
6.7:	The silica/poly(ethylene oxide) model system	147
6.8:	The effect of changing the pH	153
6.9:	The influence of adsorbent type	155
6.10:	Surface modifications	160

REFERENCES:		163
-------------	--	-----

CHAPTER 7: RESULTS AND DISCUSSION 164

-OIL DISPERSIONS

7.1:	Rheology-oil medium	165
7.2:	Rheology-Polymeric binder in solution	166
7.3:	Rheology-carbon black dispersions	168
7.4:	Comparison of particle types	173
7.5:	Low shear viscosity, high shear viscosity and yield stress	175
7.6:	Colour measurements	180
7.7:	Colour data interpretation	183

REFERENCES:		190
-------------	--	-----

CHAPTER 8: RESULTS AND DISCUSSION 191

-MIXED PARTICLE DISPERSIONS

8.1:	Aqueous mixed particle dispersions	191
8.2:	Mixed particle in oil dispersions	195

REFERENCES:		208
-------------	--	-----

CHAPTER 9: FINAL CONCLUSIONS	209
REFERENCES:	215
APPENDIX	

CHAPTER 1: INTRODUCTION

A colloid is a dispersion of one material in another, where the dispersed component has a size in the range $1\text{nm} - 1\mu\text{m}^1$. In general, colloidal "particles" (the dispersed phase) are aggregates of numerous atoms or molecules whose dimensions are below the limits of resolution of simple optical microscopes. The term colloid is used to describe a broad array of such two phase systems. However, the variety of different two phase combinations has led to a more distinct classification. A "dispersion" is the name given to a solution of solid particles within a liquid² whereas a liquid within a liquid is termed an "emulsion".

There have been a great number of studies concerned with the stability of emulsions and the properties of polymers at a fluid-fluid interface. For example, the adsorption of a homopolymer at the interface between oil and water has been discussed by Halperin and Pincus³; the crossing of the liquid-liquid interface by short chain polymers, by Ishinabe⁴; SANS studies concerning the volume fraction profiles of two pluronic polymers at the interface of a toluene-in-water emulsion were carried out by Cosgrove *et al.*^{5,6} and the rheology of emulsions is discussed by Tadros⁷, Pal⁸, Robins *et al.*⁹ and Bressy *et al.*¹⁰

However the principal focus of this thesis is predominantly that of solid in liquid dispersions (sometimes called suspensions). More specifically, the unusual rheological behaviour (that is not observed with common polymer solutions) which is associated with solid in liquid dispersions has been studied. Dispersions, like emulsions, are thermodynamically unstable in nature however, there are two mechanisms commonly used in order to promote stability; 1) steric stabilisation- this occurs when a layer of polymer or surfactant is adsorbed onto the particle surface and 2) electrostatic stabilisation, this occurs when a charge is imparted on the particles. Consequently, dispersions fall into one of four categories; hard sphere, sterically stabilised, electrostatically stabilised or flocculated.

Many properties of dispersions are concentration dependent. For example, the *viscosity* of a system can be increased/decreased upon increasing/decreasing the concentration of particles. Newton postulated in 1687 that *"there is a resistance that arises from the lack of slipperiness of the parts of the liquid"* and Bingham proposed that viscosity can be thought of being analogous to electrical resistance¹¹. Both of these have been proven to be viable statements, hence viscosity is therefore commonly defined as the measure of the resistance of a liquid to flow.

From a calculation of energy dissipation in a suspension, Einstein^{12,13} derived that a dilute suspension of rigid spherical particles behaves as a Newtonian fluid with relative viscosity (η_r) represented by the following:

$$\eta_r = 1 + 2.5 \phi \quad (1.1)$$

where ϕ is the volume fraction of the dispersed phase and η_r , the relative viscosity, is the ratio of dispersion viscosity to continuous-phase viscosity. The assumptions made whilst deriving this equation were that the particles are separated by such a distance so as there is NO interaction between them and that inertia is neglected when describing the flow around each particle. It is, therefore, not surprising that this formula becomes invalid when $\phi > 0.02$ ¹⁴. Generally, dilute dispersions are not of great industrial interest, however concentrated dispersions of particles dispersed in a complex fluid matrix are ubiquitous in chemical and materials processing¹⁵. For example, concentrated suspensions of colloidal latex particles dispersed in associative polymeric thickeners are the basis of water-borne paints and coatings¹⁶.

The first step towards understanding the properties of dispersions is to analyse the distribution of particles within the system¹⁷. For this, a schematic two-dimensional diagram representing the equilibrium distribution of particles in a dispersion of hard spheres (For more information, see chapter 2), with a radius of a , suspended in a Newtonian fluid of viscosity η_F , is shown in figure 1.1:

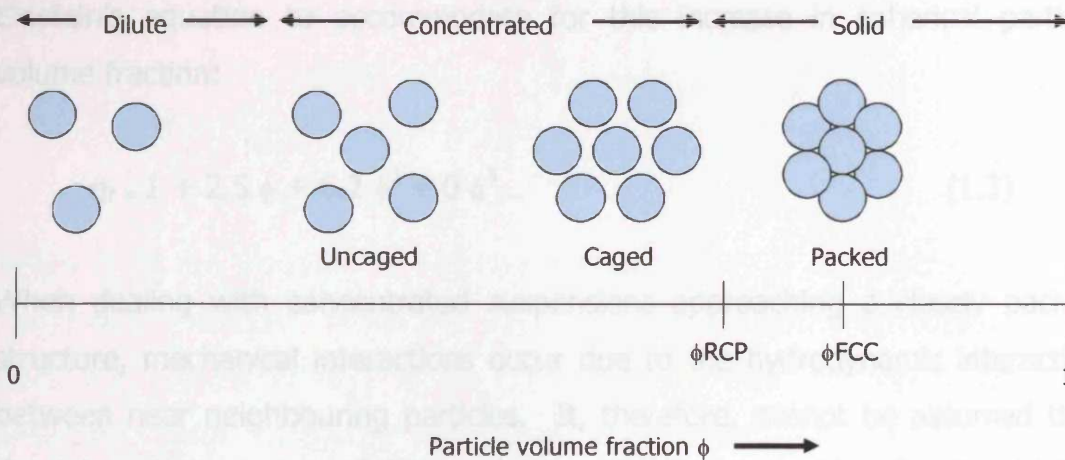


Fig 1.1: Schematic diagram of the equilibrium distribution of particles in a dispersion of hard spheres, where the volume fraction for random close packing is $\phi_{RCP} = 0.637$ and for face centred cubic, $\phi_{FCC} = 0.74$ (redrawn from Quemada and Berli¹⁸).

The volume fraction ϕ is therefore the key parameter for characterisation of the microstructure and the arrangement of particles within the system. The equation used to calculate the volume fraction of a system is:

$$\phi = n 4 \pi a^3 / 3 \quad (1.2)$$

where n is the number density of particles and a is the particle radius.

In the dilute regime, $\phi \ll 0.1$, the distance between neighbouring particles is on average significantly larger than the particle radius. Hence, free movement of the particles throughout the medium (driven by Brownian motion) is permitted. As ϕ increases, i.e. the system becomes more concentrated, the mean particle separation distance decreases.

For moderately concentrated systems where $0.1 < \phi < 0.2$, the particles are able to detect their nearest neighbours, hence a deviation from the Einstein

equation is observed. Batchelor^{19,20,21} noticed this during his extensive studies on a wide variety of concentrated dispersions and proceeded to modify Einstein's equation to accommodate for this increase in spherical particle volume fraction:

$$\eta_r = 1 + 2.5 \phi + 6.2 \phi^2 + 0 \phi^3 \dots \quad (1.3)$$

When dealing with concentrated suspensions approaching a closely packed structure, mechanical interactions occur due to the hydrodynamic interaction between near neighbouring particles. It, therefore, cannot be assumed that the interactions are negligible and they MUST be considered. For higher concentrations, up to $\sim \phi=0.55$, the viscosity is covered by Thomas²² empirical formula:

$$\eta_r = (1 + 2.5 \phi + 10.05 \phi^2 + 2.73 \times 10^{-3} \exp(16.6 \phi)) \quad (1.4)$$

This is similar to the Einstein equation, except that higher order terms have been added to compensate for the effects of particle collision. In addition to Thomas' empirical equation, the following proposed formulas by Mooney²³ (1.5) and Krieger and Dougherty²⁴ (1.6) are some of the most commonly used equations that also include a contribution from the hydrodynamic interactions.

$$\eta_r = \exp(2.5\phi / 1-K\phi) \quad (1.5)$$

$$\eta_r = (1-K\phi)^{-2.5/K} \quad (1.6)$$

where K is an adjustable parameter- the so-called "crowding" effect. From equation 1.6, it can be seen that the viscosity becomes infinite when $\phi = 1/K$, hence we can relate $1/K$ with the maximum packing fraction ϕ_m . Krieger and Dougherty's theory also states that, in the general case, the 5/2 (2.5) factor (the intrinsic viscosity for an ideal suspension of spherical particles) could be replaced by the intrinsic viscosity $[\eta]$, allowing particles of any shape to be

accounted for. The full, more generalised, Krieger-Dougherty equation (K-D)²⁵ can, therefore, be written as:

$$\eta = \eta_s \left(1 - \frac{\phi}{\phi_m} \right)^{-[\eta]\phi_m} \quad (1.7)$$

where η is the viscosity of the suspension and η_s is the viscosity of the suspending medium. When the volume fraction is further increased above 0.55, the system is said to be "crystallised". This behaviour has been predicted using computer simulations by Hoover and Ree²⁶ and also experimentally confirmed by Pusey and Megan²⁷ and Russel *et al.*²⁸. At this point, the motion of the particles is inhibited by the close proximity of neighbouring particles. A further increase in the volume fraction up to 0.637 requires a randomly closely packed structure²⁹ and for 0.74, a face-centred cubic array of particles is required.

A number of experimental investigations on the rheology of dispersions of asymmetric particles have used the Krieger-Dougherty equation to fit the data obtained. These include studies on: silica spheres (submicron)³⁰, spheres (40 μm)³¹, titanium dioxide³², quartz grains³³ and glass fibres³¹. In addition, models have also been developed using the Krieger-Dougherty equation as a basis. On studying the shear viscosity of non-dilute suspensions containing strongly interacting particles, Buscall³⁴ and Quemada³⁵ described the volume fraction dependency of the shear viscosity in theoretical models using the K-D equation for hard-sphere suspensions. This equation describes how the viscosity, η , of a colloidal dispersion at high concentrations (where the linear Einstein formula is not obeyed) varies rapidly with the volume fraction of particles within the dispersion (for more information, see chapter 4).

To summarise, the explanation behind the associated increase in viscosity (dilute \rightarrow concentrated \rightarrow solid-like) with an increase in particle concentration for a suspension is attributed to a restriction in the relative motion (closer

packing) of the particles which then leads to an increase in the frictional forces as the particles in the suspension bump each other. However, the above mentioned transitions only occur at the specified volume fractions for monodisperse hard sphere systems that only interact through hydrodynamics and it must be noted that the distribution of particles is highly sensitive to shape, size and surface charge of the particles considered.

Most industrial systems are not true hard sphere systems and therefore more complicated theories are employed to govern their behaviour. In most industrial systems, in addition to the mechanical interactions, when the concentration of the dispersed phase is high, aggregation/ flocculation of the particles can also occur. This can significantly alter the system's flow properties (e.g. viscosity) and hence promote non-Newtonian rheological behaviour.

The terms "Rheology" and "rheological behaviour" have, until now, only been mentioned superficially. However, more detailed studies will now be made to define what is meant by these terms. "Rheology" is the study of the deformation and flow of matter resulting from the application of a force³⁶. The "matter" we investigate however, can be both simple or of a complex nature and it is this degree of complexity that determines the ease of rheological measurements³⁷. When describing a material, the terms "solid" or "liquid" are often the first used, however, the classification of the "matter" as either a solid (elastic material) or liquid (viscous material) is not descriptive enough and, more often than not, inappropriate. The vast majority of materials have both solid-like and liquid-like properties and therefore can be classified as either a solid or a liquid only if accompanied by the conditions (range of shear stress, timescale of observation, temperature etc) at which that particular behaviour is observed.

The rheological behaviour of a material can essentially be classified as one of two types, of which both have already been mentioned (and are discussed in more detail in chapter 4): a) Newtonian or b) non-Newtonian. If a material is

said to behave in a Newtonian way, it means that an applied force has NO effect on the viscosity of the material and so remains constant. On the other hand, if a material is said to behave in a non-Newtonian way, application of an external force (shear) decreases the viscosity (shear-thinning) or increases the viscosity (shear- thickening) depending on the nature of the material and the external force applied (for more information, see chapter 4). The rheological behaviour that is observed from a given material is, however, related to the type of experiment conducted. There are two types of experiment that can be conducted in order to characterise the rheological behaviour of the material: linear or non-linear.

A non-destructive, linear experiment involves the use of small amplitude oscillations to probe the microstructure of the material causing only small deformations. A non-linear experiment involves the application of a continuously increasing shear stress. As a result, this experiment has a destructive character in which the material is largely deformed (for more information regarding these experiments, see chapter 4).

The bulk properties, e.g. rheological properties, of both stable concentrated dispersions, stabilised either sterically or electrostatically, and flocculated colloidal particle dispersions (often induced by non-adsorbing polymers) are of great importance in many technological applications, such as paint/ ink formulations, food concentrates and pharmaceuticals³⁸. The recognised fundamental importance of non-adsorbing polymer induced phase separated materials or flocculated colloidal particulate systems, prompted Asakura and Oosawa³⁹ to predict the underlying theory back in 1958, before any experiments had even been conducted. Their theory basically states that the polymer is excluded from the region between two colloidal particles when their surface separation is less than the diameter of the polymer coil. Since then, this theory has been extensively studied; Vincent *et al.*⁴⁰ observed a phase separation of particles into a colloid-rich and a colloid-poor phase during their studies on non-adsorbing polymer induced flocculation of colloidal particles; Vrij⁴¹ used a study on nonaqueous colloidal particles to propose the concept of

particle phase separation and Sperry⁴², after studying an aqueous system, did the same. Furthermore, if a system is flocculated, there is a marked difference between the rheological behaviour obtained and the associated rheological behaviour of the analogous non-flocculated system.

Stein *et al.* have described the apparent break-down of a particle network by shear, as the development of shear planes. In the giant floc model^{43,44} proposed by Stein *et al.*, these shear planes (that develop as a result of the network destruction by shear) were found to divide the floc into separate domains where, it is assumed that, the particles remain temporarily surrounded by the same neighbouring particles.

It has been observed that the flocculation of silica nanoparticles can influence nanocomposite (a material created by dispersing nano-sized single materials with complimentary properties into a continuous matrix) viscoelasticity in several ways. First, long-range particle-particle interactions,⁴⁵ such as van der Waals forces and electrostatic forces, are enhanced by close approach of particles in a flocculated composite. Second, bridging of nanoparticles with adsorbed polymer molecules is expected to be substantially stronger for flocculated systems than for materials containing well isolated nanoparticles. On studying a system consisting of PEO-PPO-PEO (PEO, poly(ethylene oxide); PPO (poly(propylene oxide)) adsorbed onto small polystyrene latex particles at full coverage, and the corresponding system that was flocculated by nonadsorbing hydroxycellulose, Faers and Luckham⁴⁶ found that the typical Newtonian behaviour that is associated with unflocculated structures was not observed for the flocculated suspensions. In this case, the flocculated structures exhibited plastic flow (see chapter 4) with a yield stress (see chapter 4) that corresponded to the force required to completely breakdown the flocculated structure.

Similar dispersions consisting of two different sized polystyrene latex particles stabilised with ABA block copolymers of ethylene oxide (A) and propylene oxide (B), have also been employed to investigate the resulting viscosity of bimodal dispersions. Greenwood *et al.*⁴⁷ prepared a small particle,

monodisperse suspension with the polystyrene latex particles having a diameter of 78nm and another large particle suspension with particle diameters of 372nm (hence the diameter ratio of these lattices was 4.76). Firstly, the rheology of the monomodal dispersions was investigated as a function of volume fraction. Following this, the monomodal dispersions were combined in a variety of different ratios and the rheology of the resulting bimodal dispersions was investigated, also as a function of volume fraction. It was already shown by Greenwood *et al.* that broadening the particle size distribution leads to an increase in the maximum packing fraction, where small particles fit in the gaps between the large particles. Ultimately, this allows a greater particle loading that does not increase the viscosity. However, the aim of their research was to test the theoretical predictions and compare with the existing values^{48,49,50,51,52} at which the maximum packing fraction and minimum viscosities were said to occur. The conclusions drawn from these studies stated that, at a diameter ratio of 4.76, a bimodal suspension with a composition of $\phi_{\text{small particles}} = 0.15-0.20$ by volume yielded a minimum viscosity value. This value was recalculated to $\phi_{\text{small particles}} = 0.27-0.36$, when considering the adsorbed polymer layer thickness, which is the lower limit of the theoretical values already proposed. In the same paper, Greenwood *et al.* also disagree with the Farris theory⁴⁸, which they found to underestimate the viscosity, stating that the effective volume fraction cannot be calculated correctly from it. On similar systems, Greenwood *et al.*⁵³ also studied the effect of particle size on the adsorbed layer thickness. For particles ranging in size from 20-217 nm it was concluded that the layer thickness increases with particle size. However if the concentration of polymer is the only variable, on increasing the volume fraction of the polymer a decrease in the layer thickness, due to polymer layer compression/interpenetration, was reported. These results were not in total agreement with those of Faers and Luckham⁵⁴, who stated that the adsorbed amount is, within experimental error, independent of the particle size (over the size range of 70-500 nm), however different polymers were used. Also, the adsorbed amount and the layer thickness are two different parameters that are dependent on the polymer

type, adsorption mechanism and the conformation of adsorbed polymer. It was concluded by Greenwood *et al.* that the polymer is adsorbed in a different way on the small particles compared to the large ones, but the strong dependence of particle size on the adsorbed layer thickness remains unexplained. However, molecular dynamics (MD) simulations using a system comprising of a high molecular weight poly(ethylene oxide) adsorbed onto colloidal silica was investigated by Cosgrove, Griffiths and Lloyd⁵⁵ to explain the effect of the relative sizes of the adsorbent and adsorbate. Two cases were studied: 1) when the polymer is larger than the particle and 2) when the size of the polymer is comparable to the size of the particle. When the polymer is larger it “wraps” itself tightly around the particle. Here, the bound fraction is high, the thickness is low and bridging between surfaces is expected. For the situation where the polymer and particle sizes are comparable, the chains are much less tightly adsorbed, the bound fraction is smaller and the thickness is considerably larger due to the formation of extended tails.

Polymer dispersions exhibit a complete spectrum of rheological behaviour from pure viscosity to dominating elasticity⁵⁶. At low concentrations, the viscosity shows Newtonian behaviour as described by Einstein’s law. However, at moderate concentrations, non-Newtonian behaviour can be observed with noticeable viscoelastic and elastic properties. Polymers have proved to be very useful in modifying the viscosity of a solution for many industrial applications. Currently, it is their ability to increase a solutions viscosity that has prompted their use as thickening agents in paints/inks etc. Following studies on poly(acrylamide), PAM, in various glycerol-water mixtures, Briscoe *et al.*⁵⁷ have proposed a mechanism for the commonly observed shear thickening behaviour of polymer solutions and they have also explained the influence of the glycerol content, the polymer solute concentration and the presence of electrolytes in addition to the variation of pressure and temperature on the behaviour of their PAM system. An increase in the glycerol content or polymer concentration both resulted in an increase in viscosity of the solutions, whereas an increase in temperature resulted in a decrease in viscosity and a less pronounced shear

thickening region was observed. Upon addition of NaCl, both the associated critical shear rate and the critical shear stress were increased. In general, previous studies by Geerissen *et al.*⁵⁸; Kiran and Sen⁵⁹; Kiran and Gokmenoglu⁶⁰, have all concluded that the application of a hydrostatic pressure to a system leads to a contraction of the volume that consequently increases the viscosity. For dilute polymer systems, the increase in the viscosity is believed to be the most important factor contributing to the shear thickening however, Briscoe *et al.* found the shear thickening of their PAM system to be more complicated, but thought it to be in agreement with many other workers^{61,62,63,64,65} a result of the formation of a transient network between the polymer chains.

Many factors have been found to contribute to the flow behaviour of particle/polymer systems, but most importantly, the size, shape and concentration of the dispersed particles/polymers, coupled to the dispersion stability are known to be the main flow determining factors. Under flow, Ma and Cooper found that aqueous solutions of hydrocarbon end-capped poly(ethylene) oxide⁶⁶ exhibit Newtonian behaviour at low shear rates, shear thickening behaviour above some critical shear rate and then upon further increasing the shear rate, shear thinning behaviour is observed. The unusual rheological properties of this associating polymer system have been attributed to the formation of a physically cross-linked network. Shear thickening is rarely observed in common polymer solutions, although, along with associating polymer systems, the shear-induced structural changes have promoted thickening in complex fluids including wormlike micelles and dense suspensions. These findings prompted further studies to fully describe the behaviour of associating polymer solutions, hence leading to several proposed theoretical models^{67,68,69,65}.

Concentrated suspensions of solids however, frequently show shear-thinning behaviour⁷⁰. With increasing shear rate, a decrease in the viscosity is observed (1.8):

$$\sigma = \eta \dot{\gamma} \quad (1.8)$$

where η is the viscosity, $\dot{\gamma}$ is the shear rate and σ is the shear stress.

Experiments conducted with spherical particles, sterically stabilized with thin layers of grafted polymers, have shown that large particles can behave in a similar way to hard spheres^{71,72,73,74}. On studying a well-known^{75,76} hard sphere model suspension of silica particles coated with 3-(trimethoxysilylpropyl) methacrylate (TPM) and dispersed in tetrahydrofurfuryl alcohol (THFFA), O'Brien and Mackay⁷⁷ found that the viscous-like or hydrodynamic viscosity component was approximately independent of shear rate. They also report a continuous shear thickening for a suspension with $\phi=0.54$ but, upon increasing the volume fraction to 0.59 and then to 0.63, a discontinuous shear thickening, indicated by a rapid rise in the viscosity at a critical shear rate. This result was consistent with previous studies by Boersma *et al.*^{78,79} of the shear thickening of hard sphere suspensions. The shear thickening of these silica samples was described by Brady's⁸⁰ theory of particle clustering- a higher concentration increases the effective volume fraction and hence promotes a closer packed structure. Monodisperse systems of hard spheres can theoretically pack in several ways ranging from simple cubic (maximum packing fraction, $\phi_{\max} = 0.524$) to face centred cubic and hexagonal close packed ($\phi_{\max} = 0.740$). However, a transition from viscous-like shear thickening for the two lower volume fraction suspensions (0.54 and 0.59) to elastic-like shear thickening for the $\phi=0.63$ suspension indicated an increasing formation of clusters on approaching the maximum packed solid-like structure. Theoretical analysis of Brownian hard sphere suspensions have shown that the stress developed under shear can be separated into two components, viscous-like (hydrodynamic component) and elastic-like

(thermodynamic component). Further, the flow behaviour is affected ONLY by viscous forces and Brownian motion of the particles⁸¹. The viscous-like component is due to the hydrodynamic interaction between and drag on the particles whereas the elastic-like component is due to Brownian motion. At very low shear rates, the Brownian motion of the particles is dominant and tends to restore the structure of the suspension when it is perturbed from the rest state. Usually these systems display Newtonian behaviour at very low shear rates, shear thinning behaviour at high shear rates, and another shear-independent viscosity at very high shear rates⁷¹. Other structural and rheological studies have been conducted on systems composed of a filled poly(ethylene oxide) matrix with silica nanocomposites⁸² as the filler. Within highly filled polymers the filler interactions are so strong that yield phenomena characteristic of solid-like materials, (which is attributed to the existence of a filler network that spans large sections of the polymer matrix) is observed^{83,84,85,86,87}. Based on this, Zhang and Archer decided to investigate a highly interactive polymer-particle system. PEO is a non-ionic polymeric additive that is known to have a high affinity for silica particles;⁸⁸ therefore due to the irreversible^{89,90} adsorption of PEO via strong hydrogen bonding to the silica, strong polymer-particle interactions occur in this system. These studies have shown that two closely spaced silica particles can be easily bridged by adsorbed PEO molecules, simultaneously enhancing particle connectivity and reducing the mobility of the polymer chains. After weakening the PEO/silica interactions by the grafting of organosilanes to the silica surface, a partial break-down of the existing network was observed. Aqueous silica and uncharged adsorbed polymer systems have also been utilised in an attempt to study the effect of high molecular weight polymers on the rheology of the dispersed system. However, most of these studies^{91,92,93,94} concern either dilute or moderately concentrated systems. For this reason, Neel *et al.*⁹⁵ has studied the rheology of a concentrated system ($\phi > 0.2$) consisting of aqueous silica particles with adsorbed low molecular weight PEO. It was found that, on increasing the molecular weight of the PEO, the adsorbed amount and the layer thickness was also increased. For example, for PEO with a molecular

weight of 2000, the maximum adsorbed amount was 0.21mg m^{-2} and the layer thickness was 4nm, whereas, for PEO with a molecular weight of 35000, the values obtained were 0.55mg m^{-2} and 15nm respectively. These estimates are in agreement with those extracted from previous dispersion viscosity measurements⁹⁶ and also from SANS data⁹⁷ however, both studies were conducted on more dilute systems. As a result of this increasing layer thickness, the stability was also increased to a point. For silica with adsorbed PEO of molecular weight 2000, the adsorbed layer proved to be too thin to prevent the particles from aggregating, but for PEO 35000, interpenetration of the thick adsorbed layers, caused chain entanglements hence an increase in rheological parameters also. The systems that consisted of adsorbed PEO with molecular weights of 5000 and 10000 and intermediate layer thicknesses of 7 and 9nm respectively, proved to be stable in comparison.

Through optical and rheological measurements on near hard-sphere suspensions of silica particles, it was concluded by Bender and Wagner that the characteristic shear thinning in concentrated dispersions is due to changes in the thermodynamic contribution to the stress tensor while the hydrodynamic contribution remains relatively constant⁹⁸. However, shear thickening was attributed to increased hydrodynamic interactions and is, therefore, a result of strong lubrication forces generated by the formation of non-permanent clusters. Further studies on the effects of added polymer on the stability of fumed silica particles by Kawaguchi *et al.*⁹⁹, state that after being fumed and dispersed in trans-decalin, the resulting suspensions showed strong elastic responses due to the formation of gel-like materials.

Hard sphere behaviour is, however, not observed when the thickness of the adsorbed polymer layer is larger than the core particle radius. In this case, Kapnistos *et al.* described the particles as behaving like multi arm star polymers¹⁰⁰. In addition, an interesting intermediate regime consisting of both hard sphere and polymer star behaviour can also be found, when the adsorption layer thickness of the polymer is comparable to the core particle radius¹⁰¹.

Non-spherical particles such as montmorillonite clay are often stabilised by surfactants and/or polymers. An investigation by Rossi, Luckham and Tadros¹⁰² shows that the flow curves (curves relating stress to rate of shear) for the suspensions at maximum coverage of adsorbing species exhibited a more pronounced shear-thinning behaviour compared to those with lower surfactant concentrations. It was also noticed that, on increasing the clay content above 3%, an apparent deviation from the (practically) Newtonian behaviour was observed and the shear-thinning behaviour of the suspension was enhanced. Flocculation of the suspension (attributed to the bridging of micelles between the particles) occurs below the maximum surfactant coverage and occurs to a greater extent at approx. 50% coverage.

Over the years, there has also been considerable interest in the rheology of dispersions containing pigments. Pigments are and will remain a very important area of research in order to gain an understanding that is essential for the printing inks/paints industry.

One such pigment, carbon black, because it is a strong absorber of light over the entire spectrum, has largely become the preferred black pigment and filler^{103,104,105,106}. Carbon black is employed in many industrial processes, but more specifically for ink applications. Aspects of carbon particle science relating to ink (apart from colour) are those concerned with size and surface chemistry. These two properties determine the ability of the particles to disperse and interact with solvents (dispersion), to function as artists' media (paints), and to be useful conductive additives (rubber and plastics). More importantly, these properties directly impact colour strength, gloss (see chapter 5) and transparency of carbon based pigments¹⁰⁷. Carbon black is an intensely black, finely divided powdered form of highly dispersed elemental carbon manufactured by the controlled vapour phase pyrolysis of hydrocarbons¹⁰⁸. In general, primary carbon black particles are amphoteric substances in aqueous solutions, consisting typically of sp^2 hybridized carbon atoms in planes of fused aromatic rings with weak van der Waals forces holding the layers together¹⁰⁹. These primary particles instantaneously fuse

together during combustion to form small stable aggregates, which represent the characteristic physical unit of the carbon black (see chapter 3). Carbon black has many characteristics that distinguish it from conventional fillers. It has a large specific surface, a capacity for preferential wetting by hydrocarbon fluids, the potential for a high degree of structure due to its infinite variety of irregularly shaped particles, and a surface rich in various functional groups.

Carbon blacks exhibit peculiar rheological behaviour depending on the process of formation and the degree of disruption of the flocculated network structure that is present¹¹⁰. On studying the rheology of dispersed furnace carbon black particles, it is impossible to avoid taking into account the flocculated structures present because it is these structures that introduce properties such as shear thinning/thickening and yield stress. The microscopic structure that is known to be present in a strongly aggregated dilute system of carbon black in dodecane has been studied by Collins and Spencer¹¹¹ using a variety of techniques. The results obtained indicated that the internal structure of the flocs are highly fractal in nature (yielding a fractal dimension of 1.45 ± 0.02) and that they are also, in agreement with previous studies by Detler *et al.*¹¹²; Bremer *et al.*¹¹³ and Chen and Russel¹¹⁴, independent of the particle volume fraction. More recently, Wu *et al.*¹¹⁵ have used dynamic rheological measurements to try and estimate the flocculation structure of carbon black and short-carbon-fiber-filled polymer composites. Two types of carbon black with different characteristics and a short carbon fiber were used as model fillers. They were mixed with various polymer matrices including high-density polyethylene (HDPE), polypropylene (PP) and poly(methyl methacrylate) (PMMA). All of the suspensions showed yield behaviour- a common feature found for most highly filled polymer composites¹¹⁶. This yield behaviour is attributed to the formation of three-dimensional interparticle networks. It has previously been noted that, carbon black has a tendency to self-aggregate and easily forms three-dimensional networks (flocculation structure) in a polymer matrix. This network has a high density that usually results in a high storage modulus. It is believed that this storage modulus at low frequencies and strains can be used as a sensitive experimental parameter reflecting the

degree of flocculation of the ultra-fine-particle-filled polymer composites. Generally, the contribution of filler to the storage modulus of the composite (G'_c) can be analysed in terms of three inter-related effects¹¹⁷: a hydrodynamic effect (G'_h), a viscoelastic effect (G'_p), and the interparticle network (G'_n),:

$$G'_c = G'_h + G'_p + G'_n \quad (1.9)$$

Here, the hydrodynamic term contains the effect of the filler geometry and filler-polymer interactions. The viscoelastic term refers to the frequency dependence of the polymer matrix itself. It is also possible to consider the relative storage modulus, G'_r ;

$$G'_r = G'_c / G'_p \quad (1.10)$$

it is this term that Wu *et al.* analysed in order to reveal that the three-dimensional interparticle network starts to form throughout the matrix when its value is increased to 7, regardless of the system type.

The incorporation of solid "filler" particles into a polymeric "binder" network can dramatically change the nature of its flow by altering the structure. Considering the fact that the viscoelastic behaviour is a reflection of the internal structure, Yamovsky *et al.*¹¹⁸; Zhang and Yi¹¹⁹ have both studied the dynamic rheological behaviour of high-density polyethylene filled with carbon black to try and understand the structure of the filled system. At low carbon black content, Zhang and Yi, found that the viscoelastic properties of the polymer matrix were dominant, but on increasing the carbon black loading, the newly formed network structure became the prevailing character that affected the viscosity. The loss factor, $\tan \delta$, is defined as the ratio of the viscous modulus G'' to the elastic modulus G' (for more information, see chapter 4). G'' is related to the filler network which remains unchanged during dynamic strain, and G' to the breakdown and reconstruction of the network after deformation has occurred. It is, therefore, not surprising that $\tan \delta$ is very sensitive to the carbon black structure and that the onset and strength of the

secondary filler network have a major impact on $\tan \delta$. Hence, the addition of solid carbon black particles to HDPE polymeric systems has been noted to increase the modulus G' . Zhang and Yi also found that the incorporation of finer sized carbon black particles further increased the modulus allowing for easier dispersal in the matrix, but on increasing the temperature, the modulus was decreased.

Recently, there have also been studies that have probed the effect of filler-filler interaction on rheological behaviour, using natural rubber compounds filled with both carbon black and silica. As is already documented by a few research groups^{120,121}, silica has a large number of hydroxyl groups on the surface, which result in strong filler-filler interactions hence an irreversible aggregation. In contrast, carbon black also has a variety of polar functional groups on its surface such as hydroxyl, carboxyl, ketone, etc, however the quantity is small in comparison^{122,123}. It is, therefore, not surprising that the filler-filler interaction of silica is much stronger than that of carbon black. Choi *et al.*¹²⁴ found that, in these compounds containing both silica and carbon black, the compounds containing a higher concentration of silica had an increased viscosity in addition to an increasingly apparent abnormal behaviour, represented by "hump regions". These regions consisted of a sudden increase in the viscosity followed by a decrease after certain storage times during the measurement. They attributed this behaviour to the existence of the high density of silanol groups on the silica surface and the strong hydrogen bonding resulting in the formation of tightly held (irreversible) aggregates.

As well as filled polymer solutions and melts, carbon black filled bitumen¹²⁵ has also prompted a great interest from many scientific teams. Bitumen is produced from oils and, unmodified, its rheological properties are highly susceptible to changes in temperature. Carbon black is known to impart dramatic reinforcing effects as an additive to bitumen road binder hence the resulting rheological properties of the carbon black filled bitumen dispersions are of great interest. Chaala *et al.* found that, for systems comprising of between 5-30% pyrolytic carbon black dispersed in a 150/200 penetration

grade bitumen, the presence of carbon black results in higher viscoelastic properties (i.e. higher values of G' and G'' at a given frequency) compared to the values for the un-filled bitumen and also, it was found that the influence of temperature (a problem that causes the cracking of road surfaces) on the physical response characteristics of the blend was reduced.

For 10-15wt% carbon black particles suspended in low molecular weight silicone oil¹²⁶, it was found by Kawaguchi *et al.* that structural breakdown is observed at low shear rates but this is reversed at higher shear rates. The values of G' and G'' (~3000 Pa and ~200 Pa respectively) obtained for a 12.5wt% carbon black suspension in silicone oil from this same experiment, indicates solid-like viscoelastic behaviour for all carbon black suspensions.

Due to the fundamental industrial importance of electrical¹²⁷, rheological and morphological properties of polymeric materials compounded with filler particles, studies on carbon black dispersions have been ongoing for many years. Amari¹²⁸ has previously studied dispersions consisting of carbon black in linseed oil varnish, although, with his co-worker Watanabe, many other concentrated suspensions^{129,130,131,132,133} have also been studied. However, his studies on carbon black in linseed oil also discussed the non-linear viscoelastic properties, such as storage (G') and loss (G'') moduli and relaxation modulus ($G(t)$), by observing the results obtained from rheological experiments that varied the strain, strain rate and strain history. The flocculated network structures were found to be responsible for a series of relaxation mechanisms with longer relaxation time. The equilibrium moduli (G' in the lower frequency region and $G(t)$ in the longer time region) exhibited remarkable strain dependence, attributable to the network structure break down. The network structures were also observed to be highly sensitive to changes in the strain amplitude and the strain rate, a consequence of complicated non-linear viscoelastic properties. In the stress relaxation experiment (where a constant strain was applied at various rates), $G(t)$ showed a strong time dependence at the initial time region which, upon increasing the shear rate, shifted to a shorter time. These observations were explained with the box type relaxation

spectrum, in which the dimensions of the box, the height and width, are related to the rheological variables studied e.g. the magnitude of shear strain and the rate of shear respectively.

The rheology resulting from the adsorption of poly(ethylene oxide)-poly(propylene oxide) ABA block copolymers on carbon black has also been studied¹³⁴. The results showed a decrease in the amount of adsorption with an increase in the ethylene oxide (EO) chain length and it was, therefore, concluded that the adsorption is governed by the size of the PEO chain. Incorporating the results from their previous studies, Miano *et al.* deduced that the ABA block copolymers were not as effective in stabilising of carbon black dispersions compared with ABC surfactants containing a nonylphenyl group in addition to the PPO chain. The results indicated that anchoring of the chain to the carbon black surface is enhanced in the presence of the nonylphenyl group.

Aoki *et al.*^{135,136} have studied the rheology of carbon black dispersed in various media – an alkyd resin(AR), a modified phenol resin(PR) and a polystyrene/dibutyl phthalate solution(PS/DBP). Three different types of rheological behaviour were observed, depending on the affinity of the suspending media for the particles. When the medium has a poor affinity for the particles (PS/DBP), the rheology was characterised by a network of agglomerates i.e. “highly nonlinear elasto-plastic”. With moderate affinity (PR), the suspension showed a sol-gel transition with increasing particle concentration. This behaviour suggested the formation of a self-similar, fractal agglomerate. Further, increasing the affinity of the suspending media for the particles (AR), the particles become more evenly dispersed, forming no agglomerates.

Carbon black is used in ink formulations where surfactants and amphiphilic polymers are also present. This application is dependent on the control of the surface chemistry, particle size and aggregate structure. Interaction of the particle surface with a dispersion medium involves adsorption at the solid-

liquid interface, which in turn affects the dispersibility and stability of the dispersion. In this respect changes in the surface chemistry can have a major effect on the performance of a carbon black¹³⁷.

The composition of carbon black particles is typically 90-99% elemental carbon with oxygen and hydrogen being two other major constituents¹³⁸. Therefore, carbon black particles are strongly hydrophobic and prone to aggregation in water dispersions. To improve the dispersibility in aqueous media, carbon black can be treated with oxidising solutions to form surface oxides with acidic functional groups that render the carbon black surface, polar in character¹³⁹. To try and characterise the surface in more detail, it might be useful to state that; carboxyl, phenolic hydroxy, lactone, and quinionic oxygen groups have, typically, all been found to exist on the carbon black surface^{140,141}.

The modification of carbon black surfaces by both chemical and physical methods has been extensively studied in recent years and there are several methods that have been employed. The surface grafting of polymers, in itself, holds many different processes; grafting onto process, grafting from process, polymer reaction process and stepwise growth process¹⁴².

Polymers can be grafted onto carbon surfaces via a termination reaction between growing polymer radicals and functional groups on the carbon surfaces, and by a polymerisation reaction initiated from initiating groups that have been previously introduced on the carbon surfaces. Alternatively, polymers may be grafted onto carbon surfaces by reaction of the carbon surface groups with functional polymers. These methods require some complicated pre-treatments and multiple steps with special coupling agents.

A simple impregnation method that can effectively graft polymers or organic compounds, with functional groups such as hydroxy or amine groups, onto carbon blacks without a coupling agent has been reported¹⁴³. In this case, Poly(ethylene glycol) with a molecular weight of 6000 was grafted onto a FW200 grade carbon black (which had a specific surface area of 460 m² g⁻¹ and a volatility of 20wt%), to produce a stable colloidal dispersion in water

and onto N330 (which had a specific surface area of $83 \text{ m}^2 \text{ g}^{-1}$ and a volatility of 0.8wt%) that had been nitric acid pre-treated.

More recent data have shown how polyethylene (PE) was grafted onto a carbon black surface by γ -ray radiation of the PE adsorbed carbon black^{144,145}. A two-step method was adopted, in which, the PE was adsorbed onto the carbon black surface from a *m*-xylene solution firstly, followed by γ -irradiation, at a dose rate of 20 kGy/h up to 300 kGy at 120°C in nitrogen. Carbon surfaces can also be modified using elevated temperature chlorination^{146,147}.

In addition to polymers, several authors have studied the adsorption of ionic^{148,149} and non-ionic¹⁵⁰ surfactants onto carbon black in aqueous solution. Lin, Smith and Alexandridis¹⁵¹ adsorbed a "rake-type" siloxane surfactant (consisting of a poly(dimethylsiloxane) backbone with grafted polyether) onto carbon black, although incomplete coverage occurred. The chemical composition of CB particles obtained by XPS showed that a small portion of the particles had been oxidised to form COO^- . Supporting SANS data confirmed that the adsorbed surfactant layer had a structure and dimensions similar to that of the surfactant micelles in aqueous solution in the absence of any particles. The micelles formed by the surfactant in aqueous solution are spherical at room temperature with a core diameter of $\sim 15\text{nm}$ hence the adsorbed layer has a structure in the form of spherical micelles.

An extensive study, undertaken by Trawczynski, Suppan, Sayag and Djega-Mariadassou¹⁵², consisted of the comparison of various carbon black composite (CBC) surface activation procedures: oxidation by nitric acid, oxidation by hydrogen peroxide, gasification with water steam, ammoxidation and doping with quinoline or silica gel. In their conclusions, emphasis was placed on the change in surface acidity. It was found that, on oxidising with nitric acid or hydrogen peroxide, there was an increase in the number of surface oxygen groups (acidic sites) that decompose to CO and CO_2 . The nitric acid activated CBC was also found to contain carboxylic groups on the surface, whereas the

CBC activated by gasification with water steam showed no surface acidity at all.

Concerning the rheology, Ishii *et al.*¹⁵³ have investigated how altering the particle size and surface morphology can affect the flow behaviour of carbon black suspensions. They compared two identical carbon blacks in linseed oil, one which was in pristine condition and another that had been heat treated to 3073K in order to increase its micrographitic structure. Using the Casson model (see chapter 4), it was found that the yield value was significantly lower for the graphitized carbon black (5.8 Pa) compared to that of the pristine carbon black (114 Pa). This indicated a degeneration of the flocculated network structure as a result of the heat treatment. In addition to this the carbon black that had been heat-treated, was not as easily wet with the linseed oil and often showed pigment settling.

Summary:

In most studies on filled polymers, the filler carbon black is of considerable industrial interest. However, more regularly shaped silica particles have proved to be more useful for systematic studies. Consequently, there have been a vast number of rheological studies conducted using carbon black, silica or polymer solutions/polymer melts that contain both particles. To date, there is strong evidence of some general patterns that have emerged from the published data of linear dynamic moduli and steady-state shear viscosities.

Firstly, on adding particles to a polymer solution/melt, the dynamic moduli and the viscosity is always systematically increased, regardless of the frequency or shear rate¹⁵⁴. However, the relaxation modes of the polymer remain unchanged. This can be attributed to the hydrodynamic effects caused by the rigid particles "upsetting" the ordering in the flow. The volume effects of the particles that are present also induce a corresponding increase in the stress.

At small interparticle distances there is an additional increase in the moduli obtained at low frequencies depicted by a low-frequency plateau and the viscosity obtained at low shear rates-denoted by the appearance of a yield

stress. The presence of these additional features suggests that the attractive forces between the particles have ultimately induced the formation of a weak solid-like, space-filling network.

A schematic representation of the networked polymer configuration in the presence of highly interactive filler during the stages of rest and flow can be seen in figure 1.2:

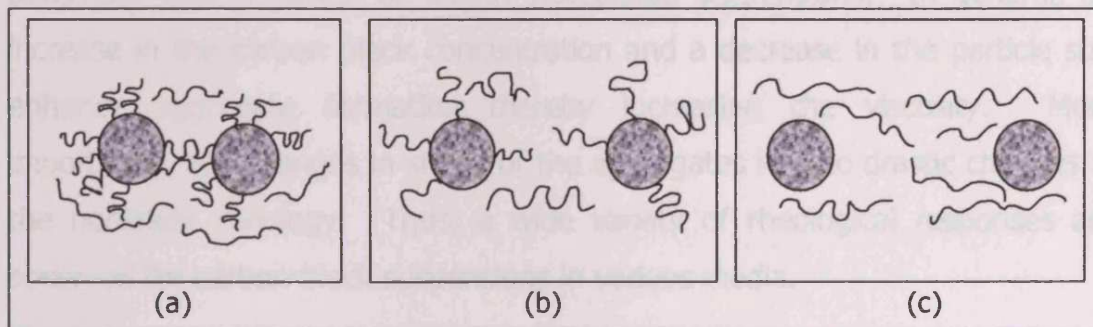


Fig 1.2: Configuration of the polymer-filler mixture: (a) at rest; (b) at low shear rates and (c) at high shear rates. Redrawn from Havet and Isayev¹⁵⁵

The polymer chains can be considered as one of three different forms. They can move freely throughout the solution forming a coil, they can be adsorbed to a single particle, or they can be adsorbed to two particles, forming a bridge. This is represented by situation (a); as the shear rate is increased slightly (b), the bridges are deformed to the point of breaking, however the brushes are still adsorbed to their respective particles and the hydrodynamic reinforcement is still in operation. As the shear rate is further increased, the adsorbed brushes detach themselves from the particle surface (c), in this case, the reinforcement is only due to the presence of the filler particles and the corresponding volume fraction of the filler.

At low particle volume fractions, stable dispersions exhibit Newtonian behaviour, whereas flocculated systems exhibit pseudoplastic flow. Flocculation is thus accompanied by a large increase in both yield value and storage modulus of the dispersion¹⁵⁶.

There are many other variable properties associated with a polymer-filler system that are known to alter the rheological properties; particle surface charge, particle size/shape and the volume fraction of the filler are to name but a few. Below a critical particle volume fraction, hydrodynamic effects dominate the rheology of the suspensions. This critical volume fraction decreases with decreasing particle size. Increasing the volume fraction beyond the critical value gives rise to drastic changes in the rheological behaviour that is typical of weakly flocculated suspensions. In general, an increase in the carbon black concentration and a decrease in the particle size enhance aggregate formation thereby increasing the viscosity. More importantly, the changes in shape of the aggregates lead to drastic changes in the nonlinear rheology. Thus, a wide variety of rheological responses are observed for carbon black suspensions in various media.

References:

- 1 Everett, D.H., *Basic Principles of Colloid Science*, Royal Society of Chemistry, (1988).
- 2 Pal, Rajinder., *Ind.Eng.Chem.Res.* (1999), 38, 5005-5010
- 3 Halperin, A., Pincus, P., *Macromolecules*, 19, (1986), 79
- 4 Ishinabe, T., *J. Chem. Phys.*, 80, (1984), 1318
- 5 Mallagh, L., Ph.D. Thesis Bristol, (1989)
- 6 Cosgrove, T., Mallagh, L.M., Ryan, K., Scheutjens, J.M.H.M., *J. Surface. Sci. Technol.*, 4, (1988), 81
- 7 Tadros, Th. F., *Colloids and Surfaces A*, 91, (1994), 39-55
- 8 Pal, R., *Ind. Eng. Chem. Res.*, (1999)
- 9 Robins, M.M., Watson, A.D., Wilde, P.J., *Current opinion in Colloid and Interface Science*, 7, (2002), 419-425
- 10 Bressy, L., Hébraud, P., Schmitt, V., Bibette, J., *Langmuir*, (2002)
- 11 Severs, E.T., *Rheology of polymers*, Reinhold publishing corporation, New York(1962), chapter 2
- 12 Einstein, A., Eine neue Bestimmung der Molekul dimension. *Ann.Phys*, (1906), 19, 289
- 13 Einstein, A., Berichtigung zu meiner Arbeit: Eine neue Bestimmung Molekul dimension. *Ann. Phys.* (1911), 34, 591
- 14 Batchelor, G.K., Green, J.T., The determination of the bulk stress in a suspension of spherical particles to order c^2 . *J. Fluid Mech.* (1972), 56, 401
- 15 Solomon, M.J., Lu, Qiang., Rheology and dynamics of particles in viscoelastic media, *Current opinion in colloid and interface science* 6, (2001), 430-437
- 16 Glass, J.E., Prud'homme, R.K. *Coating rheology: component influence on the rheological response and performance of water-borne coatings in roll applications*. In:Kistler, S.F., Schweizer, P.M., editors.Liquid film coating. London: Chapman and Hall, (1997)
- 17 Tadros, Th.F., *Adv. Colloid Interface Sci.*, 68, (1996), 97
- 18 Quemada, D., Berli, C., *Adv. Colloid Interface Sci.*, (2001)
- 19 Batchelor, G.K., *J. Fluid Mech.*, (1970), 41, 545
- 20 Batchelor, G.K., *Ann. Rev. Fluid Mech.*, (1974), 6, 227
- 21 Batchelor, G.K., *J. Fluid Mech.*, (1977), 83, 97
- 22 Thomas, D.G., *J. Colloid Sci*, 20, 267, (1965)
- 23 Mooney, M., The viscosity of a concentrated suspension of spherical particles. *J. Colloid Sci.* (1951), 6, 162

- 24 Kreiger, I.M., Dougherty, T.J. A mechanism for non-Newtonian flow in suspensions of rigid spheres. *Trans.Soc.Rheol.* (1959), 3, 137.
- 25 Barnes, H.A., Hutton, J.F., Walters, K., *An introduction to Rheology*, Elsevier Science, (1989), 115-137
- 26 Hoover, W.G., Ree, F.H., *J. Chem. Phys.*, 49, (1968), 3609
- 27 Pusey, P.N., Megen, W. van., *Nature*, 320, (1986), 340
- 28 Russel, W.B., Saville, D.A., Schowalter, W.R., *Colloidal Dispersions, 2nd ed.*, Cambridge University Press, Cambridge, (1991)
- 29 Scott, D.G., *Nature*, 188, (1960), 908
- 30 de Kruijff, C.G., van Iersel, E.M.F., Vrij, A., Russel, W.B., *J. Chem. Phys.*, 83, 4717-4725, (1985)
- 31 Giesekus, H., Disperse systems: dependence of rheological properties on the type of flow with implications for food rheology, in *Physical Properties of Foods*, Jowitt et al., Applied Science Publishers, Chap. 13, (1983)
- 32 Turian, R., Yuan, T-F., *AIChE J.*, 23, 232-243, (1977)
- 33 Clarke, B., *Trans. Inst. Chem. Eng.*, 45, 251-256, (1967)
- 34 Buscall, R., *J. Chem. Soc. Faraday Trans.*, 87, 1365, (1991)
- 35 Quemada, D., *Europhys. Lett.*, 25, 149, (1994)
- 36 Goodwin, J.W., Hughes, R.W. *Rheology for Chemists; an introduction*, The Royal Society of Chemistry, (2000)
- 37 Wagner, N.J., Prud'homme, R.K., Editorial overview-Rheology and rheological techniques, *Current Opinion in Colloid and Interfac Science* 6, (2001), 421-422
- 38 Luckham, P.F., Ukeje, M.A., *J.Colloid.Interf.Sci* 220 (1999) 347-356
- 39 Asakura, S., Oosawa, F. *J. Polym. Sci.* (1958), 33, 183
- 40 Vincent, B., Edwards, J., Emmett, S., Jones, A. *Colloids Surf.* (1986), 18, 261
- 41 Vrij, A. *Pure Appl. Chem.* (1976), 48, 471
- 42 Sperry, P.R. *J. Colloid Interface Sci.* (1984), 99, 97.
- 43 Dieman, A.J.G. van., Stein, H.N., *Rheol. Acta*, 22, (1983), 41-50
- 44 Schreuder, F.W.A.M., Stein, H.N., *Rheol. Acta*, 26, (1987), 45-54
- 45 Leonov, A.I., *J. Rheol.*, (1990), 34, 1039
- 46 Faers, M.A., Luckham, P.F. *Langmuir*, (1997), 13, 2922-2931
- 47 Greenwood, R., Luckham, P.F., Gregory, T., *Coll. Surf. A: Physicochemical and Engineering Aspects*, 144, (1998), 139-147

- 48 Farris, R.J., *Trans. Soc. Rheol.*, 12, (1968), 281
- 49 White, H.E., Walton, S.F., *J. Am. Ceram. Soc.*, 20, (1937), 155
- 50 Westman, A.E.R., Hugill, H.R., *J. Am. Ceram. Soc.*, 13, (1930), 767
- 51 Furnas, C.C., *Ind. Eng. Chem.*, 23, (1931), 1052
- 52 Fraser, R., *J. Geol.*, 43, (1935), 910
- 53 Greenwood, R., Luckham, P.F., Gregory, T., *Coll. Surf. A: Physicochemical and Engineering Aspects*, 98, (1995), 117-125
- 54 Faers, M.A., Luckham, P.F., *Colloids Surfaces A*, 86, (1994), 317-327
- 55 Cosgrove, T., Griffiths, P.C., Lloyd, P.M., *Langmuir*, (1995), 11, 1457-1463
- 56 Tadros, Th.F., *Progr. Colloid Polym. Sci.*, 79 (1989) 120
- 57 Briscoe, B., Luckham, P., Zhu, S., *Rheol Acta*, 38, 224-234, (1999)
- 58 Geerissen, H., Schmidt, J., Wolf, B., *J Appl Polym Sci*, (1982), 27, 1277-1291
- 59 Kiran, E., Sen, Y., *Int J Thermophys*, (1992), 13, 411-442
- 60 Kiran, E., Gokmenoglu, Z., *J Appl Polym Sci*, (1995), 28, 2307-2324
- 61 Choplin, L., Sabatié, J., *Rheol Acta*, (1986), 25, 570-579
- 62 Biggs, S., Selb, J., Candau, F., *Langmuir*, (1992), 8, 838-847
- 63 Hu, Y., Wang, S., Jamieson, A., *Macromolecules*, (1995), 28, 1847-1853
- 64 Wang, L., Tiu, C., Liu, T., *Colloid Polym Sci*, (1996), 274, 138-144
- 65 Ballard, M.J., Buscall, R., Waite, F.A. *Polymer*, (1988), 29, 1287
- 66 Ma, S.X., Cooper, S.L., *Macromolecules*, October 12, 2000
- 67 Marrucci, G., Bhargava, S., Cooper, S.L., *Macromolecules* (1993), 26, 6483
- 68 Witten, T.A., Cohen, M.H. *Macromolecules*, (1985), 18, 1915
- 69 Tanaka, F., Edwards, S.F. *J. Non-Newtonian Fluid Mech.* (1992), 43, 247
- 70 Stein, H.N., Laven. J., *Advances in colloid and interface Science*, 93, (2001), 77-90
- 71 Zaman, A.A., Bjelopavlic, M. and Moudgil, B.M., *J. Colloid Interface Sci* 226 (2000) 290-298
- 72 Killmann, E., Wild, TH., Gutling, N., and Maier, H., *Colloids Surf.* 18, 241 (1986)
- 73 Pusey, P.N., van Meegen, W., Bartlett, P., Ackerson, B.J., Rarity, J.G., Underwood, J.M. *Phys. Rev. Lett.* 1989, 63, 2753

- 74 Lekkerkerker, H.N.W. In *Structure and Dynamics of Strongly Interacting Colloids and Supramolecular Aggregates in Solution*, Chen, S.H., Huang, J.S., Tartaglia, P., Eds., Kluwer Academic Publishers, Dordrecht. The Netherlands, 1992, p97
- 75 Philipse, A.P., Vrij, A., *J. Colloid Interface Sci.*, (1989), 128, 121
- 76 Marshall, L., Zukoski, C.F., *J. Phys. Chem.*, (1990), 94, 1164
- 77 O'Brien, V.T., Mackay, M.E., *Langmuir*, (2000), 16, 7931-7938
- 78 Boersma, W.H., Laven, J., Stein, H.N., *AIChE J*, (1990), 36, 321
- 79 Boersma, W.H., Baets, P.J.M., Laven, J., Stein, H.N., *Rheol.*, (1991), 35, 1093
- 80 Brady, J.F. *J. Chem. Phys.*, (1993), 99, 567
- 81 Kreiger, I.M., *Adv. Colloid Interface Sci.* 3, 111, (1972)
- 82 Zhang, Q., Archer, L.A., *Langmuir*, (2002)
- 83 Yurekli, K., Krishnamoorti, R., Tse, M.F., Mcelrath, K.O., Tsou, A.H., Wang, H.C., *J. Polym. Sci., Part B: Polym. Phys.*, (2001), 39, 256
- 84 Wang, M.J., *Rubber Chem. Technol.*, (1998), 71, 520
- 85 Tanaka, H., White, J.L., *Polym. Eng. Sci.*, (1980), 20, 949
- 86 Carreau, P.J., Lavoie, P.A., Bagassi, M., *Macromol. Symp.*, (1996), 108, 111
- 87 Kim, K.J., White, J.L., *Polym. Eng. Sci.*, (1999), 39, 2189
- 88 Wind, B., Killmann, E., *Colloid Polym. Sci.*, (1998), 276, 903
- 89 Rubio, J., Kitchener, J., *J. Colloid Interface Sci.*, (1976), 57, 132
- 90 Howard, G.J., McConnell, P., *J. Phys. Chem.*, (1967), 71, 2974
- 91 Otsubo, Y., *J. Colloid Interface Sci.*, 153, 584, (1992)
- 92 Liu, S.F., Lafuma, F., Audebert, R., *Colloid Polym. Sci.*, 272, 196, (1994)
- 93 Aubry, T., Largentou, B., Moan, M., *Langmuir*, 15, 2380, (1999)
- 94 Kawaguchi, M., *Adv. Colloid Interface Sci.*, 53, 103, (1994)
- 95 Neel, O., Ducouret, G., Lafuma, F., *J. Colloid Interface Sci.*, 230, 244-253, (2000)
- 96 Lafuma, F., Wong, K., Cabane, B., *J. Colloid Interface Sci.*, 143, (1991), 9.
- 97 Cosgrove, T., Griffiths, P.C., Lloyd, P.M., *Langmuir*, (1995), 11, 1457-1463
- 98 Bender, Wagner, *J. Colloid Interf. Sci.* 172 (1995) 171-184
- 99 Kawaguchi, M., Mizutani, A., Matsushita, Y., Kato, T., *Langmuir*, (1997), 13, 6339-6341

- 100 Kapnistos, M., Semenov, A.N., Vlassopoulos, D., Roovers, J., *J. Chem. Phys.* (1999), 111, 1753.
- 101 Nommensen, P.A., D. van den Ende, Duits, M.H.G., Mellema, J., *Langmuir*, (2001), 17, 5757-5767
- 102 Rossi, S., Luckham, P.F., Tadros, Th.F., *Colloids and Surfaces*, 201 (2002) 85-100
- 103 Luo, Y., Wang, G., Zhang, B., Zhang, Z., *Eur Polym J*, (1998), 34, 1221
- 104 Dishovsky, N., Grigorova, M., *Mater Res Bull*, (2000), 35, 403
- 105 Sumita, M., Sakata, K., Hayakawa, Y., Miyasaka, K., Tanemura, M., *Colloid Polym Sci*, (1992), 270, 134
- 106 Mallette, J.G., Marquez, A., Manero, O., Castro-Rodriguez, R., *Polym Eng Sci*, (2000), 40, 2272
- 107 Battersby, G., *Dispersions of Pigments into Printing Inks*, Marcel Dekker Inc., New York, (1994)
- 108 Donnet, J., Bansal, R. and Wang, M., *Carbon Black 2nd edition*, Marcel Dekker Inc.. (1993) 1-66
- 109 Swider, J.R., Hackley, V.A., Winter, J., *Journal of Cultural Heritage*, 4, (2003), 175-186
- 110 Ishii, C., Akao, K., Koseki, K., Amari, T., *J. Jpn Soc Colour Mater*, (1997), 70 (90), 584-590
- 111 Collins, I.R., Taylor, S.E., *J. Colloid and Interface Sci.* 155, 471-481, (1993)
- 112 Detler, G., Aubert, C., Cannell, D.S., Wiltzius, P., *Phys. Rev. Lett.*, 57, 3117, (1986)
- 113 Bremer, L.G.B., van Vliet, T., Walstra, P., *J. Chem. Soc. Faraday Trans.*, 85, 3359, (1989)
- 114 Chen, M., Russel, W.B., *J. Colloid Interface Sci.*, 141, 564, (1991)
- 115 Wu, G., Asai, S., Sumita, M., Hattori, T., Higuchi, R., Washiyama, J., *Colloid Polym Sci*, 278, 220-228, (2000)
- 116 Malkin, Y., *Adv Polym Sci*, (1990), 96, 69
- 117 Medalia, A.I., *Rubber Chem Technol*, (1978), 51, 437
- 118 Yamovsky, Y.G., Vinogradov, G.V., Gevorgyan, A.M., et al., *Vysokomol Soedin*, (1985), 28, 238
- 119 Zhang, Jian-Feng., Yi, Xiau-Su., *J Appl Polym Sci*, (2002), 86, 3527-3531
- 120 Wolff, S., Wang, M.J., *Rubber Chem Technol*, 65, 329, (1992)
- 121 Li, Y., Wang, M.J., Zhang, T., Zhang, F., Fu, X., *Rubber Chem Technol*, 67, 693, (1994)
- 122 Ayala, J.A., Hess, W.M., Dotson, A.O., Joyce, G.A., *Rubber Chem Technol*, 63, 747, (1990)

- 123 Donnet, J.B., *Rubber Chem Technol*, 71, 323, (1998)
- 124 Choi, Sung-Seen., Nah, Changwoon., Lee, Seung Goo., Joo, Chang Whan., *Polym Int*, 52, 23-28, (2003)
- 125 Chala, A., Roy, C., Ait-Kadi, A., *Fuel*, 75, 13, 1575-1583, (1996) and references within.
- 126 Kawaguchi, M., Okuno, M., Kato, T., *Langmuir*, (2001), 17, 6041-6044
- 127 Rwei, S.P., Ku, F.H., Cheng, K.C., *Colloid Polym Sci*, (2002), 280, 1110-1115
- 128 Amari, T., *Progress in Organic Coatings*, 31, (1997), 11-19
- 129 Amari, T., Watanabe, K., *Polym. Eng. Rev.*, 3, (1983), 277
- 130 Amari, T., Watanabe, K., *J. Soc. Rheol. Jpn.*, 14, (1986), 37
- 131 Amari, T., Watanabe, K., *Curr. Topics Polymer Sci*, vol.2. L.A. Utracki *et al.* (eds.), Hanser, (1987), 182
- 132 Amari, T., Watanabe, K., *J. Jpn. Soc. Colour Material*, 62, (1989), 728
- 133 Amari, T., Watanabe, K., *J. Rheol.*, 34, (1990), 207
- 134 Miano, F., Bailey, A., Luckham, P.F., Tadros, Th.F., *Colloids and Surfaces*, 68 (1992)9-16
- 135 Aoki, Y., Hatano, A., Watanabe, H., *Rheol Acta*, (2003) 42: 209-216
- 136 Aoki, Y., Hatano, A., Watanabe, H., *Rheol Acta*, (2003) 42: 321-325
- 137 Rouquerol, F., Rouquerol, J., Sing, K., *Adsorption by powders and porous solids principles, methodology and applications*, Academic press, (1999), chapter 9.
- 138 Donnet, J.B.; Bansal, R.C.; Wang, M.J. *Carbon Black second edition*; Marcel Dekker: New York, (1993)
- 139 Donnet, J.B.; Voet, A. *Carbon Black*; Marcel Dekker: New York, (1976)
- 140 Studebaker, M.L, *Rubber Chem. Technol.*, 30, 1400, (1957)
- 141 Boehm, H.P., *Adv. Catal.*, 16, 198, (1966)
- 142 Tsubokawa, Norio. *Functionalization of Carbon Material by Surface Grafting of Polymers*, *Bull. Chem. Soc. Jpn.*, 75, 2115-2136, (2002)
- 143 Jarm-Horng Lin, Hsiu-Wei Chen, Kuo-Tung Wang and Feng-Hsiung Liaw, *Journal of Materials Chemistry*, (1998), 8(10) 2169-2173
- 144 Chen, J., Iwata, H., Tsubokawa, N., Maekawa, Y., Yoshida, M., *Polymer* 43 (2002) 2201-2206
- 145 Chen J, Maekawa Y, Yoshida M, Tsubokawa N. *Polymer* (2002); 34:30-5.

-
- 146 Hall CR, Holmes RJ. The preparation and properties of some chlorinated activated carbons. Part II. Further observations. *Carbon* (1993);31(6):881-6
- 147 Baker SL, Branton PJ, Norman PR, Stanton D., April (1996)
- 148 Bele, M., Kodre, A., Arcon, I., Grdadolnik, J., Pejovnik, S., Besenhard, J.O., *Carbon*, 36, 1207, (1998)
- 149 Ogura, T., Tanoura, M., Tatsuhara, K., Hiraki, K.A., *Bull. Chem. Soc. Jpn.*, 67, 3143, (1994)
- 150 Douillard, J.M., Pougnet, S., Faucompre, B., Partyka, S., *J. Colloid Interface Sci.*, 154, 11, (1992)
- 151 Lin Y, Smith Thomas.W, Alexandridis P, *Langmuir* (2002), 18, 6147-6158
- 152 Trawczynski.J, Suppan.S, Sayag.C, Djega-Mariadassou.G, *Fuel Processing Technology* 77-78 (2002) 317-324
- 153 Ishii, C., Koseki, K., Amari, T., Hanzawa, Y., Yoshizawa, N., Hatori, H., Yamada, Y., Yamazaki, S., *Letters to the Editor/Carbon*, 39, (2001), 2369-2386
- 154 Le Meins, J-F., Moldenaers, P., Mewis, J., *Ind. Eng. Chem. Res.*, (2002), 41, 6297-6304
- 155 Havet, G., Isayev, A.I., *Rheol Acta*, (2003), 42, 47-55
- 156 Liang, W., Tadros, Th.F., *Langmuir*, (1993), 9, 2077- 2083

CHAPTER 2: COLLOIDAL DISPERSIONS

2.1: Polymers

2.1.1: Description

Polymers are long chain molecules that can either be naturally occurring or synthetic, consist of a large number of one or more monomer units and whose size falls within the colloidal range, typically $10 < 100$ nm. However, the large number of materials that fall into the category of polymers is so extensive a classification that distinguishes them from one another has been devised and is shown in figure 2.1

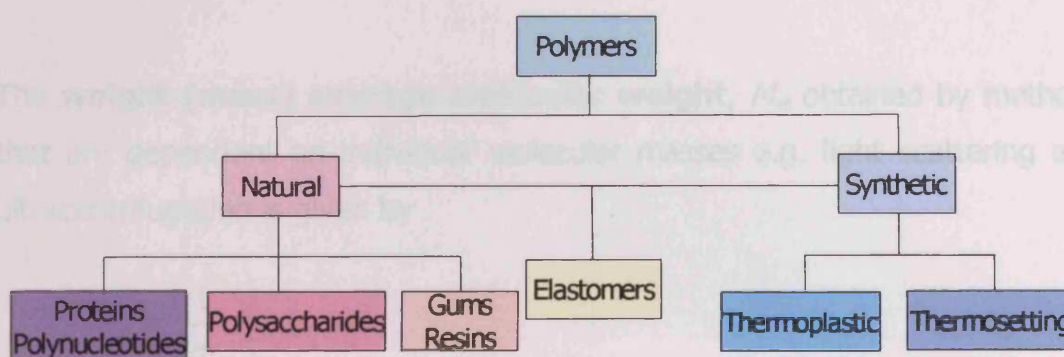


Fig 2.1: The classification of polymers (redrawn from Cowie (1973))¹

Note that elastomers, in general, can either be natural or man-made and are classified as a common sub-group.

Due to the great number of atoms and molecules that make up these structures, polymers tend to have a high relative molecular mass or molecular weight associated with them.

2.1.2: Relative molecular mass, molar mass and molecular weight

One of the most important features that distinguishes a polymer from a simple molecule is the inability to assign an exact polymer molecular mass. Most polymers are *polydisperse* - they consist of a mixture of molecules with various

chain lengths and molar masses. As a consequence of this, it is common to use mean values, determined by different techniques, to describe a polymer:

The **number average molecular weight**, M_n , which is obtained by methods that depend on end-group analysis or colligative properties (where each molecule contributes equally regardless of weight), is given by

$$\bar{M}_n = \frac{1}{N} \sum_i N_i M_i \quad (2.1)$$

where N_i is the number of molecules with molar mass M_i and there are N molecules in total.

The **weight (mass) average molecular weight**, M_w obtained by methods that are dependent on individual molecular masses e.g. light scattering and ultracentrifugation is given by

$$\bar{M}_w = \frac{1}{m} \sum_i m_i M_i \quad (2.2)$$

where m_i is the total mass of molecules of molar mass M_i and m is the total mass of the sample.

Due to the contributions of the individual molecules within a polymer in determining M_w , M_w is always greater than M_n . However, a special case exists when all molecules are of the same weight, here $M_w = M_n$. Hence, the narrower the molecular weight range, the closer are the values of M_w and M_n . This relationship gives rise to the **polydispersity index**, P , which is a measure of the molecular weight distribution in a sample

$$P = M_w / M_n \quad (2.3)$$

Many of the physical properties of polymers are highly dependent on the molecular weight, it is therefore good practice to experimentally determine one of the mean values (e.g. by viscosity measurements, osmometry etc) and to

state an estimation of the polydispersity, in order to select the most suitable polymer for the specific application in mind. However for a vast majority of research it is common to use an industrially derived polymer that is known to be fairly monodisperse.

2.1.3: Composition

The molecular building blocks and configuration of the molecules within a polymer are the fundamental basis to many of its associated properties. Most polymer molecules have a "backbone" of carbon, but there are some that have other backbones, such as silicone oxide which is represented in figure 2.2.

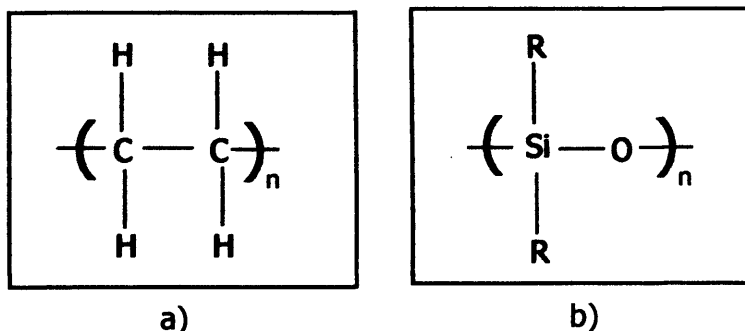


Fig 2.2: *Representative structures of a) a polymer with a carbon backbone and b) a silicone oxide backbone.*

The polyolefins have a continuous carbon backbone, whereas other polymers may have amide, ester or ether linkages. It is the nature of these linkages, amongst other properties e.g. molecular weight, that drastically affect the properties of the polymer.

2.1.4: Polymer structure

The process in which the monomers are joined together greatly influences the final structure of the polymer, of which there are two main types:

1. Homopolymers-a polymer that can either be ionic or non-ionic which consist of the same monomeric repeat unit,
2. Copolymers-a polymer that can either be ionic or non-ionic that consist of more than one type of monomer. Copolymers can be subdivided into further categories:
 - block or comb copolymers- when long chains of one monomer are connected to long chains of another monomer,
 - random/statistical copolymers- when the monomers are distributed randomly,
 - alternate copolymers- where the monomers alternate and
 - graft copolymers- which are slightly different, but compose of segments that *covalently* bond to the surface of particles. (The previous three mentioned copolymers *physically* adsorb to surfaces.)

Note: If a polymer consists of one or more monomer unit that is carrying an ionisable group (if it is ionic), it is termed a Polyelectrolyte.

2.1.5: Polymer architecture

One can also describe polymers (figure 2.3) as *linear*, *branched*, and *cross-linked* (network). A linear polymer has no branching other than the pendant groups associated with the monomer². Branched polymers contain branch points (junctions) that connect three or four sub-chains which may be side-chains or part of the main chain. However, cross-linked (network) polymers are formed when linear or branched polymer chains are joined together by covalent bonds, by intermolecular physical junctions or by entanglements of the chains.

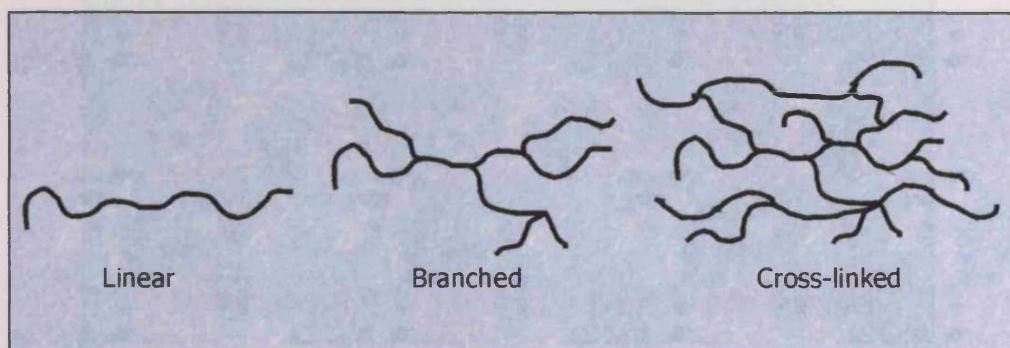


Fig 2.3: Representation of polymer types.

In the solid state, in addition to classifying a polymer as linear, branched or cross-linked, it is also necessary to take into account the assembly of the polymer chains. There are two ideal types of assemblies; Amorphous or crystalline. *Amorphous* polymers have no definite order and there are no points of attachment between adjacent molecular chains (liquid-like). *Crystalline* polymers have their molecular chains arranged in an ordered fashion (solid-like) enabling these chains to approach one another close enough for intermolecular forces to bind the chains together. Crystalline and amorphous arrangements are ideal structures and their behaviour as solids and fluids constitutes ideal states. However, there are also arrangements of polymer assemblies that show order similar to crystals and, at the same time, fluidity like liquids. Polymers of this "intermediate" type are called *mesomorphous*³.

Technically, there is also another class of highly branched (hyperbranched) polymers called dendrimers that were discovered in 1985 by Donald A. Tomalia⁴. A dendrimer is a synthetic, three-dimensional macromolecule that is formed by the step-wise addition of monomers into a regular branching "tree-like" structure^{5,6,7}. When produced by a step-wise synthesis, dendrimers are monodisperse with a precise molecular weight and size.

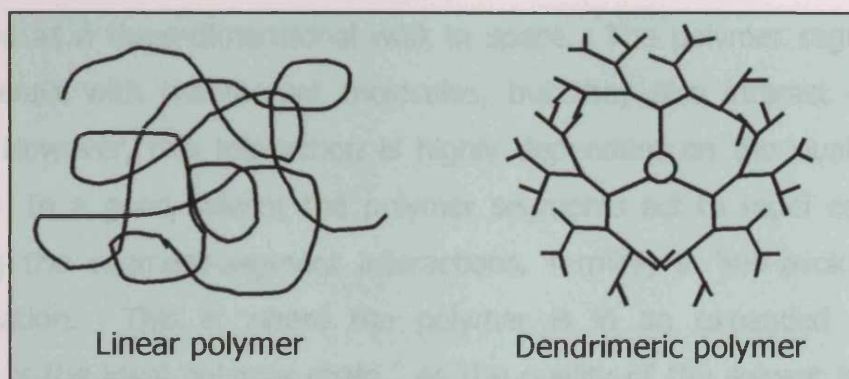


Fig 2.4: A schematic illustration of a conventional linear polymer and a dendrimer.
 (Adapted from Dr. Gavin Kirton's home page, Indiana University-Purdue University
 Indianapolis)

In principle this unique monodispersity is determined during the synthesis, where the conditions of formation can be finely tuned in order to produce a dendrimer of exactly the right shape, size, flexibility etc. required. Dendrimers tend to form symmetrical spherical shapes, as shown in figure 2.4, with a well-defined interior and exterior and with their chemistry being dominated by the nature of the groups on the branch end.

2.1.6: Polymers in solution

When a polymer is dissolved in a solvent an increase in the solution viscosity is observed. Owing to their large size, polymers move slowly in solution compared to the small solvent molecules and therefore act to slow down the solvent molecules by inhibiting their flow. As a consequence of this, the solution becomes more viscous. However, not only do the polymer molecules block the motion of the solvent molecules, they also slow them down through intermolecular forces. If there are any attractive secondary interactions between the polymer and the solvent molecules, the small solvent molecules can become bound to the polymer.

Polymer molecules generally form random coils in solution, which may be described as a three-dimensional walk in space. The polymer segments not only interact with the solvent molecules, but they also interact with each other. However, this interaction is highly dependent on the quality of the solvent. In a good solvent the polymer segments act to repel each other, reducing the segment-segment interactions, forming a "self-avoiding walk" conformation. This is where the polymer is in an expanded form and represents the ideal polymer chain. As the quality of the solvent is reduced, the number of segment-segment interactions, due to the unfavourable entropic contribution associated with segment-solvent interactions, increases. As a consequence of this increase, the polymer is in a more contracted conformation. So by altering the conformation of polymers in solution, it is possible to alter many of the solution properties e.g. the viscosity.

Therefore, polymers are used as thickeners in things like shampoo and even ice cream. The extent of the thickening, however, is highly dependant on the molecular weight of the polymer. When a polymer has a high molecular weight, it has a large hydrodynamic volume (the volume the coiled polymer takes up in solution) and is able to block the motion of more solvent molecules. Also, for higher molecular weight polymers, the secondary forces are stronger hence the more strongly a solvent molecule or neighbouring polymer segment will be bound to the polymer.

2.1.7: Polymer solution thermodynamics

The solvation of a polymer is governed by the magnitude of the free energy of mixing, ΔG_{mix} :

$$\Delta G_{\text{mix}} = \Delta H_{\text{mix}} - (T \Delta S_{\text{mix}}) \quad (2.4)$$

where ΔH_{mix} is the enthalpic component, T is the temperature and ΔS_{mix} is the change in entropy upon mixing. Note, for spontaneous dissolution, ΔG_{mix} must be negative. The resultant solution, following spontaneous dissolution, has a lower free energy than the sum of the free energies of the constituents. Due

to the solvated chains having an increased conformational mobility, the change in entropy upon mixing of the polymer and solvent is always large and positive and hence, the dissolution of the polymer is controlled by the magnitude of ΔH_{mix} , which should be small, zero or negative for dissolution to be favoured.

2.1.8: Polymer-solvent interactions

The properties and the interaction mechanism of polymers in solution are highly dependent on the solvent quality. Upon dissolving a polymer in a solvent, there will be attractive forces between certain polymer segments that induce cohesion. To remove a given molecular species from its nearest neighbours would, therefore, require energy. This measure of energy, which is termed the cohesive energy, is related to ΔH_{mix} , the volume of mixing, the volume fractions and the cohesive energy densities of the components. The cohesive energy density- $\Delta E_n / V_n$ is analogous to the heat of vaporisation per unit volume. Furthermore, the term $(\Delta E_n / V_n)^{1/2}$ is known as the solubility parameter, δ_n .

It therefore follows that:

$$\Delta H_{\text{mix}} = V_{\text{mix}} (\delta_1 - \delta_2)^2 \phi_1 \phi_2 \quad (2.5)$$

where V_{mix} is the volume of mixing, δ_1 and ϕ_1 are the solubility parameter and volume fraction of solvent respectively and δ_2 and ϕ_2 are the solubility parameter and volume fraction of the polymer. For spontaneous dissolution, ΔH_{mix} must be small, and thus the solubility parameters of the solvent and polymer must be as close as possible in value; if the values of δ_1 and δ_2 differ widely, the polymer segments prefer contact with themselves and phase separation occurs.

2.1.9: Flory-Huggins theory

This approach uses the principles of statistical thermodynamics to describe the criteria required for mixing a polymer and solvent. By obtaining a value for the entropy of mixing ΔS_{mix} , using the Boltzmann equation, the Flory Huggins

parameter, χ_{sp} , can be obtained. χ_{sp} is a measure of the interaction energy of a given polymer-solvent system and is related principally to the enthalpy of mixing for the polymer solution. χ_{sp} is small for good solvents whilst poor solvents have a high value of χ_{sp} . $\chi_{sp} = 0$ corresponds to a solvent very similar to the monomer⁸. This theory also predicts that mixing of polymer and solvent is favourable when the temperature is increased, based on the fact that at higher temperatures the solvent properties are improved as $\chi_{sp} \rightarrow 0$. However, this is not always found experimentally and at large temperature ranges there is a deviation from the expected behaviour.

2.1.10: Solvent quality

The situation where $\chi_{sp} = 0.5$ corresponds to the θ condition, where polymer-solvent contact is minimised and phase separation is incipient. In a good solvent (where $\chi_{sp} < 0.5$) the segments of the polymer chain have no preference for other segments over the solvent molecules. Usually, in a good solvent, the solvent molecules are similar in properties to those of the polymer, and a given segment of the polymer would have as much preference for a solvent molecule as for another polymer segment. The result is a random configuration of the extended chains, just as in a polymer melt. In a poor solvent (where $\chi_{sp} > 0.5$), there is much greater affinity between polymer segments than between the segments and the solvent molecules. The result is a contraction of the chains. This random extension in a good solvent and a contraction in a poor solvent is an important factor affecting the viscosities of solutions.

2.1.11: Size and shape

The dimensions and shapes of single polymer molecules can only be studied in solution because these molecules degrade at the temperatures required for their vaporization. Solvents may or may not interact with polymer molecules to generate additional varieties of sizes and conformational shapes.

When a polymer is dissolved in a high excess of solvent the polymer-polymer interactions can be neglected. Depending on the configuration (degree of

branching, molecular weight), the nature of the solvent and the temperature, when dissolved, a single flexible linear chain has many internal degrees of freedom (by rotation about the single bonds in the backbone) and may fold in different ways in order to minimize polymer-solvent contact. This folding of the polymer chain commonly forms structures, such as; unperturbed coils, wormlike coils, perturbed coils and even various more or less compact structures that resemble Euclidian bodies (e.g. spheres or rods).

The size of a polymer coil is, however, characterised by its radius of gyration, R_g which measures the r.m.s. distance of the polymer segments from the centre of mass of the molecule. Figure 2.5 illustrates three extreme types of polymer configuration: the stiff rod, the compact (spherical) globule and the coil. For a solid sphere of radius R , the radius of gyration is $(3 / 5)^{1/2} R$, and for a long thin rod of length l , $R_g = l (2 \sqrt{3})$.

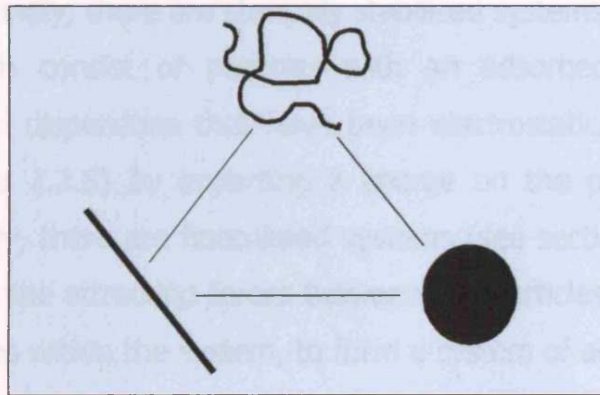


Fig 2.5: *The triangle of Haug, representing three different types of chain folding.*

It should also be noted here that the radius of gyration is dependent on the molar mass, M . In the compact state $R_g \propto M^{0.33}$, for a linear configuration $R_g \propto M$, while for a random coil $R_g \propto M^\alpha$, where $1 > \alpha > 0.33$.

2.2: Colloids

2.2.1: Classification of a colloid

Simple colloidal dispersions are two-phase systems consisting of a disperse phase (for example a powder) finely distributed in a dispersion medium⁹. When the disperse phase is a solid and the dispersion medium is a liquid, the widely used Ostwald classification of dispersions distinguishes this further to be called a suspension.

As a result of the size of the particles/molecules (1nm-1 μ m), a colloid will neither dissolve nor precipitate. However, the size is not the dominant factor, rather the total surface area. From a thermodynamic perspective, colloidal dispersions are inherently unstable, but kinetically stable. There are four main types of colloidal dispersions, the most simple being "hard sphere" systems. The nature of these systems has been discussed in chapter one, but they basically consist of a low concentration of particles, which screens out any interparticle interactions because of the large distances between nearest neighbours. Secondly, there are sterically stabilised systems (see section 2.2.5 and 2.2.6) which consist of particles with an adsorbed polymeric layer. Thirdly, there are dispersions that have been electrostatically stabilised (see section 2.2.7 and 2.2.8) by imparting a charge on the particles, to induce repulsion. Lastly, there are flocculated systems (see section 2.2.18). These are formed when the attraction forces between the particles predominate over all the other forces within the system, to form a system of aggregates.

2.2.2: Preparation of colloidal dispersions

In 1928, Svedberg divided the preparation of colloidal dispersions into two categories: dispersion and condensation¹⁰, dispersion being the most suitable method for fine particulate materials. In the dispersion method, a sample of bulk material is broken down to colloidal dimensions by some kind of mechanical process. The most widely used (e.g. colloidal mill, high shear mixing) utilises a shearing action in which the particles are torn apart. This results in a colloidal dispersion, provided that the solution contains a suitable dispersing agent to prevent re-aggregation of the small particles¹¹. However,

the method employed in the preparation of a colloidal suspension is highly dependent on the magnitude of the particle-particle interactions and the particle concentration¹².

2.2.3: Colloidal motion

It was the English botanist Robert Brown, who first observed the rapid erratic motions of small particles. Since then, further experimental evidence has shown that "Brownian motion" has been found to exist within colloidal dispersions, in fact, all systems that have small enough particles tend to exhibit this behaviour.

The kinetic-molecular theory of matter was employed to explain this motion, which showed that the motion was a result of the continuous bombardment of particles by the solvent molecules that surround them.

2.2.4: Stabilisation of a colloid

Colloidal particles undergo Brownian motion and hence are continuously forced into colliding with one another. The intensities of these bombardments are varied and sometimes the collisions can result in a permanent association of two or more particles. This formation of aggregates (referred to later as *flocculation*) renders the system unstable. Colloidal particles attract each other over large distances, so there is a long-range force (van der Waals force) that tends to condense them into larger particles. At the point where these larger particles are formed, the free energy of the system is at its lowest. In order to stabilise colloidal systems there are two mechanisms that have proved effective in opposing this long-range interaction and hence prevent aggregation of the particles during collisions;

1. *steric stabilisation*-where the particles can be coated with an adsorbed layer of material (e.g. a polymer) which will then shield the "hairy" particles from contacting each other or
2. *electrostatic stabilisation*-where all the particles can be given either a positive or negative electrical charge to induce the coulombic repulsion

operative between charged colloidal particles and their respective double layers.

2.2.5: Steric stabilisation

In effect, the surface of a lyophobic (solvent-repelling) colloidal particle is covered with a lyophilic (solvent-attracting) material of a polymeric nature, thus giving the particles a "hairy" surface. When two such particles approach, they repel each other due to the interaction between the adsorbed polymer chains on either particle. In fact, the repulsion is due to two effects, an *osmotic effect* caused by the high concentration of polymer chains in the region of particle overlap, and a *volume restriction effect* due to the loss of possible conformations in the narrow gap between the two particle surfaces. In essence, this repulsion is sufficient to overcome the long-range attractive forces and therefore introduces stability within the system. The colloidal stability of dispersed particle systems depends largely on the adsorbed amount and the hydrodynamic thickness of the adsorbed polymeric layer^{13,14}. In practice, steric stabilizers are usually block copolymers with lyophobic "anchor" groups, to provide firm attachment to the surface, and highly lyophilic "buoy" groups, to provide a suitably thick layer of polymer that acts as the steric barrier. For example, polymers/surfactants are expected to adsorb onto particles, typical ingredients of ink formulations, by their hydrophobic parts and extend their hydrophilic parts into the aqueous medium, thus providing steric stabilization.

2.2.6: Factors that influence steric stabilisation

Steric stabilisation can be influenced by many factors; by changing the nature or the length of the adsorbing polymer chains (the hairs), by altering the adsorption energy (altering the particle surface properties) or by changing the solvent properties. In worse than theta conditions or when the surfaces are not completely covered, the hairs may collapse rendering the interaction attractive, therefore promoting aggregation of the particles.

2.2.7: Electrostatic stabilisation

At any interface between two phases, there is a tendency for charges (electrons or ions) to accumulate. As a result of the different affinities of different species (coulombic interactions) for the surfaces that may be present within a colloid, an uneven charge distribution may occur that renders one surface positively charged and the other negatively. Negative counter-ions are attracted to a positive surface by the electric field generated by the positive charges as well as being distributed uniformly throughout the surrounding medium by their thermal motion. The outcome, therefore, consists of a few negative ions strongly bound to the particle surface and a distribution of the negative charge that decreases in concentration as the distance approaches the bulk solution. This arrangement of charge is what is called the *diffuse electrical double layer* of the particle, which can be seen in figure 2.6.

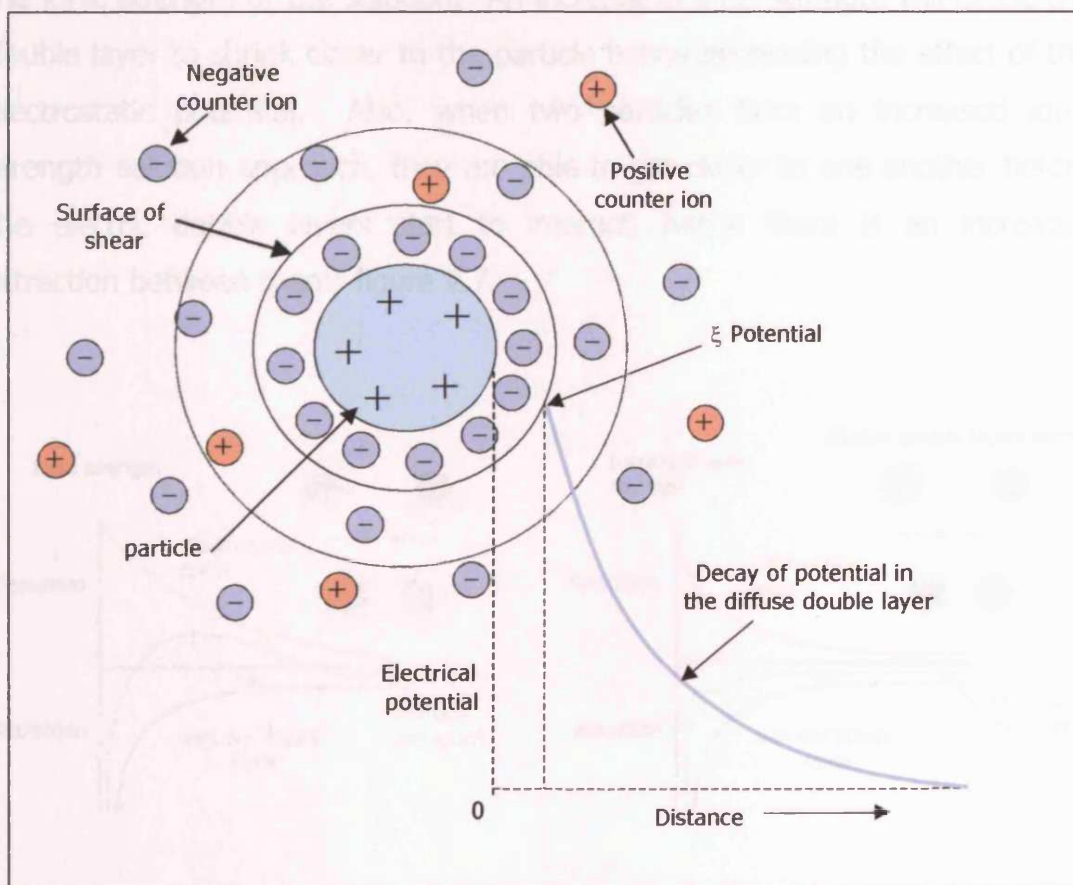


Fig 2.6: The electrostatic double layer of a particle and the dependence of the electrical potential on the distance a counter-ion is from the layer.

The inner layer near the particle (the Stern layer) can always be assumed to be fixed to the particle, however as the distance from the particle is increased the layer becomes more diffuse and the liquid begins to move with respect to the particle. The point at which this movement occurs is termed the surface of shear. The electrostatic potential in this plane relative to the bulk is called the zeta potential (ξ)¹⁵. The zeta potential is, in many cases, a good estimate of the diffuse layer potential and it is determined by measuring the velocity of the particles in an electric field.

2.2.8: Factors that influence electrostatic repulsion

The extent of the diffuse electrical double layer can be altered by changing the magnitude of the surface charge or the concentration of the electrolyte (adding an excess of positive or negative charge) in solution. This acts to alter the ionic strength of the solution. An increase in ionic strength will cause the double layer to shrink closer to the particle hence decreasing the effect of the electrostatic potential. Also, when two particles from an increased ionic strength solution approach, they are able to get closer to one another before the electric double layers start to interact, hence there is an increased attraction between them; figure 2.7.

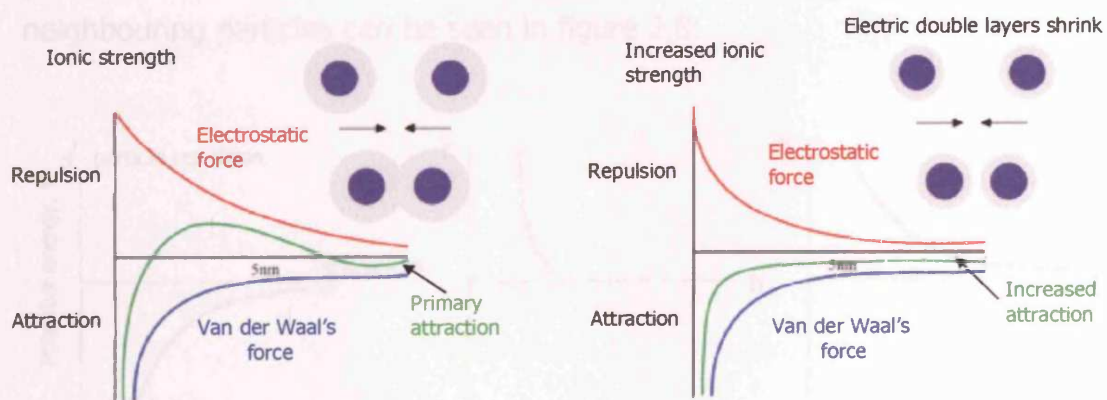


Fig 2.7: A schematic diagram to represent the forces between two approaching particles in a solution and the effect of increasing the ionic strength.

There are, as can be seen in figure 2.7, two main forces that act on charged colloidal particles in a solution;

- 1) electrostatic repulsion and
- 2) van der Waal's attractive forces

Deryagin, Landau, Verway and Overbeek summarised that by adding these two opposite forces together it is possible to describe the overall force acting on a colloidal particle as it approaches another particle or charged surface. This is the basis of the **DLVO** theory. However, it is very important to realise that the overall shape of this resultant force (the green lines in fig 2.7) depends on the ionic strength, which in turn affects the depth of the electric double layers and the resultant electrostatic repulsion.

Basically, in order to stabilise a colloidal system, the ever present attractive van der Waals forces that exist between the particles have to be overcome and the above two methods (imparting of a charge or adsorption of a polymeric species) have proved effective in promoting particle repulsion which opposes this attraction. To illustrate the effect of the two methods, the inter-particle potential of a) an un-stabilised colloidal system (showing van der Waals attraction), b) a sterically stabilised colloidal dispersion and c) an electrostatically stabilised dispersion with respect to the distance between neighbouring particles can be seen in figure 2.8:

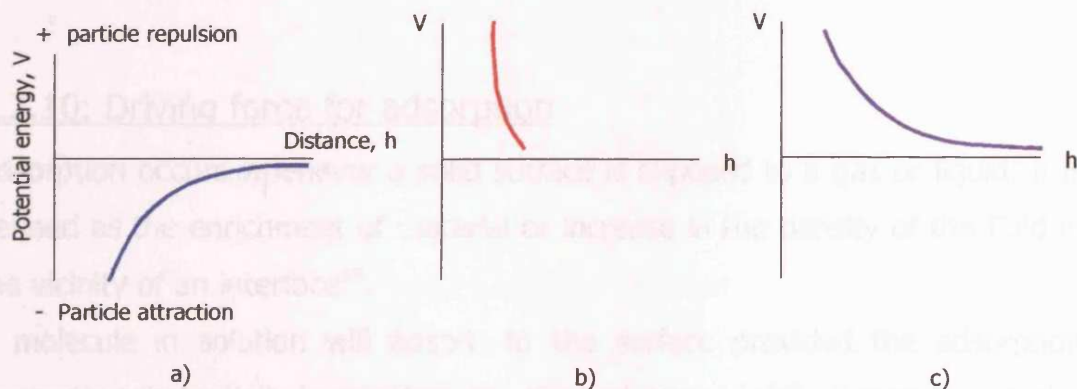


Fig 2.8: *Interparticle potential vs. separation diagrams for unstable and stabilised colloidal systems.*

Although both methods are successful, to retain good flow properties steric stabilisation, is the preferred method for the manufacture of concentrated dispersions since no electroviscous effects occur. The stabilisation of colloidal dispersions by naturally occurring polymers has been exploited continuously since the ancient Egyptians produced "instant" ink for writing on papyrus¹⁶. Nowadays colloidal stabilisation by either natural or synthetic polymers is essential for many applications within the pharmaceutical, food and detergents industry in addition to its continuing use as a basis for inks and paints.

2.2.9: Colloidal forces

The force **F** between two surfaces or particles at a separation **h** and a constant external pressure is determined by the change in Gibbs free energy **G** with separation¹⁷

$$F = -(\Delta G / \Delta h)_T = -(\Delta H / \Delta h)_T + T (\Delta S / \Delta h)_T \quad (2.6)$$

The sign convention is such that the repulsive force is positive.

When the surfaces are covered with adsorbed polymer, interaction begins when the surface separation is approximately twice the distance of the radius of gyration of the polymer. At this distance, which is typically 10-100 nm, van der Waals and double-layer forces between the bare surfaces are negligible leaving the polymer-polymer overlap to provide the dominant contribution to the resultant force.

2.2.10: Driving force for adsorption

Adsorption occurs whenever a solid surface is exposed to a gas or liquid: it is defined as the enrichment of material or increase in the density of the fluid in the vicinity of an interface¹⁸.

A molecule in solution will adsorb to the surface provided the adsorption energy is substantially larger than the thermal energy, kT . Depending on the polymer type and the filler material chosen, as with any spontaneous process, adsorption of a polymer from solution to a surface is driven by a reduction in

the overall free energy, ΔG , e.g. if the free energy of polymer segment-surface contacts is lower than that of the solvent-surface contacts. Basically, adsorption is driven by the competition between the net energy change on adsorption (enthalpy of adsorption), the loss of conformational entropy of the adsorbed polymer, and the gain in entropy of the solvent molecules that are replaced by the polymer molecules at the particle surface.

2.2.11: Kinetics of polymer adsorption

The kinetics of polymer adsorption involves several distinct processes that occur simultaneously, but each of which has a characteristic time scale. The first process is concerned with the mass transport, via diffusion or convection, of the polymer from the solution to the surface. Upon reaching the surface, the polymer must then attach itself to any available surface sites however this is dependent on the magnitude of any local activation energy barrier. The last process is the rearrangement of the polymer from the solution conformation to the new "tail-loop-train" conformation. Following initial contact of the polymer solution to the surface, an increase in the adsorbed amount is observed with increasing time. However, at first this increase is rapid but on approaching surface saturation the molecules arriving at the surface are unable to adsorb immediately and the rate is therefore slowed. Upon adsorption up to about 75% coverage, the concentration of non-adsorbed polymer at and around the surface is much greater than that of polymer in the bulk solution. This mass transport effect is therefore regarded as the kinetically dominant process of adsorption.

2.2.12: Methods of adsorption

A polymer can adsorb to a particle surface as a result of: van der Waals interactions, coulombic (charge-charge) interactions, dipole interactions or hydrogen bonding. Whatever the mode of adsorption, the size of a polymer molecule makes it extremely unlikely that all the segments of the macromolecule will be in contact with the surface at any one time. Hence, the usual result is that the polymer chain is adsorbed by more than one point, with

the tail extending into the solvent. The common representation, first proposed by Jenckel and Rumbach in 1951, of an adsorbed polymer to a particle surface can be shown in figure 2.9, with the so-called *trains* (the surface contact points), *loops* (the train connecting points) and the *tails* (the non-adsorbed portion of the polymer).

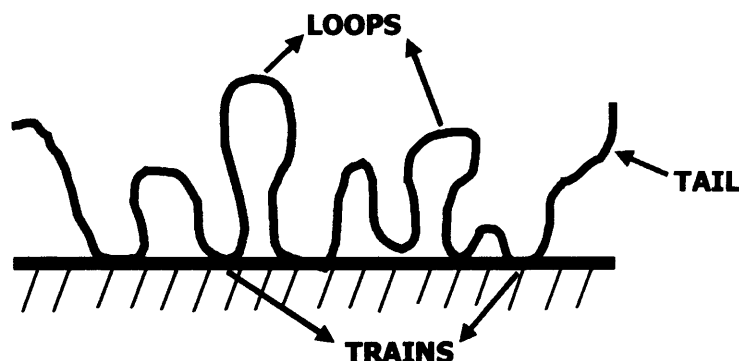


Fig 2.9: A schematic diagram to represent the adsorption of a polymer to a particle surface.

Multipoint attachment of the molecule to the surface makes it difficult for all the segments to desorb simultaneously therefore, polymer adsorption can essentially be classified as an irreversible process even though each of the separate contact points may easily be desorbed.

2.2.13: Polymer segment-surface interactions

The adsorption characteristics of a polymer are highly dependent on the interaction energy of a given polymer-solvent system, χ_{sp} . However, it is very important, for adsorption to occur, that the polymer has an affinity for the surface in question, expressed in terms of the segment-surface interaction parameter χ_s . When χ_s is large, there is a strong attraction between the polymer segment and the surface hence the adsorption is strong. When χ_s is small, the adsorption is weak. Upon adsorption, this interaction parameter strongly influences the conformation of a polymer at the solid-liquid interface. When χ_s is large, the polymer density at the surface will increase and may

result in less extension of the polymer into solution. However, χ_s and the adsorption of polymer to the surface are greatly influenced by many factors, the main two being; the interfacial surface characteristics and the chemistry that defines how the polymer behaves in solution.

2.2.14: Surface characteristics that affect adsorption

The surface roughness and porosity can greatly influence the degree of adsorption of a polymer at that surface. The hydrophobicity of a surface may be varied by the presence of high energy sites, such as crystal edges, ridges or corners that usually expose active sites that can then accommodate polymer adsorption. If a surface is porous, the total surface area available for polymer adsorption can be greatly underestimated, in this case, the polymer may be able to penetrate the surface¹⁸.

If a surface is heterogeneous, the presence, distribution and nature of functional groups found at the surface also contribute significantly in the polymer adsorption process. These groups ultimately determine the energy of the surface and hence the nature and strength of the interaction/bonds responsible for adsorption between the polymer and the surface, whether they be chemical bonds, hydrogen bonds or hydrophobic interactions.

Another important adsorption determining factor is the surface curvature¹⁷. The conformation, amount of adsorbed polymer and the adsorbed layer thickness, δ can be influenced by the particle size, specifically, the radius of curvature of the particle surface, r_{curv} . Particles with a small radius allow polymer segments greater access to the regions immediately adjacent to the particle surface. This results in a higher polymer density near the surface but on the other hand, a thinner adsorbed layer is observed.

2.2.15: Adsorption and the properties of polymers in solution

The adsorption behaviour and the resulting conformation of a polymer is, as mentioned before, greatly influenced by many solution properties that are associated with the polymer e.g. solvency, molecular weight and concentration. The solvency of the polymer is very important because the resulting interaction between the polymer and the solvent determines the adsorbed layer thickness, due to either elongation of chains into the solvent or contraction of chains to the surface. Also, the molecular weight of the polymer has a profound effect on the adsorption characteristics. Generally, the polymer adsorbed amount increases with molecular weight due to the resultant decrease in adsorption entropy. A high molecular weight polymer tends to contract on the surface in order to minimise polymer-solvent mixing, hence also minimise entropic loss. It must be mentioned however, that a high molecular weight polymer takes longer to reach equilibrium adsorption levels than the equivalent low molecular weight polymer. Two factors contribute to this^{19,20,21,22}: firstly, when a polymer is larger it has a lower diffusion coefficient compared to a smaller polymer and secondly, larger polymer chains require more time to rearrange from their solution conformation to their adsorbed conformation. The first effect is rate determining at low concentration and the second is rate determining at high concentration. Lastly, as the concentration of polymer is increased in solution, the extent of the surface coverage also increases until eventually maximum coverage is achieved. Upon the continued addition of polymer, the osmotic and steric forces between adsorbed chains hinder any further adsorption, rendering the excess polymer un-bound in solution.

2.2.16: Measurement of adsorbed amount

The adsorption of a polymer from solution onto a surface is usually described in terms of an *adsorption isotherm* which relates the amount of polymer at the particle surface, Γ (mg/m^2) to the amount of polymer left in solution, c (ppm or mg/L). The shape of the isotherm is dependent on the nature of the system however there are four main types which can be seen in fig 2.10: "S"

shaped which indicate an increase in adsorption sites by an increase in slope, type "L" (Langmuir) which indicates the difficulty of finding vacant sites on increasing the polymer concentration, "H" types (high affinity) which are very common and show monolayer coverage onto the surface and "C" type (constant partition) which, for porous adsorbents, indicates the creation of new sites as the adsorption process progresses.

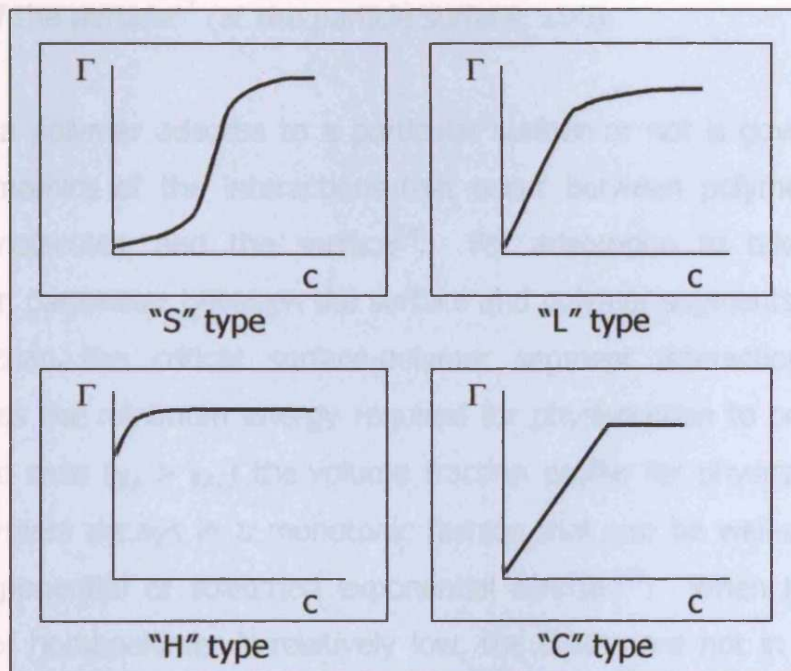


Fig 2.10: Different types of polymer adsorption isotherms

The most widely used methods for obtaining an isotherm are those which require physical separation of the surface layer from the continuous phase, after which the supernatant is analysed (indirect methods). Alternatively, the substrate is analysed either *in situ* or after separation of the solid material (direct methods). Isotherms are studied in order to understand the mechanisms and forces involved in the adsorption process and to gain an understanding of the structure of the adsorbed species. Control of the extent

of adsorption and the orientation of the adsorbate can be useful for controlling the transport and equilibrium properties of a suspension.

2.2.17: Volume fraction profiles

The resulting conformation of an adsorbed polymer is a very important parameter because the way in which a polymer arranges itself ultimately determines the volume fraction profile it will produce. The volume fraction profile of an adsorbed polymer, $\phi(z)$, quantifies the fractional volume occupied by polymer segments in relation to the distance the segment is from the surface of the particle²³ (at the particle surface, $z=0$).

Whether a polymer adsorbs to a particular surface or not is governed by the thermodynamics of the interactions that occur between polymer segments, solvent molecules, and the surface²⁴. For adsorption to take place, the interaction parameter between the surface and polymer segments, χ_s , must be greater than the critical surface-polymer segment interaction parameter (defined as the minimum energy required for physisorption to occur), χ_{sc} . If this is the case ($\chi_s > \chi_{sc}$) the volume fraction profile for physically adsorbed homopolymers decays in a monotonic fashion that can be well-approximated by an exponential or stretched exponential function²⁵. When the adsorbed amount of homopolymer is relatively low, the chains are not in contact with their nearest neighbours and can form one of two conformations depending on the values of χ_s and χ_{sc} . If $\chi_s > \chi_{sc}$, the volume fraction profile resembles a "pancake" (fig 2.11). However, if $\chi_s < \chi_{sc}$, the volume fraction profile exhibits a maximum some distance from the interface, best described by a Gaussian function, and forms a "mushroom".

On increasing the adsorbed amount, the distance between the grafting points of the polymer is decreased. In order to accommodate this extra material at the interface, the polymers are forced to extend and form what is known as a "brush" conformation where the profile is described by a "step"^{26,27}.

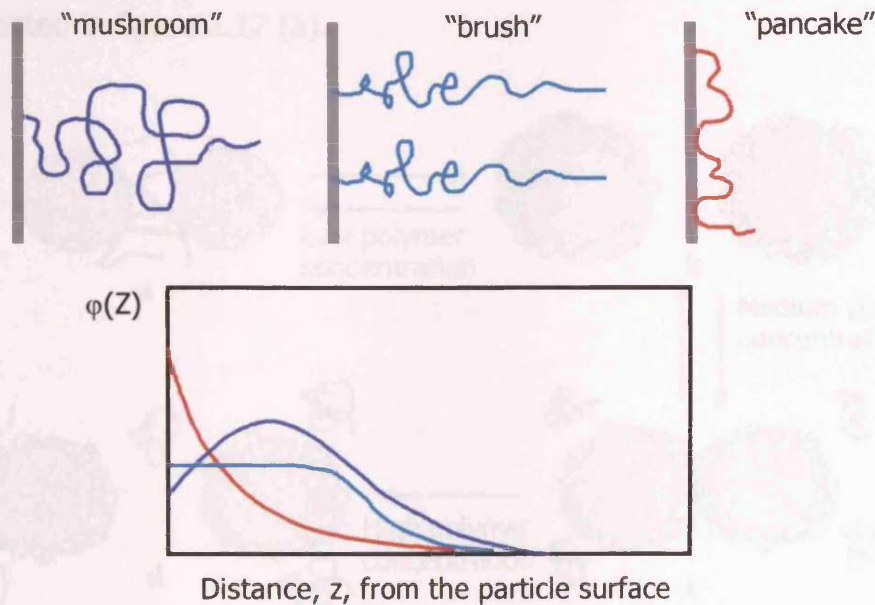


Fig 2.11: The "mushroom", "brush" and "pancake" conformations and their respective volume fraction profiles²³.

The situation, however, becomes rather more complicated when dealing with copolymers. Copolymers consist of more than one monomer hence the volume fraction profiles are determined not only by the distribution of certain monomers within the chain, but also by considering their different interaction parameters.

2.2.18: Polymer coated particle interactions

As already mentioned, the stability of a colloidal dispersion is greatly influenced by the addition of a polymer solution. At a low polymer-particle concentration ratio, colloidal instability may be observed due to a phenomenon called *bridging flocculation*. Bridging flocculation occurs readily with high molecular weight polymers over a narrow range of concentrations (of the order of several parts per million) when there is insufficient polymer to coat the particles resulting in the adsorption of the polymer to more than one particle. The floc structures formed, which tend to be rather loose, sediment

rapidly and are easily removed from solution by filtration. The conditions that promote flocculation and the resulting flocculated structures are schematically represented in figure 2.12 (a).

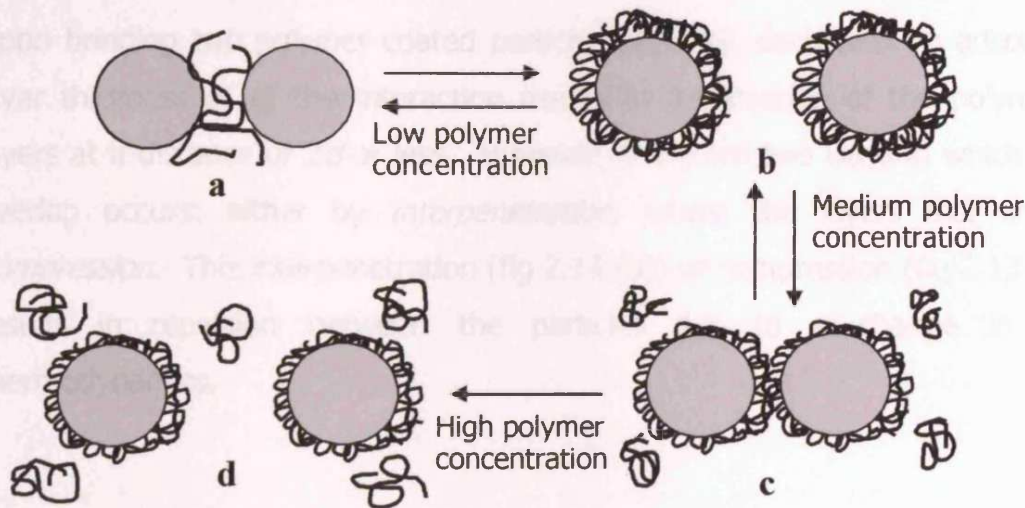


Fig 2.12: Schematic representation of the effects of adsorbed polymer on the stability of colloids showing: a) bridging flocculation at low polymer concentrations, b) steric stabilisation, c) depletion flocculation at medium polymer concentrations and d) depletion stabilisation at higher polymer concentrations (modified from Hunter, 2001)

At medium polymer concentrations, *steric stabilisation* (fig 2.12 (b)) of the colloidal particles is a result of polymer coated particle repulsion. This requires a high surface coverage, in addition to good solvency conditions for the polymer. Figs 2.12 (c) and 2.12 (d) show the effects of non-adsorbing polymer on the stability of colloids. Non-adsorbing polymers influence the interactions of particles by modifying the effective osmotic pressure or the activity of the solvent in the gap between two approaching particles. Polymer is excluded from the gap between particles. The osmotic pressure difference in the bulk solution, due to these non-adsorbing polymers, also excludes the solvent from the gap and hence induces an attractive force that pushes the particles together. This is called *depletion flocculation* and is shown in fig 2.12 (c). When the polymer concentration is high, *depletion stabilisation* (fig 2.12

(d)) may occur as a result of a repulsive force induced by the work required in creating a polymer free region between the two approaching polymer coated particles.

Upon bringing two polymer coated particles together, each with an adsorbed layer thickness of d , the interaction results in the overlap of the polymeric layers at a distance of $2d$ or less. However, there are two ways in which this overlap occurs: either by *interpenetration*, where the layers mix or by *compression*. This interpenetration (fig 2.13 (b)) or compression (fig 2.13 (a)) results in repulsion between the particles due to a change in the thermodynamics.

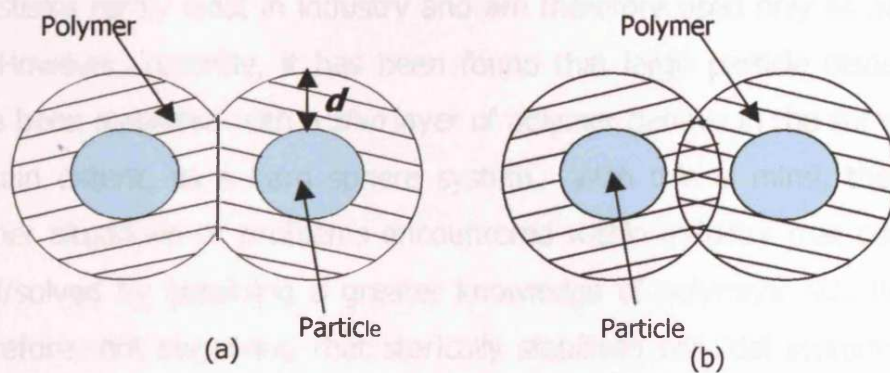


Fig 2.13: Interaction of particles coated with polymers: a) compression; b) interpenetration. Redrawn from Mollet and Grubenmann, page 165⁹

Summary:

In industry, where the control of a materials flow properties plays an important role e.g. paints/inks, food industry etc, the most widely used method employed to stabilise a colloidal dispersion is to adsorb a polymeric material on to the particle surface. However, the nature of the polymeric material must be chosen with care because many associated factors such as the molecular weight, polydispersity, degree of crystallinity and charge greatly affect the resulting rheological properties. Owing to the vast choice of available adsorbants and the varying concentrations that can be used, a variety of systems, each with their own unique properties, have been prepared and studied. Previously, it has been mentioned that the simplest colloidal system is that of a true "hard sphere" where there is no interaction between the particles and the only force acting is the weak van der Waals attraction. These systems rarely exist in industry and are therefore used only as an ideal model. However, recently, it has been found that large particle dispersions that have been stabilised with a *thin* layer of polymer behave in the same way, to a certain extent, as a hard sphere system. With this in mind, there are many other situations or problems encountered within industry that could be improved/solved by obtaining a greater knowledge of polymeric stabilisation. It is therefore, not surprising that sterically stabilised colloidal systems have been the basis of scientific research for many years already and will, I'm sure, continue to be so for many years to come.

References:

- 1 Cowie, J.M.G., *Polymers: Chemistry and physics of modern materials*, International Textbook Company Limited, Bucks, (1973)
- 2 Stevens, M.P., *Polymer Chemistry- an introduction 3rd edition*, Oxford University Press, New York, (1999)
- 3 Elias, Hans-Georg., *An Introduction to Polymer Science*, VCH, New York, (1997)
- 4 Tomalia, D.A., Baker, H., Dewald, J., Hall, M., Kallos, G., Martin, S., Roeck, J., Ryder, J., Smith, P., *Polym. J.*, 17, (1), 117-132, (1985)
- 5 Inoue, K., *Progr. Polym. Sci.*, 25, (4), 453-571, (2000)
- 6 Matthews, O.A., Shipway, A.N., Stoddart, J.F., *Progr. Polym. Sci.*, 23, (1), 1-56, (1998)
- 7 Aulenta, F., Hayes, W., Rannard, S., *European Polymer Journal*, 39, (9), 1741-1771, (2003)
- 8 Griffiths, P.C., *Ph.D. Thesis*, (1991)
- 9 Mollet, H., Grubenmann, A., *Formulation Technology-Emulsions, Suspensions, Solid Forms*, WILEY-VCH, (2001)
- 10 Svedbeg, T., *Colloid chemistry*, Chemical Catalog., New York, (1928)
- 11 Hunter, R.J., *Foundations of Colloid Science 2nd edition*, Oxford University Press, Oxford, (2001)
- 12 Russel, W.B., Saville, D.A., Schowalter, W.R., *Colloidal Dispersions*, Cambridge University Press, Cambridge, (1989)
- 13 Sato, T., Ruch, R., *Stabilization of Colloid Dispersions by Polymer Adsorption.*, Dekker, New York, (1980)
- 14 Napper, D.H., *Polymeric Stabilization of Colloid Dispersions.*, Academic Press, London, (1983)
- 15 Hunter, R.J., *Introduction to Modern Colloid Science*, Oxford Science Publications, Oxford, (1993), 233-235
- 16 Napper, D.H., Polymeric Stabilization-paper given at a review symposium on colloid science, Special Publication No. 43, *Colloidal Dispersions*, The Royal Society of Chemistry, (1981)
- 17 Evans, D.F., Wennerstrom, H., *The Colloidal Domain-where physics, chemistry, biology and technology meet 2nd edition*, WILEY-VCH, (1999)
- 18 Rouquerol, F., Rouquerol, J., Sing, K., *Adsorption by powders and porous solids-principles, methodology and applications*, Academic press, (1999), chapter 1.
- 19 Obey, T.M., Griffiths, P.C., *Polymer Adsorption Fundamentals, Principles of Polymer Science and Technology in Cosmetics and Personal Care*, Marcel Dekker, (1999)

- ²⁰ Couture, L., Van de Ven, T.G.M., *Colloids Surf.*, (1991), 54(3-4), 245-60.
- ²¹ Polverari, M., Van de Ven, T.G.M., *Coll. Surf. A: Physicochemical and Engineering Aspects*, (1994), 86, 209-28
- ²² Van de Ven, T.G.M., *Adv. Colloid Interface Sci.*, (1994), 48, 121-40
- ²³ Griffiths, P.C., King, S.M., *Encyclopedia of Surface and Colloid Science*, Marcel Dekker, Inc., New York, Reprint program, (2002), 4700-4717
- ²⁴ Fler, G.J., Cohen Stuart, M.A., Scheutjens, J.M.H.M., Cosgrove, T., Vincent, B., *Polymers at interfaces*, Chapman and Hall, London, (1993)
- ²⁵ Cosgrove, T., Crowley, T.L., Ryan, K., Webster, J.R.P., *Colloids Surf.*, (1990), 51, 255-269
- ²⁶ Alexander, S., *J. Phys. (France)*, (1977), 38, 983
- ²⁷ de Gennes, P.G., *Macromolecules*, (1980), 13, 1069

CHAPTER 3: MATERIALS

The subject of this thesis is principally concerned with solid in liquid dispersions and their associated rheological behaviour. The main focus will be that of carbon black particles in both aqueous and oil media. The systems chosen were such that they are representative, initially, of model systems. Firstly, in order to relate this study directly to applications within industry, concentrated dispersions consisting of carbon black with a variety of different adsorbants in both aqueous solutions and oils were prepared and studied. Various grades of carbon black, which differ in aggregate size, structure, surface properties etc, have been investigated with either:

- an adsorbed acrylic resin layer,
- a poly(ethylene glycol) / poly(propylene glycol) / poly(ethylene glycol) block copolymer layer or
- a bitumen binder layer.

The second system comprised of an aqueous system of silica with an adsorbed polyethylene oxide layer. Silica and poly(ethylene oxide) systems have been employed in many areas of research as model systems hence are very well documented within past and present scientific literature. As a result, the broad knowledge and published detailed characterisation of this system provided a perfect model in which to compare the, not so well documented, but industrially important carbon black systems with.

3.1: Carbon black

3.1.1: Introduction

Carbon black is an intensely black, finely divided powdered form of highly dispersed elemental carbon manufactured by the controlled vapour phase pyrolysis of hydrocarbons¹. Its principal use is as a reinforcing agent in automobile tyres and other rubber products, but because carbon blacks are strong absorbers of light over the entire spectrum they are also used

extensively as extremely black pigments with high hiding power suitable for use in printing inks, paints and carbon paper.

3.1.2: Microstructure of carbon black

The blackness and tint properties of such ink coatings are all highly dependent on the particle size distribution, particle morphology and structure. Carbon black particles are usually spherical in shape and less crystalline than graphite². The precise structure is intermediate between graphite and a truly amorphous material - small crystallites made up of parallel graphitic layers 0.35-0.38nm apart. These localized graphitic layers are disordered in the centre of the particles, but tend to lie parallel to the particle surface³.

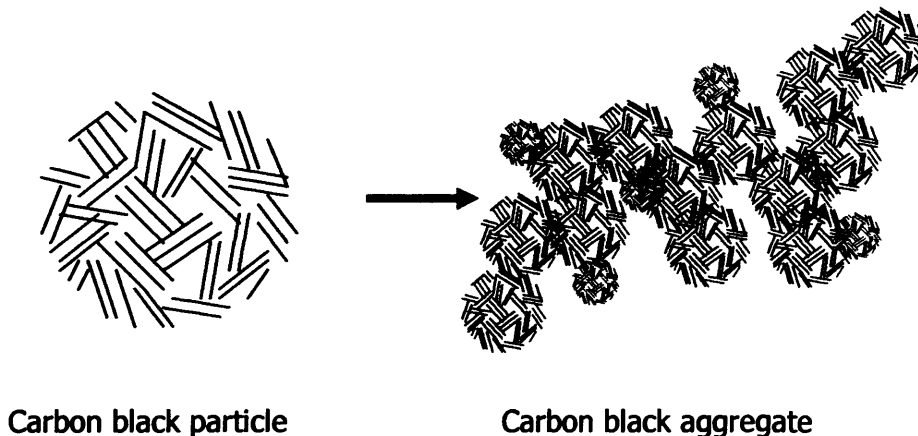


Fig 3.1: *A schematic diagram of the microstructure of a carbon black particle and how a typical aggregate may look.*

3.1.3: Manufacture of carbon black

Carbon black is made, primarily, from a petroleum-based feedstock. The oil is pumped into a specially designed furnace, where it is heated continuously above 1000°C with a mixture of fuel (oil or gas) and air. This elevated heating process “cracks” the oil to produce a gas stream laden with carbon black powder. The gas stream that is obtained is then passed through a series of

filters, which ultimately leads to the carbon black particles being separated from the gases.

3.1.4: Formation of carbon black

The formation of carbon black involves three important stages; nucleation of soot precursors, thus producing a particulate system from a molecular system, precursors which subsequently agglomerate to form particles with typical dimension 1-2nm. The final step involves the association of these particles, forming roughly spherical, primary particles. Aggregation of these primary particles thus determines the ultimate morphology of carbon black aggregates henceforth, termed fractal or spherical particles. Average aggregate diameters range from 0.1 to 0.8 μ m.

3.1.5: Important properties of carbon black

Carbon black is described by four fundamental properties. These include; fineness (which is dependent on the particle size distribution), structure (based on aggregate shape and size), porosity and surface chemistry (types of active functional groups present at the carbon black surface). Recognition of these fundamental properties and the non-fundamental properties such as surface area and tint strength that can be derived from them is, therefore, the key to understanding the nature of carbon blacks and their importance in industry.

- Particle size

The particle diameter (fineness) is the single most important property of carbon blacks which exerts a primary influence on the colour properties and the reinforcement properties. A finer particle size leads to jetter colour (Jetness is a measure of the blackness of a printed image and is also known as the optical density), more effective reinforcement and a higher viscosity, but requires increased dispersion energy. The particle size of a carbon black is a stable property and does not change when a sample is mixed into a particular vehicle system.

- Structure

When describing carbon black, the term "structure" is used to define the formation of the particles within an aggregate. Carbon black aggregates vary widely in shape, some being almost spherical (low structure), whereas others are more clustered and fibrous (high structure). There are four distinctly different categories described by Herd and coworkers⁴, shown in figure 3.2, that group together all possible aggregate types found within all carbon blacks.

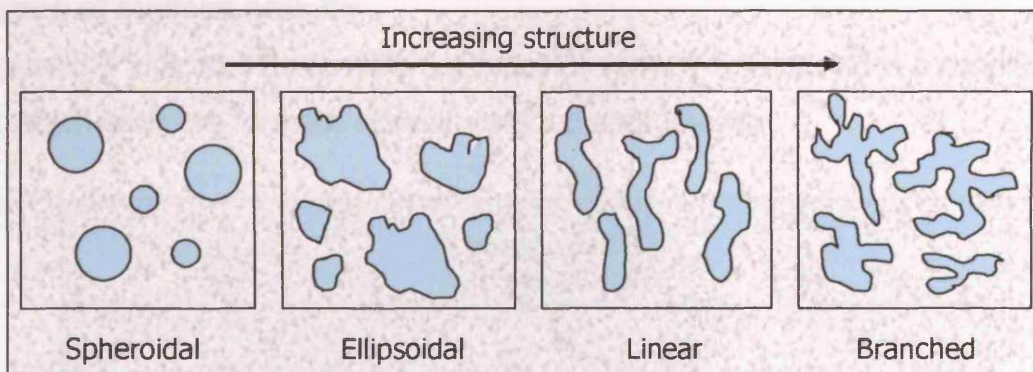


Figure 3.2: *The four types of carbon black aggregates. Redrawn from⁵*

In liquid or polymeric systems, the presence of a highly structured carbon black raises the viscosity and improves dispersibility. Structure is a system dependent property and the aggregate size/shape distribution will vary according to vehicle type and the shearing forces that are generated during the dispersing process.

- Porosity

The porosity in carbon blacks can be divided into two categories, open and closed porosity. The open porosity can be in the form of small pores of the order of nanometers of an undefined shape on the surface which may or may not provide access to internal voids. If the internal voids are not accessible to the surface, they represent closed porosity.

- Surface activity

Of the four fundamental properties of carbon black, surface activity is the most difficult to characterize, but in essence, it is described as the interaction (either physical or chemical) of the carbon black surface with its surroundings. Most carbon blacks have a low affinity for water, i.e. they are hydrophobic. However, Walker and Janov⁶ and later Bradley⁷ *et al* have reported that the level of hydrophobicity is reduced by the presence of chemisorbed oxygen and certain functional groups. However, the oxygen and hydrogen content are dependent on the manufacturing procedure employed and varies with the type of carbon black. In addition, the nature of the adsorbate and the conditions of adsorption, the nature of the adsorbent and the

Types of surface activity

Figure 3.3 indicates three different types of surface activity and the conditions at which each are formed; normal, oxidized and graphitic.

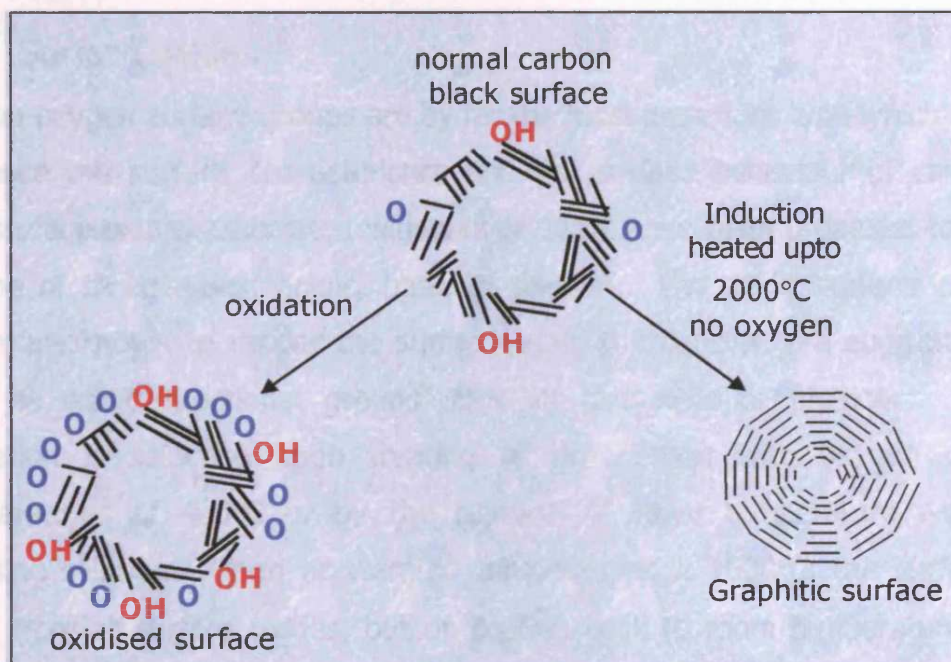


Fig 3.3: A schematic to represent three types of carbon black surface activity⁵

The surface activity of the carbon black dominates polymer-filler interactions and filler aggregate-aggregate interactions for many industrial applications, it is, therefore, of the utmost importance that the chemistry involving the

functional groups present at the surface be fully understood. Carbon blacks are invariably associated with varying amounts of oxygen and hydrogen. In addition they may also be associated with atoms of chlorine, nitrogen and sulphur. These atoms become part of the chemical structure, whilst being introduced to the sample during the manufacturing process. Carbon blacks typically contain about 90-99% elemental carbon with oxygen (typical oxygen content between 0.2 and 8.5%) and hydrogen (between 0.1 and 0.7%) as the other major constituents. However, the oxygen and hydrogen content are dependent on the manufacturing procedures employed and values vary from batch to batch. In addition, the nature of the feedstock and the manufacturing conditions are also responsible for the sulphur that is commonly found in carbon blacks (typical content of ~0.6%).

Surface oxides

Carbon-oxygen surface groups are by far the most important type which act to influence the surface characteristics and the surface behaviour of carbons. The surface oxides associated with carbon black have been proposed to exist as one of three types; acidic, basic or neutral. The acidic surface oxides, which are known to render the surface polar in character, are suggested to exist as acidic functional groups such as carboxylic or phenolic. Their formation is selective upon treating of the carbon with oxygen up to temperatures of 400°C or by the reaction at room temperature with an oxidising solution. Upon accelerated temperatures $\geq 1000^\circ\text{C}$, the surface is freed from all surface oxides, but on cooling back to room temperature, the presence of oxygen gas promotes the production of basic surface oxides that have a heterocyclic oxygen-containing ring structure. Lastly, the neutral surface oxides are formed by the irreversible adsorption of oxygen at the unsaturated sites present on the carbon black surface.

Carbon-Hydrogen surface groups

It has been observed that hydrogen, the second hetero atom associated with carbon black, is adsorbed as atoms at carbon sites situated at the edges and

corners of the graphitic crystallites⁸. The hydrogen in carbon black is present as chemisorbed water and as part of the hydroxyl, phenol and hydroquinone groups. In addition hydrogen is also bound to surface carbon atoms as C-H bonds that are more stable than the carbon-oxygen compounds that are also present in carbon black.

Carbon-Nitrogen and Carbon-Sulphur surface complexes

A typical carbon black does not contain a significant amount of nitrogen or sulphur (< 1%) however, the amounts present are highly dependent on the processing conditions during the manufacturing of the carbon black. The carbon nitrogen surface complex is stable to thermal treatments hence temperatures in the range of 900°C-1200°C are essential for desorption to occur. Sulphur, however, is present in many different forms such as elemental sulphur, inorganic sulphate and as organo-sulphur compounds. The carbon-sulphur surface compounds are extremely stable and are not readily decomposed, however, on specific heating (500°C-700°C) with hydrogen, complete desorption as H₂S is apparent.

Carbon-Halogen (Chlorine) surface compounds

The adsorption of halogens onto carbon black results in the formation of stable carbon-halogen surface compounds, however the amount adsorbed is highly dependent upon the nature of the carbon surface, the reaction conditions and the nature of the halogenating species. Further, the oxygen and hydrogen contents of the carbon also affect the adsorption of a halogen because it is through mechanisms involving the exchange with chemisorbed hydrogen, addition at unsaturated sites and surface oxidation, that the halogen is adsorbed onto the surface.

3.1.6: The use of fractal geometry

So far, the carbon black aggregate shape and size has only been described by models based on geometrical objects (e.g. spheres and ellipsoids) which are amenable to the laws of Euclidean geometry. However, due to the complexity

encountered in trying to fully describe the highly irregular nature of carbon black aggregates, which are typically non-Euclidean, fractal geometry has emerged as a particularly useful tool that is widely used. Small angle neutron scattering on fractally rough surfaces has the potential to scale the surface geometry by the wavelength of the incident radiating source and hence a direct analysis of the carbon black surface can be made. The surface fractal dimension, D_s , of the two different grades of carbon black, Raven L and Raven M used here, have been determined by SANS (see chapter 6). It was found that D_s ranged from 2.42 to 2.53 which is in total agreement with Gerspacher and O'Farrell's nearly constant value for D_s of ~ 2.4 obtained for fifteen different grades of carbon black.

Another scattering method utilizes Transmission Electron Microscopy (TEM) to assess the fractal dimension of the carbon black aggregate. TEM carbon black aggregate micrographs are contrasted using a binary technique (black and white).

3.1.7: The influence of carbon black properties on applications performance.

The fundamental properties of carbon black (particle size, structure, porosity and surface chemistry) can be, specifically, related to many important application properties. For inks and coatings, the single most important property in terms of carbon black usage is colour (blackness). However, rheological properties are also highly important, both in the mixing and actual coating process.

- A small particle size increases blackness and tint, increases viscosity and lowers dispersibility.
- A higher structure black reduces blackness and tint, increases viscosity and improves dispersibility.
- Higher porosity increases viscosity.
- Higher surface activity improves wetting, microdispersion and stability and reduces the viscosity of liquid systems.

It is, therefore, of the utmost importance that the correct grade of carbon black is chosen which is suitable for all of the aspects associated with the final application process.

3.1.8: Carbon black grades that were studied

The two principal grades of carbon black that were investigated are Raven[®] L and Raven[®] M which are ink grade carbon blacks supplied by the Columbian Chemicals Company, Avonmouth, UK. Ink grade carbon blacks are generally medium to coarse in particle size and are used for their masstones (the masstone is a measure of how evenly covered an area that has been coated in carbon black is. It is used to determine colour matches between samples) rather than tint (the tint is a gradation of colour made by adding white to it to lessen its saturation) properties. Raven[®] L and Raven[®] M are untreated, medium colour blacks that are used for news inks. Raven L has a medium-low structure and is used for inks in which a typical carbon content of 16-20% is required. In contrast Raven M shows medium-high structure and is generally the chosen black for inks where the carbon content required is lower (10-13%). The structure of carbon blacks is measured by their ability to adsorb dibutyl phthalate (DBP), where the higher the value, the higher the structure. For Raven M, the dibutyl phthalate adsorption is $108 \pm 5 \text{ cm}^3/100\text{g}^9$ and for Raven L the value is $75 \pm 5 \text{ cm}^3/100\text{g}^9$.

The principal characteristics of the two particles are presented in Table 3.1 and the corresponding transmission electron micrographs can be seen as figures 3.4(a) and 3.4(b).

	"Spherical" Raven® L	"Fractal" Raven® M
Structure	medium-low	medium-high
Carbon content (%) of a typical ink	16 – 20	10 – 13
Mean particle diameter (nm)	30.0	31.4
Particle surface area (m ² /g)	91.4	85.9
Dry state aggregate diameter (nm)	86.8	104.5

Table 3.1: *Characterisation of carbon black particles*

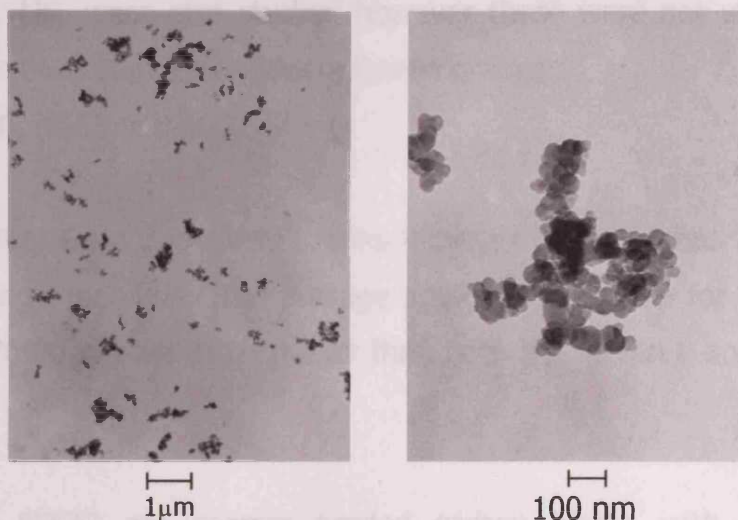


Fig 3.4(a): *Transmission electron micrographs of the "Spherical" Raven L particles at two different magnifications. On the left is a picture of the dry material in bulk whereas the micrograph on the right represents a typical aggregate within the bulk.*

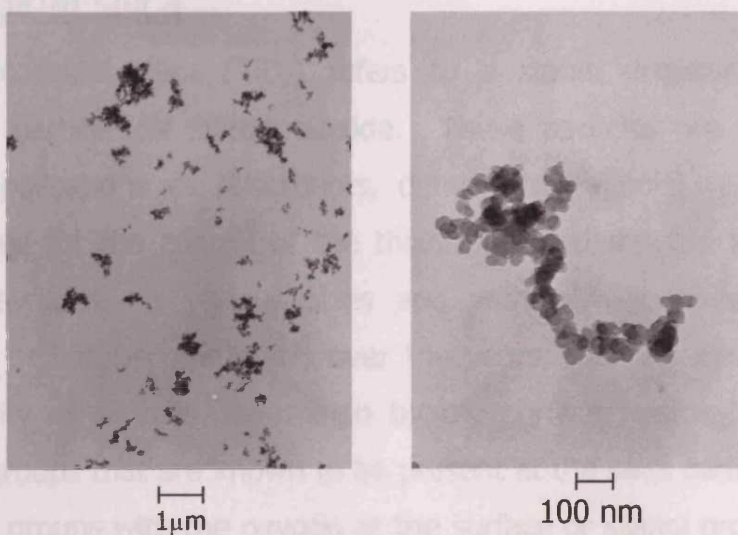


Fig 3.4(b): *Transmission electron micrographs of the "Fractal" Raven M particles at two different magnifications. On the left is a picture of the dry material in bulk whereas the micrograph on the right represents a typical aggregate within the bulk.*

Further carbon black grades, all supplied by Columbian Chemicals Company, Avonmouth, UK, were also studied however these were not studied in such depth as the two, above mentioned, Raven grades;

R760, R1060, N660 and N772

R760 and **R1060** are identical grades however the R760 has had its surface oxidised using ozonolysis. The average aggregate diameter for both R760 and R1060 is ~70-80 nm which is smaller than both the Raven L and M aggregate diameters.

N660 and **N772** are coarser graded carbon blacks with large average aggregate diameters compared to the Raven L and Raven M grades. N660 has an average aggregate diameter of ~215-225 nm and is classed as a medium-low structured black whereas N772 has a slightly smaller average aggregate diameter of ~195-205 nm but is more highly structured.

3.2: Colloidal silica

The term colloidal silica (SiO_2) refers to a stable dispersion of discrete amorphous particles of silicon dioxide. These particles are used in many industrial applications as adsorbents, dehydrating agents, reinforcing fillers and additives for the control of the thixotropic and rheological properties¹⁰. They are available in various sizes and with a wide variety of surface treatment. It has become clear, over the years, that the surface chemistry and reactivity of silica is determined by the surface hydroxyl groups. The functional groups that are known to be present at the silica surface, can either be siloxane groups with the oxygen at the surface or silanol groups, shown in fig 3.5; a) free (isolated) OH, b) vicinal (bridged) OH, c) geminal OH, d) siloxane bridge and e) triple hydroxyl group.

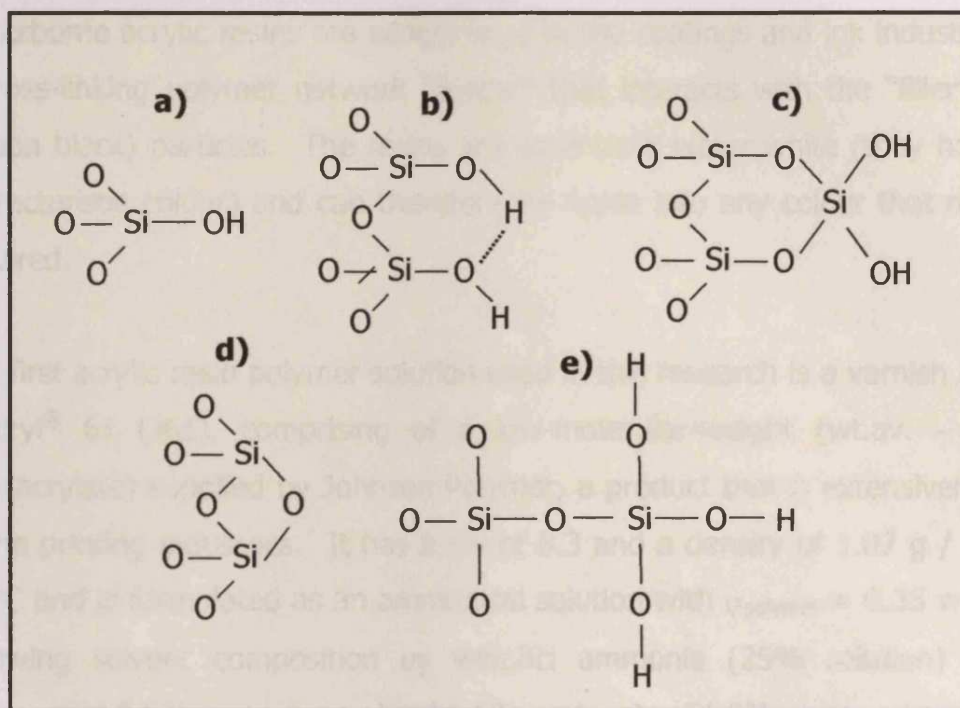


Fig 3.5: The various types of hydroxyl groups on the silica surface¹¹.

The silica particles under investigation here were obtained from Eka Chemicals AB, AKZO NOBEL as a 40wt% colloidal suspension in weakly alkaline aqueous solution, stabilised with a small amount of sodium hydroxide. They are more commonly known as Bindzil 40/170. This Bindzil grade silica has a pH of 9.5, a density of 1.295 g/cm^3 at 20°C and a specific surface area of $170 \text{ m}^2/\text{g}$. As for the particle size, Bindzil 40/170 has a wide particle size distribution with particle diameters ranging from 5 to 100 nm.

3.3: Adsorbents

3.3.1: Acrylic resins

Waterborne acrylic resins are widely used in the coatings and ink industries as a cross-linking polymer network “binder” that interacts with the “filler” (e.g. carbon black) particles. The resins are essentially water white (they have no characteristic colour) and can therefore be made into any colour that may be required.

The first acrylic resin polymer solution used in this research is a varnish named Joncryl[®] 61 (J61), comprising of a low-molecular-weight (wt.av. ~ 8500) poly(acrylate) supplied by Johnson Polymer, a product that is extensively used in the printing industries. It has a pH of 8.3 and a density of 1.07 g / cm³ at 25 °C and is formulated as an ammoniacal solution with $\phi_{\text{polymer}} = 0.35$ with the following solvent composition by weight: ammonia (25% solution) 9.5%, isopropanol 3.0%, propylene glycol 1.5% and water 51.0%.

The viscometry data for two separate batches of J61 is represented in figure 3.6. All measurements were taken at 25° C using an Ostwald U-tube grade D viscometer that had been calibrated using distilled water (for more information see chapter 4).

Relative viscosity

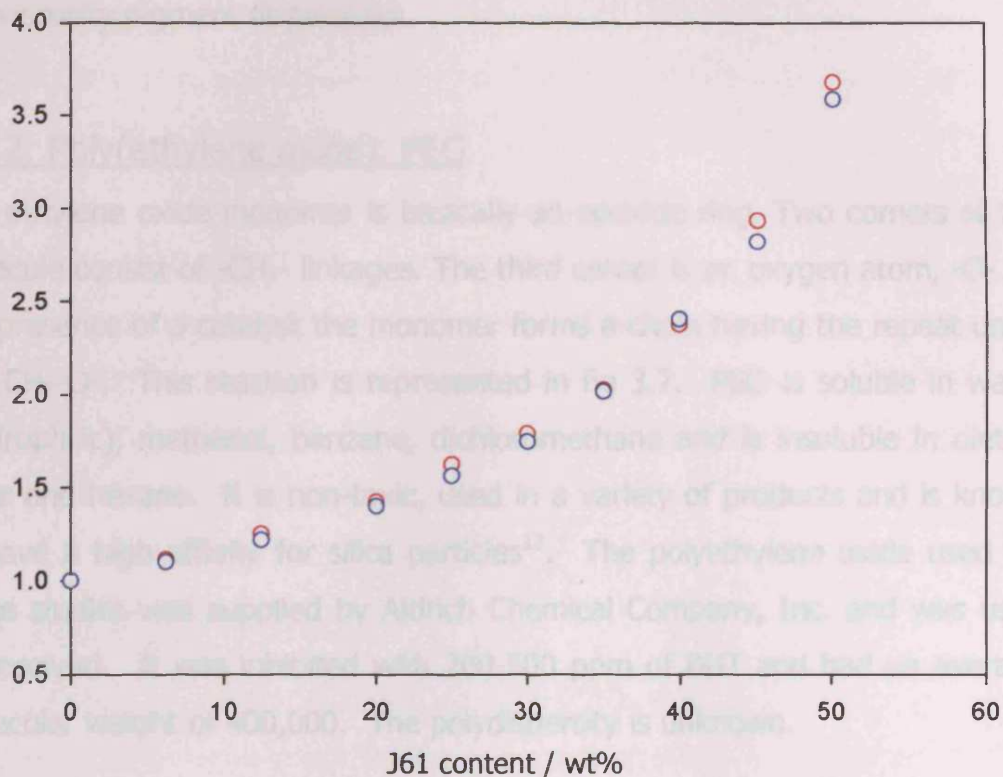


Fig 3.6: The U-tube viscometry data for the acrylic resin polymer solution used in this research, named Joncryl[®] 61. As shown (○) and (○) represent different batches of the same solution obtained from Johnson Polymer. All solutions were diluted with distilled water.

It is clear to see that the sample variation between batches is minimal. By comparing the relatively small change in viscosity of a 50wt% J61 solution in water and a 6.25wt% J61 solution in water, these data are evidence that the polymer resin flakes that are dispersed within the acrylic resin (where $\phi_{\text{polymer}} = 0.35$) have a low molecular weight. The R_h value obtained from diffusion measurements for J61 = 2.5nm. This is approximately the same as an SDS micelle.

The second, Joncryl[®] HPD 96 E, from the same suppliers, is a high molecular weight (wt.av. ~ 16,500) styrene acrylic ammonia neutralised resin solution with a pH of 8.5 and a relative density of 1.07 g / cm³ at 25 °C. It is typically used for pigment dispersions which promotes high colour strength and stable, low viscosity pigment dispersions.

3.3.2: Poly(ethylene oxide), PEO

The ethylene oxide monomer is basically an epoxide ring. Two corners of the molecule consist of -CH₂- linkages. The third corner is an oxygen atom, -O-. In the presence of a catalyst the monomer forms a chain having the repeat unit -CH₂-CH₂-O-. This reaction is represented in fig 3.7. PEO is soluble in water (hydrophilic), methanol, benzene, dichloromethane and is insoluble in diethyl ether and hexane. It is non-toxic, used in a variety of products and is known to have a high affinity for silica particles¹². The polyethylene oxide used for these studies was supplied by Aldrich Chemical Company, Inc. and was used as received. It was inhibited with 200-500 ppm of BHT and had an average molecular weight of 400,000. The polydispersity is unknown.

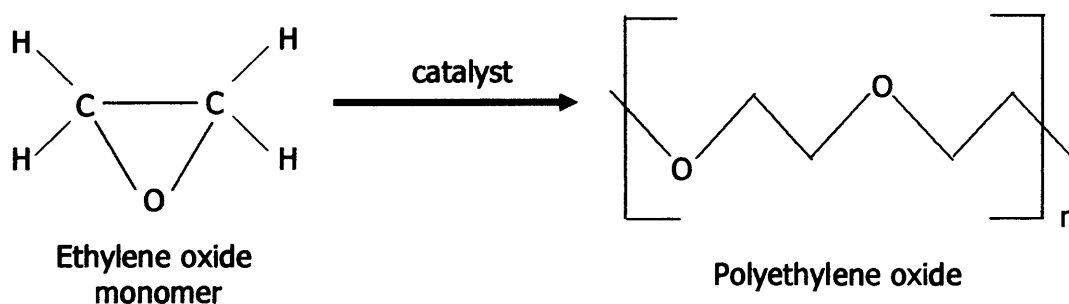


Fig 3.7: The production of polyethylene oxide from the ethylene oxide monomer.

3.3.3: PEG / PPG / PEG block copolymer

Poly(ethylene glycol) / poly(propylene glycol) / poly(ethylene glycol) (PEG / PPG / PEG) block copolymers are commercially available non-ionic macromolecular surface active agents¹³.

The pluronic block copolymer used for these studies was supplied by Aldrich Chemical Company, Inc., it had an average molecular weight of 8400 and a composition ratio of 80% PEG to 20% PPG.

3.3.4: Bitumen

The bitumen used was supplied by the Lion Oil Company, El Dorado and is a very long chain petroleum hydrocarbon that has the trade name, Lion Flux.

3.3.5: The oil medium

The oil is a blended petroleum hydrocarbon lubricant base stock consisting of ~ 65% - 80% heavy naphthenic hydrotreated distillate and ~ 20% - 35% naphthenic bright stock. Its full name is N-1200-HT Inkol, but is more commonly referred to as Magie oil.

3.4: Sample preparation

3.4.1: Aqueous dispersions of carbon black and J61

Initially, samples were prepared using a paint shaker. A concentrated stock carbon black dispersion was prepared by shaking the desired amount of carbon black with steel ball bearings for 30mins. This stock was then diluted to the desired carbon black loading, ~ 15 wt% (In practice, the realistic loading of carbon black powders is about 15%^{14,15,16}) and then further shaken for 15mins to ensure even dispersion. It was found subsequently that a normal high-shear unipellar mixer was sufficient (and easier) to disperse the desired amount of carbon black directly into the polymeric vehicle. Using the high shear mixer, samples were stirred for 24hours, left to equilibrate overnight, and then analyzed. For example, a typical sample would comprise 15 wt% particles and 60 wt% polymer resin (of which 21 wt% is polymer and 39 wt% is solvent), the remainder (25 wt%) being water- this is denoted as $\phi_{\text{particles}} = 0.15$, $\phi_{\text{polymer}} = 0.21$.

During this equilibration period, the isopropanol (IPA) in the J61 evaporates. No attempt was made to counter this and NMR was used to check that there is no substantial difference between the various samples. Such NMR studies have not been applied to the carbon black systems, but it is assumed that they would be no different from the simple polymer solutions. Indeed, duplicate rheological measurements performed upwards of a week later show that there are no discernible differences in the observed behaviour (see chapter 6, figures 6.1(a) and 6.1(b)). This criterion is how the distinction of "stable" and "unstable" was made and hence, how the adsorbed amount of 50 mg of polymer per $13 \text{ m}^2 (\pm 1)$ of particle surface area was arrived at.

3.4.2: Oil dispersions of carbon black

For each sample a dry bead vehicle containing 24.5 wt% bitumen (which acts as a polymeric binder) in oil (Magie oil) was prepared using an industrial grade mixer for 30mins. Once mixed, this was left to stand for 24 hours (to reach equilibrium) before preparing a mill base. The mill base was prepared by taking 105 g of the dry bead vehicle and adding to that 45 g of carbon black particles. After cooling, 75g of the mill base was mixed with a further 50g of oil. This mixture was triple roll milled three times to ensure a sufficient dispersion. The grind gauge values were checked for all of the stock solutions. For the four particles involved in the oil studies; Raven L, Raven M, N660 and N772, this meant that 18wt% stock samples in oil were prepared. The stocks were then diluted with oil to various carbon black loadings.

3.4.3: Carbon black in oil for colour measurements

Two samples, 18wt% Raven L in oil and 18wt% N660 in oil were prepared by adding the required amount of particles to a solution of bitumen in oil in the same way as stated in the above section (3.4.2).

3.5: Equipment

3.5.1: Rheology

The controlled stress rheology measurements were performed on a Bohlin CS10 rheometer employing either a cone and plate geometry (with a diameter of 40 mm and a cone angle of 4°) or a roughened double gap geometry (the diameters of the inner and outer cylinders being 24 and 27 mm, respectively). The double gap geometry allows the user to facilitate accurate measurements of low-viscosity samples. The shear rate sweep and oscillatory shear stress sweep measurements were conducted on a StressTech (ReoLogica Instruments AB) with a cone and plate geometry (the cone has a diameter of 40 mm and an angle of 4°).

3.5.2: Small-angle neutron scattering studies

The SANS measurements were performed on the D22 diffractometer at the ILL, Grenoble. Neutron wavelengths of 8 Å were taken with three instrument configurations to span a Q-range of approximately 0.002 to 0.4 Å⁻¹. The samples were contained in 2 mm pathlength UV-spectrophotometer-grade quartz cuvettes (Hellma) mounted in aluminium holders on top of an enclosed computer controlled sample changer. Sample volumes were approximately 0.4 cm³. All scattering data were (a) normalized for the sample transmission, (b) background-corrected using an empty quartz cell (this also removes the inherent instrumental background arising from vacuum windows, etc.), and (c) corrected for the linearity and efficiency of the detector response. The data were put onto an absolute scale by reference to a flat scatterer such as water.

3.5.3: High-resolution ultrasonic measurements

The velocity (ν) and attenuation coefficient (α) of longitudinal ultrasonic waves in carbon black dispersions were measured with a HR-US 102 high-resolution ultrasonic spectrometer (Ultrasonic Scientific, Dublin). The limiting resolution of the spectrometer is 10⁻⁵ % for ultrasonic velocity and better than 0.2 % for ultrasonic attenuation. Two identical cells of volume 1 cm³ were used; the measuring cell was filled with a sample of carbon black dispersion, while the

reference cell was filled with water. Ultrasonic velocity and attenuation in the sample and reference solution were measured at frequencies between 2 and 15 MHz at 25 °C. The particle sizes of the carbon black particles in the dispersion were analyzed using the HR-US 102 particle size software module, based on the scattering theory described by Allegra and Hawley¹⁷ and Waterman and Truell¹⁸. The following parameters were used in the calculations: aqueous phase (volume fraction of 0.925, density = 1049 kg/m³, ultrasonic velocity = 1574 m/s, intrinsic attenuation coefficient normalized per square of frequency $\alpha / f^2 = 4 \times 10^{-13} \text{ s}^2/\text{m}$), solid particles (volume fraction = 0.08, density = 2600 kg/m³, ultrasonic velocity = 4600 m/s).

3.5.4: Colour measurements

Prior to the colour measurements, prints of the various different dispersions were obtained. The prints were taken by loading the printing roller with 0.8ml of the dispersion using an inker pen. The loaded roller was weighed, a print was taken and the roller was then re-weighed, this process was then repeated approximately 20 times. Following this, the print/optical density for each print was recorded using a Gretag-Macbeth handheld densiometer.

The colour measurements were performed using a benchtop Hunter Labscan[®] XE automated spectrophotometer. This spectrophotometer measures reflected colour the way the eye sees it, including the effect of gloss. During these investigations, the colour instrument measured with a sensor angle of 0°/45°. The angle of the light is 0° (i.e. perpendicular to the surface) and the angle of the detector is 45°. This angle measures apparent colour changes due to both the sample colour and surface shine or texture. A D65 illuminant¹ was

¹ An illuminant is the specification for a potential light source. They are normally specified in terms of the relative energy tabulated for each wavelength or wavelength band. There are several illuminants that are widely used by the colour industry, D65 in this instance. The D class of illuminants specify relative energy distributions that closely correspond to the radiation emitted by a so-called black-body. As the temperature (in Kelvin) of a black body is increased there is a shift in the emitted radiation to shorter wavelengths. For example, the illuminant D65 has a spectral energy distribution that closely matches that of a blackbody at 6500K. The illuminant D65 also resembles the relative spectral energy distribution of the natural north-sky daylight.

employed and a xenon lamp was used to provide a broad spectral source and also for greater stability.

The machine was normalized at wide aperture by taking a black tile reading to establish a zero reflectance, taking a white tile reading to establish 100% reflectance and finally, to verify the accuracy, a green tile is used on a daily basis to check the tolerance (allowed tolerance is ± 0.10) in XY and Z (see chapter 5 for more information). For small aperture readings (i.e. prints), the procedure was repeated, however, the green tile was replaced by the white tile for verification. The white tile has an allowed tolerance of ± 0.05 in XY or Z.

Following this normalizing procedure, the print was placed over the aperture and supported with a backing tile. Three readings were taken at different points along the print and the average was recorded using Hunter Lab units (L = jetness, a= red/green and b= blue/yellow).

References:

- 1 Donnet, J., Bansal, R. and Wang, M., *Carbon Black 2nd edition*, (1993) 1-66
- 2 Donnet, J., Bansal, R. and Wang, M., *Carbon Black 2nd edition*, (1993) 89-163
- 3 Rouquerol, F., Rouquerol, J., Sing, K., *Adsorption by powders and porous solids-principles, methodology and applications*, Academic press, (1999), chapter 9.
- 4 Herd, C.R., McDonald, Hess, W.M., *Rubber Chem. Technol.*, 65, 1, (1991)
- 5 Columbian Chemicals Company information booklet, *CARBON BLACK-manufacturing processes and important properties*, march (1994)
- 6 Walker, P.L., Janov, J., *J. Colloid Interface Sci.* 28, (1968), 499
- 7 Bradley, R.H., Sutherland, I., Sheng, E., *J. Chem. Soc., Faraday Trans.*, 91, (1995), 3201
- 8 Baugham, D.H., Stafford, J., *J. Chem. Soc.*, 127, 1985, (1925)
- 9 Columbian Chemicals Company, Atlanta, Georgia USA, information leaflet on Raven[®] L and Raven[®] M
- 10 Yziquel, F., Carreau, P.J., Tanguy, P.A., *Rheol Acta*, 38, 14-25, (1999)
- 11 Alkan, M., Dogan, M., *Encyclopedia of Surface and Colloid Science*, Marcel Dekker, Inc., (2002), 5014-5027
- 12 Wind, B., Killmann, E., *Colloid Polym. Sci.*, (1998), 276, 903
- 13 Alexandridis, P., Hatton, T.A., *Colloids and Surfaces A: Physicochemical and Engineering Aspects*, 96, (1995), 1-46
- 14 Chan, C.M., Cheng, C.L., *Polym Eng Sci*, (1997), 37, 1127
- 15 Lee, G.J., Suh, K.D., Im, S.S., *Polym Eng Sci*, (2000), 40, 247
- 16 Accorsi, J., Romero, E., *Plastics Eng*, (1995), April, 29
- 17 Allegra, J.R., Hawley, S.A., *J. Acoust. Soc. Am.*, 51, (1972), 545
- 18 Waterman, P.C., Truell, R., *J. Math. Phys.*, 2, (1961), 512

CHAPTER 4: RHEOLOGY

4.1: Introduction to rheology

4.1.1: Definition

The term "rheology" was invented by Professor Bingham of Lafayette College, Indiana, on the advice of a colleague, the Professor of Classics. It means:

The study of the deformation and flow of matter¹.

The type of deformation that occurs is, however, dependent on the state of matter. For example, gases and liquids will flow when a force is applied, whilst solids will deform by a fixed amount².

4.1.2: Uses of rheology

The study of the rheology of a particular sample allows the experimentalist to gain a greater insight into the forces that operate in the sample. It is a useful technique that is employed to study the control and flow of complex fluids such as polymers, pastes, suspensions and foods, but is not suitable for describing simple fluids e.g. water and air, here, the well-defined field of fluid mechanics is utilised³.

4.1.3: Solids and Liquids

There is a marked difference in the response of a solid and a liquid when subjected to an applied force. When considering their rheology, it is convenient to think of a behaviour scale, where they are at opposite extremes (see fig 4.5).

The solid response is explained by Robert Hooke's "*True Theory of Elasticity*" 1678, whereas, the behaviour of liquids was proposed in Isaac Newtons "*Principia*", published in 1687.

4.1.4: Shear stress, shear rate and viscosity

The two most important factors relevant to rheological studies are:

- 1) **The Shear Stress**, σ , which is the resistance of a body to an applied force and defines a force per unit area with units Nm^{-2} or Pa.

2) **The Rate of Shear**, $\dot{\gamma}$, which is the rate at which a material is sheared, taking into account the distance between the shearing planes with dimensions of reciprocal time (s^{-1})

It is, therefore, not surprising that one of the principle studies of rheology is to determine the relationship between the rate of shear and the shearing stress.

Consider the application of a shear stress, σ , to a body (figure 4.1). This results in the generation of a deformation (strain, γ). If, on removal of this stress, the strain does not return to zero then *flow* has occurred and the material is characterised as a liquid.

If two plates (area, A), separated by a height, H , of liquid are moved (at a velocity, V by a force, F) relative to one another, Newton's law states that the shear stress (F/A) is proportional to the shear rate (V/H).

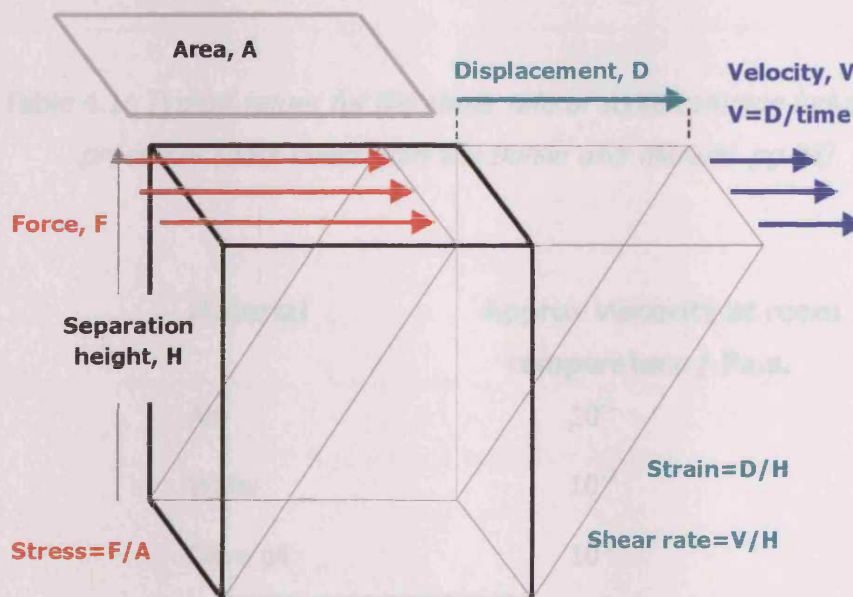


Figure 4.1: *Shear stress applied to a volume of material*

The proportionality constant is known as the (dynamic) **viscosity**, it has the symbol η , units of Pa.s. and is defined as the tendency of the fluid to resist flow.

Hence, the fundamental equation relating the important rheological parameters is:

$$\sigma = \eta \dot{\gamma} \quad (4.1)$$

Some typical data on shear rates and viscosities are shown in table 4.1 and 4.2 respectively.

Process	Shear rates / s⁻¹
Sedimentation	10 ⁻¹ – 10 ⁻³
Pumping	10 ⁰ - 10 ³
Stirring	10 ¹ – 10 ³
Spraying	10 ⁴ – 10 ⁵
Rubbing	10 ⁴ - 10 ⁵

Table 4.1: *Typical values for the shear rate of some common industrial processes.(data taken from the Bohlin user manual, pg.28)*

Material	Approx viscosity at room temperature / Pa.s.
Air	10 ⁻⁵
Water	10 ⁻³
Olive oil	10 ⁻¹
Glycerol	10 ⁺⁰
Molten polymers	10 ⁺³
Bitumen	10 ⁺⁸

Table 4.2: *Typical viscosities of some common materials⁴*

4.2: Solids and liquids

4.2.1: Classification of materials

Solids respond to shear in a completely different manner to liquids. Figures 4.2 and 4.3 summarise the differences that are observed.

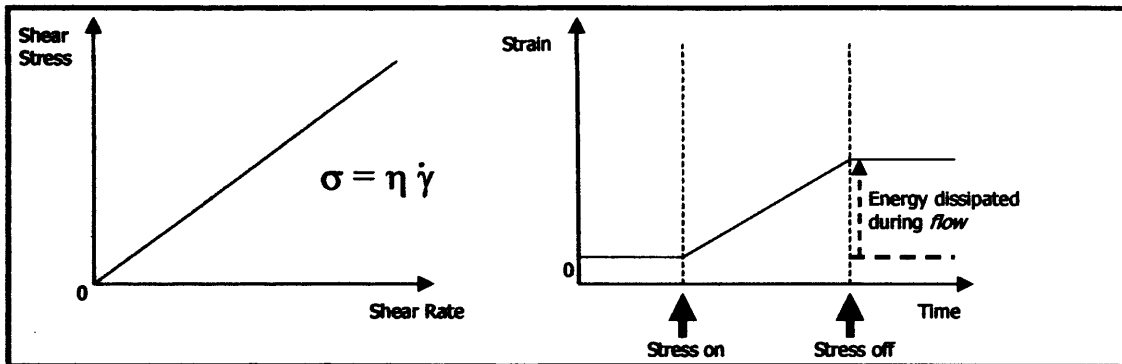


Fig 4.2: *Perfect liquid behaviour*

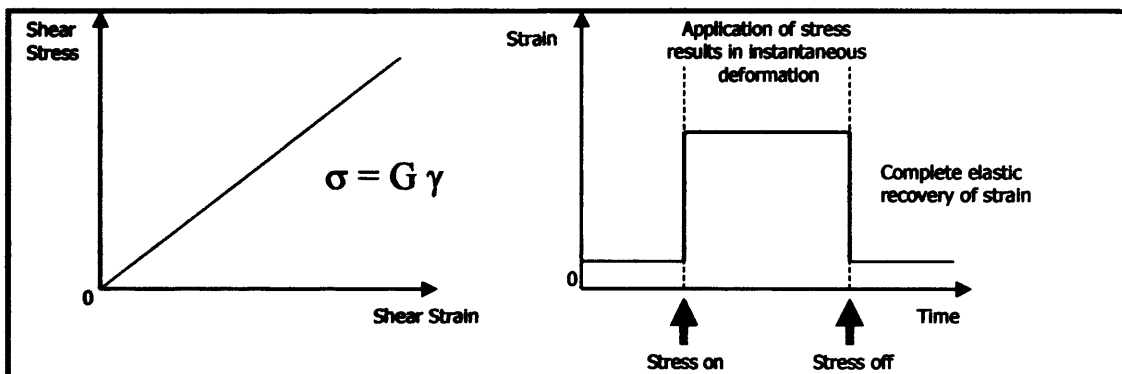


Fig 4.3: *Perfect solid behaviour*

For a perfect (Newtonian) liquid, there is a linear relationship between the applied stress and the resultant shear rate.

For a perfect (Hookean) solid, there is a linear relationship between the applied stress and the resultant deformation or strain.

When considering the strain / time plots, the observed response of the perfect liquid indicates that on application of a stress, a continuous deformation is generated until the stress is removed. On removal of this stress, the strain does not return to the original position hence, energy has been dissipated as

heat to the surroundings and it is said that *flow* has occurred. In contrast, a perfect solid instantly deforms upon application of a stress, but there is a complete recovery of strain upon removal of this stress hence, flow has not occurred. In this case, all of the energy put into the system is stored elastically by the microstructure and not dissipated as heat.

A mechanical representation that is often employed to simplify the idea is shown in figure 4.4. A model of a perfect Newtonian (viscous) liquid is shown as a dashpot and a spring is used to represent the mechanics of a perfect Hookean (elastic) solid.

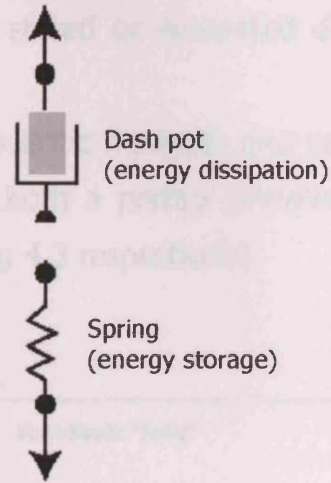


Figure 4.4: Schematic to represent the classical behaviour of solids and liquids

The two classical extreme behaviours described so far are generally not observed for “real” systems. Depending on the time scale, most systems have a behaviour that is intermediate of the two. These systems are known as *viscoelastic materials*, fig 4.5.

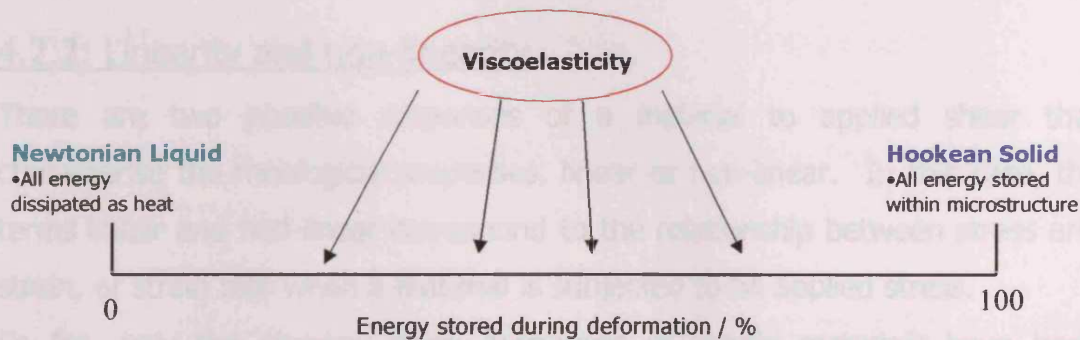


Fig 4.5: The classical behaviour of materials under shear

Viscoelastic materials have the capacity to store some of the energy that is put into the system (solid behaviour) within their microstructure, but at the same time, dissipate the remainder as heat, whilst flowing like a liquid. Systems that exhibit viscoelastic behaviour can neither be classified as solid-like or liquid-like, but they are termed viscoelastic "fluid" or viscoelastic "solid" depending on the percentage of energy that is stored or dissipated during deformation.

Figure 4.6 depicts the strain / time plots for viscoelastic materials and can be directly compared to the strain / time plots for both a perfect (Newtonian) liquid and a perfect (Hookean) solid (fig 4.2 and fig 4.3 respectively).

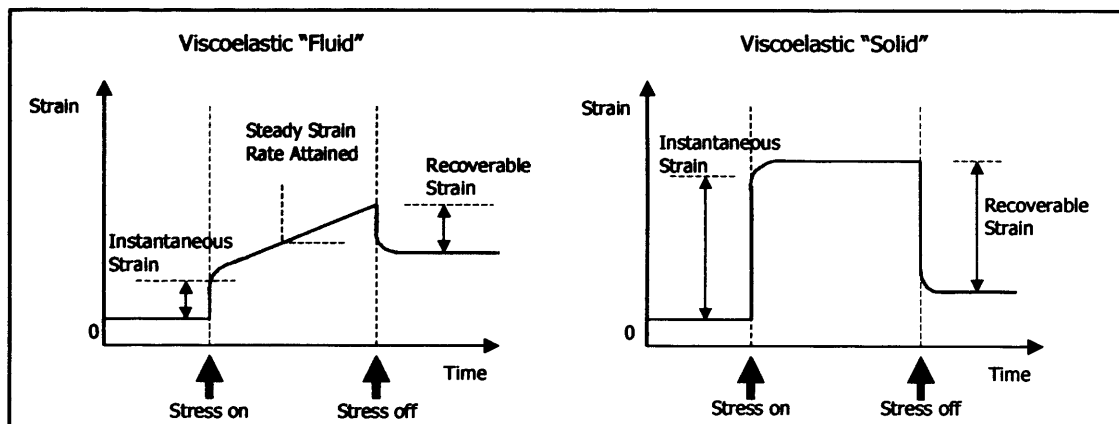


Fig 4.6: *The two types of viscoelastic behaviour*

4.2.2: Linearity and non-linearity

There are two possible responses of a material to applied shear that characterise the rheological properties, linear or non-linear. In this case, the terms linear and non-linear correspond to the relationship between stress and strain, or strain rate when a material is subjected to an applied stress.

So far, only the classical linear responses of simple materials have been discussed, however, in more complex systems the range of stress over which materials behave linearly is invariably limited and if exceeded, deviations from

linear behaviour can occur. Along with Newtonian flow, the four main types of non-Newtonian flow are shown in figure 4.7.

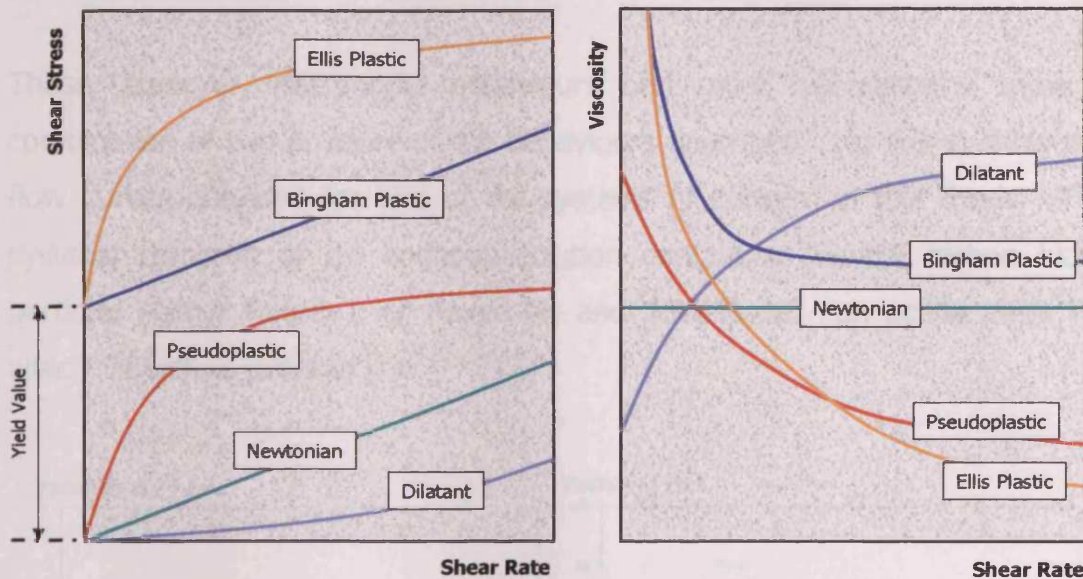


Fig 4.7: Flow curves of types of flow behaviour (redrawn from "Noveon"- Bulletin 12: Flow and Suspension Properties)

1. Dilatant behaviour (shear thickening) – when the shear rate increases, the viscosity increases. This occurs in dispersions that contain a high concentration of closely-packed solids.
2. Newtonian behaviour – this is characterised by the direct proportionality between shear stress and shear rate. The viscosity is, therefore, totally independent of external shear and remains constant regardless.
3. Pseudoplasticity (shear thinning) – when the shear rate increases, the viscosity decreases.
4. Bingham plastic – a certain amount of shear stress must be applied to initiate flow. Once the flow begins, it is not affected by any further changes in shear.

5. Ellis plastic (viscoplastic) – a yield stress point must be reached (c.f. Bingham plastic) before flow begins. The fluid then exhibits shear thinning behaviour – decreasing viscosity with increasing shear.

These, however, are model behaviours and most real systems show a combination of two or more of the behaviours described. Fig 4.8(a) show the flow curves obtained for two of the systems of concern in this thesis. The systems comprise of an aqueous solution containing 15wt% carbon black particles (either Raven L or Raven M) and 15wt% J61- an acrylic resin (of which, 35wt% is polymer).

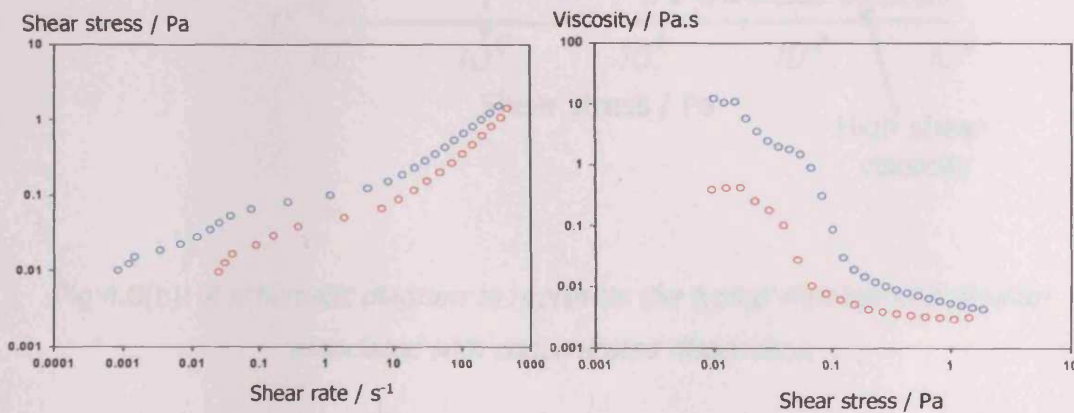


Fig 4.8(a): Flow curves to represent the rheological behaviour of two aqueous carbon black/acrylic resin dispersions where $\varphi_{particle} = 0.15$ and $\varphi_{polymer} = 0.053$ for (○) Raven L and (○) Raven M.

Figure 4.8(a) is an example of the typical rheological behaviour associated with a concentrated dispersion. At low shear stresses, a high viscosity Newtonian plateau is common. The viscosity remains constant until a critical stress value is reached, at which the viscosity dramatically reduces to a high shear stress Newtonian plateau. The critical stress point at which the viscosity suddenly decreases is termed the “yield stress” and the region of rapid decrease is termed “shear thinning”.

Shear thinning is very common in concentrated systems and a schematic graph to represent the behaviour is shown in figure 4.8(b):

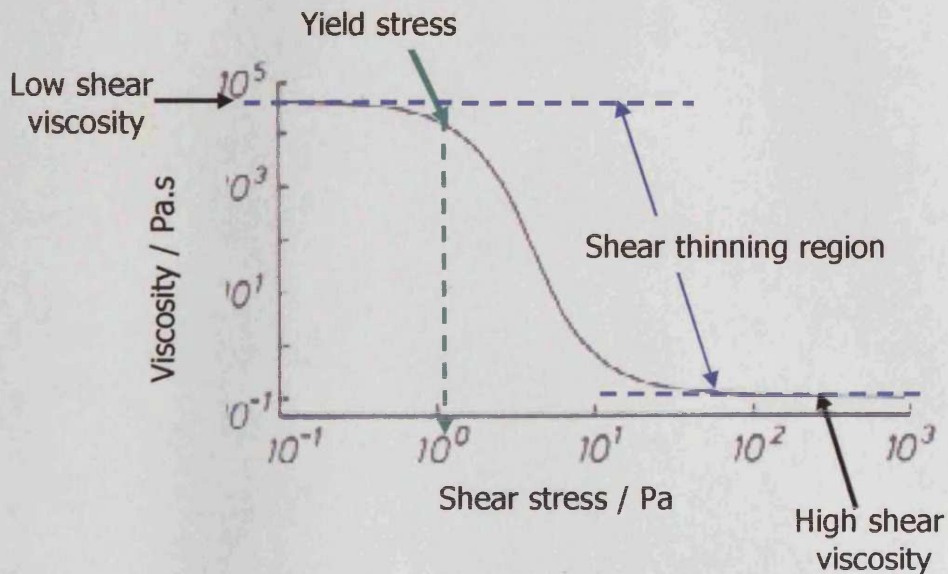


Fig 4.8(b): A schematic diagram to represent the typical rheological behaviour associated with concentrated dispersions.

When a concentrated system flows at very low shear rates, the particles have to move around each other or “bounce off” each other for overall flow to occur. This involves large resistance and the resulting viscosity is high. At slightly higher shear rates, the imposed velocity gradient induces an orientation of the particle structure that allows free movement past one another, hence the viscosity is lowered.

4.2.3: Yield stress

The yield stress of a material is the stress point at which a material will start to deform. Below this yield value point, flow does not occur. However, this definition of a yield stress is questionable because it is believed by many, including one of the founders of rheology, Professor Marcus Reiner, “everything flows if you wait long enough”.

However, in practice, the use of the term is common, but due care must be taken as the theoretical value is highly dependent upon, not only the stress but also the measured strain and elapsed time.

4.2.4: Deborah number

As already mentioned, the idea of yield stress is highly dependent on the scaling of time. In rheology, understanding the timescale of flow is achieved by means of the *Deborah number*, D_e . This dimensionless quantity is so-called after it was noticed by Professor Reiner, in the Old Testament, that Deborah claimed "The mountains flowed before the Lord..."

So, on the basis that everything will flow if you wait long enough, the Deborah number is defined as:

$$D_e = \tau / T \quad (4.2)$$

where T is a characteristic time of the deformation process being observed and τ is a time characteristic of the material. For a perfectly Newtonian viscous liquid, τ has a value of zero, whereas for a perfectly elastic Hookean solid, τ is infinite. In practice, if a material has a high Deborah number, it is said to be solid-like, however, it can appear solid-like for one of two reasons; either the material has a very long characteristic time or because the deformation process employed is very fast.

4.2.5: The Péclet number

The Péclet number, P_e is a dimensionless quantity that is used to compare the effect of applied shear with the effect of thermal (Brownian) motion.

It is defined as:

$$P_e = r^2 \dot{\gamma} / D_T \quad (4.3)$$

where r is the particle radius, $\dot{\gamma}$ is the shear rate and D_T is the translational

diffusion coefficient. For $P_e \ll 1$, particle behaviour is dominated by diffusional relaxation (Brownian motion), whereas for $P_e \gg 1$, hydrodynamic effects dominate.

The D_T of a molecule is the ratio of the energy that the molecule has, which is dependent on temperature, and the frictional force that opposes the motion, commonly expressed via the Stokes-Einstein equation:

$$D_T = kT / f \quad (4.4)$$

where kT is the usual unit of thermal energy and f is the frictional force. By replacing f with Stokes's law, we obtain:

$$D = kT / 6 \pi \eta a \quad (4.5)$$

where η is the viscosity and a is the spherical particle radius.

4.3: Measurements

4.3.1: Measurement of viscoelasticity

There are two types of experiment (represented in fig 4.9) that can be conducted in order to characterise the rheological properties of a viscoelastic material.

1. Steady shear experiments
2. Small amplitude oscillatory shear experiments.

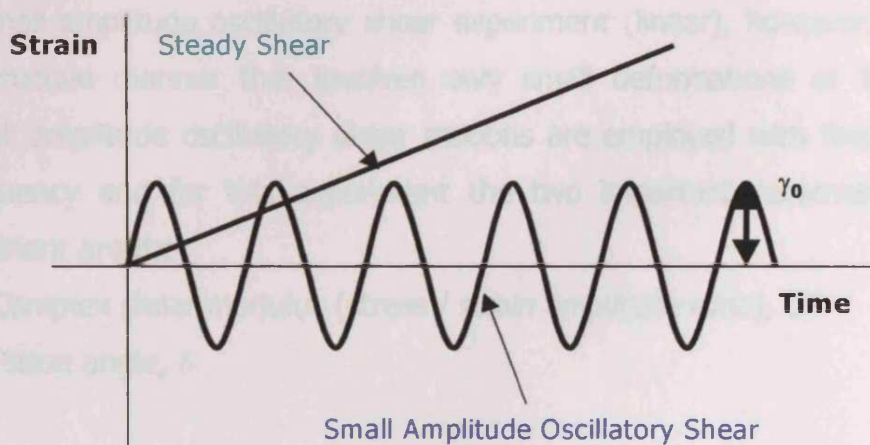


Fig 4.9: Two different methods to determine the rheological properties of materials

A steady shear experiment consists of a continuous stress sweep, it has a destructive manner and large deformations of the material are involved. From this particular type of experiment, flow curves as shown in fig 4.7 are obtained and the important parameters pertinent to this experiment are the;

- Shear rate, $\dot{\gamma}$

This is calculated using the following equation;

$$\dot{\gamma} = \frac{dy}{dt} \quad (4.6)$$

where γ is the strain and t is the time.

- Shear stress, σ
- Viscosity, η

The viscosity is, as mentioned before, the proportionality constant between the shear rate and the shear stress.

This type of experiment can also be known as a non-linear experiment. This is because the large deformations that occur can promote a deviation from a linear relationship between the shear stress and shear rate.

A small amplitude oscillatory shear experiment (linear), however, has a non-destructive manner that involves only small deformations of the material. Small amplitude oscillatory shear motions are employed with fixed or varying frequency and for this experiment the two important parameters that are pertinent are the;

- Complex shear modulus (stress / strain amplitude ratio), G^*
- Phase angle, δ

During small amplitude oscillatory shear measurements, the application of a harmonic strain on the sample, results in the generation of a harmonic stress. The equation that represents the strain is sinusoidal in nature;

$$\gamma = \gamma_0 \sin(\omega t) \quad (4.7)$$

where γ is the strain, γ_0 is the strain amplitude (see fig 4.9), ω is the angular frequency of oscillation and t is the time.

The stress varies with the same angular frequency, ω , has an amplitude of σ_0 , but is shifted out of phase with the strain by an angle, δ , the phase angle. Equation 4.8 shows the form of the stress wave;

$$\sigma = \sigma_0 \sin(\omega t + \delta) \quad (4.8)$$

It is the relationship between the strain wave and the corresponding stress wave that yields all of the important properties of the material being sheared.

If a small amplitude oscillatory shear experiment was to be conducted on a perfect Hookean Solid, the stress and the strain waveforms would be found to be exactly in phase with each other, hence the phase angle, $\delta = 0$.

If the same experiment was then conducted using a perfect Newtonian liquid, the stress and strain waveforms are in quadrature, therefore, the phase angle, $\delta = 90^\circ$.

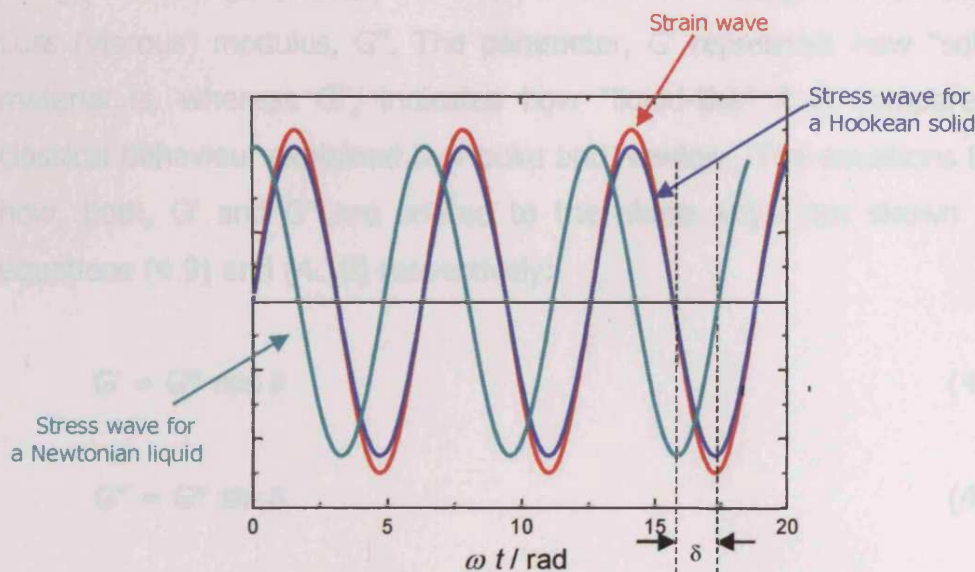


Fig 4.10: *The stress waveforms of a Hookean solid and a Newtonian liquid when subjected to a harmonic strain.*

Since most materials have neither perfect solid nor perfect liquid behaviour, rather a combination of solid and liquid properties, the phase angle for "real" materials therefore lies somewhere in between 0 and 90° .

The other important factor obtained from the stress/strain amplitude ratio in a **linear** experiment is the complex shear modulus, G^* . This is a characteristic measure of the consistency of a material or, if you like, how "stiff" a material is. If $G^* > 10^3$ Pa, the material is fairly "stiff", if $G^* < 10^2$ Pa, the material is

considered more “runny”. (Notice that a great emphasis is put on the word “linear” when talking about G^* and δ . A “non-linear response” - a consequence of increasing the stress amplitude to a point where the microstructure is disrupted - will render the values of G^* and δ uncharacteristic of the material.)

The consistency is a useful parameter to know, but it doesn't reveal how “solid-like” or “liquid-like” a material really is. A suitable approach, therefore, is to resolve the complex modulus, G^* into two components. The “real” part being the Storage (elastic) modulus, G' and the “imaginary” part being the Loss (viscous) modulus, G'' . The parameter, G' represents how “solid-like” a material is, whereas G'' , indicates how “liquid-like” it is compared to the classical behaviour explained by Hooke and Newton. The equations that show how, both, G' and G'' are related to the phase angle are shown below as equations (4.9) and (4.10) respectively:

$$G' = G^* \cos \delta \quad (4.9)$$

$$G'' = G^* \sin \delta \quad (4.10)$$

Hence, the complex modulus can therefore be expressed as:

$$G^*(\omega) = G'(\omega) + i G''(\omega) \quad (4.11)$$

where all the moduli (G^* , G' and G'') are frequency (ω) dependent and i is the square root of -1 .

As mentioned earlier, G'' is the viscous modulus that is dependent on the frequency (ω). If measured in the region where the rheological parameters are independent of the amplitude (the viscoelastic region), the ratio between G'' and ω defines a parameter, obtained by an oscillation experiment, known as the dynamic viscosity η' :

$$\eta' = G'' / \omega \quad (4.12)$$

4.3.2: How to measure the viscosity of a solution

There are two common methods used for rheometric measurements on fluid systems: capillary (or tube) and rotational. For a simple Newtonian material, if the viscosity is the **only** area of interest, the measurement is quite simple and a u-tube viscometer, like the one shown in figure 4.11, can be used.

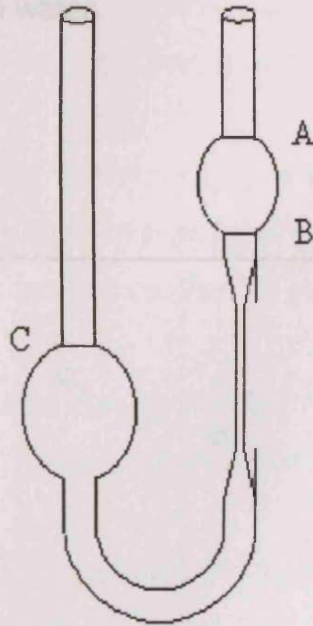


Fig 4.11: An Ostwald type capillary viscometer⁵

In this technique, the viscometer is filled with the dilute sample to the mark C. The fluid is then drawn up the right arm, to the point A, where it is held. Upon releasing the fluid, a timer is started in order to record how long it takes for the fluid to flow from A to B. The basis for this capillary method is *Poiseuille's law*, which relates the flow time, t , to the liquid's viscosity, η as follows:

$$\frac{\eta}{\rho} = At + \frac{B}{t} \quad (4.13)$$

where A and B are instrument constants and ρ is the density of the material. It is good practice to calibrate the viscometer using a standard material (with a

known viscosity) at the measurement temperature concerned, e.g. water at room temperature. The viscosity of a solution is highly dependent on the temperature at which it is measured. Fig 4.12 shows the temperature dependence on the efflux time of the main resin/varnish, J61, (Joncryl® 61 (J61) is a varnish, comprising of a low-molecular-weight (wt.av. ~ 8500) poly(acrylate) supplied by Johnson Polymer) used in this research at three different concentrations in water.

Average efflux time / s

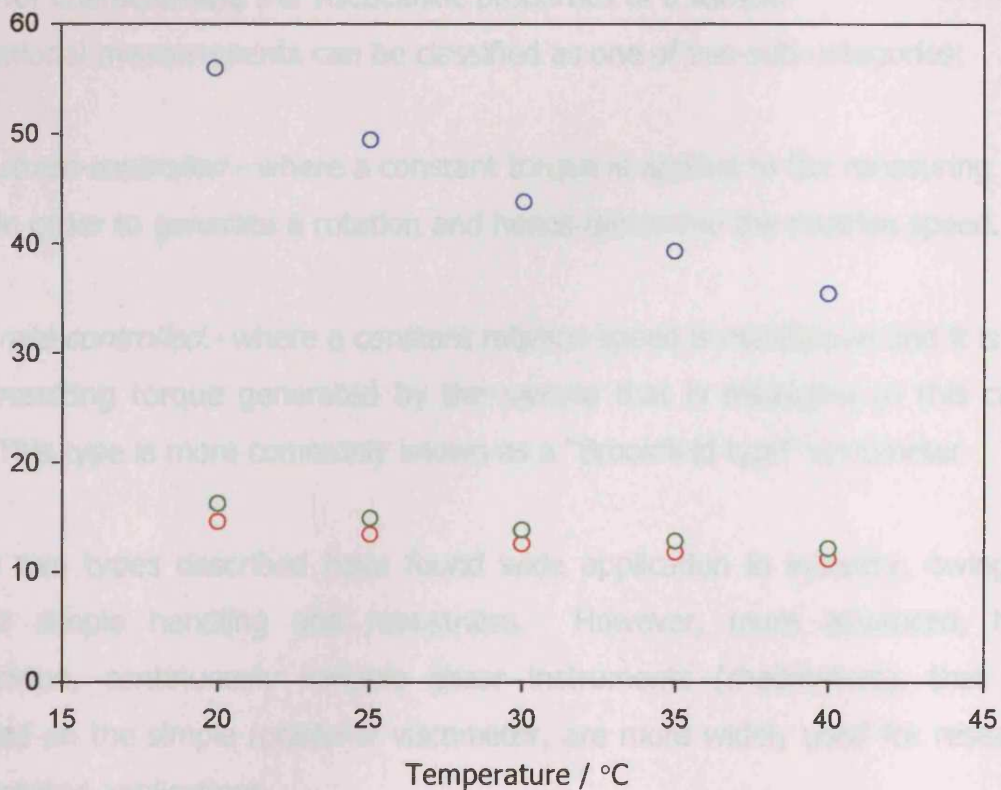


Fig 4.12: The temperature dependence on the efflux time of solutions of Joncryl 61 (J61) at three different concentrations, where: (O) $\phi_{\text{varnish}} = 50\text{wt}\%$, (O) $\phi_{\text{varnish}} = 12.5\text{wt}\%$ and (O) $\phi_{\text{varnish}} = 6.25\text{wt}\%$.

It is also useful to choose the most suitable viscometer carefully. The Ostwald viscometer is available with a variety of different diameters to accommodate materials with different viscosity ranges.

Although the capillary method is very precise, if the viscosity of concentrated suspensions, gels or pastes is required a rotational viscometer is the alternative. Here, the material is continuously sheared between two surfaces, one or both of which are rotating, hence allowing an equilibrium state to be achieved under controlled conditions.

Rotational methods can also incorporate oscillatory measurements (see page 95) for characterising the viscoelastic properties of a sample

Rotational measurements can be classified as one of two sub-categories:

1. *stress-controlled* - where a constant torque is applied to the measuring tool in order to generate a rotation and hence determine the rotation speed.
2. *rate-controlled* - where a constant rotation speed is maintained and it is the resulting torque generated by the sample that is measured in this case. This type is more commonly known as a "Brookfield type" viscometer.

The two types described have found wide application in industry, owing to their simple handling and robustness. However, more advanced, high precision, continuously variable shear instruments (rheometers), that are based on the simple rotational viscometer, are more widely used for research orientated applications.

4.3.3: Rotational rheometer

The basic rotational system consists of four parts:

- 1) A measurement tool with a well-defined geometry,
- 2) a device to apply a constant torque or rotation speed to the tool over a wide range of *shear stress* or *shear rate* values,
- 3) a device to determine the stress or shear rate response, and

4) a means of temperature control for the test fluid and tool.

The instrument available here was the Bohlin CS10 (see figure 4.13). This is a controlled stress instrument that applies a torque (force) to the material and measures the resultant displacement (movement). Many different measuring systems can be used on the rheometer. These fall broadly into three categories, namely:

- cup and bob (coaxial cylinder),
- cone and plate or
- parallel plate

With reference to figure 4.13, the two systems utilised were the cone and plate and the double gap, which fits into the coaxial cylinder category. A parallel plate was available, but not used for this research.



Double gap measuring geometry



Cone and plate measuring geometry

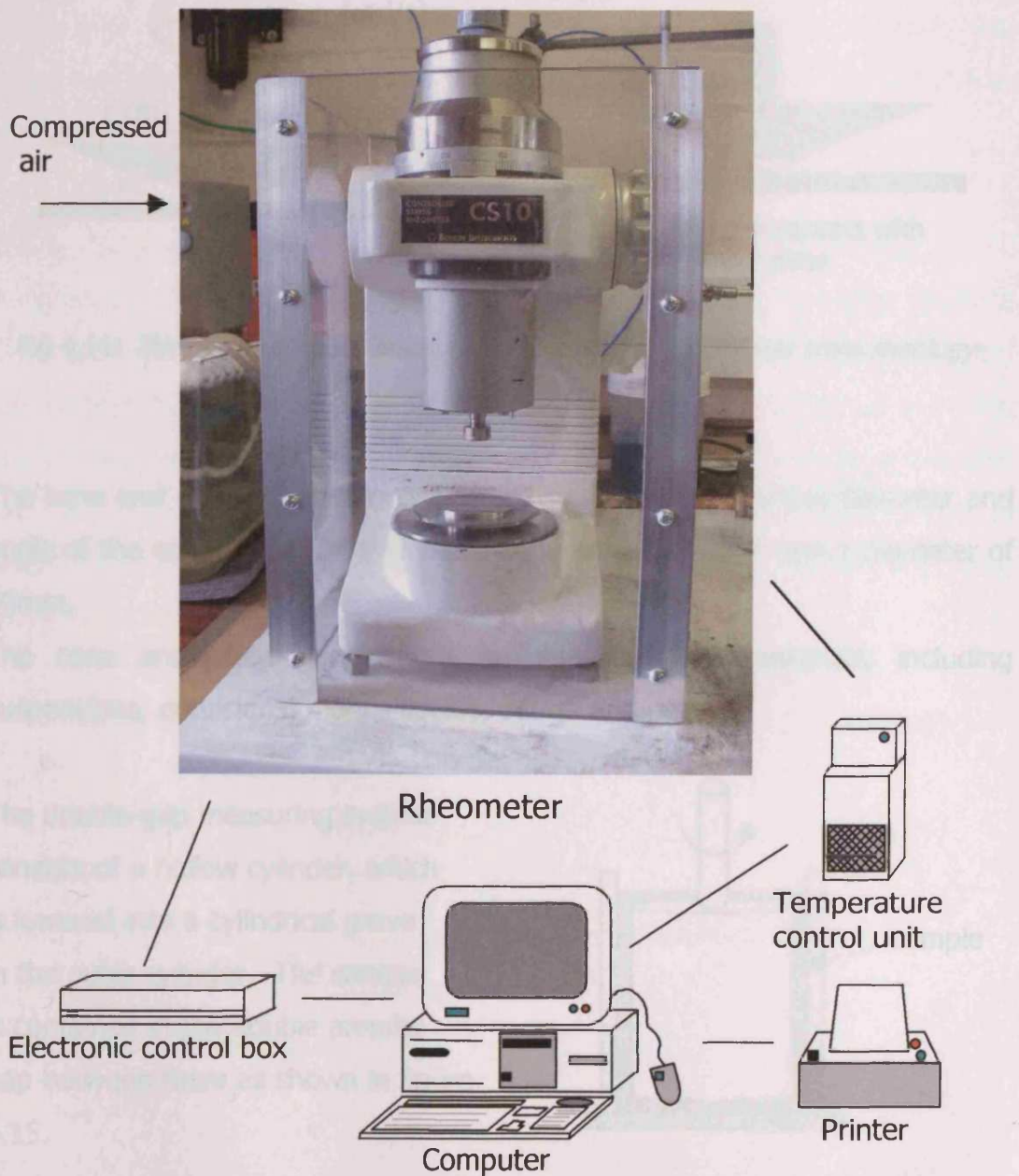


Fig 4.13: The Bohlin CS10 rheometer, the different measuring geometries and associated peripherals

4.3.4: Selection of appropriate measuring system

The cone and plate measuring system consists of a rotating upper cone and a fixed lower plate with the sample being contained between them (as shown in fig 4.14(a)). However, the cone is often truncated by a small amount (typically $\sim 0.15\text{mm}$) as shown in figure 4.14(b). An accurate gap setting mechanism is then employed to ensure that the "virtual" tip is in contact with the lower plate when measuring samples.

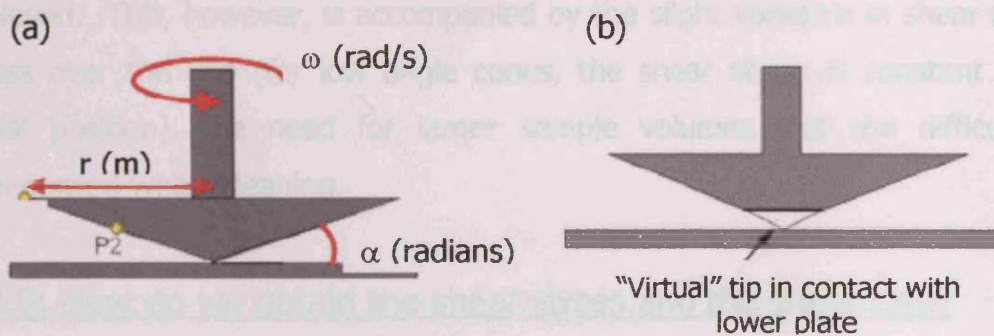


Fig 4.14: *The cone and plate measuring geometry (adapted from www.rheology-online.com)*

The cone and plate measuring system is usually denoted by the diameter and angle of the cone e.g. a CP 4/40 has a cone angle (α) of 4° and a diameter of 40mm.

The cone and plate geometry is suitable for most materials, including suspensions, emulsions, mobile liquids, dough and pastes.

The double-gap measuring system consists of a hollow cylinder, which is lowered into a cylindrical groove in the outer cylinder. The sample is contained in the double annular gap between them as shown in figure 4.15.

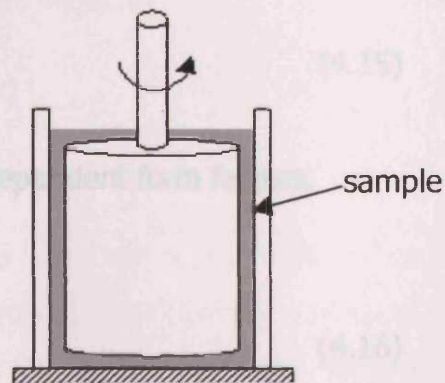


Fig 4.15: *The double-gap measuring geometry*

The double-gap measuring system is denoted by the inner and outer diameters e.g. a DG 24/27 comprises of a hollow inner cylinder with a diameter of 24mm and an outer cylinder with a diameter of 27mm.

The double-gap system is more suited to low viscosity samples.

The advantages of the double-gap over the cone and plate are few, but ultimately, particulate materials can be measured (they "jam" in the gap for the cone and plate) and, for low viscosity samples, maximum sensitivity can be achieved. This, however, is accompanied by the slight variation in shear rate/stress over the gap (for low angle cones, the shear stress is constant with radial position), the need for larger sample volumes and the difficulties experienced whilst cleaning.

4.3.5: How do we obtain the shear stress and the shear rate?

Rheometers and viscometers work with torque and angular velocity, hence a method is required to convert these "instrument numbers" into the rheological parameters that are normally used, shear stress and shear rate. This conversion is dependent on the measuring system that has been used because each measuring system has an associated *form factor* to convert torque to shear stress (equation 4.14) and to convert angular velocity to shear rate (equation 4.15).

$$\text{Shear stress} = C_1 \times \text{torque} \quad (4.14)$$

$$\text{Shear rate} = C_2 \times \text{angular velocity} \quad (4.15)$$

where C_1 and C_2 are the measuring system dependent form factors.

It follows that, for a cone and plate:

$$C_1 = \frac{3}{2} \pi r^3 \quad (4.16)$$

where r is the radius of the cone and

$$C_2 = 1/\theta \quad (4.17)$$

where θ is the cone angle in radians.

However, for coaxial cylinders (including the double-gap), the equations are:

$$C_1 = 1 / 2 \pi r_a^2 H \quad (4.18)$$

where H is the height of the cylinder and

$$r_a = (r_i + r_o) / 2 \quad (4.19)$$

where r_i is the radius of the inner cylinder and r_o is the radius of the outer cylinder. Ultimately, knowing the values of r_i and r_o makes the calculation of C_2 rather straightforward since these are the only terms required for determination of the form factor:

$$C_2 = (2 (r_i^2 \times r_o^2)) / (r_a^2 (r_o^2 - r_i^2)) \quad (4.20)$$

Most commercial rheometers have an in-built program that automatically calculates the shear stress and the shear rate from the associated C_1 and C_2 values respectively, but knowledge of the origin of these parameters is essential to assist in the understanding of their meaning.

4.4: Analysis of results

4.4.1: Flow curves and flow models

It has already been mentioned that there are five main flow curves commonly obtained, either exclusively or in various combinations, from the values of the shear stress, shear rate and hence viscosity for a given material: Newtonian flow, pseudoplastic flow, dilatant flow, Bingham plastic flow and Ellis plastic flow. The fundamental behaviour that these curves depict can therefore be

described using one of many models that have been devised to try and characterise a given materials flow behaviour.

The simplest model is the **Newtonian** model, the equation for which has already been discussed on page 12 and 86. Non-Newtonian Pseudoplastic (shear thinning) and dilatant (shear thickening) materials are best described by the **Power law** (Ostwald model) given as equation 4.21 below. This law is good for describing a materials (e.g. polymer solutions, melts and some solvent based coatings) flow under a small range of shear rates, however, most materials will deviate from this behaviour as the shear rate is increased.

$$\sigma = \eta \times \dot{\gamma}^n \quad (4.21)$$

where σ is the shear stress, η is the viscosity, $\dot{\gamma}$ is the shear rate and n is the power law index of the material. For shear thinning materials $n < 1$ and for shear thickening materials $n > 1$.

If a stress is applied to a plastic material, flow will not be observed until a yield stress is reached, at which point, flow will occur. Models that express this behaviour are the **Bingham plastic** model (4.22) and the **Herschel-Bulkley** model(4.23):

$$\sigma = \sigma_B + \eta_{pl} \dot{\gamma} \quad (4.22)$$

$$\sigma = \sigma_{HB} + (\eta_{pl} \dot{\gamma})^n \quad (4.23)$$

where σ_B and σ_{HB} are the Bingham and Herschel-Bulkley model yield stresses respectively and η_{pl} is the plastic viscosity.

If the effect of particle self-crowding on suspension viscosity needs to be considered, this is incorporated into the **Krieger-Dougherty** model (4.24):

$$\eta_r = (1 - (\phi / \phi_m))^{-[\eta] \phi_m} \quad (4.24)$$

where ϕ is the particle volume fraction, ϕ_m is a parameter representing the maximum packing fraction and $[\eta]$ is the intrinsic viscosity (for ideal spheres $[\eta] = 2.5$see chapter 1 for more information).

These models are suitable for describing the flow of many concentrated suspensions, colloidal systems and are also widely used in industry.

The fundamental models mentioned above are very effective at describing the flow over a small shear rate range, however the incorporation of model enhancements allow the flow of more complex systems to be predicted over a wider range of conditions. For example, in trying to model the behaviour of pseudoplastic materials at shear rates higher than is valid for the power law, one can use the **Cross** (4.25) model:

$$(\eta - \eta_\infty) / (\eta_0 - \eta_\infty) = 1 / (1 + ((K \dot{\gamma})^m)) \quad (4.25)$$

where η_0 and η_∞ refer to the asymptotic values of viscosity at very low and very high shear rates respectively, K is a constant parameter with the dimension of time and m is a dimensionless constant.

For plastic materials at a stress much higher than the yield stress, the **Casson** (4.26) model can be used as an extension to the Bingham plastic and the Herchel-Bulkley models to describe the behaviour of suspensions, in particular the properties of molten chocolate:

$$\sigma^{1/2} = (\sigma_c^{1/2} + \eta_{pl}^{1/2} \dot{\gamma}^{1/2}) \quad (4.26)$$

where σ_c is the Casson model yield stress and η_{pl} is the plastic viscosity.

4.4.2: Factors that affect the rheology of a material

Apart from the nature of the material, the choice of measuring system used and the magnitude of the applied force, some other important factors that can affect the rheology of a given sample are temperature, pressure and time.

Temperature

The viscosity of a sample is very sensitive to the temperature, for water, the viscosity at room temperature is just about half that at the freezing point and the viscosity of water at the boiling point is about one-third that at room temperature. It is known that, for Newtonian liquids, as the temperature is increased, the viscosity is decreased according to the Arrhenius equation below:

$$\eta = A e^{-k/T} \quad (4.27)$$

where A is the pre-exponential factor, T is the absolute temperature in Kelvin and k is related to the flow activation energy E_a and the Boltzmann constant R by:

$$k = E_a / R \quad (4.28)$$

This equation assumes that there are no physical/chemical changes being induced by the applied heat energy.

Pressure

The effect of pressure on the viscosity of a material is based on a free volume theory, proposed by Batchinski⁶ at the beginning of this century. In essence, this theory states that in a solution, the total volume of the solid material subtracted from the volume that the same amount of liquid would occupy gives a value for the free space. Therefore, if the molecules have more space for movement, there would be less resistance to flow.

Mathematically, the inverse of viscosity is proportional to the free volume.

In effect, external pressure forces the molecules together, reduces the amount of free space and consequently increases the viscosity.

Time

Some materials have flow characteristics that are highly dependent on the "shear history". Take tomato ketchup for example, when it has been left for

some time, the inter-particle interactions cause an increase in viscosity and it becomes stiff. In order to then get ketchup to flow, the internal structure must be destroyed hence a shearing motion (shaking of the bottle) must be applied. This is an example of a reversible decrease of viscosity (shear thinning) with time and is termed *thixotropy* (the term negative thixotropy is used to describe a temporary increase in viscosity).

4.4.3: Time effects-thixotropy

The measured shear stress and hence the viscosity of a non-Newtonian fluid can either increase or decrease with time of shearing. Such changes can be reversible or irreversible. A gradual decrease of the viscosity under shear stress followed by a gradual recovery of structure on removal of the stress is termed "thixotropy".

To combat this time dependent effect, when investigating the rheology of a sample, a "pre-shear" is usually carried out. During a pre-shear, the sample is subjected to a high shear rate for a time that is sufficient to completely break down the structure and then allowed to recover before any measurements are taken.

4.5: Common rheological problems

The measurement of the rheological behaviour of concentrated dispersions is of paramount importance to both academia and industry. It is therefore essential that the measurement conditions selected have been carefully considered. A few of the more common problems that are encountered when measuring the rheology of such systems are described below:

4.5.1: Turbulent flow

When investigating the rheological properties of a fluid material using a rotational rheometer, it is assumed that the flow is laminar (steady) at all times. However, at high shear rates this may not be the case and the flow may become turbulent. This happens when the inertial forces exceed the

viscous forces in the liquid. The value of this ratio is of the utmost importance and is given by the Reynolds number. For a double-gap geometry, this is given by:

$$\text{Re} \approx \frac{\dot{\gamma}(R_o - R_i)^2 \rho}{\eta} \quad (4.29)$$

where R_o and R_i are the radii of the outer and inner cylinders respectively and ρ is the density of the fluid.

For a cone and plate measuring geometry, the equation becomes:

$$\text{Re} \approx \frac{\dot{\gamma} \rho}{\eta} \left(\frac{\pi R \alpha}{180} \right)^2 \quad (4.30)$$

where R is the radius of the cone and α is the angle of the cone (in degrees).

The onset of this secondary (turbulent) flow will produce a sudden increase in the torque required to obtain a given shear rate and hence a rapid increase in the viscosity is observed. As a consequence, it is a good idea to calculate the Reynolds number for the instrument and measuring geometry being used and ensure that all measurements are taken below this figure.

4.5.2: Wall slip

If we refer back to the definitions of shear stress and shear rate (section 4.1.4), a cube of material with one fixed surface was considered. Since the material is not physically "glued" onto the surface it is possible that some movement of the fixed surface may occur. As a result of this movement, the rheometer will measure a greater strain than should be correct and so the measured viscosity will appear lower than it should be. This phenomenon appears to be more common when using smooth measuring geometries, small cone angles (in the case of the cone and plate) and a smaller gap between surfaces.

Figure 4.16 suggests three different methods employed to try and eliminate slippage during measurements. The method in (a) suggests using ribbed (roughened) cylinders instead of a pair of smooth parallel plates, in (b) a 4° cone angle is used instead of a 1° cone angle and in (c) increasing the gap between parallel plates tends to eliminate the slippage.

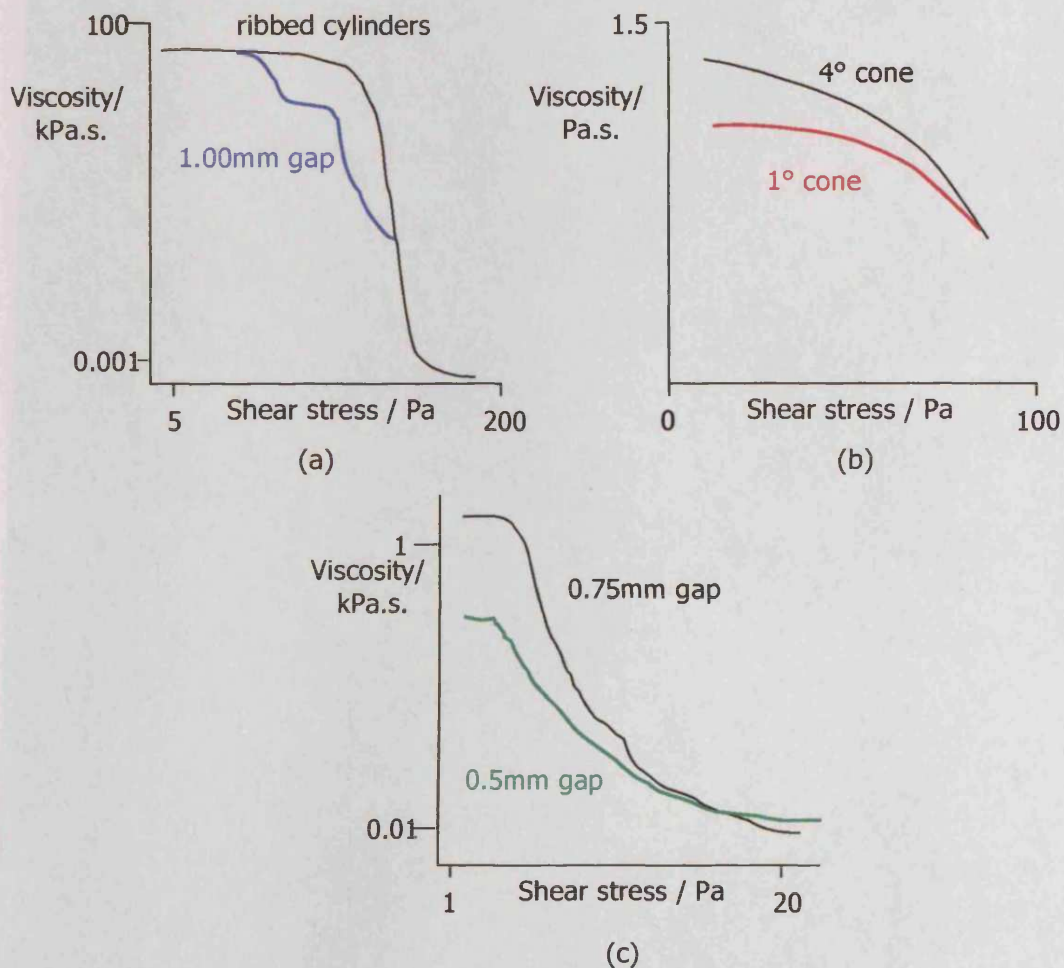


Fig 4.16: *Methods suggested in order to eliminate slippage*⁷.

To support these ideas, it has also been demonstrated on a number of occasions that concentrated colloidal dispersions^{8,9,10,11,12,13} and emulsions^{14,15} show slip flow when sheared between **smooth** concentric cylinders or **smooth** cones and plates, but on using roughened geometries all evidence of slip was eliminated. As a result of these studies, several explanations for the occurrence of wall slip have been proposed, all of which agree that it is due to

the reduction in concentration of particles adjacent to the solid wall surface. The phenomenon is said to arise because of the interactions between the flowing dispersion and the solid surface and the resulting non-linearity of velocity profiles at the wall. Figure 4.17 represents this situation schematically:

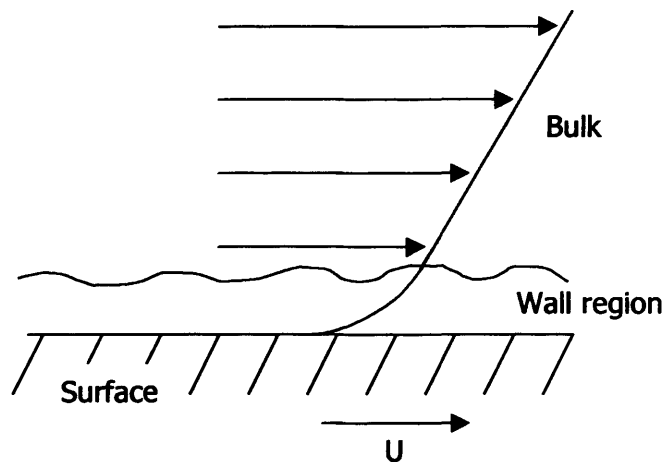


Fig 4.17: A diagram to represent the velocity profiles of a sheared liquid.

In addition, it has also been suggested that wall slip is a consequence of three other factors:

- 1) it is geometrically impossible that the particle arrangement near the geometry surface (the wall) is the same as that in the bulk solution,
- 2) the particles migrate from regions of high shear to regions of low shear and
- 3) the particles are hydrodynamically redistributed during flow.

In essence, if the flow of a material deviates from the expected behaviour, it is very important to obtain comparative data from flow geometries of a different design with both smooth and roughened surfaces in order to determine if wall slip has occurred.

References:

- ¹ Barnes, H.A., Hutton, J.F., and Walters, J.F., *An Introduction to Rheology*, Elsevier, 1989, pg 1
- ² Goodwin, J.W., and Hughes, R.W., *Rheology for Chemists- an introduction*, The Royal Society of Chemistry 2000, pg 1
- ³ Morrison, F.A., *Understanding Rheology*, Oxford university press, 2000, Chapter 1
- ⁴ Science Data Book, edited by R.M. Tennent, Oliver & Boyd ISBN 005 002487 6
- ⁵ Hackley, V.A., Ferraris, C.F., *Guide to rheological nomenclature: Measurements in Ceramic Particulate Systems*, National Institute of Standards and Technology Special Publication 946, January 2001
- ⁶ Batschinski, A.J., *Z., physik. Chem.*, 84, 643, (1913)
- ⁷ Application Note by Bohlin Instruments Limited
- ⁸ Buscall, R., McGowan, J.I., Morton-Jones, A.J., *J. Rheol.*, 37(4), 1993
- ⁹ Gregory, T., Mayers, S., *Surface coatings international*, 76(2), 82-86, (1993)
- ¹⁰ Léger, L., *et al, J. Phys.: Condens. Matter*, 9, 7719-7740, (1997)
- ¹¹ Léger, L., Hervet, H., *C.R. Physique*, 4, (2003), 241-249
- ¹² Russel, W.B., Grant, M.C. *Colloids and Surfaces A: Physicochemical and Engineering Aspects*, 161, 2, (2000), 271-282
- ¹³ Aral, B.K., Kalyon, D.M., *J. Rheol.*, 38, 957-972, (1994)
- ¹⁴ Pal, R., *Colloids and Surfaces A: Physicochemical and Engineering Aspects*, 162, (2000), 55-66
- ¹⁵ Sanchez, M.C., Valencia, C., Franco, J.M., Gallegos, C., *Journal of Colloid and Interface Science*, 241, 226-232, (2001)

CHAPTER 5: OTHER TECHNIQUES

5.1: Colour measurements

5.1.1: What is colour?

The colour we observe a material to have is the result of the interaction of the optical properties of the pigments and polymer used. Most pigments are selective in that they absorb and scatter certain portions of the visible spectrum more completely than others. If a surface **reflects** all visible light in a diffuse way and with complete reflectance, it appears to the human eye as white. Carbon black, on the other hand, **absorbs** light very efficiently across the whole visible spectrum (400 – 750nm)¹ and is hence perceived as black. If a constant fraction of light is absorbed in the whole range between 400 and 750 nm it appears grey. White, grey and black are called achromatic colours². In contrast to achromatic colours, materials that show one or more bands, i.e. absorption maxima and minima in the visible spectrum, are classified as chromatic.

5.1.2: Chromatic colours

The portion of the electromagnetic spectrum lying between about 400 and 750 nm is the **visible** region³, figure 5.1.

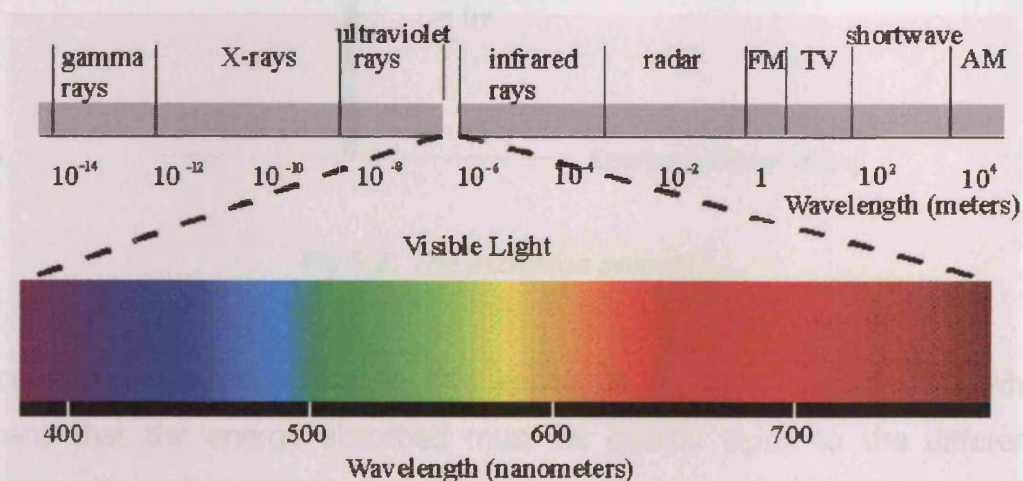


Fig 5.1: The electromagnetic spectrum with an emphasis on the visible region (taken from www.yorku.ca/eye/spectru.htm).

If a light wave has a wavelength that falls between these limits it appears coloured to the human eye. Although this may seem relatively simple, the phenomenon of coloured compounds is, in fact, rather more complicated. In brief, if a substance absorbs visible light, it appears to have a colour. However, the colour observed is not directly associated with the light that is absorbed but is related to the wavelength of the light that is reflected. Therefore, an inverse relationship exists between the observed colour and the colour that is absorbed.

5.1.3: Electronic excitations

When radiation with a wavelength belonging in the visible region (400-750 nm) is absorbed, the associated energy of the radiation is sufficiently high to promote various electronic transitions within a sample. Upon absorption, the electrons pass from a state of low energy (the initial or ground, state) to a state of higher energy (the excited state) e.g. from an occupied orbital to an unoccupied orbital of greater potential energy (fig 5.2).

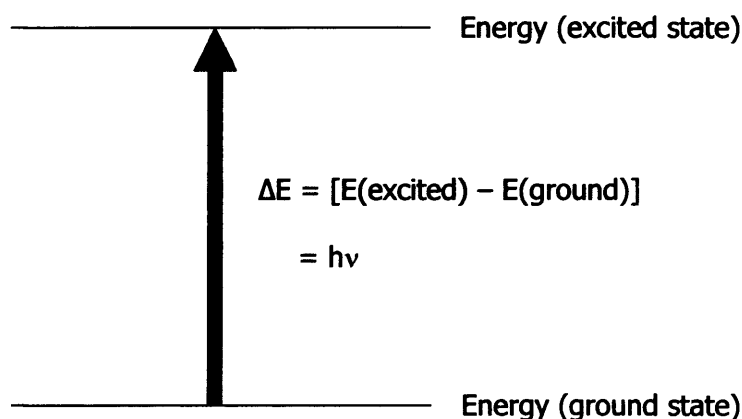


Fig 5.2: *The excitation process*³.

According to quantum theory, this excitation process is quantized, which means that the energy absorbed must be exactly equal to the difference between the energies of the two states, $h\nu$, where h is Planck's constant and ν is the frequency of the radiation. These energy quanta are also called photons.

5.1.4: Beer-Lambert law

In accordance with the Beer-Lambert law (eq. 5.1), the intensity of absorption by a sample varies with the length, l , of the sample:

$$\log I / I_0 = -\epsilon [J] l \quad (5.1)$$

where I_0 is the incident intensity (at a particular wavenumber), I is the intensity after passage through a sample of length l , and $[J]$ is the molar concentration of absorbing species J . The quantity ϵ is called the molar absorption coefficient (also known as the "extinction coefficient") and is a measure of the amount of light absorbed per unit concentration, normally expressed in $\text{L mol}^{-1} \text{cm}^{-1}$. A compound with a high molar absorptivity (e.g. $100,000 \text{ L mol}^{-1} \text{cm}^{-1}$) is very effective at absorbing light (of the appropriate wavelength), and hence low concentrations of a compound with a high molar absorptivity can be easily detected.

$\log I / I_0$ is also known as the absorbance, A (also known as the "optical density") which is dimensionless and the ratio I / I_0 is the transmittance, T of the sample and is a measure of the amount of radiation absorbed. T can also be expressed as a percentage, hence, when T is 100%, none of the radiation has been absorbed so the absorbance is zero. If all the light is absorbed, then percent transmittance is zero, and absorption is infinite.

5.1.5: Measurement of colour

The colour properties of a material can be measured instrumentally. Greatly simplified, instrumental readings can be used to describe the colour by converting spectral reflectance data into a position in three dimensional colour space. The Hunter L,a,b colour measurement method system positions the specimen's colour in a space defined by its position along one of three orthogonal axes as shown in figure 5.3:

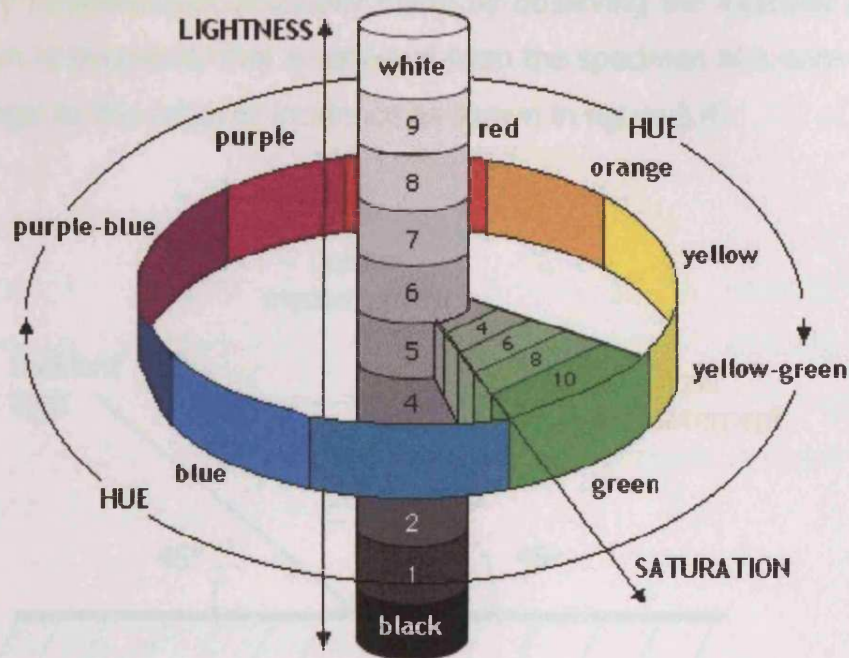


Fig 5.3: Three dimensional colour space (taken from <http://home.wanadd.nl/paulschils>).

Hunter colour

- "L" axis for lightness/darkness
- "a" axis for redness/greenness
- "b" axis for yellowness/blueness

Colour is therefore classified three dimensionally, where the L axis, which is aligned vertically, represents the lightness or brightness and the a and b axes, which form a horizontal colour wheel, represent the hue or colour tone. In addition to these two classifications, a material's colour also has a horizontally changing degree of saturation, also known as the purity and is a measure of the vividness or dullness of the apparent colour. The quantities L, a and b are obtained from the tristimulus values which are related to the amounts of the three primary stimuli; blue, green and red⁴ that are required to produce a colour match to a known colour.

The primary measurement is usually made by observing the intensity of light as a function of frequency that is reflected from the specimen at a non-specular angle to the angle of incidence as shown in figure 5.4.

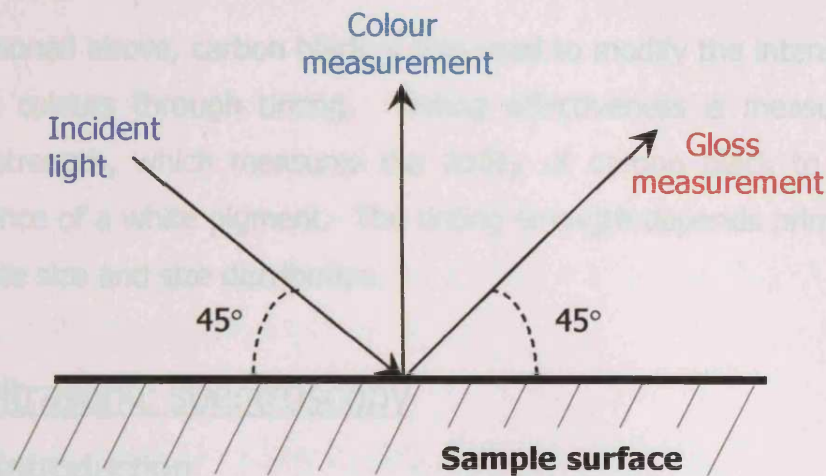


Fig 5.4: *Angles of measurement.*

Note: Gloss measurements depend on the intensity of the light measured at the specular reflectance angle. Small imperfections on the surface can scatter light in a variety of directions, hence the total intensity of light reflected to the measuring point is reduced, which, in turn, reduces the gloss.

5.1.6: Colour applications of carbon black

The use of carbon black in plastics and inks is common for two colour applications. Firstly, it is simply used to make black products and secondly to modify the colour imparted by other pigments present. The two applications however are highly dependent on different aspects of the ability of carbon black to interact with light. An important attribute is that carbon black has the ability to impart a degree of blackness, or "jetness", in its dispersed form. Jetness is a complex function of the primary particle size (surface area), the primary aggregate size (tint) and the degree of dispersion. Finer particles have more surface area for adsorbing light and they are more efficient at

forward scattering of light. For colour applications there is another important attribute of carbon black, the undertone, or "masstone". This is a complex function of the scattering and absorption efficiencies as a function of the wavelength of light.

As mentioned above, carbon black is also used to modify the intensity of other pigment colours through tinting. Tinting effectiveness is measured by the tinting strength, which measures the ability of carbon black to modify the appearance of a white pigment. The tinting strength depends primarily on the aggregate size and size distribution.

5.2: Ultrasonic spectroscopy

5.2.1: Introduction

Up until recent times, electromagnetic radiation has dominated the field of material analysis and is extensively used in many optical spectroscopic methods e.g. NMR, UV and IR. However, low energy ultrasound can provide an alternative wave (high frequency (20 MHz) sound waves) for the non-destructive analysis of materials⁵. Unlike some conventional spectroscopic methods that use light waves, ultrasonic spectroscopy utilises waves that can propagate through most materials including opaque samples (e.g. carbon black) and allow direct probing of the intermolecular forces (microelasticity) that make up matter. Another advantage of ultrasonic waves over light is that, because they are electronically synthesised (whereas light waves originate from a light source), it is fairly simple to alter the wavelength and probe a material with a variety of waves that differ in wavelength by more than an order of magnitude.

5.2.2: Uses of ultrasonic spectroscopy

Ultrasonic spectroscopy allows easy measurements of:

- the critical micelle concentration (CMC) and characterization of elasticity of the micellar hydrophobic core, as well as other parameters of micelles.

- the stability of suspensions and emulsions with regard to temperature induced transitions (e.g. aggregation)
- particle sizing within a sample hence kinetics of sedimentation and of chemical and physical processes in materials (e.g. adsorption on particle surfaces)
- crystal formation
- particle and polymer gelation (network formation)

In addition to the measurement applications listed above, the clever construction of modern ultrasonic cells allows controlled stirring of the sample, hence permitting measurements under shear.

5.2.3: Ultrasonic attenuation and ultrasonic velocity

Ultrasonic spectroscopy is a non-destructive (the amplitudes of the waves employed are extremely small) analytical technique that is based on the measurement of two independent parameters; the ultrasonic attenuation coefficient (α) of the wave and the ultrasonic velocity (ν) of the propagating wave. The attenuation, which is indicative of the energy losses experienced during compressions (which promote inter-molecular repulsions and give a peak in the wave) and decompressions (which are attractive and give a trough) of the molecules, is mainly determined by the scattering of ultrasonic waves on particles (microstructure) in non-homogeneous samples such as emulsions and dispersions and by fast chemical relaxation in homogeneous samples. The attenuation can therefore be expressed in terms of viscosity of the medium or its longitudinal loss modulus. On the other hand, the ultrasonic velocity is determined by the density and the elastic response of the sample to the oscillating pressure in the ultrasonic wave and thus can be expressed in terms of compressibility, which is extremely sensitive to intermolecular interactions, or the storage modulus.

5.2.4: Methods for obtaining the attenuation and velocity

There are two main methods for the precision measurements of ultrasonic attenuation and ultrasonic velocity that have been distinguished; the pulse technique and the resonator technique. In the pulse technique, the attenuation can be obtained by measuring the change in amplitude of the pulse and the velocity can be determined through both, direct or indirect measurements of the time of propagation of the transmitted ultrasonic pulse through the liquid sample. In contrast, in the resonator technique the ultrasonic cell forms an acoustic resonator. For this method, the velocity is obtained by measuring the frequency (or the wavelength) of the ultrasound in the resonance. A travelling wave has a velocity as shown in equation 5.2:

$$u = \lambda f \quad (5.2)$$

where u is the velocity, λ is the wavelength and f is the frequency.

However, the velocity of the propagating wave will be affected by the physical properties of the medium through which it is travelling, hence:

$$u = u_{\text{intrinsic}} + u_{\text{scattering}} \quad (5.3)$$

where $u_{\text{intrinsic}}$ is determined by the micro-elasticity of the sample and $u_{\text{scattering}}$ is due to the elasticity and density of the medium and is dependent on a structural contribution in non-homogeneous samples.

The attenuation is determined by the energy losses experienced during the resonance. When an "input" wave is propagated through a sample there is always a reduction in the amplitude associated with the "output" wave- this is due to a loss of energy (via collisions with particles etc.). The wave can, therefore, be represented by the following equation:

$$A = A_0 e^{-\alpha t} \quad (5.4)$$

where A is the amplitude of the wave, A_0 is the initial amplitude of the wave, t is the time and α is the attenuation coefficient. As with the velocity, the attenuation coefficient can also be regarded as the sum of two separate components:

$$\alpha = \alpha_{\text{intrinsic}} + \alpha_{\text{scattering}} \quad (5.5)$$

where $\alpha_{\text{intrinsic}}$ is due to the absorption of energy and $\alpha_{\text{scattering}}$ is due to the actual scattering of the wave.

At first, the pulse method, being simple to construct with a low cost of instrumentation, was the most popular method employed. However, the requirement of relatively high sample volumes in order to obtain precise measurements and its limitations in biomolecular studies and pharmaceuticals, due to the high cost of materials, prompted scientists into developing the resonator technique. As a result, for the past fifteen years or so, the resonator technique has been the preferred method for ultrasonic measurements owing to the low resolutions achieved (~1ppm for velocity and ~1% for attenuation) and the small sample volumes that are required (30 μ l - 4 ml).

5.2.5: Principles of ultrasonic spectroscopy

In the resonator technique, the ultrasonic parameters of liquids are obtained through the measurements of resonance characteristics of acoustic resonators. There are two main elements; the resonator chamber, where the acoustic resonance is formed and the piezotransducers, which excite and detect the ultrasonic vibrations.

As is schematically represented in fig 5.5, the generated electronic signals are converted into ultrasonic waves by the continuous vibrating of the surface of a piezotransducer, which are then passed back and forth through the sample chamber before finally being converted, by another piezotransducer, back into an electronic signal ready for analysis. Oscillating compression (and decompression) in the ultrasonic wave causes an oscillation of molecular

arrangements in the sample, which responds by intermolecular attraction or repulsion.

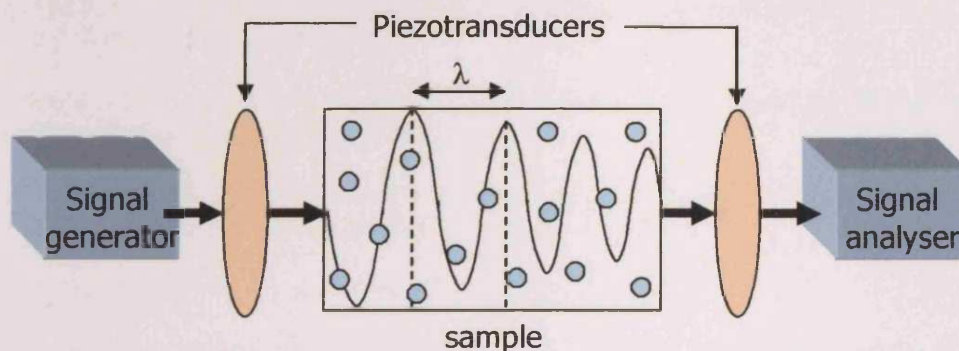


Fig 5.5: *Ultrasonic waves and ultrasonic measurements (taken from www.thesupplyline.org/Issue50/feature.html).*

5.2.6: Interpretation of ultrasonic results

If, after probing the system with the high frequency sound waves, the **ultrasonic velocity** has dropped this suggests that an elastic network has been formed or partially formed. Oscillating sound waves can also cause structural rearrangements within the sample being measured. This rearrangement of particles ultimately disrupts the wave and consequently increases the **attenuation**. If there appears to be a decrease in both the ultrasonic attenuation and the velocity this is indicative of the complete collapse of the network.

5.2.7: Comparison with rheology measurements

In an ultrasonic wave, oscillating pressure (stress) causes oscillation of compressions within a sample (mechanical deformation) and therefore can be regarded as a rheological wave (see chapter 4). Hence, ultrasonic parameters map to rheological ones; for ultrasonic velocity, elasticity/longitudinal storage modulus and for attenuation, viscosity/longitudinal loss modulus. However

there is a difference between the two, as classical rheology deals with slow or low frequency (typically below 1 KHz) deformations, ultrasound involves fast or high frequency deformations (above 100 KHz)⁶.

References

- ¹ Donnet, J.-B., Bansal, R.C., Wang, M.-J., *Carbon Black, Second Edition, Revised and Expanded*, Marcel Dekker, Inc, New York, (1993)
- ² Zollinger, H., *Color Chemistry, Syntheses, Properties and Applications of Organic Dyes and Pigments*, VCH, Weinheim, (1987)
- ³ Pavia, D.L., Lampman, G.M., Kriz, G.S., *Introduction to Spectroscopy, second edition*, Saunders College Publishing, USA, (1996)
- ⁴ MacAdam, D.L., *Color Measurement, Theme and Variations*, Springer Series in Optical Sciences, Volume 27, Springer-Verlag, Germany, (1981)
- ⁵ Buckin, V., Smyth, C., *Sem Food Anal*, (1999), 4(2), 113-130
- ⁶ Buckin, V., Kudryashov, E., O'Driscoll, B., High-resolution ultrasonic spectroscopy for material analysis, reprinted from *Spectroscopy Perspectives A Supplement to American Laboratory*, March (2002).

CHAPTER 6: RESULTS AND DISCUSSION – AQUEOUS DISPERSIONS

6.1: Reproducibility

Before presenting any of the data associated with this research, it seems appropriate, here, to verify the reproducibility of the data, more specifically, the rheological data. For carbon black dispersions, the rheological data obtained can depend on many factors, both in the processing of the carbon black and the method in which the carbon black is dispersed and also upon the conditions under which the experiments are conducted. For these reasons, a great emphasis was placed on the reproducibility of the results and only data that showed acceptable reproducibility is contained within this thesis.

Firstly, the bulk of this thesis and indeed the great majority of this chapter (chapter 6) is concerned with an aqueous system of carbon black, either Raven[®] L or Raven[®] M, with a waterborne acrylic resin polymer named Joncryl[®] 61 (J61). The carbon black particles were supplied by Columbian Chemicals Company and all experiments were conducted using a portion taken from the same batch. However, carbon black is composed of aggregates that vary in size (shown by the TEM'S in chapter 3) hence the need for consistent data was recognised as a priority at the beginning of the research. The acrylic resin polymer was supplied on demand, by Johnson Polymer, therefore several different batches were used throughout.

All samples were prepared with the use of a mechanical mixer and left to equilibrate overnight. The rheology of the equilibrated samples was then measured. Following the completion of this initial measurement, a thermal equilibrium time of 15minutes was allowed, before a repeat measurement was taken. The sample was then tightly sealed and stored for a week until a third measurement was taken. All three sets of data were then compared in order to detect any time dependent effects and to see if the reproducibility is acceptable for repeat data. In addition to the "day to day" reproducibility, a "sample to sample" reproducibility test was also conducted. This consisted of

an identical sample being prepared in the same way and measured under the same conditions.

Figure 6.1(a) represents repeat rheological data obtained for an aqueous carbon black and Joncryl 61 dispersion, chosen at random, i.e. typical data.

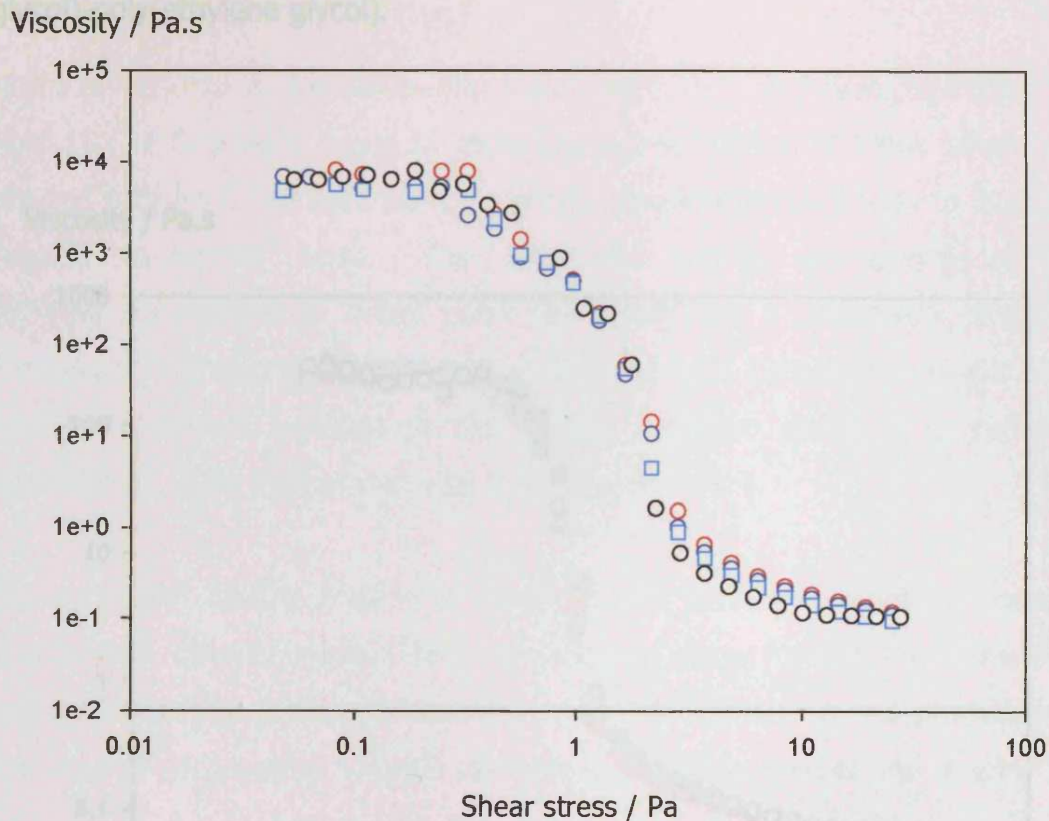


Fig 6.1(a): Typical viscosity-shear stress curves for a dispersion of Raven[®] L particles in an aqueous Joncryl[®] 61 solution of $\varphi_{\text{particle}} = 0.15$ and $\varphi_{\text{polymer}} = 0.21$, where (○) initial measurement (following an overnight equilibrium), (○) repeat data obtained 15 minutes later, (○) repeat data obtained 7 days later and (□) data obtained after an identical sample was remade and measured.

For the carbon black and poly(ethylene glycol)-poly(propylene glycol)-poly(ethylene glycol) dispersions all the polymer used was from the same batch, supplied by Aldrich, however this block copolymer is polydisperse.

Just as fig 6.1(a) represents an aqueous carbon black and Joncryl 61 dispersion, fig 6.1(b) represents repeat rheological data obtained for a typical aqueous dispersion of carbon black and poly(ethylene glycol)-poly(propylene glycol)-poly(ethylene glycol).

Viscosity / Pa.s

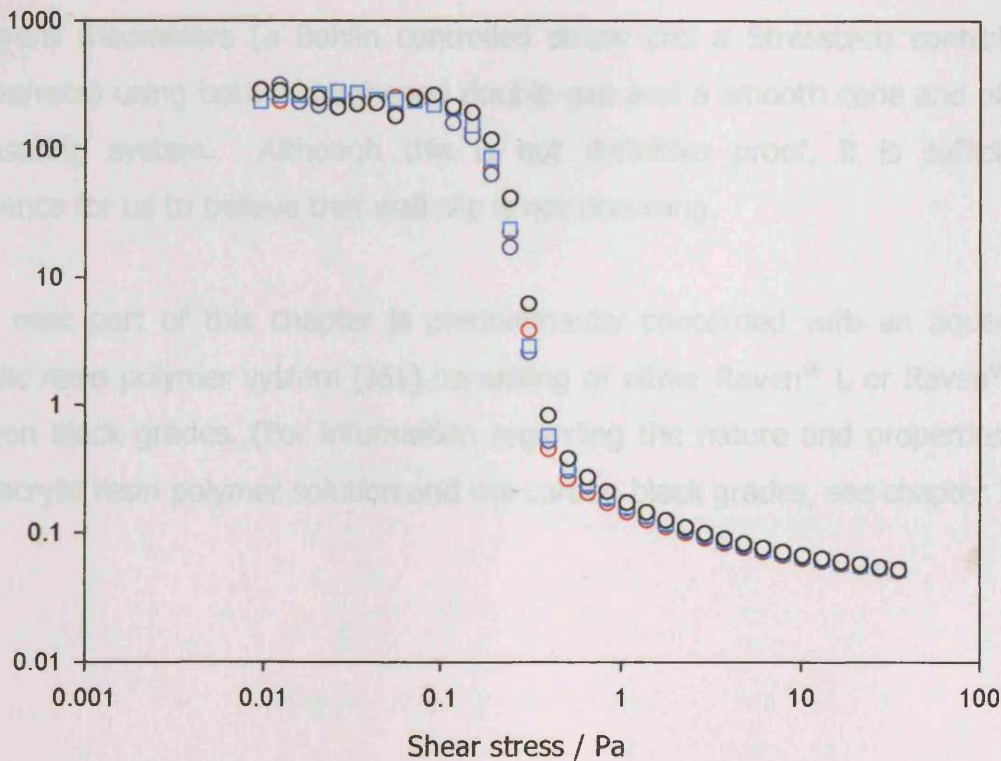


Fig 6.1(b): Typical viscosity-shear stress curves for a dispersion of Raven® L particles in an aqueous poly(ethylene glycol)-poly(propylene glycol)-poly(ethylene glycol) solution of $\varphi_{particle} = 0.15$ and $\varphi_{polymer} = 0.21$, where (○) initial measurement (following an overnight equilibrium), (○) repeat data obtained 15 minutes later, (○) repeat data obtained 7 days later and (□) data obtained after an identical sample was remade and measured.

On considering the reproducibility of "day to day" and "sample to sample" measurements obtained for the above two systems shown in (6.1(a) and 6.1(b)), it is clear to see that the data has been verified on more than one occasion and is indeed reproducible to a satisfactory standard. All data contained in this thesis were measured in exactly the same way and the results were also confirmed more than once. However, only the initial data (after overnight equilibrium) have been presented.

Some of the data in this section (fig 6.3(a), fig 6.3(b), fig 6.5(a), fig 6.5(b) and fig 6.10), at first sight, seem to show flow curves typical of those where wall slip has occurred¹. All data were, however, reproducible on a "day to day" and "sample to sample" basis. They were also entirely reproducible on two different rheometers (a Bohlin controlled stress and a Stresstech controlled stress/rate) using both a roughened double-gap and a smooth cone and plate measuring system. Although this is not definitive proof, it is sufficient evidence for us to believe that wall slip is not occurring.

The next part of this chapter is predominantly concerned with an aqueous acrylic resin polymer system (J61) consisting of either Raven[®] L or Raven[®] M carbon black grades. (For information regarding the nature and properties of the acrylic resin polymer solution and the carbon black grades, see chapter 3).

6.2: Particle characterisation

The morphology of the two main carbon black particles has been examined by small-angle neutron scattering (fig 6.2(a)), in the presence of polymer, and by microscopy i.e. in the absence of polymer (see chapter 3). Fig 6.2(a) shows a typical scattering curve for each of the two particles, Raven L and Raven M, studied.

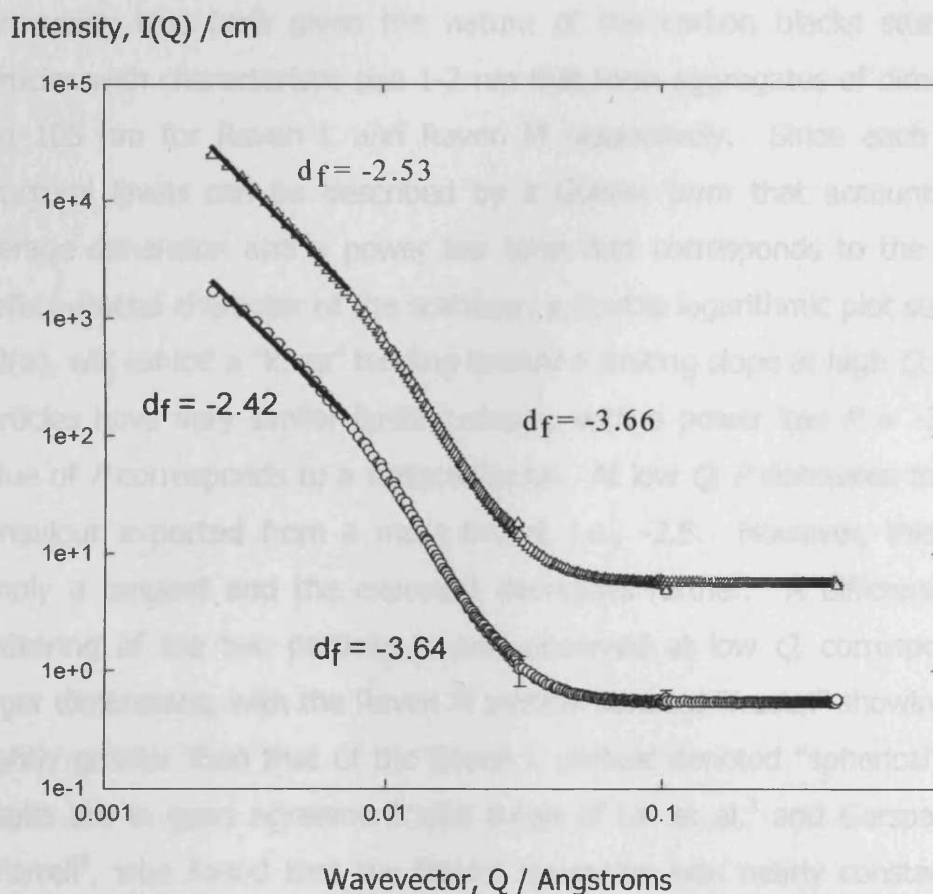


Fig 6.2(a): Particle characterization by SANS. Small-angle neutron scattering data for 0.5 wt% carbon black particles, where (O) is the Raven L and (Δ) is the Raven M, dispersed in water with 0.18% polymer. The polymer is "invisible" in this experiment due to the low contrast.

Many materials show different structural levels when examined over a range of dimensions². A general representation for the scattering on a particular level is:

$$I(q) \cong G \exp(-q^2 R_g^2 / 3) + B(1 / q^*)^P \quad (6.1)$$

Where $q^* = q / [\text{erf}(k q R_g / 6^{1/2})]^3$, G is the Guinier prefactor defined by the specifics of the particle composition and the concentration of the particles, and B is a prefactor specific to the type of power-law scattering. B is defined according to the regime in which the exponent P falls. Such a behaviour is particularly true here given the nature of the carbon blacks studied, viz., particles with characteristic size 1-2 nm that form aggregates of dimension 87 and 105 nm for Raven L and Raven M respectively. Since each of these structural levels can be described by a Guinier term that accounts for the average dimension and a power law term that corresponds to the mass- or surface-fractal character of the scatterer, a double logarithmic plot such as fig. 6.2(a), will exhibit a "knee" tending toward a limiting slope at high Q . The two particles have very similar limiting slopes, with a power law $P = -3.6$. This value of P corresponds to a surface fractal. At low Q , P decreases toward the behaviour expected from a mass fractal, i.e., -2.5. However, this slope is simply a tangent and the exponent decreases further. A difference in the scattering of the two particles is only observed at low Q , corresponding to larger dimensions, with the Raven M particle denoted "fractal" showing a slope slightly greater than that of the Raven L particle denoted "spherical". These results are in good agreement with those of Lin et al.³ and Gerspacher and O'Farrell⁴, who found that the fractal dimension was nearly constant for 15 different grades of carbon black. The SANS data presented here confirm the TEM results that the fractal particle (Raven M) has a more open structure.

The particle types could also be differentiated by their ultrasonic parameters, as shown in figure 6.2(b) and 6.2(c). Two samples comprising of $\varphi^{\text{spherical}}$ Raven L = 0.15, $\varphi_{\text{polymer}} = 0.11$, and φ^{fractal} Raven M = 0.15, $\varphi_{\text{polymer}} = 0.11$ were investigated.

Ultrasonic attenuation, 1/m

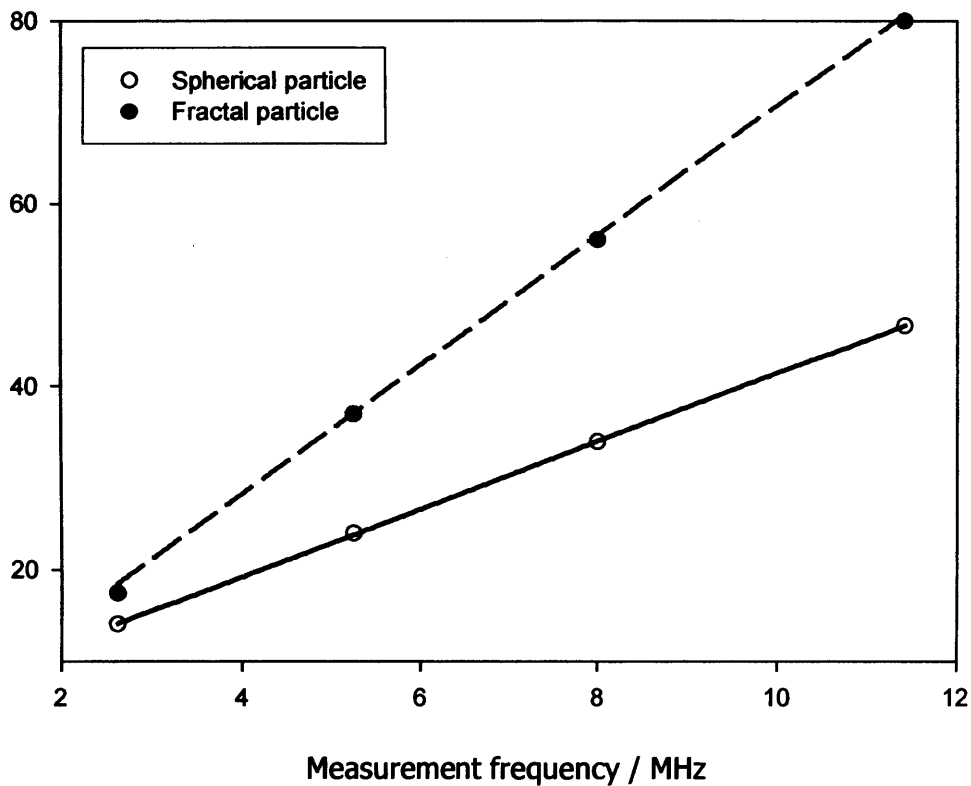


Fig 6.2(b): Frequency dependence of ultrasonic attenuation in carbon black dispersions in water, where (O) $\varphi^{\text{spherical}}$ Raven L = 0.15, $\varphi_{\text{polymer}} = 0.11$, and (●) φ^{fractal} Raven M = 0.15, $\varphi_{\text{polymer}} = 0.11$.

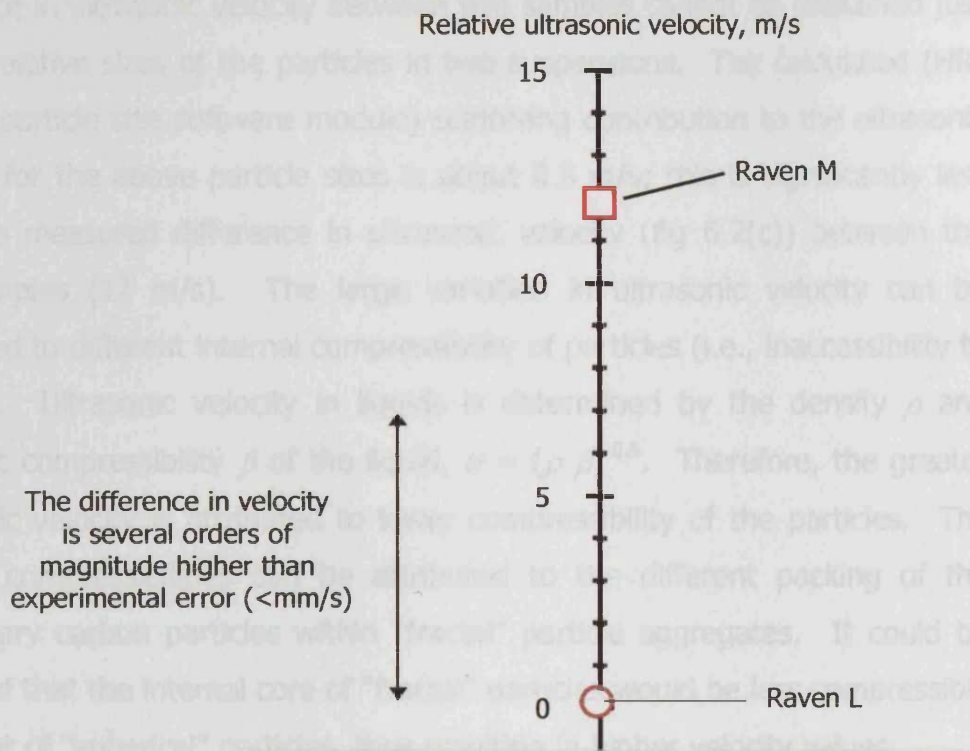


Fig 6.2(c): The relative difference in ultrasonic velocity of the two different particle carbon black dispersions in water, where (○) $\varphi^{\text{"spherical" Raven L}} = 0.15$, $\varphi_{\text{polymer}} = 0.11$, and (□) $\varphi^{\text{"fractal" Raven M}} = 0.15$, $\varphi_{\text{polymer}} = 0.11$.

Both the ultrasonic velocity and the ultrasonic attenuation in the dispersion of "fractal" Raven M particles are higher than those in samples with "spherical" Raven L particles. The differences in ultrasonic velocity and attenuation between the two samples are 7 m/s and 25.7 m^{-1} respectively, at a frequency around 8 MHz. This difference in attenuation can be attributed to the scattering contribution to ultrasonic attenuation, which depends on the particle size. The second line in fig 6.2(b) shows the calculated (via the HR-US 102 particle size software module) difference in ultrasonic attenuation based on the best-fit-average sizes of particles in both of the suspensions, 0.08 and 0.11 μm . As can be seen from the figure, the attenuation data are well described by the scattering of ultrasonic waves due to particles of different sizes.

Further, the sizes of the particles are in good agreement with the (dry state) aggregate diameters determined by microscopy (Table 1, chapter 3). The difference in ultrasonic velocity between two samples cannot be explained just by the relative sizes of the particles in two suspensions. The calculated (HR-US 102 particle size software module) scattering contribution to the ultrasonic velocity for the above particle sizes is about 0.3 m/s; this is significantly less than the measured difference in ultrasonic velocity (fig 6.2(c)) between the two samples (12 m/s). The large variation in ultrasonic velocity can be attributed to different internal compressibility of particles (i.e., inaccessibility to solvent). Ultrasonic velocity in liquids is determined by the density ρ and adiabatic compressibility β of the liquid, $u = (\rho \beta)^{-0.5}$. Therefore, the greater ultrasonic velocity is attributed to lower compressibility of the particles. The relative compressibilities can be attributed to the different packing of the elementary carbon particles within "fractal" particle aggregates. It could be expected that the internal core of "fractal" particles would be less compressible than that of "spherical" particles, thus resulting in higher velocity values.

However, another factor that could be responsible for these differences in ultrasonic velocity is the interaction of polymer with the particles. Adsorption of polymer onto the surface of a particle will be accompanied by solvation effects, which in turn affect the compressibility of the suspension^{5,6}.

6.3: Rheology-the effect of polymeric binder concentration

Figs. 6.3(a) and 6.3(b) show a series of typical viscosity vs shear stress behaviours for both the Raven L and Raven M particle types with a fixed particle volume fraction $\phi_{\text{particle}} = 0.15$ and a range of polymer volume fractions: $\phi_{\text{polymer}} = 0.053, 0.11, \text{ and } 0.21$.

Viscosity / Pa.s

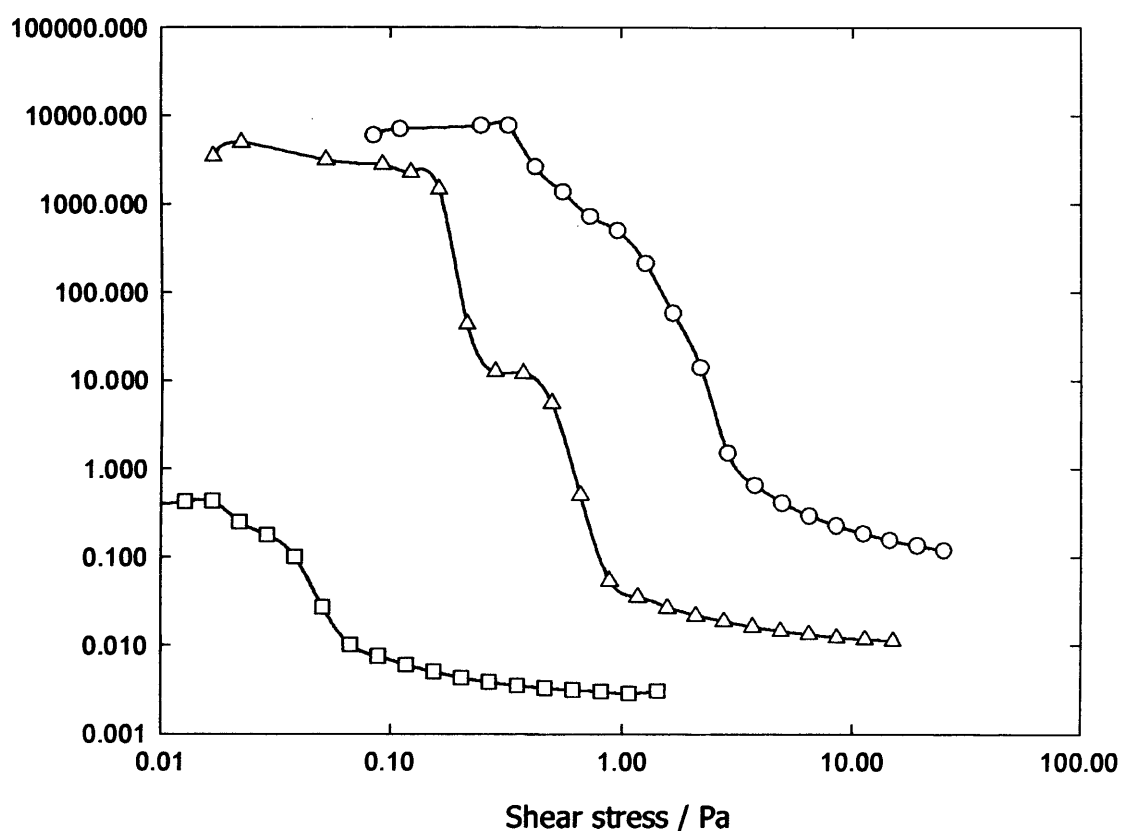


Fig 6.3(a): *Typical viscosity-shear stress curves for "spherical" Raven[®] L carbon black particles in aqueous polymer solutions with $\phi_{\text{particle}} = 0.15$ and (\square) $\phi_{\text{polymer}} = 0.053$, (Δ) $\phi_{\text{polymer}} = 0.11$ and (\circ) $\phi_{\text{polymer}} = 0.21$.*

Viscosity / Pa.s

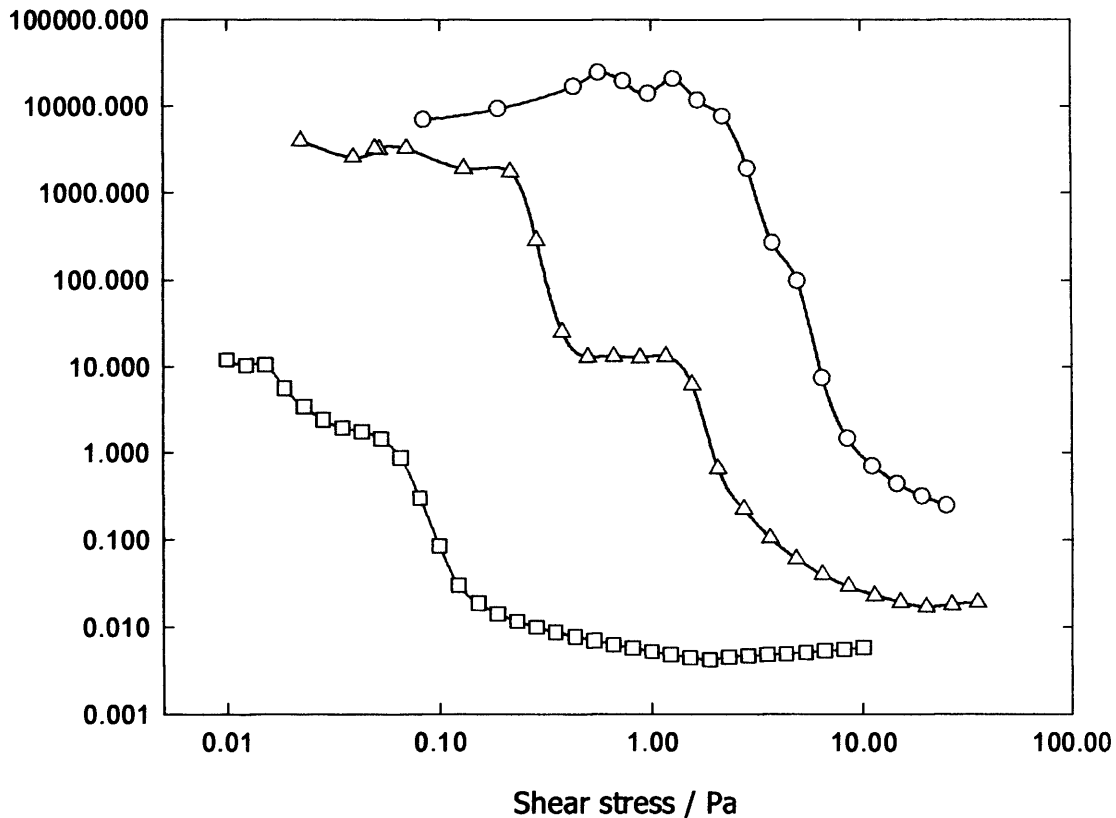


Fig 6.3(b): Typical viscosity-shear stress curves for "fractal" Raven® M carbon black particles in aqueous polymer solutions with $\phi_{particle} = 0.15$ and (\square) $\phi_{polymer} = 0.053$, (Δ) $\phi_{polymer} = 0.11$ and (O) $\phi_{polymer} = 0.21$.

All the dispersions show, in essence, similar behaviour- a Newtonian region at low shear stresses (rates), which shear thin above some critical shear stress. Sometimes a slight upturn in viscosity with increasing shear stress at high shear stress is present. This is an experimental artefact, that is attributed to the sample being spun out of the double gap geometry, and is not shown in these data; hence the data cease at different shear stresses.

Dispersions with $\phi_{polymer} < 0.053$ were unstable. Hence, we conclude that $\phi_{polymer} = 0.053$ corresponds to sufficient polymer concentration in order to stabilize the particles. Therefore, for $\phi_{polymer} > 0.053$, excess nonadsorbed

polymer will be present in the solution. In reality, excess polymer is a realistic representation of many industrial situations. Unfortunately, the adsorption isotherm could not be measured for a stable system of carbon black and Joncryl 61. Several attempts were made, but all methods adopted proved unsuccessful. The biggest problem was finding a quantitative method for the residual polymer solution in the presence of some residual carbon black e.g. NMR, IR were not sensitive enough.

The effects of nonadsorbed polymer on the dispersion viscosity are then apparent. Consider the $\phi_{\text{particle}} = 0.15 / \phi_{\text{polymer}} = 0.053$ system, i.e., where there is little or no free polymer. At low shear stresses the Raven M particle (fig 6.3(b)) has a much higher viscosity of ~ 10 Pa.s compared to a viscosity of ~ 0.45 Pa.s. for the Raven L particle (fig 6.3(a)). This is in excellent agreement with the rather limited ultrasonic spectroscopy studies. In addition, the Raven M particle dispersions undergo shear thinning at a higher shear stress (~ 0.08 Pa) than the Raven L particle (~ 0.04 Pa). The limiting high-shear viscosity is similar for both particles at ~ 0.004 Pa.s. For the dispersions with $\phi_{\text{particle}} = 0.15 / \phi_{\text{polymer}} = 0.11$, there is significant free polymer in solution- the low-shear-stress viscosity increases accordingly, some four orders of magnitude compared to the $\phi_{\text{polymer}} = 0.053$ case. Further increases in ϕ_{polymer} , i.e., $\phi_{\text{particle}} = 0.15 / \phi_{\text{polymer}} = 0.21$, have a far less pronounced effect on the low-shear-stress viscosity. However, the viscosity at higher stresses increases by about an order of magnitude and indeed the particle morphology has a negligible effect on the rheology under these conditions. However, there is a distinct difference in the yield stress vs ϕ_{polymer} behaviour for the two particle types.

To explain the details in the shear stress behaviour, we should therefore examine the rheology of the simple polymer solutions. For all concentrations, the response is largely Newtonian (to a first approximation at least) over the majority of the shear stress range, fig 6.4(a), and the viscosity increases with concentration, fig 6.4(b). The viscosity-concentration scaling behaviour

increases around $\phi_{\text{polymer}} = 0.03$, indicating interaction of the polymer molecules, such as the formation of a weak polymer network or aggregation.

6.4: Rheology-Polymeric binder in solution

Viscosity / Pa.s

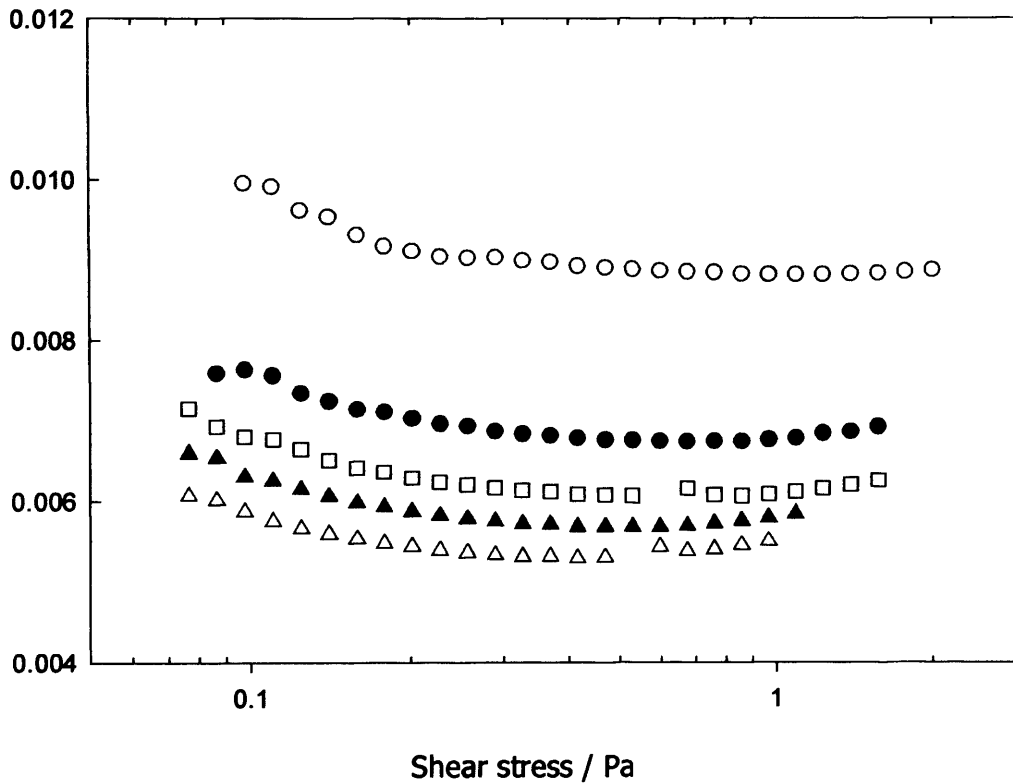


Fig 6.4(a): A series of viscosity-shear stress curves for a series of different concentration aqueous polymer solutions i.e. (Δ) $\phi_{\text{polymer}} = 0.04$, (\blacktriangle) $\phi_{\text{polymer}} = 0.09$, (\square) $\phi_{\text{polymer}} = 0.11$, (\bullet) $\phi_{\text{polymer}} = 0.14$ and (\circ) $\phi_{\text{polymer}} = 0.18$.

Newtonian viscosity / mPa.s

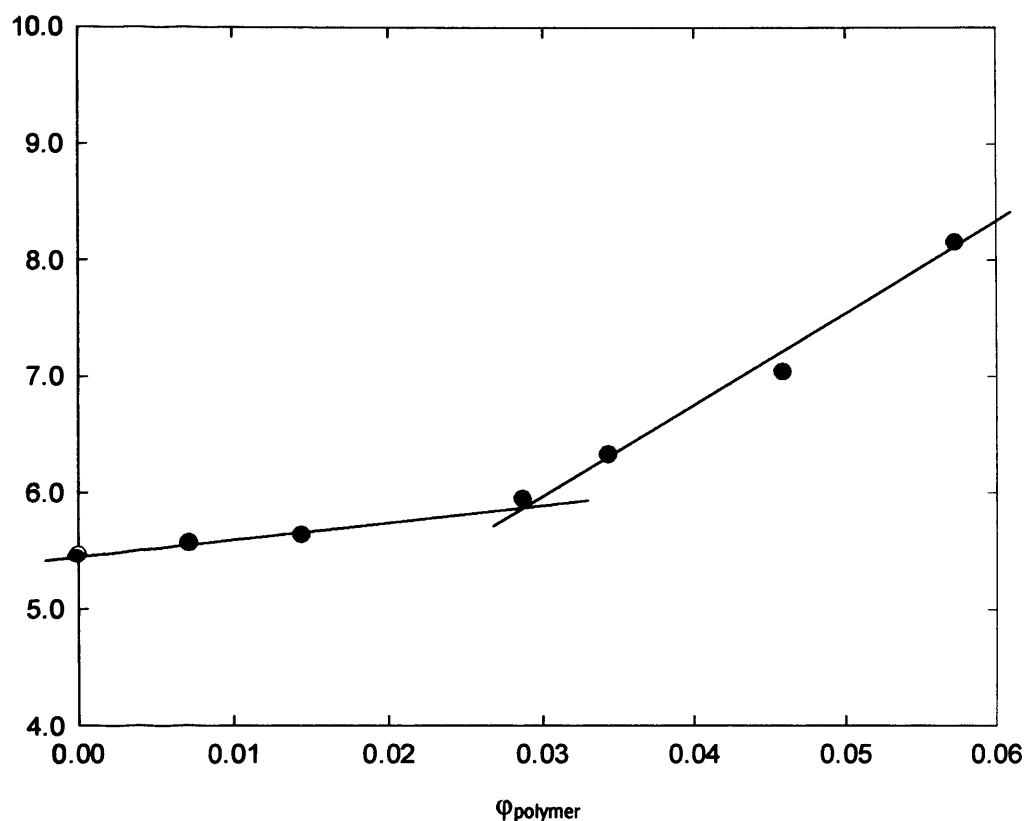


Fig 6.4(b): *Viscosity-polymer volume fraction behaviour for aqueous polyacrylamide solutions.*

Accordingly, the data presented in figs 6.3(a) and 6.3(b) correspond to 1.) a system with little or no free polymer and 2.) where sufficient excess polymer is present so that the continuous phase is a reasonably concentrated polymer solution. The substantially greater low-shear viscosity in the $\phi_{\text{particle}} = 0.15 / \phi_{\text{polymer}} = 0.11$ and $\phi_{\text{particle}} = 0.15 / \phi_{\text{polymer}} = 0.21$ cases is therefore due to polymer in solution, with the particles forming a network.

6.5: Rheology-Dilution experiments

To understand further the role of interaction between the polymer layer and the polymer in the continuous phase, "dilution experiments" were undertaken, in which the ratio ϕ_{particle} to ϕ_{polymer} was held constant, but ϕ_{particle} and therefore ϕ_{polymer} decreases. Of particular interest was the intermediate Newtonian plateau observed in the $\phi_{\text{particle}} = 0.15$, $\phi_{\text{polymer}} = 0.11$ system, i.e., where $\phi_{\text{particle}} / \phi_{\text{polymer}} = 1.4$. Typical viscosity vs shear stress plots are shown in figs 6.5(a) and 6.5(b) for dispersions with $\phi_{\text{particle}} / \phi_{\text{polymer}} = 1.4$ as a function of ϕ_{particle} .

Viscosity / Pa.s

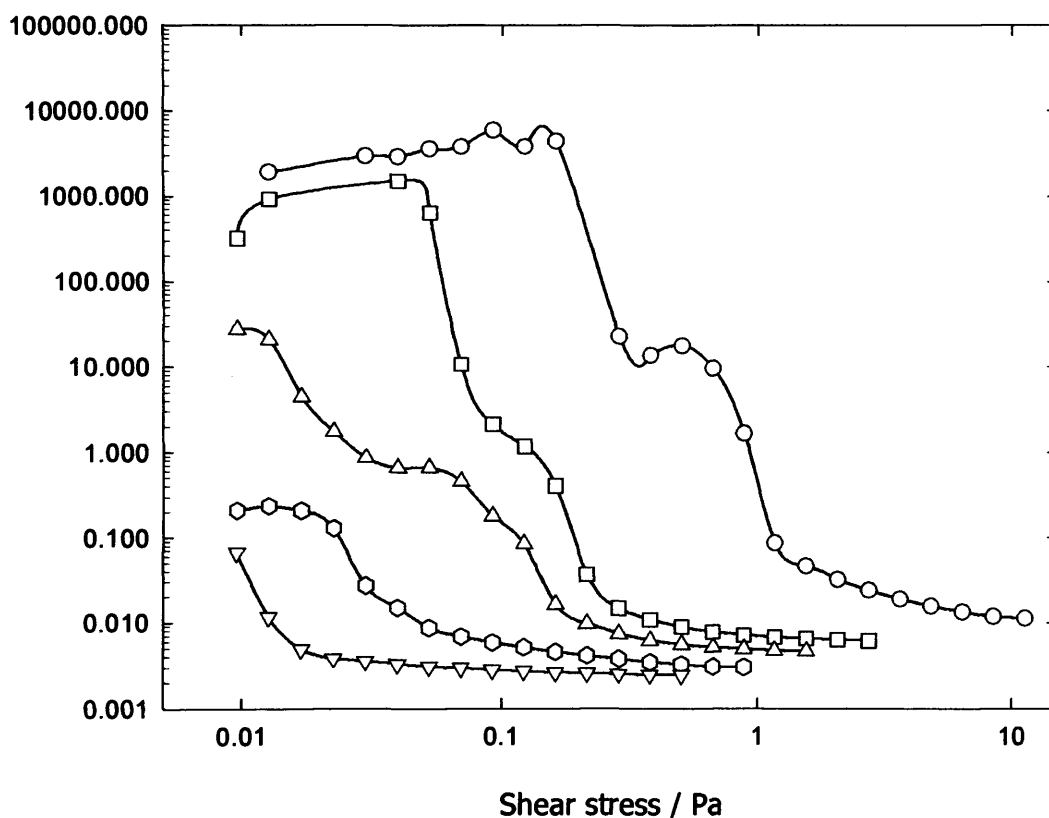


Fig 6.5(a): Typical viscosity-shear stress curves for the "spherical" Raven[®] L carbon black particles in aqueous polymer solutions at a fixed $[\text{polymer}]/[\text{particle}]$ as a function of ϕ_{particle} ; i.e. (O) $\phi_{\text{particle}} = 0.15$, (\square) $\phi_{\text{particle}} = 0.118$, (Δ) $\phi_{\text{particle}} = 0.107$, (\circ) $\phi_{\text{particle}} = 0.093$ and (∇) $\phi_{\text{particle}} = 0.081$.

Viscosity / Pa.s

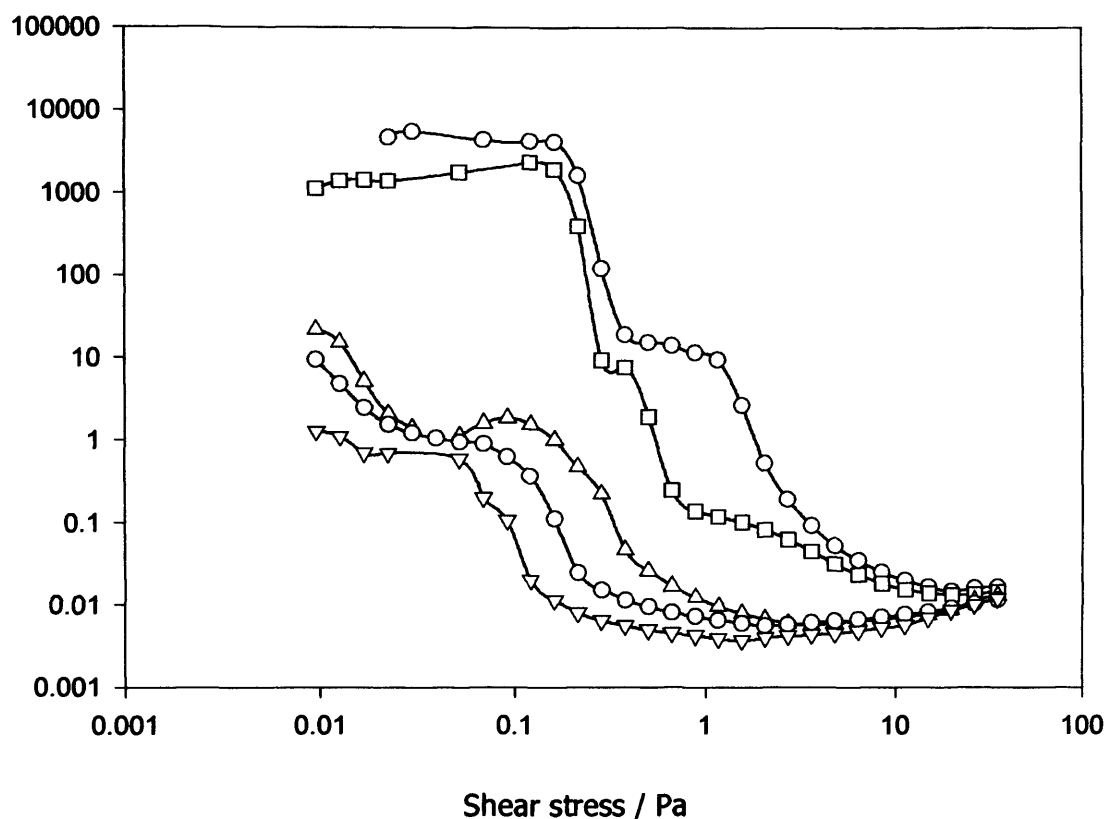


Fig 6.5(b): Typical viscosity-shear stress curves for the "fractal" Raven[®] M carbon black particles in aqueous polymer solutions at a fixed [polymer]/[particle] as a function of $\varphi_{particle}$; i.e. (O) $\varphi_{particle} = 0.15$, (□) $\varphi_{particle} = 0.128$, (Δ) $\varphi_{particle} = 0.114$, (○) $\varphi_{particle} = 0.10$ and (∇) $\varphi_{particle} = 0.092$.

Similar viscosity-shear stress behaviour is observed for all systems; a Newtonian region that shear thins above a critical point, passing through some intermediate plateau before approaching a common viscosity at high shear stresses. On dilution, the viscosity at low shear rates decreases significantly, an effect that is more pronounced for the Raven L particle (fig 6.5(a)). Note also that as the particle concentration is decreased, the intermediate Newtonian plateau shifts to lower shear rates until around $\varphi_{particle} \approx 0.10$, it cannot be distinguished.

6.6: Oscillatory rheology

Oscillation experiments were undertaken on these samples at various oscillation frequencies and amplitudes. The shear stress sweep experiments, figs 6.6(a) and 6.6(b) showed that the linear viscoelastic regions extend only over a very narrow range of shear stress. The complex viscosity of the Raven M particle (fig 6.6(b)) is slightly higher than that of the Raven L particle (fig 6.6(a)). Also, the apparent "yield" of the Raven M particle is slightly higher than the Raven L one, but otherwise the two behaviours are rather similar. As illustrated by the oval Lissajous plots, both systems are viscous at low shear stresses (a purely viscous response would be spherical, whereas an elastic response would be a diagonal line) but become elastic at higher shear stresses.

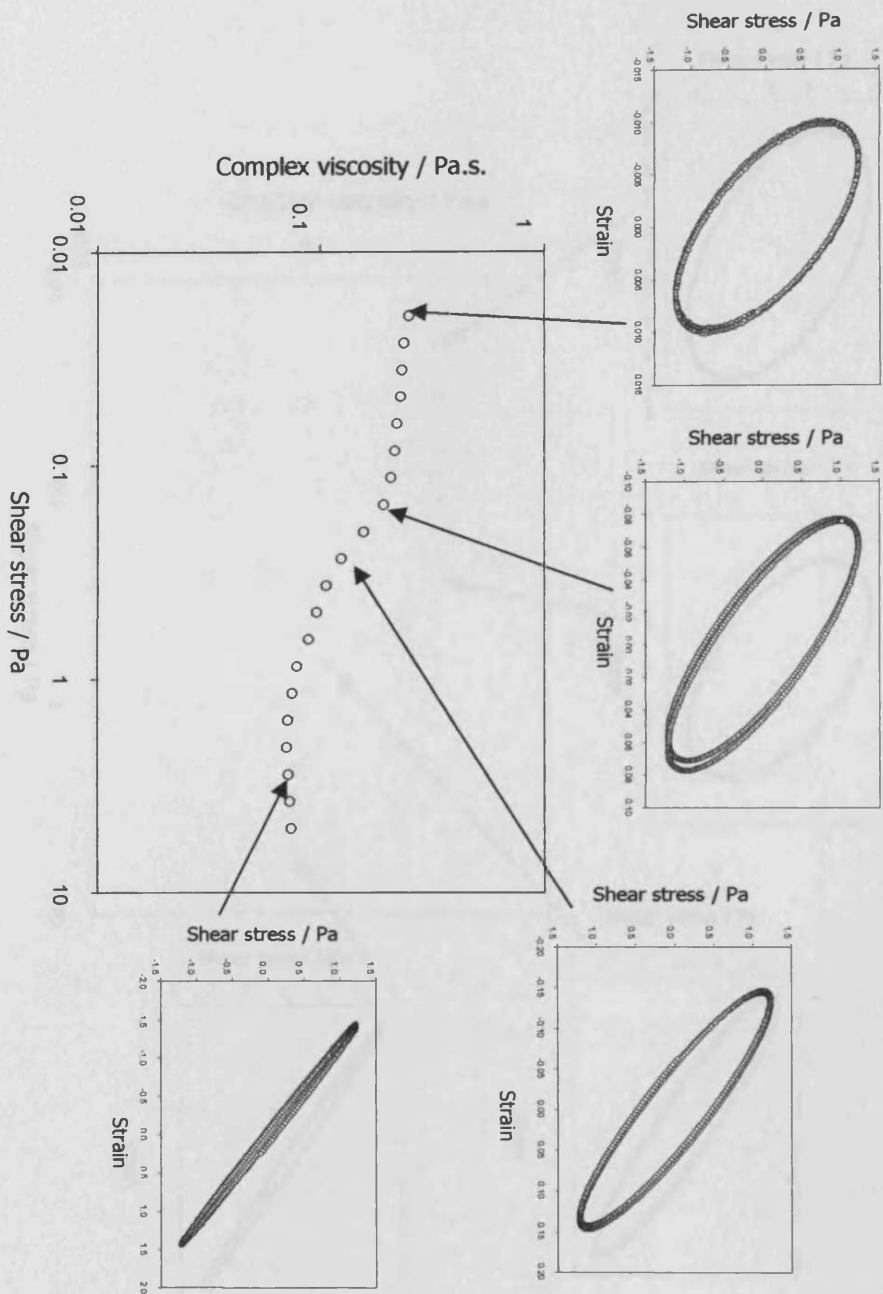


Figure 6.6(a): Typical shear stress sweep data and associated Lissajous plots at 1 Hz for a dispersion of "spherical" Raven® L particles, $\phi_{\text{particle}} = 0.15$, $\phi_{\text{polymer}} = 0.053$.

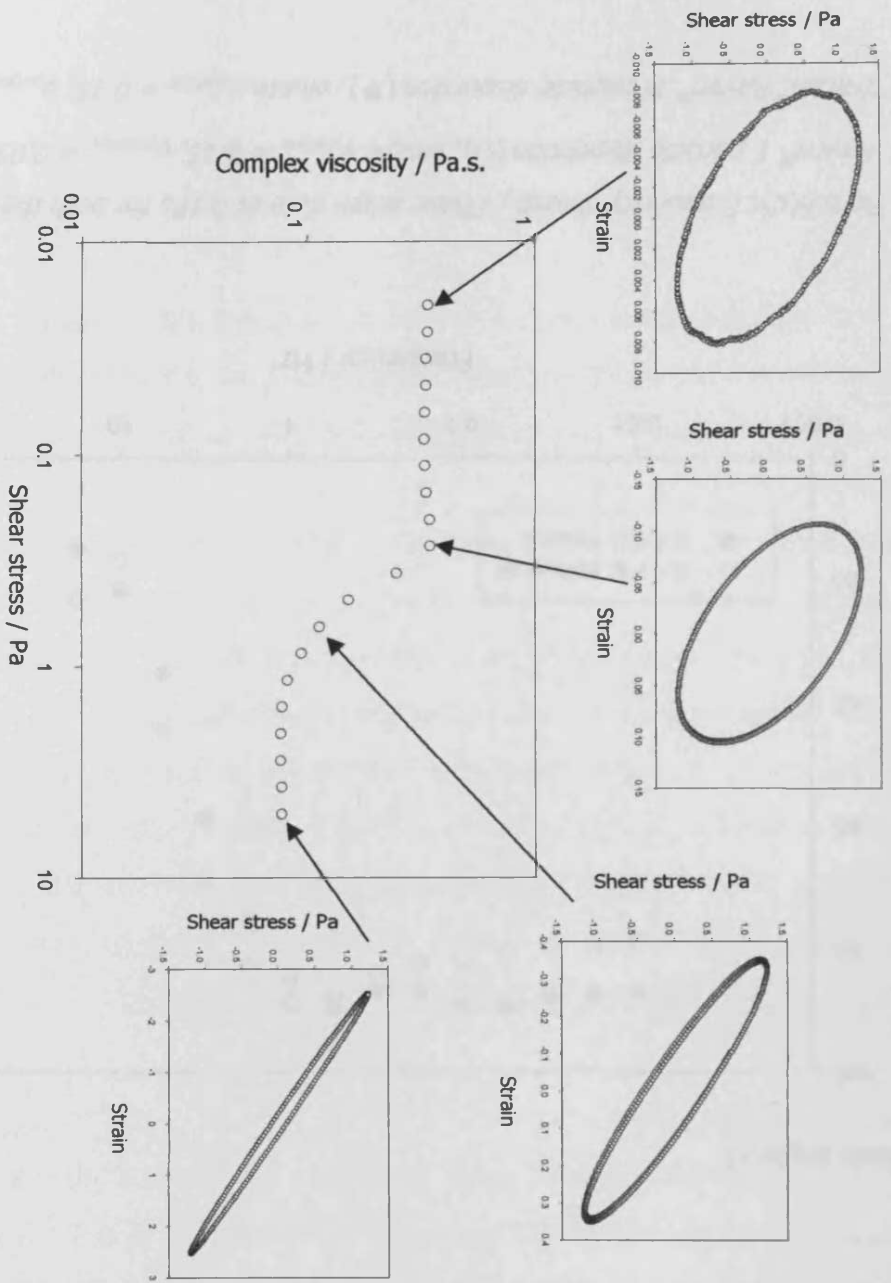


Figure 6.6(b): Typical shear stress sweep data and associated Lissajous plots at 1 Hz for a dispersion of "Fractal" Raver® M particles, $\phi_{particle} = 0.15$, $\phi_{polymer} = 0.053$.

The frequency response is presented in fig 6.6(c) for the $\phi_{\text{particle}} = 0.15$, $\phi_{\text{polymer}} = 0.053$ Raven L and Raven M dispersions at a shear stress of 0.1 Pa-toward the end of the Newtonian plateau. This representation concurs with the Lissajous data, namely that the response to deformation is viscous at low shear stresses/frequencies, but becomes more elastic with increasing shear.

Phase angle / °

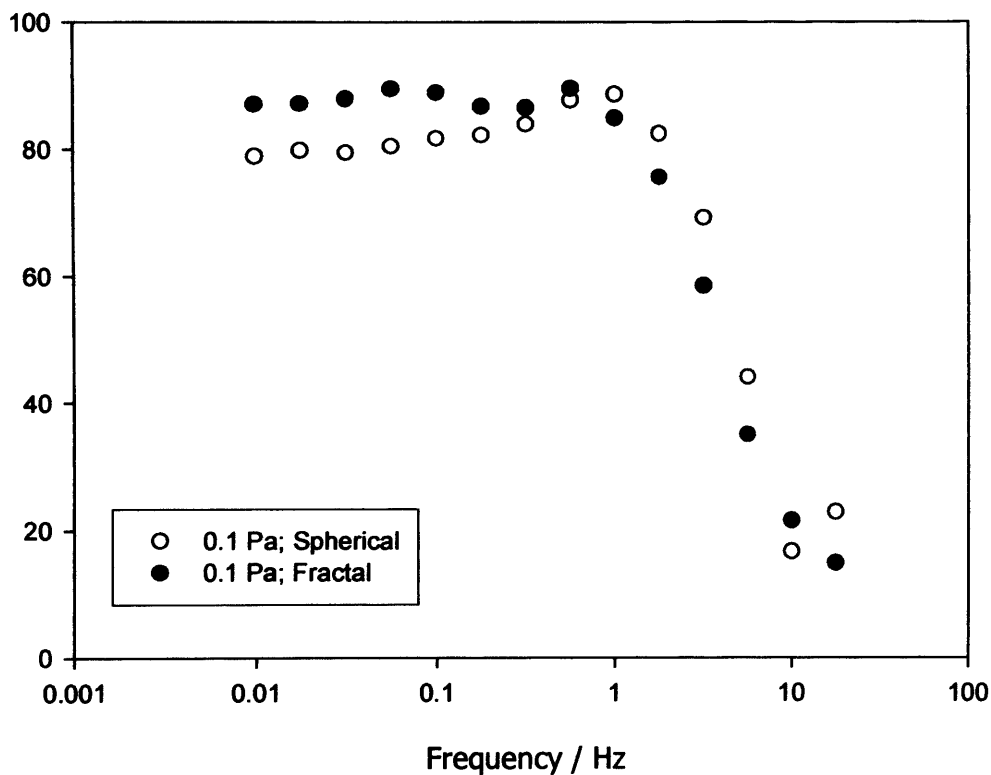


Fig 6.6(c): *Frequency sweep / Phase angle data at 0.1Pa for both the "spherical" Raven[®] L particle dispersion (O), where $\phi_{\text{particle}} = 0.15$, $\phi_{\text{polymer}} = 0.053$, and the "fractal" Raven[®] M particle dispersion (●), where $\phi_{\text{particle}} = 0.15$, $\phi_{\text{polymer}} = 0.053$.*

Summary:

The aqueous J61/carbon black systems described above have, from the experiments conducted, been well characterised which has allowed a greater

insight into the interactions present within the system. Aspects that were studied which allowed this improved understanding were: the effect of the polymeric binder content, the particle loading, the particle/polymer ratio, the role of the particles and how their structure can alter the rheology. The SANS measurements, the microscopy and the ultrasonic experiments proved useful in the characterisation and in the differentiation of the particle types, whereas the steady shear and oscillatory rheology assisted us in the understanding of the dispersion properties and the formation and deformation of a networked structure under shear.

6.7: The silica/poly(ethylene oxide) model system.

For comparison; a model system consisting of poly(ethylene oxide) chains adsorbed onto colloidal silica spheres has also been studied. Initially, the situation where full coverage of the silica particles had been obtained was considered i.e. with little or no free polymer left in the solution.

It has previously been reported that a coverage of 1mg m^{-2} (for this molecular weight) of poly(ethylene oxide) is required to coat silica⁷ so, based on this, the coverage for $\phi_{\text{particle}} = 0.2$ was calculated and the rheology of a concentrated silica dispersion with poly(ethylene) oxide at full coverage (approx 3wt% polymer) was measured.

Fig 6.7(a) represents the rheological behaviour of an aqueous silica solution, an aqueous poly(ethylene oxide) solution and an aqueous solution consisting of poly(ethylene oxide) adsorbed onto the colloidal silica particles.

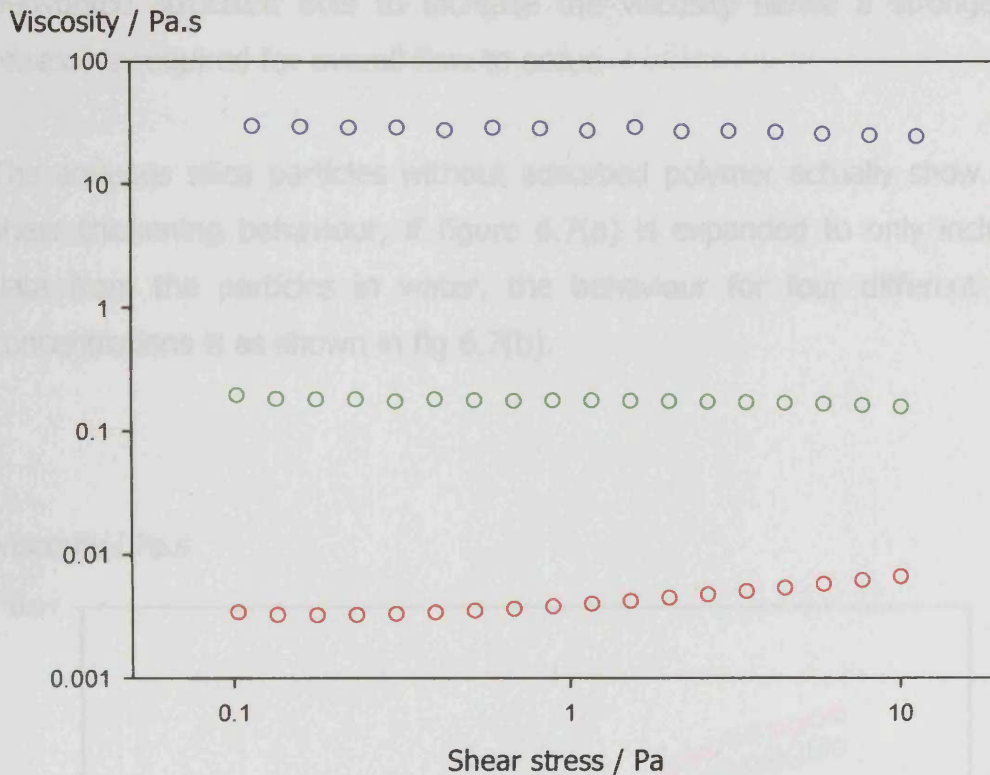


Fig 6.7(a): Typical viscosity-shear stress curves for silica in an aqueous poly(ethylene oxide) solution with (○) $\varphi_{particle} = 0.2$ and $\varphi_{polymer} = 0.03$, (○) a poly(ethylene oxide) solution with $\varphi_{polymer} = 0.03$ and (○) an aqueous silica solution with $\varphi_{particle} = 0.2$.

As can be seen from fig 6.7(a) the aqueous particle dispersion has the lowest viscosity and displays a weak shear thickening, followed by the 3wt% PEO in water solution. The solution consisting of adsorbed PEO onto silica had an increased viscosity, some two orders of magnitude higher than the polymer solution. This can be explained by considering the interaction between the polymer-coated particles. On absorption of a polymer layer to a particle surface, the effective size of the particle is increased. The distance between nearest neighbours in a concentrated system is therefore reduced, increasing the interaction between them and hence increasing the viscosity of the

system. Also, on adding particles to a polymer matrix a more viscous network is often formed, where the particles act as junction points or nodes. This networked structure acts to increase the viscosity hence a stronger force (stress) is required for overall flow to occur.

The aqueous silica particles without adsorbed polymer actually show a weak shear thickening behaviour, if figure 6.7(a) is expanded to only include the data from the particles in water, the behaviour for four different particle concentrations is as shown in fig 6.7(b).

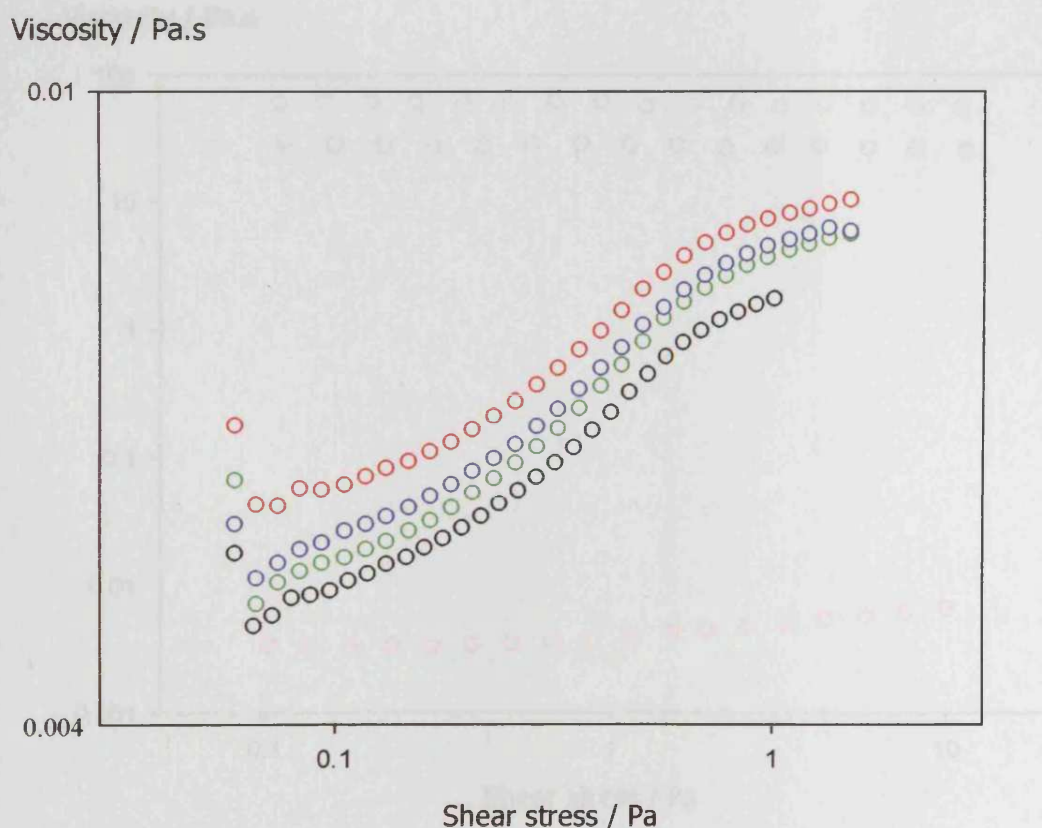


Fig 6.7(b): Typical viscosity-shear stress curves for silica in aqueous solution with (○) $\varphi_{particle} = 0.2$, (○) $\varphi_{particle} = 0.14$, (○) $\varphi_{particle} = 0.08$ and (○) $\varphi_{particle} = 0.04$.

Following the initial study (where full coverage of the silica particles had been obtained, with little or no free polymer left in the solution) a study concerning the situation where the concentration of polymer within the solution was well above the calculated "full coverage" value. In this system, there will be an excess of polymer that remains in the bulk.

Figure 6.7(c) represents the rheological behaviour of an aqueous silica solution, an aqueous poly(ethylene) oxide solution and an aqueous solution consisting of poly(ethylene) oxide adsorbed onto the colloidal silica particles in the presence of an excess of polymer (free polymer).

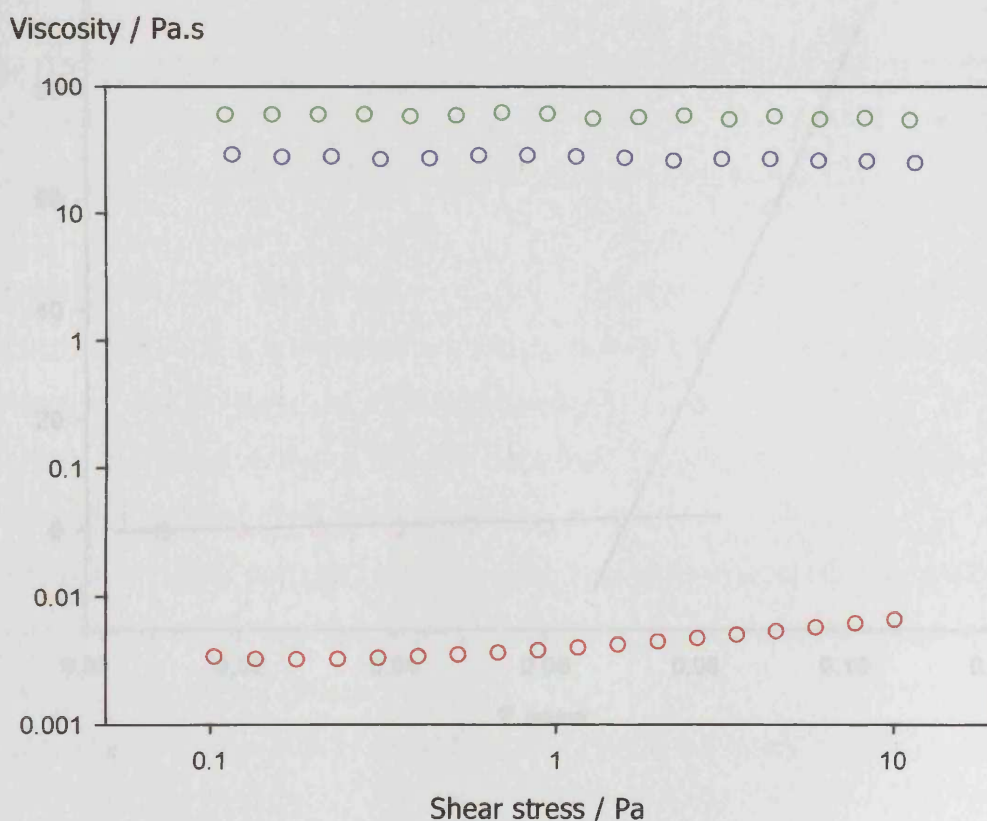


Fig 6.7(c): Typical viscosity-shear stress curves for silica in an aqueous poly(ethylene oxide) solution with (○) $\varphi_{\text{particle}} = 0.2$ and $\varphi_{\text{polymer}} = 0.10$, (○) a poly(ethylene oxide) solution with $\varphi_{\text{polymer}} = 0.10$ and (○) an aqueous silica solution with $\varphi_{\text{particle}} = 0.2$.

As can be seen from fig 6.7(c) the aqueous particle dispersion has the lowest viscosity and displays a weak shear thickening (as before), followed by the solution consisting of absorbed PEO onto silica in the presence of free polymer. In this case the PEO in water solution has the highest viscosity. Fig 6.7(d) represents the viscosity of the simple PEO solutions. For all concentrations the response is largely Newtonian over the shear stress range measured, with the viscosity increasing with increasing concentration.

Newtonian viscosity / Pa.s

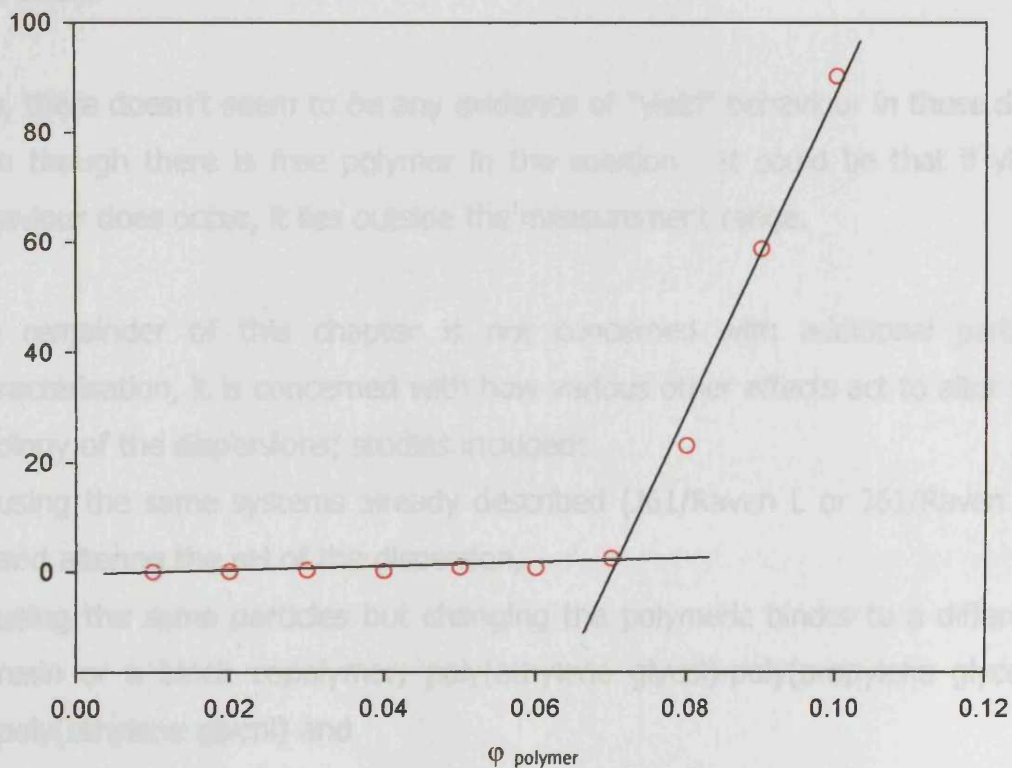


Fig 6.7(d): Viscosity-polymer volume fraction behaviour for aqueous poly(ethylene oxide) solutions.

The viscosity- concentration scaling behaviour increases around $\phi_{\text{polymer}} 0.07$, indicating a strong interaction of the polymer chains and therefore C^* - the

critical overlap concentration and the possible onset for the formation of a polymer network.

Hence in this case at this high polymer concentration (10wt%), the PEO is highly entangled, this hinders the flow and results in a high viscosity. However, the viscosity is slightly lowered on adding silica particles. A portion of the polymer in solution will adsorb onto the particles, lowering the concentration of polymer in the bulk hence decreasing the extent of entanglement and lowering the resulting viscosity. For this system, it seems that any excess polymer in solution somewhat surprisingly appears to have little effect

Also, there doesn't seem to be any evidence of "yield" behaviour in these data even though there is free polymer in the solution. It could be that if yield behaviour does occur, it lies outside the measurement range.

The remainder of this chapter is not concerned with additional particle characterisation, it is concerned with how various other effects act to alter the rheology of the dispersions; studies included:

- using the same systems already described (J61/Raven L or J61/Raven M) and altering the pH of the dispersion,
- using the same particles but changing the polymeric binder to a different resin or a block copolymer; poly(ethylene glycol)-poly(propylene glycol)-poly(ethylene glycol) and
- using different particle types that have or have not been surface modified.

These experiments were conducted in the hope that the results would provide a reinforced picture of how the interactions between the filler particles and the polymeric binder and also the filler-filler interactions within a dispersion, ultimately determine the resulting rheological properties of the dispersion.

6.8: The effect of changing the pH

To study the effect of pH proved quite difficult for the systems of interest.

Without adjustment, the acrylic resin polymer solution (Joncryn 61) has a pH of 8.3 and is formulated as an ammoniacal solution with $\phi_{\text{polymer}} = 0.35$ with the following solvent composition by weight: ammonia (25% solution) 9.5%, isopropanol 3.0%, propylene glycol 1.5% and water 51.0%.

In an attempt to produce a more acidic solution, dilute HCl was added dropwise, however even an adjustment to pH 6 rendered the polymer unstable and caused it to "crash" out of solution. Fig 6.8(a) shows a joncryn 61 solution at both pH 12 (left) and pH 4(right)



Fig 6.8(a): *Joncryn 61 solution with the pH adjusted to 12 (left) using an ammonia solution and pH 4 (right) using dilute HCl. The solution without any pH adjustment is at pH 8.3 and looks identical to that of the pH 12 solution.*

As a result, there is no rheological data corresponding to acidic joncryn 61 solutions. In order to obtain a more basic solution, a 35% ammonia solution was added dropwise.

Fig 6.8(b) represents the changing rheological behaviour that accompanies a pH change from a solution at pH 8.3 to pH 12 for both Raven L and Raven M particle dispersions.

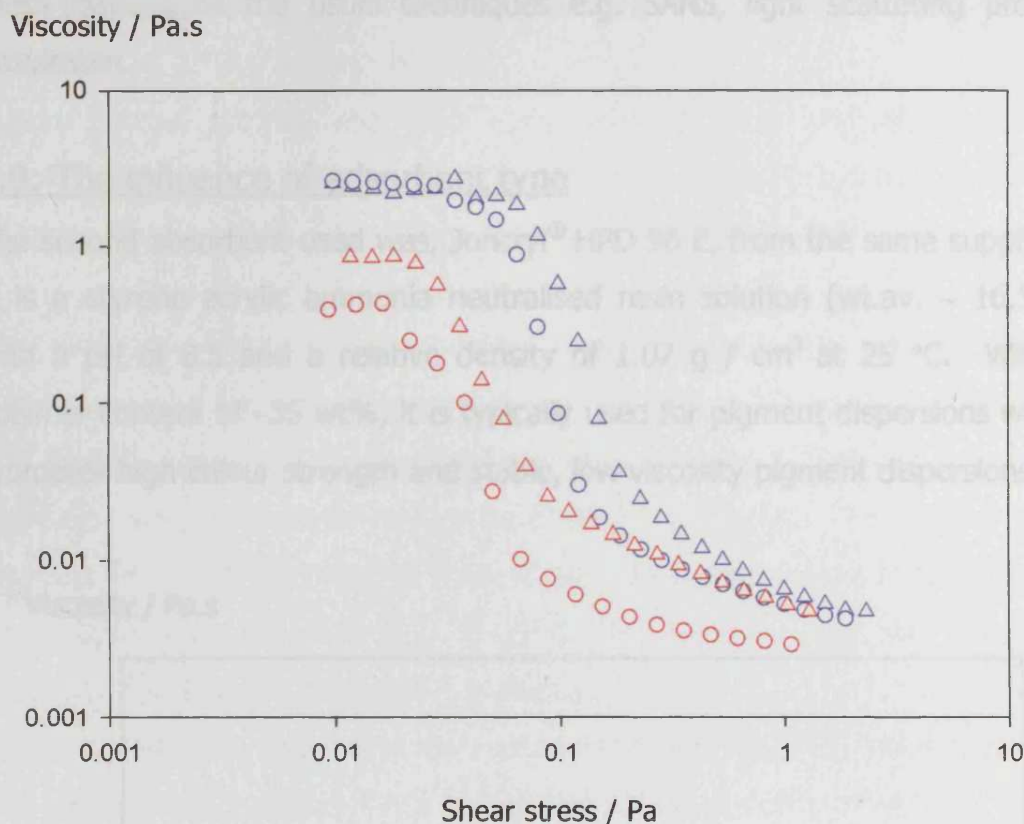


Fig 6.8(b): Typical viscosity-shear stress curves for both the "fractal" Raven[®] M and "spherical" Raven L carbon black particles in aqueous polymer solutions with $\phi_{\text{particle}} = 0.15$ and $\phi_{\text{polymer}} = 0.053$ where (Δ) Raven M at pH 12 (modified using a 35% ammonia solution), (\circ) Raven M at pH 8, (Δ) Raven L at pH 12 and (\circ) Raven L at pH 8.

It appears that altering the pH of the system has a relatively small effect on the rheology of the carbon black dispersions. Having said this however, the effect is slightly more pronounced for the Raven L particle dispersion than for the Raven M. A possible explanation is that increasing the pH results in the increase of the negative charge on the carbon black surface, the interaction between the polymer and particle is then increased resulting in the increase of coverage and the stiffening of the polymer chains. This leads to the thickness of the adsorbed polymer layer being increased, where the "enlargement" of

the particle acts to increase the solution viscosity. However, for this system the layer thickness could not be measured. Due to the colour and opacity of these dispersions the usual techniques e.g. SANS, light scattering proved unsuitable.

6.9: The influence of adsorbent type

The second adsorbent used was, Joncryl[®] HPD 96 E, from the same suppliers. It is a styrene acrylic ammonia neutralised resin solution (wt.av. ~ 16,500) with a pH of 8.5 and a relative density of 1.07 g / cm³ at 25 °C. With a polymer content of ~35 wt%, it is typically used for pigment dispersions which promotes high colour strength and stable, low viscosity pigment dispersions.

Viscosity / Pa.s

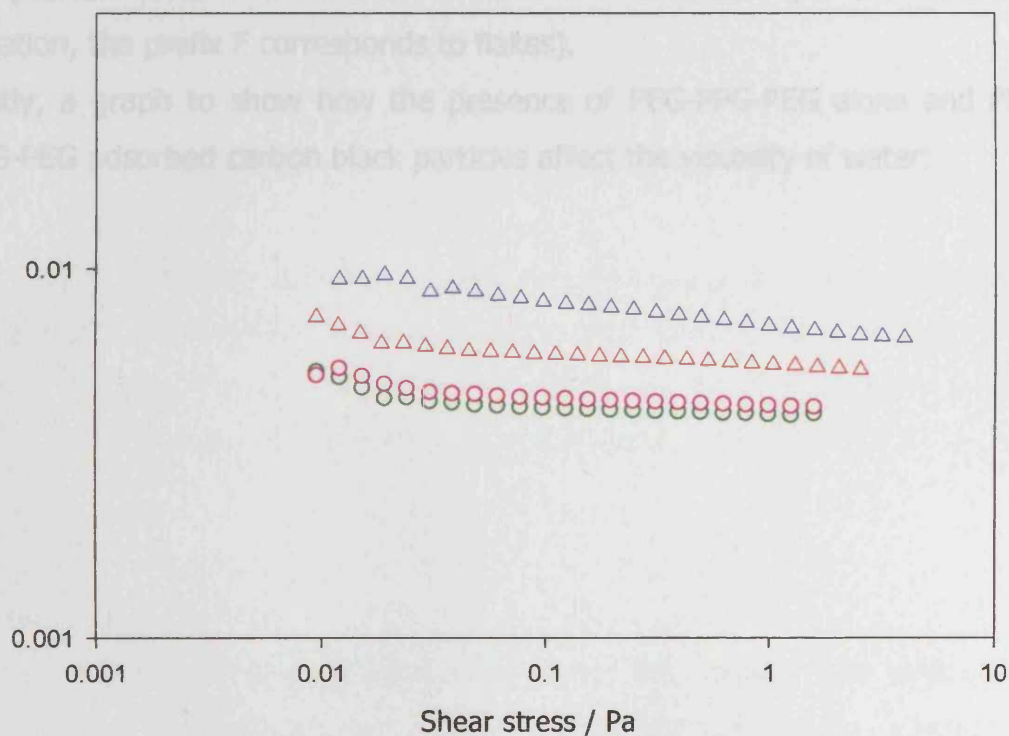


Fig 6.9(a): Typical viscosity-shear stress curves for aqueous dispersions of carbon black and JHPD-96E $\phi_{particle} = 0.15$ and $\phi_{polymer} = 0.105$ for (Δ) Raven M, (Δ) Raven L, (○) R1060 and (○) R760.

All dispersions displayed an approximate Newtonian behaviour and the typical rheology associated with concentrated dispersions was not observed. Also, the viscosity exhibited by the dispersions consisting of Joncryl® HPD 96 E in place of Joncryl® 61 was much lower.

Following the studies with the resin solutions, the rheology of block copolymers, Poly(ethylene glycol)-poly(propylene glycol)-poly(ethylene glycol) in particular, adsorbed onto carbon black was the next area of study.

Poly(ethylene glycol)-poly(propylene glycol)-poly(ethylene glycol) block copolymers are non-ionic macromolecular surface-active agents. PEG-PPG-PEG is also known as a pluronic block copolymer that is available in a range of molecular weights and differing ratios of PEG/PPG blocks. The polymer used here has the shorthand label of F 68, it had a molecular weight of 8,400 and a composition ratio of 80% PEG to 20% PPG content. (In the shorthand notation, the prefix F corresponds to flakes).

Firstly, a graph to show how the presence of PEG-PPG-PEG alone and PEG-PPG-PEG adsorbed carbon black particles affect the viscosity of water:

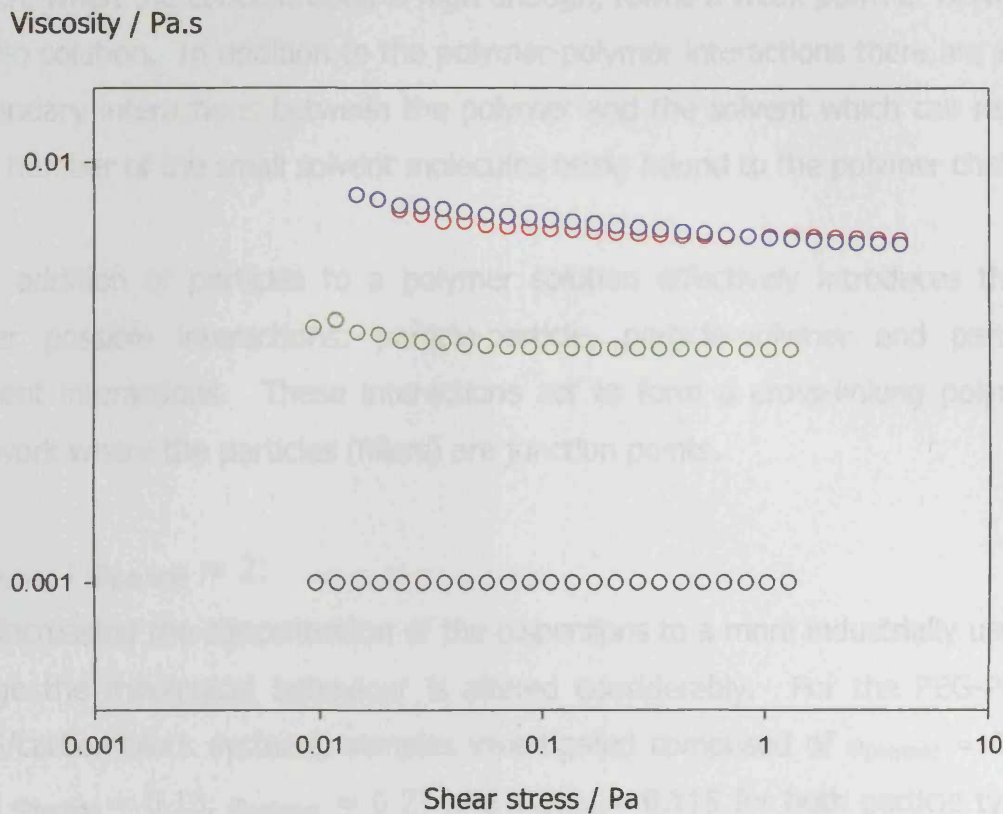


Fig 6.9(b): Typical viscosity-shear stress curves for aqueous dispersions of PEG-PPG-PEG and PEG-PPG-PEG adsorbed onto carbon black particles at room temperature, where (○) Raven M $\phi_{particle} = 0.10$, PEG-PPG-PEG $\phi_{polymer} = 0.10$, (○) Raven L $\phi_{particle} = 0.10$, $\phi_{polymer} = 0.10$, (○) $\phi_{polymer} = 0.10$ and (○) is distilled water.

$$\phi_{polymer} : \phi_{particle} = 1:$$

All data were approximately Newtonian, hence the viscosity was independent of the shear stress/shear rate. However, the viscosity of the polymer and particle solution (which showed slight shear thinning) was greater than that of the polymer solution, which in turn had a greater viscosity than the viscosity of pure water. For the polymer solution, the polymer-polymer interactions must be considered. In solution the polymer is in the form of coils, which act to hinder the motion of the small solvent molecules. When the concentration of polymer is low, this effect is not so apparent, but as the concentration is

increased, polymer overlapping increases the interactions between chains which, when the concentration is high enough, forms a weak polymer network within solution. In addition to the polymer-polymer interactions there are also secondary interactions between the polymer and the solvent which can result in a number of the small solvent molecules being bound to the polymer chains.

The addition of particles to a polymer solution effectively introduces three other possible interactions: particle-particle, particle-polymer and particle solvent interactions. These interactions act to form a cross-linking polymer network where the particles (fillers) are junction points.

$\phi_{\text{polymer}} : \phi_{\text{particle}} = 2:$

On increasing the concentration of the dispersions to a more industrially useful range the rheological behaviour is altered considerably. For the PEG-PPG-PEG/carbon black systems, samples investigated comprised of $\phi_{\text{polymer}} = 0.26$ and $\phi_{\text{particle}} = 0.13$, $\phi_{\text{polymer}} = 0.23$ and $\phi_{\text{particle}} = 0.115$ for both particle types (Raven L and M) and a dispersion consisting of $\phi_{\text{polymer}} = 0.26$ and $\phi_{\text{particle}}^{\text{Raven L}} = 0.065 + \phi_{\text{particle}}^{\text{Raven M}} = 0.065$ was also studied. These results can be seen in figure 6.9(c) (where the viscosity of a polymer solution consisting of $\phi_{\text{polymer}} = 0.26$ is included for comparison).

In essence, all of the systems in fig 6.9(c) show shear thinning behaviour with a high low shear viscosity. At low shear rates, the particles are less mobile and their random orientation within the solution promotes a tendency for an increased resistance to flow. Increasing the shear stress induces a velocity gradient in which the particles align with the flow direction, decreasing the resistance to flow and reducing the viscosity. On considering the Raven L (Δ) and Raven M (Δ) systems comprising of $\phi_{\text{polymer}} = 0.23$ and $\phi_{\text{particle}} = 0.115$ there are only a few points to notice. Firstly, the low shear viscosity of the Raven M dispersion is higher than that of the Raven L dispersion, but at high shear rates they both tend to the same value and secondly, the point at which the dispersion starts to shear thin (the yield point) is higher for the Raven M

(0.5 Pa compared to 0.14 Pa for Raven L) also. Shear thinning starts to become more uniform as the force/area increases until complete structural breakdown has occurred, resulting in the high shear, low viscosity Newtonian plateau.

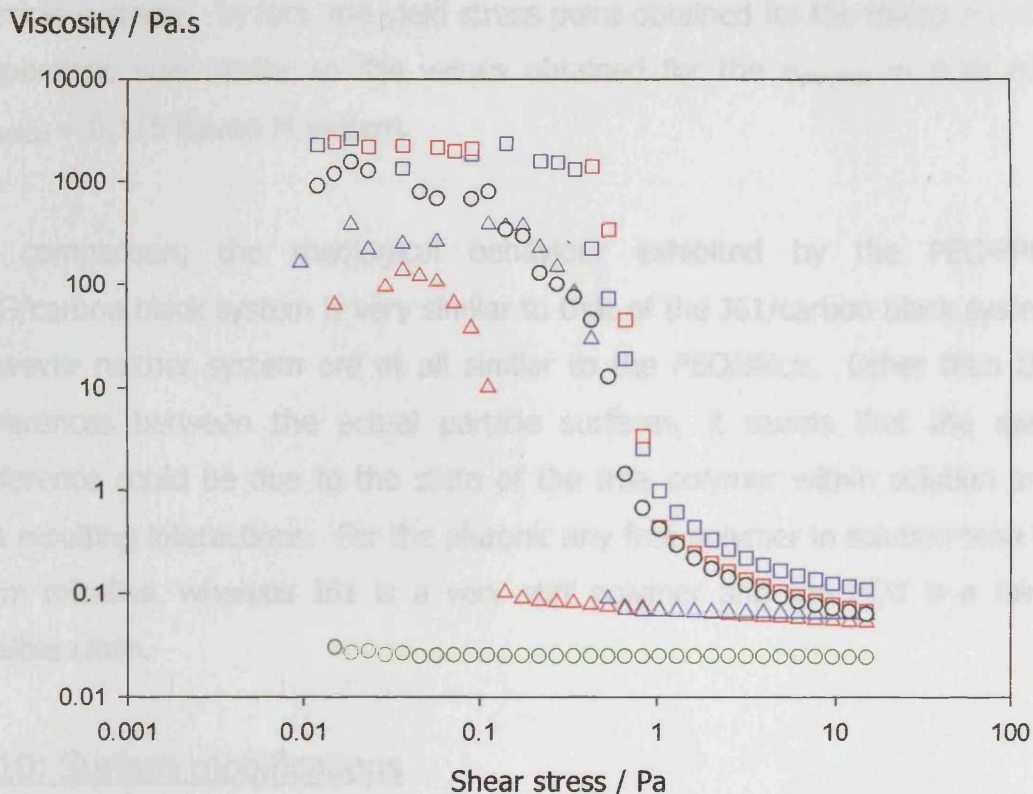


Fig 6.9(c): Typical viscosity-shear stress curves for carbon black particles in aqueous PEG-PPG-PEG polymer solutions with (\square) Raven M $\phi_{particle} = 0.13$ $\phi_{polymer} = 0.26$, (\square) Raven L $\phi_{particle} = 0.13$ $\phi_{polymer} = 0.26$, (\circ) Raven M $\phi_{particle} = 0.065$ Raven L $\phi_{particle} = 0.065$ $\phi_{polymer} = 0.26$ (Δ)Raven M $\phi_{particle} = 0.115$ $\phi_{polymer} = 0.23$, (Δ)Raven L $\phi_{particle} = 0.115$ $\phi_{polymer} = 0.23$ and (\circ) $\phi_{polymer} = 0.26$.

For the Raven L (\square) and Raven M (\square) dispersions consisting of $\phi_{polymer} = 0.26$ and $\phi_{particle} = 0.13$ the rheological behaviour is closely matched. At low shear, there is a negligible difference in the viscosity or the yield point at which the

dispersion begins to shear thin. However at high shear, the Raven M dispersion displays a higher viscosity than the Raven L dispersion, although both have higher viscosities than the same concentration polymer solution.

Combining the particle types into a mixed particle dispersion (O) where $\phi_{\text{polymer}} = 0.26$ and $\phi_{\text{particle "Raven L"}} = 0.065 + \phi_{\text{particle "Raven M"}} = 0.065$ reduces the low shear viscosity and the yield stress point compared to that of the single particle systems. In fact, the yield stress point obtained for the mixed particle dispersions was similar to the values obtained for the $\phi_{\text{polymer}} = 0.23$ and $\phi_{\text{particle}} = 0.115$ Raven M system.

In comparison, the rheological behaviour exhibited by the PEG-PPG-PEG/carbon black system is very similar to that of the J61/carbon black system however neither system are at all similar to the PEO/silica. Other than the differences between the actual particle surfaces, it seems that the main difference could be due to the state of the free polymer within solution and the resulting interactions. For the pluronic any free polymer in solution tend to form micelles, whereas J61 is a very stiff polymer and the PEO is a fairly flexible chain.

6.10: Surface modifications

The commonly found carbon-oxygen surface structures are by far the most important surface groups that influence the physico-chemical properties of carbon blacks. Further oxidation of pigment blacks produces increased polar chemical groups on the particle surface area, which possess a higher affinity to the polar groups of binders. This especially applies to carboxyl groups. The treatment thus produces better dispersion and stabilization of the pigment black in the liquid phase and better distribution in a polymer matrix.

Fig 6.10 illustrates the effect of modifying the particle surface on the rheology of carbon black dispersions. For this study, the particles R760 and R1060 were used. The particles R760 and R1060 are identical in the way they have been formed hence their particle size, aggregate size and structure are very

similar, however R1060 has been surface oxidised using ozone. R1060 has an extended built up layer of chemisorbed oxygen at the surface which is a result of the decomposition of ozone gas.

The rheology data for identical Raven L and Raven M dispersions have also been included for comparison.

Viscosity / Pa.s

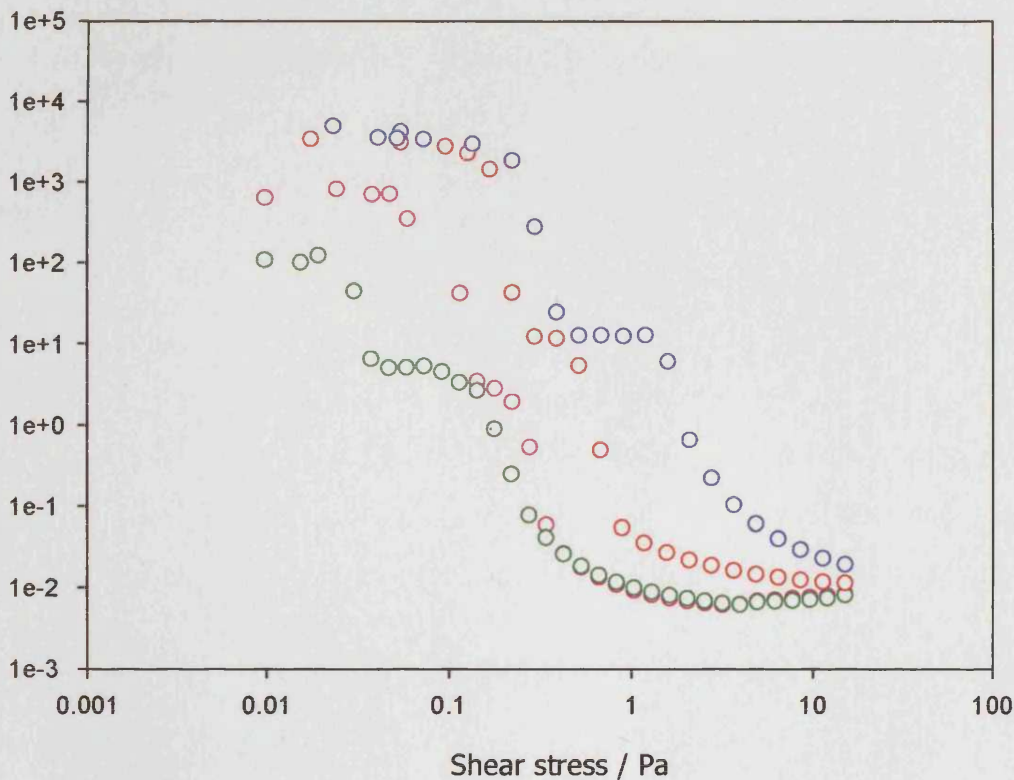


Fig 6.10: Typical viscosity-shear stress curves for aqueous dispersions of carbon black and joncryl 61 (J61) $\varphi_{particle} = 0.15$ and $\varphi_{polymer} = 0.105$ for (○) Raven M, (○) Raven L, (○) R1060 and (○) R760.

R1060 and R760 have a smaller average aggregate diameter than both Raven L and Raven M. Therefore, the dispersions formed using these particles exhibit a lower low shear viscosity, lower yield stress point and a lower high shear viscosity than the larger Raven grades. As mentioned previously, R1060

and R760 are identical grades, so the observed differences between the rheology of the R1060 dispersion and the R760 dispersion are due to the excess chemisorbed oxygen on the R1060. This excess oxygen layer acts to increase the low shear viscosity and the yield stress point however the high shear viscosities for both particle dispersions are practically identical. The excess chemisorbed oxygen on the R1060 renders the surface more active, increasing the surface/polymer attraction which affects the mode and extent of polymer adsorption to the surface and hence increasing the surface coverage.

References:

- ¹ Buscall, R., McGowan, J.I., Morton-Jones, A.J., *J. Rheol.*, 37(4), 1993
- ² Beaucage, G., *J. Appl. Crystallogr.*, 29, (1996), 134-146.
- ³ Lin, Y., Smith, T.W., Alexandridis, P., *Langmuir*, 18, (2002), 6147-6158
- ⁴ Gerspacher, M., O'Farrell, C.P., *Elastomerics*, 123, (4), (1991), 35-39
- ⁵ Buckin, V.A., Smyth, C., *Sem. Food Anal.*, 4, (2), 89-105
- ⁶ Buckin, V.A., Kankiya, B.I., Rentzeperis, D., Marky, L., *J. Am. Chem. Soc.*, 116, 9423-9429
- ⁷ Zaman, A.A., Bjelopavlic, M., Moudgil, B.M., *J. Colloid Interface Sci.*, 226, 290-298, (2000)

CHAPTER 7: RESULTS AND DISCUSSION-OIL

DISPERSIONS

In addition to being used extensively in the waterborne inks and coatings industry, carbon black is also commonly employed for the production of oil based inks. This chapter will focus, primarily, on oil based carbon black dispersions. The binder, in this case, is bitumen.

For the initial rheology study, four carbon black grades were used; Raven L, Raven M, N660 and N772.

Raven L and N772 are low-medium structured particles and Raven M and N660 are medium-high structured particles. The two Raven grades are fine to medium particles, whereas N772 and N660 are coarser grades.

For each sample a dry bead vehicle containing 24.5wt% Bitumen in oil was prepared using an industrial grade mixer. Once mixed, this was left to settle for 24hours before preparing a mill base. The mill base was prepared by taking 105g of the dry bead vehicle and adding to that 45g of carbon black particles using a high shear mixer. After cooling, 75g of this mill base was mixed with a further 50g of oil. This mixture was triple roll milled three times to ensure a sufficient dispersion. It was ensured that the grind gauge values were below 5 μ m. For all four particles, this meant that 18wt% particle stock samples in oil were prepared. The rheology of these 18wt% samples was investigated and the stocks were then diluted with oil to various carbon black loadings.

The aim of this study was to;

- Investigate the rheology of the dispersions with respect to the particle concentration.
- To combine the particle systems in different quantities and combinations in order to investigate the rheology of mixed particle systems (containing both fine and coarse particles) and to compare the results with the rheology of the single grade systems (see chapter 8).

The cone and plate geometry was used to investigate the rheology of these samples due to their high viscosities. All measurements were carried out at 25°C.

7.1: Rheology-oil medium

Firstly, the rheology of the dispersion medium (the oil) used for the dilutions was investigated (fig 7.1). The rheology of the oil is Newtonian with a viscosity of approximately 0.6 Pa.s @ 25°C.

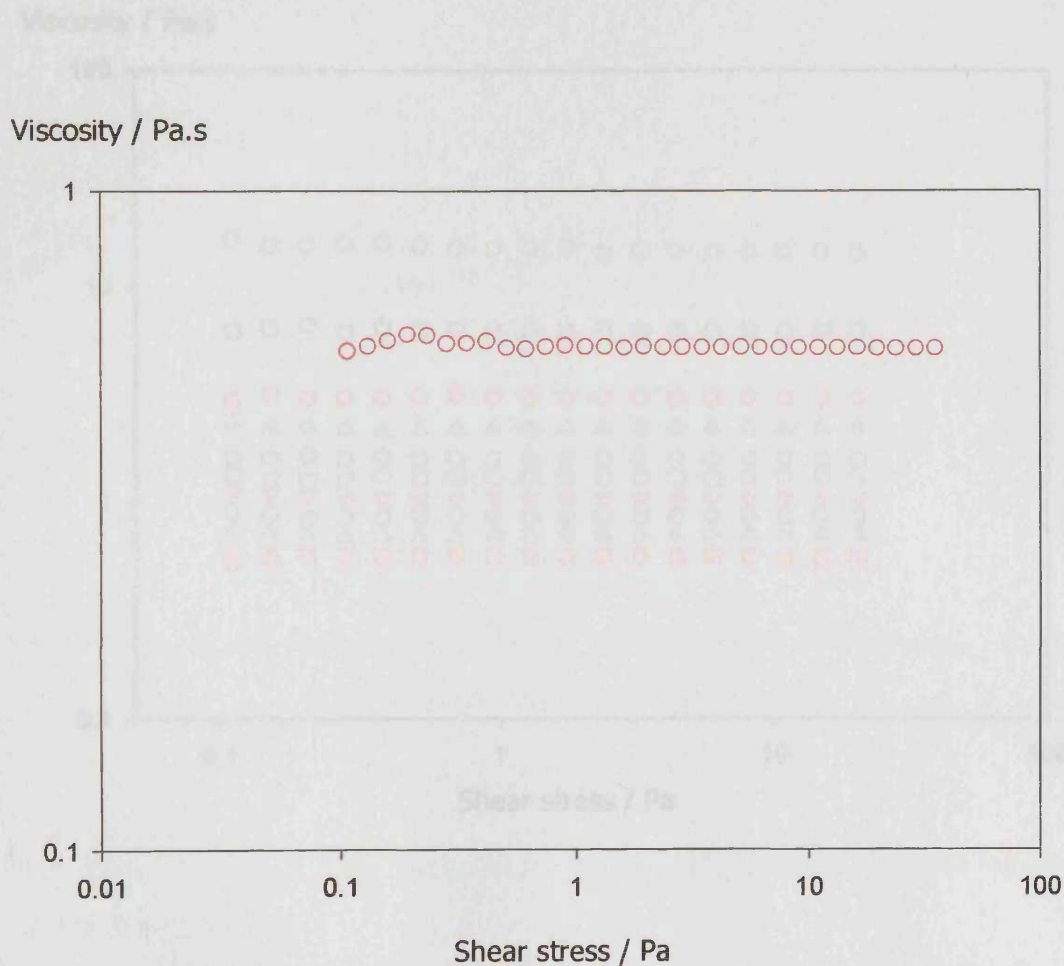


Fig 7.1: Typical viscosity-shear stress curve for the oil used in the dilution of the stock, $\phi_{particle} = 0.18$, carbon black dispersions.

7.2: Rheology-Polymeric binder in solution

Secondly, the rheology of simple solutions, comprising of varying amounts of bitumen in oil were examined. For all concentrations, the response is largely Newtonian (to a first approximation at least) over the majority of the shear stress range, fig 7.2(a), and the average viscosity increases with bitumen content, fig 7.2(b).

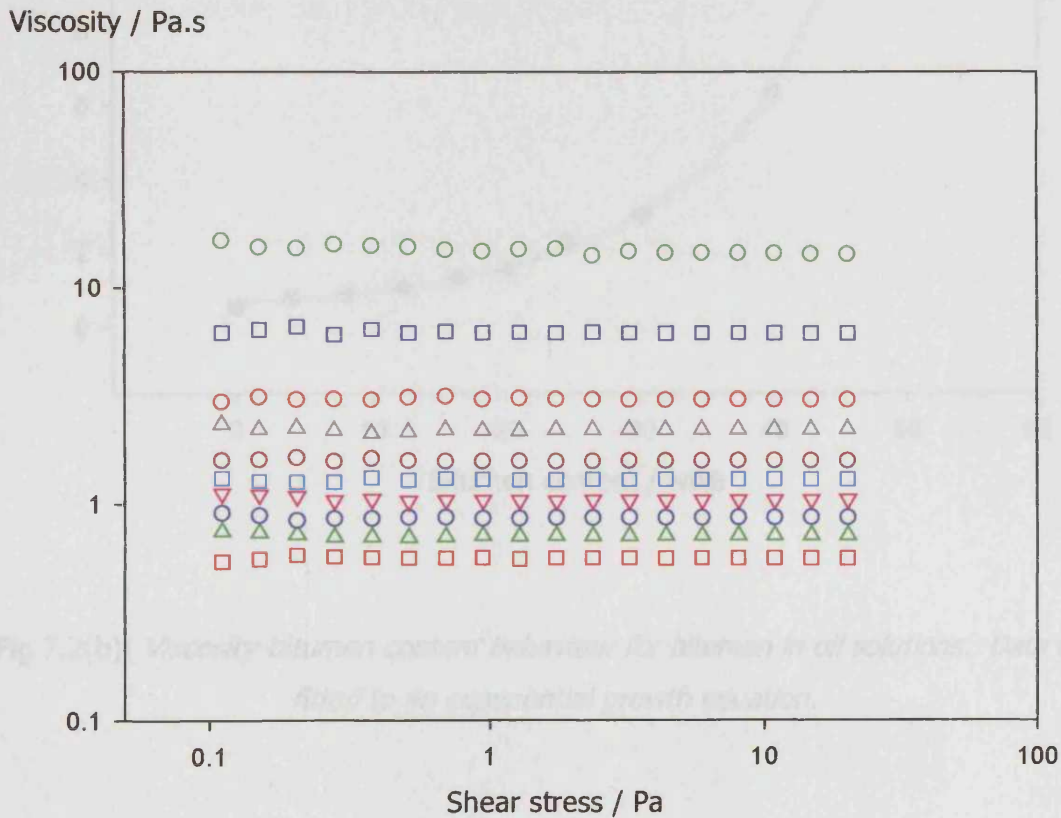


Fig 7.2(a) Viscosity-bitumen content behaviour for bitumen in oil solutions. The data was fitted to the exponential growth equation.

Fig 7.2(a): A series of viscosity-shear stress curves for a series of different concentration bitumen in oil solutions i.e. (O) $\phi_{\text{bitumen}} = 0.50$, (□) $\phi_{\text{bitumen}} = 0.40$, (○) $\phi_{\text{bitumen}} = 0.30$, (Δ) $\phi_{\text{bitumen}} = 0.245$, (○) $\phi_{\text{bitumen}} = 0.20$, (□) $\phi_{\text{bitumen}} = 0.16$, (∇) $\phi_{\text{bitumen}} = 0.12$, (○) $\phi_{\text{bitumen}} = 0.08$, (Δ) $\phi_{\text{bitumen}} = 0.04$ and (□) oil.

Average viscosity / Pa.s

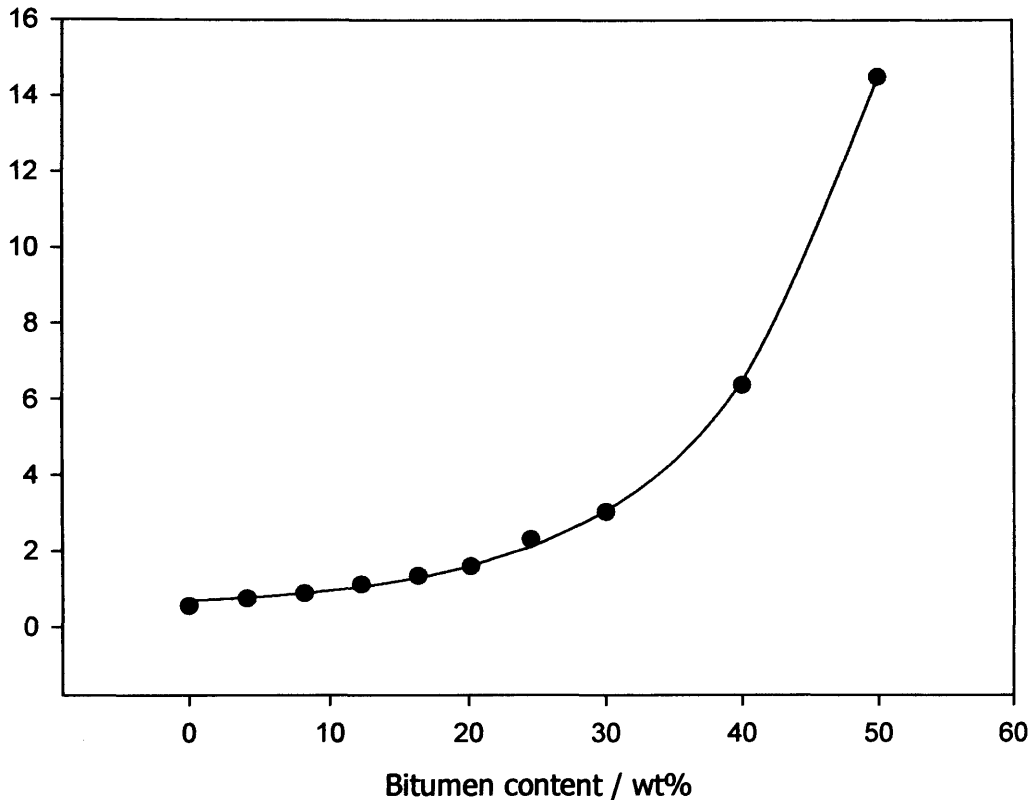


Fig 7.2(b): *Viscosity-bitumen content behaviour for bitumen in oil solutions. Data was fitted to an exponential growth equation.*

The data in fig 7.2(b) was fitted to an exponential growth equation represented as:

$$Y=Y_0 + a e^{bx} \quad (6.1)$$

Where Y is the average viscosity and x is the concentration of bitumen. However this was for the purpose of guiding the eye only and the parameters obtained have no significance.

7.3: Rheology-carbon black dispersions

Figures 7.3(a), 7.3(b), 7.3(c) and 7.3(d) represent the full data sets for all four different particle types (Raven L, Raven M, N660 and N772 respectively). Here the stock solutions containing $\phi_{\text{particle}} = 0.18$ and $\phi_{\text{bitumen}} = 0.106$ in oil were diluted using additional oil. Therefore, the ratio of particles to bitumen was kept constant (at approximately 1.7), however the concentration of both particles and bitumen was gradually decreased.

Figure 7.3(a) shows the full rheology data for Raven L:

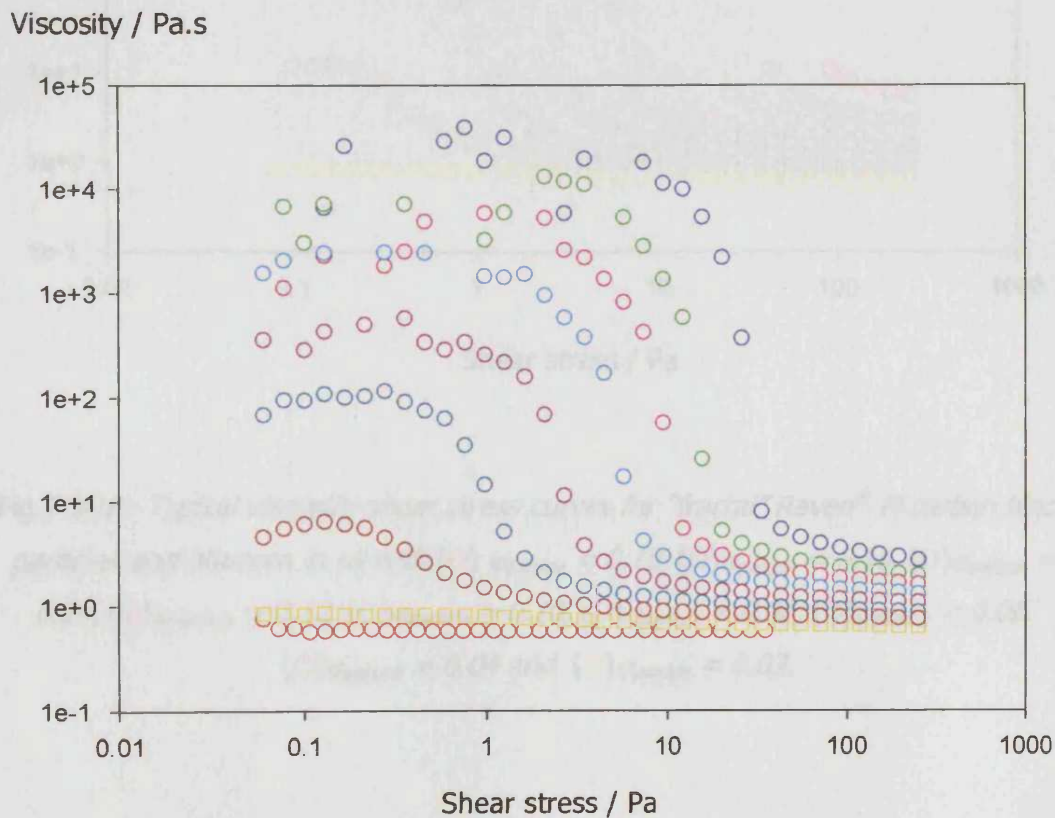


Fig 7.3(a): Typical viscosity-shear stress curves for "spherical" Raven[®] L carbon black particles and bitumen in oil with (○) $\phi_{\text{particle}} = 0.16$, (○) $\phi_{\text{particle}} = 0.14$, (○) $\phi_{\text{particle}} = 0.12$, (○) $\phi_{\text{particle}} = 0.10$, (○) $\phi_{\text{particle}} = 0.08$, (○) $\phi_{\text{particle}} = 0.06$, (○) $\phi_{\text{particle}} = 0.04$, (○) $\phi_{\text{particle}} = 0.02$ and (○) $\phi_{\text{particle}} = 0.00$ (the oil medium).

Fig 7.3(b) shows the full data for Raven M:

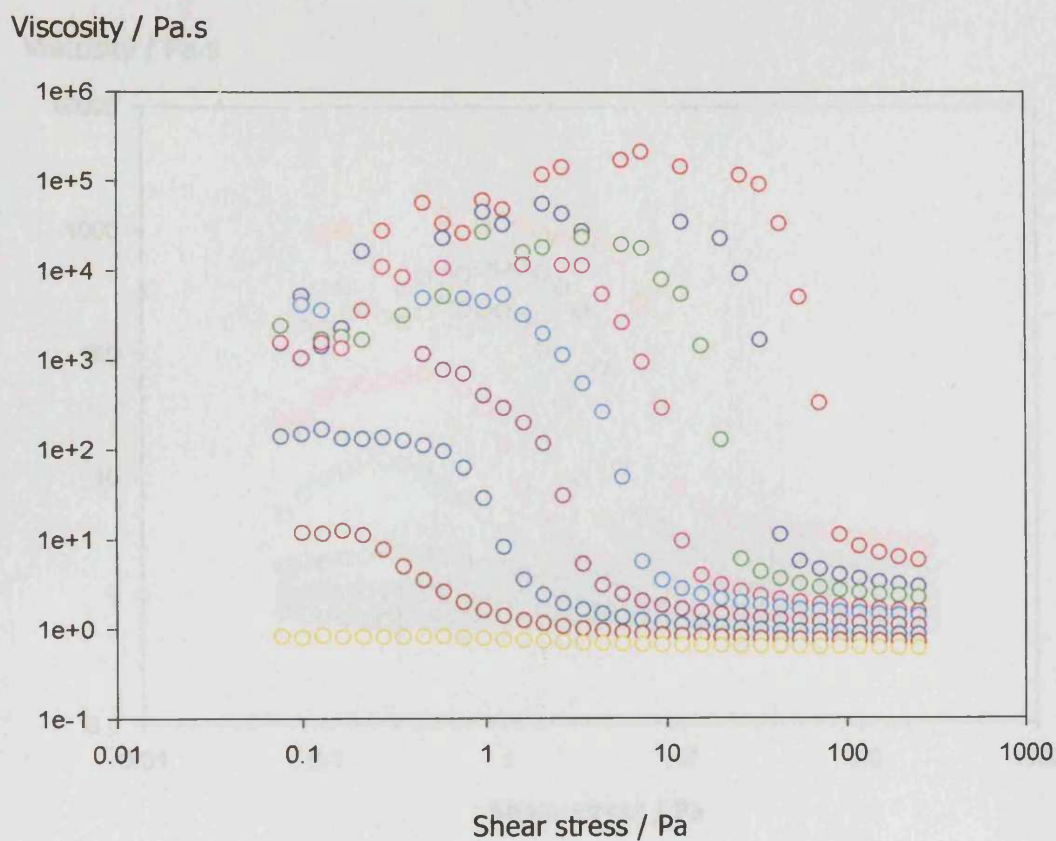


Fig 7.3(b): Typical viscosity-shear stress curves for "fractal" Raven[®] M carbon black particles and bitumen in oil with (○) $\phi_{particle} = 0.18$, (○) $\phi_{particle} = 0.16$, (○) $\phi_{particle} = 0.14$, (○) $\phi_{particle} = 0.12$, (○) $\phi_{particle} = 0.10$, (○) $\phi_{particle} = 0.08$, (○) $\phi_{particle} = 0.06$, (○) $\phi_{particle} = 0.04$ and (○) $\phi_{particle} = 0.02$.

Fig 7.3(c) shows the full data for N660:

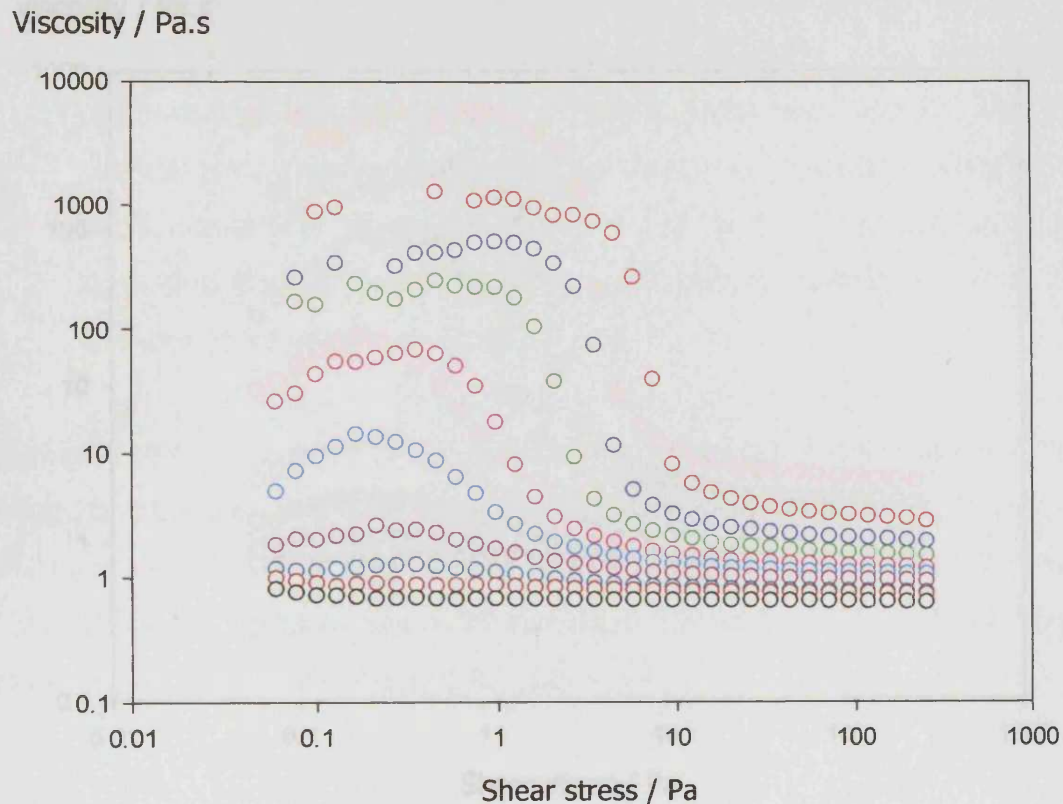


Fig 7.3(c): Typical viscosity-shear stress curves for the coarse N660 carbon black particles and bitumen in oil with (○) $\phi_{particle} = 0.18$, (○) $\phi_{particle} = 0.16$, (○) $\phi_{particle} = 0.14$, (○) $\phi_{particle} = 0.12$, (○) $\phi_{particle} = 0.10$, (○) $\phi_{particle} = 0.08$, (○) $\phi_{particle} = 0.06$, (○) $\phi_{particle} = 0.04$ and (○) $\phi_{particle} = 0.02$.

Inspection of figure 7.3(a) illustrates a few more features:

- On decreasing the particle concentration, the overall viscosity is also decreased.
- For lower particle concentrations, the "shear thinning" region is not so pronounced. The low shear viscosity decreases on decreasing the particle concentration, this again, is due to a reduction in the particle/particle and particle/polymer interactions. The high shear

Fig 7.3(d) shows the full data for N772:

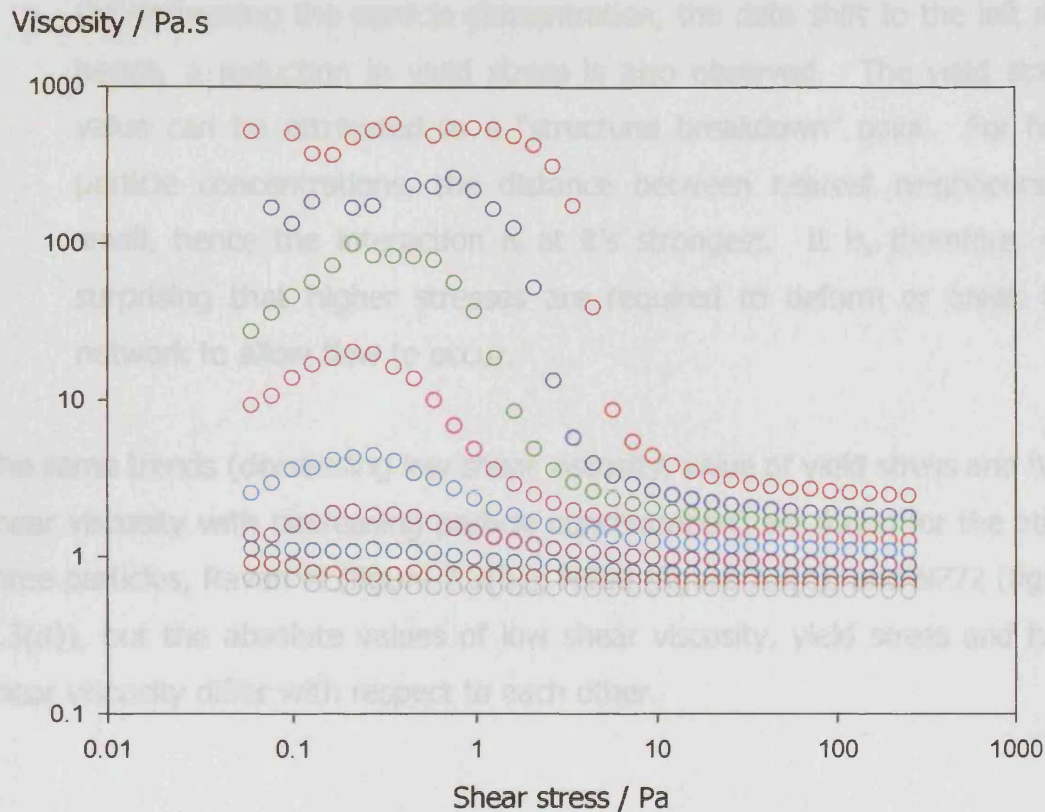


Fig 7.3(d): Typical viscosity-shear stress curves for the coarse N772 carbon black particles and bitumen in oil with $(\circ) \phi_{particle} = 0.18$, $(\circ) \phi_{particle} = 0.16$, $(\circ) \phi_{particle} = 0.14$, $(\circ) \phi_{particle} = 0.12$, $(\circ) \phi_{particle} = 0.10$, $(\circ) \phi_{particle} = 0.08$, $(\circ) \phi_{particle} = 0.06$, $(\circ) \phi_{particle} = 0.04$ and $(\circ) \phi_{particle} = 0.02$.

Inspection of figure 7.3(a) illustrates a few more features;

- On decreasing the particle concentration, the overall viscosity is also decreased.
- For lower particle concentrations, the "shear thinning" region is not so pronounced. The low shear viscosity decreases on decreasing the particle concentration, this again, is due to a reduction in the particle/particle and particle/polymer interactions. The high shear

viscosity tends to a common value (that of the oil), so the “jump” down is not as significant and leads to a less pronounced shear thinning region.

- On decreasing the particle concentration, the data shift to the left and hence, a reduction in yield stress is also observed. The yield stress value can be attributed to a “structural breakdown” point. For high particle concentrations, the distance between nearest neighbours is small, hence the interaction is at it’s strongest. It is, therefore, not surprising that higher stresses are required to deform or break the network to allow flow to occur.

The same trends (decreasing low shear viscosity, value of yield stress and high shear viscosity with decreasing particle concentration) are found for the other three particles, Raven M (figure 7.3(b)), N660 (figure 7.3(c)) and N772 (figure 7.3(d)), but the absolute values of low shear viscosity, yield stress and high shear viscosity differ with respect to each other.

7.4: Comparison of particle types

To compare the particle types, a single common particle concentration was plotted for all particles and the results are shown in figure 7.4(a). The same trends applied to all of the concentrations, so $\phi_{\text{particle}} = 0.10$ and $\phi_{\text{bitumen}} = 0.06$ was picked as being typical.

Viscosity / Pa.s

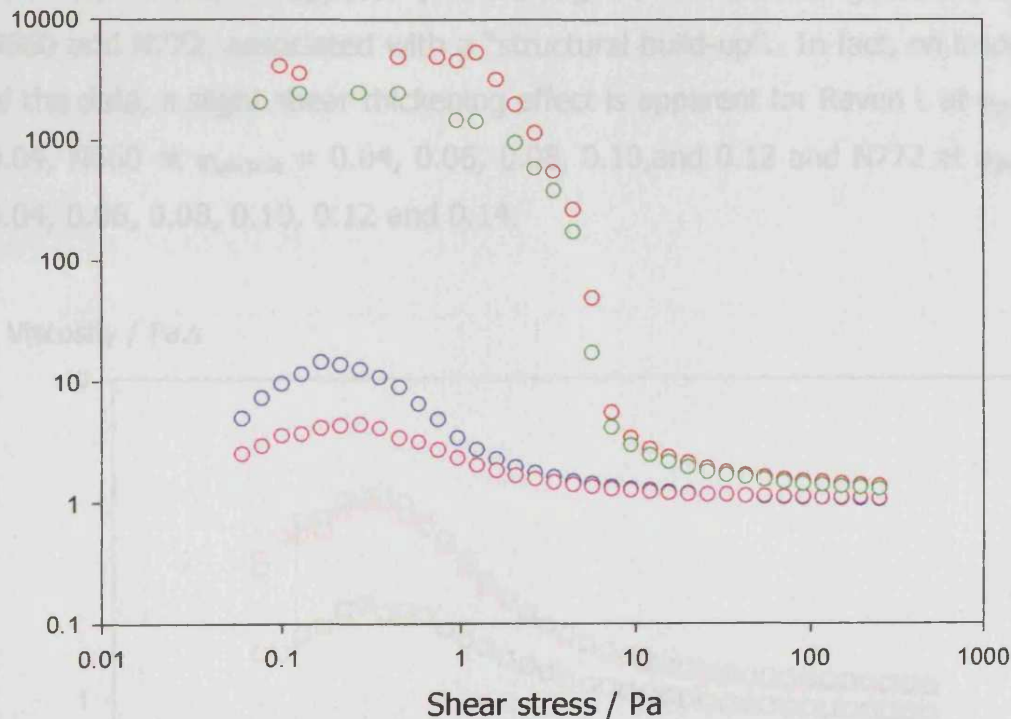


Fig 7.4(a): Typical viscosity-shear stress curves for dispersions of $\phi_{\text{bitumen}} = 0.06$ (○) Raven M $\phi_{\text{particle}} = 0.10$, (○) Raven L $\phi_{\text{particle}} = 0.10$, (○) N660 $\phi_{\text{particle}} = 0.10$ and (○) N772 $\phi_{\text{particle}} = 0.10$ carbon black particles in oil

It is apparent that the low shear viscosity, the yield stress and the high shear viscosity of Raven M > Raven L > N660 > N772.

The fine particles seem to have much higher viscosities than the coarser grades and the viscosity seems to increase with increasing structure e.g.

Raven M has a higher viscosity than Raven L because of the higher degree of structure. Raven L is composed of smaller more spherically shaped aggregates, Raven M is more "open" and the aggregates have no defined shape. In addition to the shape dependence, when considering the finer particle systems, there are a lot more of the particles per unit space than there are coarse ones. Hence, there are more "nodes" or "junction points" in the networked structure produced from these particle/polymer systems.

At low shear, there appears to be a slight shear thickening effect for both N660 and N772, associated with a "structural build-up". In fact, on inspection of the data, a slight shear thickening effect is apparent for Raven L at $\phi_{\text{particle}} = 0.04$, N660 at $\phi_{\text{particle}} = 0.04, 0.06, 0.08, 0.10,$ and 0.12 and N772 at $\phi_{\text{particle}} = 0.04, 0.06, 0.08, 0.10, 0.12$ and 0.14 .

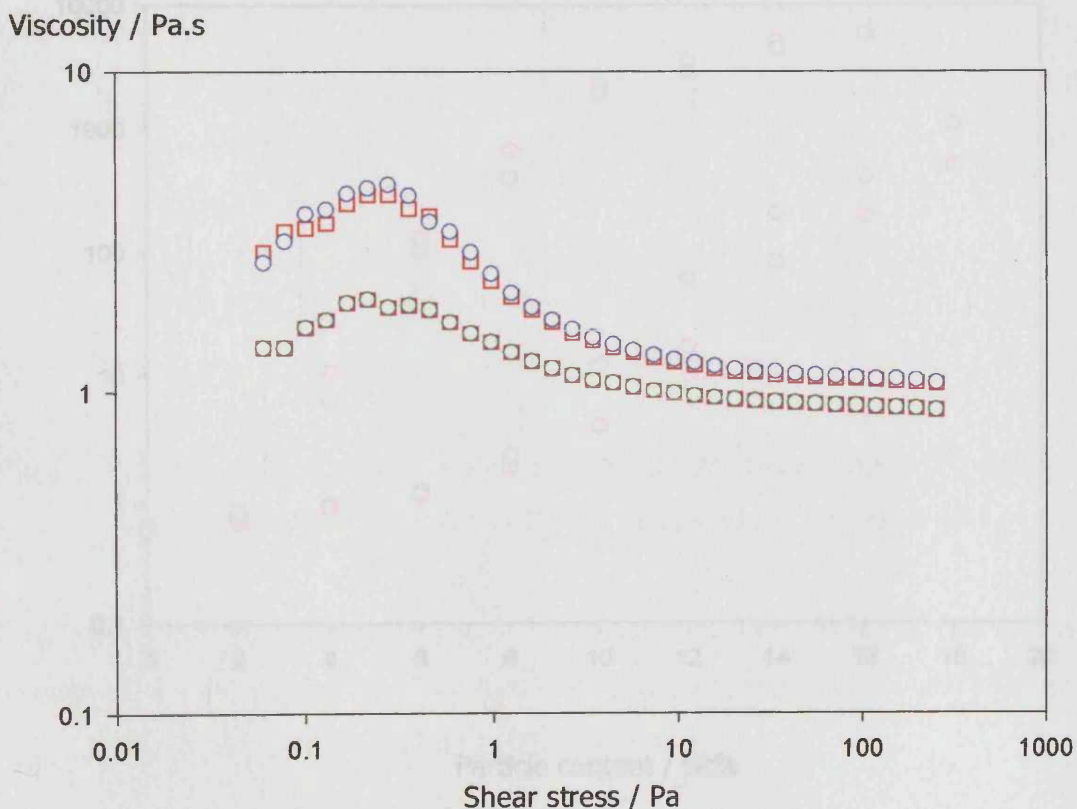


Fig 7.4(b): Typical viscosity-shear stress curves for dispersions of (O) N772 $\phi_{\text{particle}} = 0.10$, (□) repeat data for N772 $\phi_{\text{particle}} = 0.10$, (○) N772 $\phi_{\text{particle}} = 0.08$ and (□) repeat data for N772 $\phi_{\text{particle}} = 0.08$ carbon black particles and bitumen in oil.

Due to the reproducibility of the data as shown in fig 7.4(b), the slight shear thickening that is observed is attributed to an initial re-ordering of the particles, where they are encouraged to align with the direction of the applied force.

7.5: Low shear viscosity, high shear viscosity and yield stress

As shown earlier, there are three parameters that prove useful in comparing the rheology between concentrated dispersions: the low shear viscosity, the high shear viscosity and the yield stress. The following three figures (fig 7.5(a), fig 7.5(b) and fig 7.5(c)) represent these parameters respectively as a function of the particle concentration.

Low shear viscosity / Pa.s

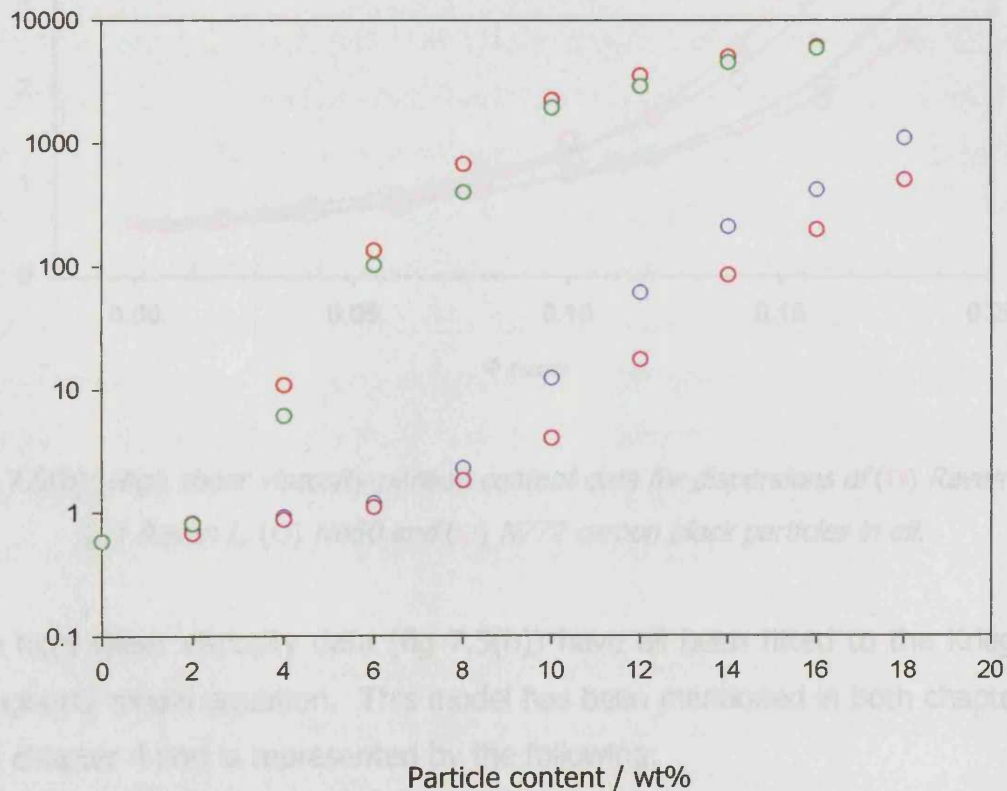


Fig 7.5(a): Low shear viscosity-particle content data for dispersions of (○) Raven M, (○) Raven L, (○) N660 and (○) N772 carbon black particles in oil.

The values obtained for the low shear viscosity (fig 7.5(a)) differed greatly hence a logarithmic scale has been used as the Y-axis. However, although the values differ by orders of magnitude, the shape of the data is essentially the same for all four particle types.

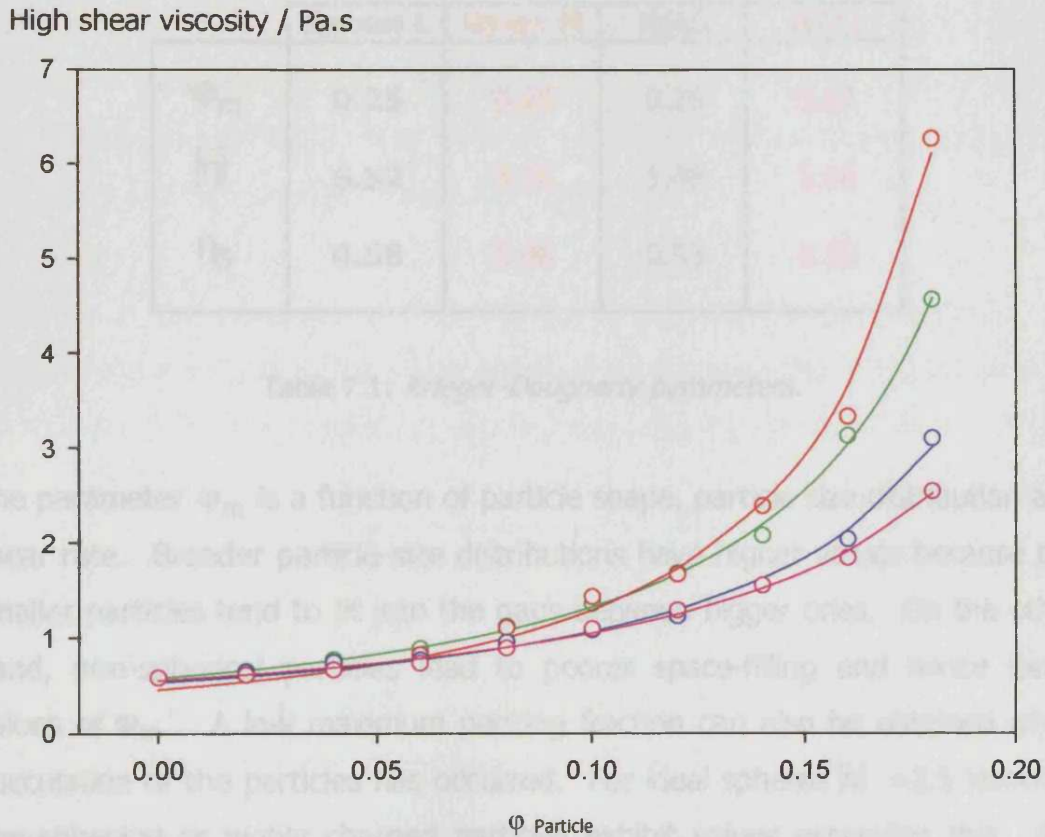


Fig 7.5(b): High shear viscosity-particle content data for dispersions of (○) Raven M, (○) Raven L, (○) N660 and (○) N772 carbon black particles in oil.

The high shear viscosity data (fig 7.5(b)) have all been fitted to the Krieger-Dougherty model equation. This model has been mentioned in both chapter 1 and chapter 4 and is represented by the following:

$$\eta_r = \eta_0 \left(1 - \frac{\phi}{\phi_m} \right)^{-[\eta]\phi_m} \tag{7.1}$$

where η_r is the relative viscosity, η_s is the viscosity of the solution in the

absence of particles, ϕ is the volume fraction, ϕ_m is the maximum packing fraction and $[\eta]$ is the intrinsic viscosity.

The values of ϕ_m , $[\eta]$ and η_s that were obtained from these fits are shown in table 7.1 for all four grades of carbon black used.

	Raven L	Raven M	N660	N772
ϕ_m	0.25	0.25	0.25	0.27
$[\eta]$	6.52	8.16	5.46	5.16
η_s	0.58	0.46	0.53	0.55

Table 7.1: Krieger-Dougherty parameters.

The parameter ϕ_m is a function of particle shape, particle size distribution and shear rate. Broader particle-size distributions have higher values because the smaller particles tend to fit into the gaps between bigger ones. On the other hand, non-spherical particles lead to poorer space-filling and hence lower values of ϕ_m . A low maximum packing fraction can also be obtained when flocculation of the particles has occurred. For ideal spheres $[\eta] = 2.5$ however non-spherical or highly charged particles exhibit values exceeding this. For example, the intrinsic viscosity has been reported as 2.7 for submicron spheres, but as high as 9-10 for laterite, glass rods and glass plates¹. The value of $[\eta]$ is also affected by the particle size distribution.

The results in table 7.1 show a low maximum packing fraction for all particle types, this is a consequence of the presence of non-spherical carbon black particles. However, the dispersion containing N772 particles had a slightly higher value. There is also a trend in $[\eta]$ where Raven M > Raven L > N660 > N772 and where all values of $[\eta]$ obtained are indicative of non-spherical particles. The two Raven grades are fine particle grades of similar size, with Raven M having a medium to high structure compared to low-medium for

Raven L, N660 and N772 are coarser grades consisting of larger particles, with N660 having a medium-high structure and N772 having a low-medium structure. Here, it seems that $[\eta]$ is dependent on, not only the "fineness" but, on the structure also. However, the "fineness" seems to be the more important variable. Fine particle grades contain more particles per unit area and therefore have a higher resistance to flow. Further examination of the parameters showed that the product of $[\eta]$ and Φ_m for each particle type did not vary a great deal (From 2 for Raven M to 1.6 for Raven L down to 1.4 for both N660 and N772). This product is useful for estimating suspension viscosities and has significant practical value.

Since η_s is the viscosity of the solution in the absence of particles, on constraining it's value to the value obtained for the viscosity of the oil medium (0.5807 Pa.s) the corresponding values of Φ_m and $[\eta]$ are shown in table 7.2:

	Raven L	Raven M	N660	N772
Φ_m	0.25	0.25	0.25	0.25
$[\eta]$	6.49	7.3	5.12	4.7

Table 7.2: *Constrained Krieger-Dougherty parameters.*

The maximum packing fraction was not altered much (if at all) on constraining the value of η_s , however the intrinsic viscosity values were all decreased.

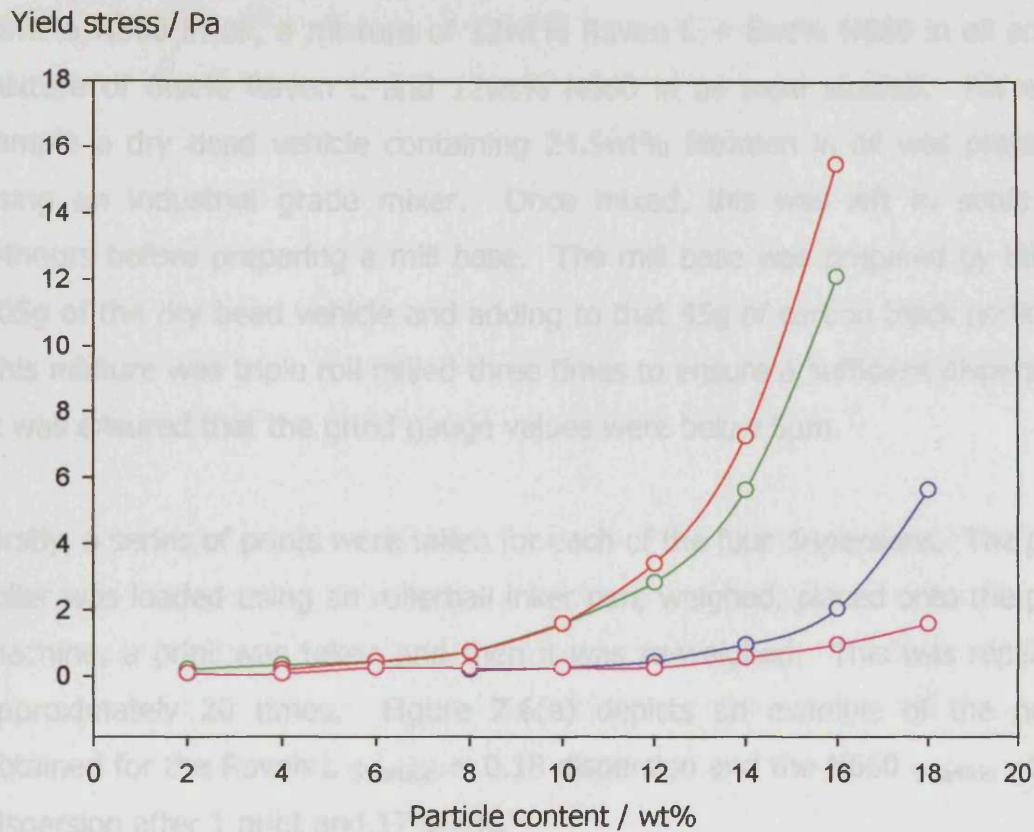


Fig 7.5(c): Yield stress-particle content data for dispersions of (O) Raven M, (O) Raven L, (O) N660 and (O) N772 carbon black particles in oil. The lines are to guide the eye only.

Here, the yield stress point is the stress value at which shear thinning commences. From the graph, at higher particle concentrations (12-18wt%) Raven M has greater yield stress values than Raven L. The two coarser particles have much lower values than Raven M and Raven L, but with N660 having slightly greater values than N772. The yield stress value is indicative of the strength of the network that has been formed between the polymer and the particles where a larger value indicates a stronger network and hence a greater stress is required for the initial breakdown. The shear thinning region is then observed on increasing the stress above the yield stress, where the network is gradually broken down to a greater extent. Eventually, the dispersion will flow freely.

7.6: Colour measurements:

For the colour measurements, systems comprising of 18wt% Raven L in oil, 18wt% N660 in oil, a mixture of 12wt% Raven L + 6wt% N660 in oil and a mixture of 6wt% Raven L and 12wt% N660 in oil were studied. For each sample a dry bead vehicle containing 24.5wt% Bitumen in oil was prepared using an industrial grade mixer. Once mixed, this was left to settle for 24hours before preparing a mill base. The mill base was prepared by taking 105g of the dry bead vehicle and adding to that 45g of carbon black particles. This mixture was triple roll milled three times to ensure a sufficient dispersion. It was ensured that the grind gauge values were below $5\mu\text{m}$.

Firstly, a series of prints were taken for each of the four dispersions. The print roller was loaded using an rollerball inker pen, weighed, placed onto the print machine, a print was taken and then it was re-weighed. This was repeated approximately 20 times. Figure 7.6(a) depicts an example of the prints obtained for the Raven L $\phi_{\text{particle}} = 0.18$ dispersion and the N660 $\phi_{\text{particle}} = 0.18$ dispersion after 1 print and 17 prints.

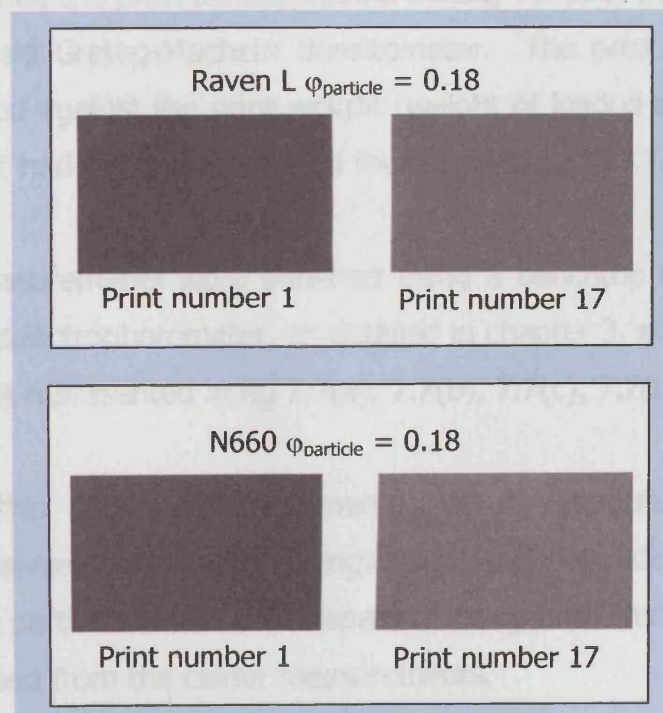


Fig 7.6(a): *The prints taken in preparation for the colour measurements.*

As can be seen from figure 7.6(a), print 1 is "more black" than print 17 for both particle types however the Raven L dispersion is "more black" than the N660 dispersion. The colour differences in matter are largely based on the interaction of light with electrons². The electrons in the graphitic layers of carbon black are free to vibrate at practically any frequency and thereby absorb all wavelengths of visible light ranging from infrared to ultraviolet. The degree of blackness in carbon blacks is dependent on the efficiency of re-emission of the light. If the particle size of the carbon black is small there is an increased amount of forward scattering. This makes the particles less efficient at re-emission, hence leading to greater light absorption.

All carbon blacks tend to selectively absorb the shorter wavelengths at the blue end of the spectrum³, however this is also dependent on particle size. The more absorbing small particles tend to reflect light of a brownish tone whereas the not-so-well absorbing larger particles reflect more of the spectrum and appear bluer in tone.

Using these prints, the print density/optical density for each print was obtained using a handheld Gretag-Macbeth densitometer. The print (optical) density was then plotted against the print weight (weight of loaded roller – weight of roller after print had been taken) for all four dispersions (fig 7.6(b)).

The colour measurements were obtained using a benchtop Hunter Labscan[®] XE automated spectrophotometer, as detailed in chapter 3, section 3.5.4. The data obtained is represented in fig 7.7(a), 7.7(b), 7.7(c), 7.7(d) and 7.7(e).

The aim of this series of experiments was to produce an **empirical** relationship between the colour strength of a particular dispersion and the composition of particles within that dispersion using both Hunter L and Hunter b values obtained from the colour measurements.

Print Density / D

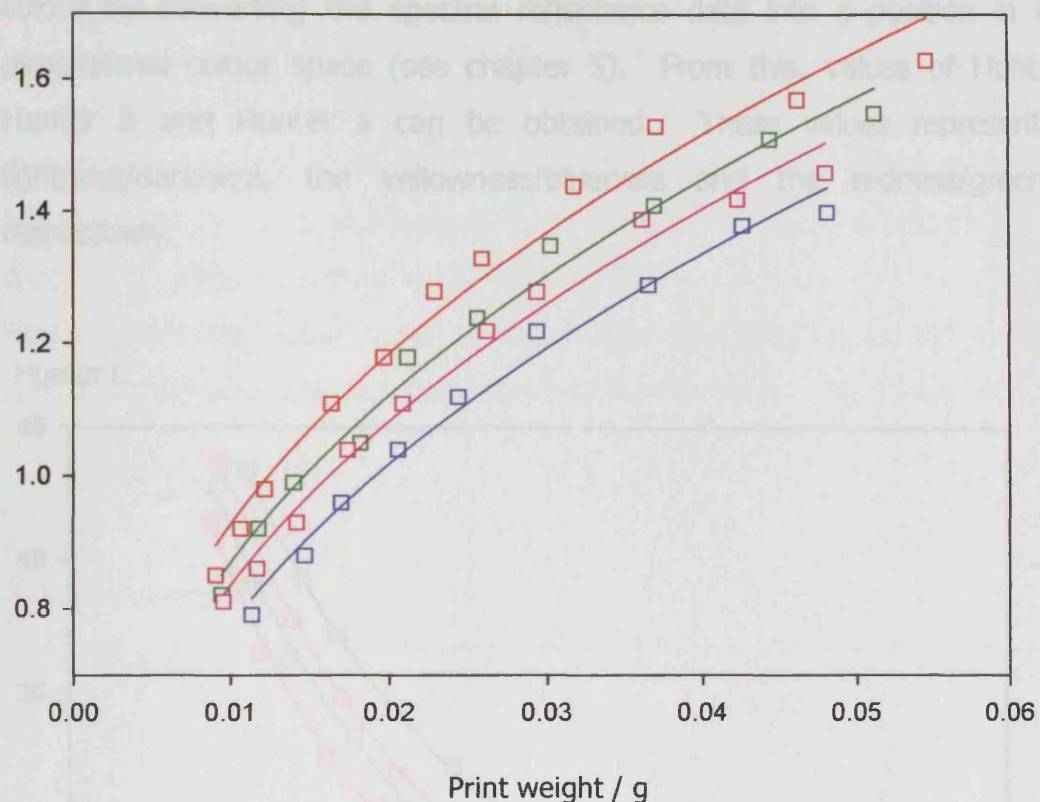


Fig 7.6(b): Print density vs print weight data for (\square) Raven[®] L, (\square) 67% Raven[®] L + 33% N660, (\square) 33% Raven[®] L + 67% N660 and (\square) N660 carbon black in oil dispersions with $\phi_{particle} = 0.18$. All data are fitted to a Power Law.

In general, samples comprising of high proportions of Raven L have a higher print density compared to samples comprised predominantly of N660.

After attempting to fit the data to a two parameter power law, it was found that the data fitted slightly better to a three parameter power law model of the form:

$$Y = Y_0 + a x^b \quad (7.2)$$

where Y is the print density and x is the print weight.

7.7: Colour data interpretation

The instrumental readings from the Hunter Labscan[®] are used to describe the colour by converting the spectral reflectance data into a position in three dimensional colour space (see chapter 5). From this, values of Hunter L, Hunter b and Hunter a can be obtained. These values represent the lightness/darkness, the yellowness/blueness and the redness/greenness respectively.

Figure 7.7(a) is a plot of colour strength ($1/\text{print weight}$) versus composition of Hunter L and represents the data obtained for Hunter L = 30, 35 and 40.

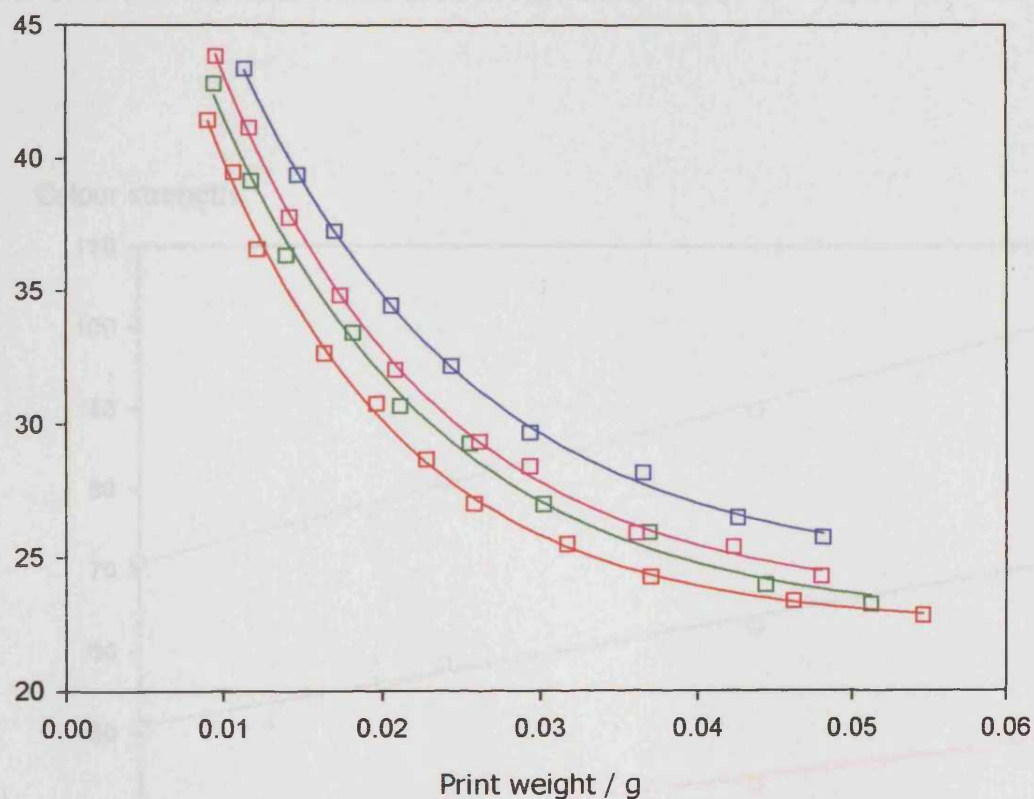


Fig 7.7(a): Hunter L vs print weight data for (\square) Raver[®] L, (\square) 67% Raver[®] L + 33% N660, (\square) 33% Raver[®] L + 67% N660 and (\square) N660 carbon black in oil dispersions with $\phi_{\text{particle}} = 0.18$. All data are fitted to an exponential decay curve.

A higher value of Hunter L denotes a “whiter” dispersion. Here, the dispersion consisting of 18wt% N660 has the highest Hunter L values which basically means that this dispersion was the lightest in colour.

All data were fitted best to a single, three parameter exponential decay curve of the form:

$$Y = Y_0 + a e^{-bx} \quad (7.3)$$

where Y is Hunter L value and x is the print weight. The obtained values for the parameters Y_0 , a and b were then used to calculate corresponding print weights for Hunter L values of 30, 35 and 40.

Figure 7.7(b) is a plot of colour strength (1/print weight) versus composition of Raven L and represents the data obtained for Hunter L = 30, 35 and 40.

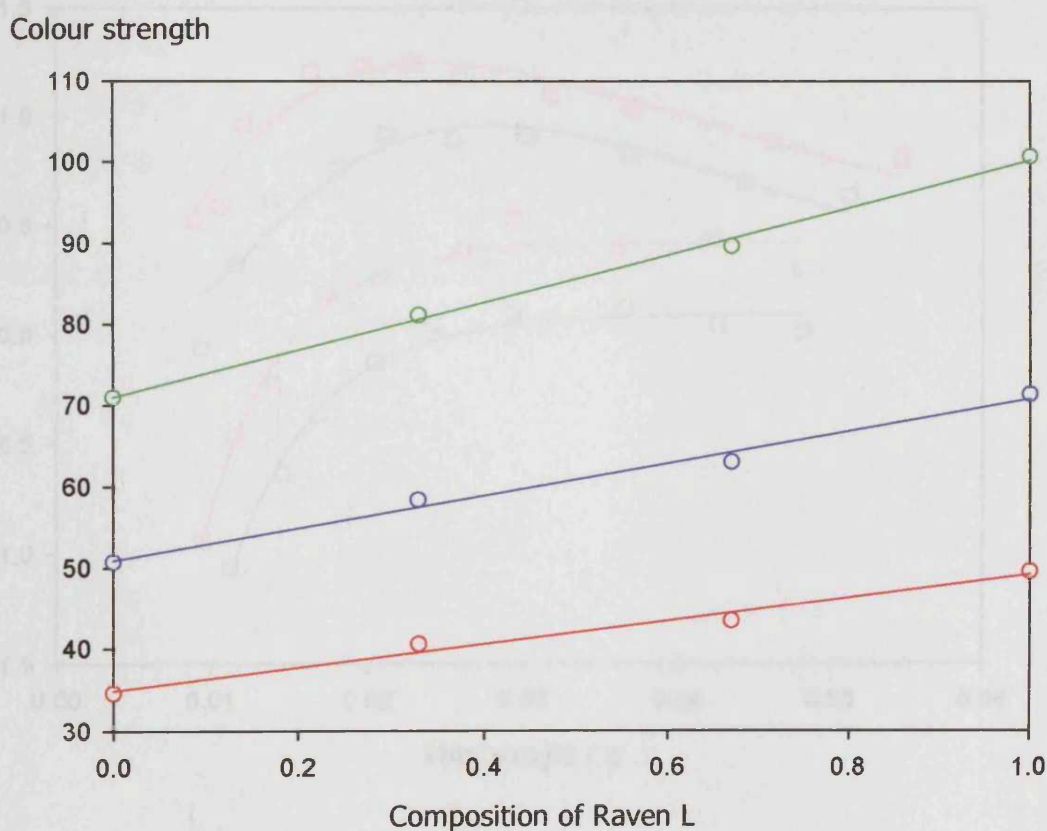


Fig 7.7(b): Colour strength versus Raven L composition data for (○) Hunter L = 30, (○) Hunter L = 35 and (○) Hunter L = 40 for mixed particle carbon black in oil dispersions.

As can be seen, the results produced a fairly linear relationship. In fact, these data were fitted to a straight line equation.

Hunter b is a measure of the blueness/yellowness of a print. A positive value indicates a blue undertone and is usually obtained with a well dispersed carbon black, on the other hand a negative value indicates a more brown undertone which is associated with less well dispersed carbon blacks. Fig's 7.7(c) and 7.7(d) represent the blueness and the undertone of the dispersions respectively.

Hunter b

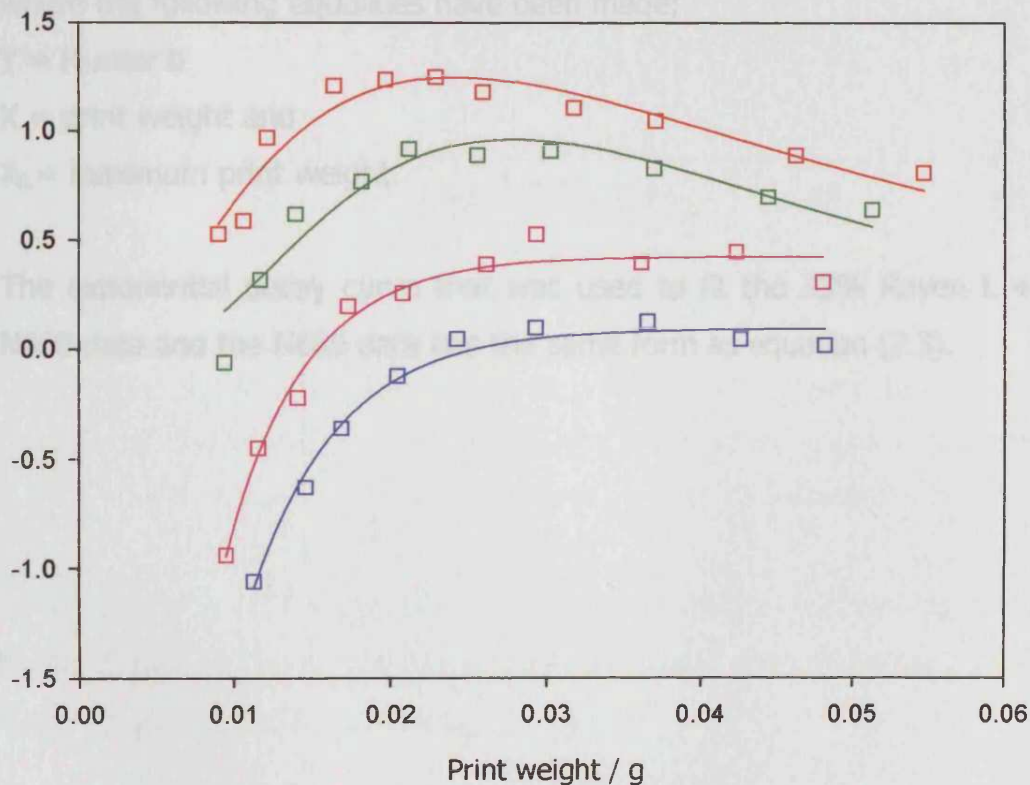


Fig 7.7(c): Hunter b vs print weight data for (\square) Raven[®] L, (\square) 67% Raven[®] L + 33% N660, (\square) 33% Raven[®] L + 67% N660 and (\square) N660 carbon black in oil dispersions with $\phi_{particle} = 0.18$. The data for the Raven L and the 67% Raven L + 33% N660 dispersions are fitted to a log normal peak, but the data for the 33% Raven L + 67% N660 and the N660 are fitted to an exponential decay curve.

Here, the increasing amount of Raven L particles in the dispersions increases the Hunter b value. Raven L is smaller and finer than N660 and is therefore more easily dispersed.

The log normal peak curve that was used to fit the Raven L data and the 67% Raven L + 33% N660 data has the form:

$$Y = a e^{-0.5 \left(\frac{\ln\left(\frac{x}{x_0}\right)}{b} \right)^2} \quad (7.4)$$

where the following equalities have been made;

Y = Hunter b

X = print weight and

X₀ = maximum print weight.

The exponential decay curve that was used to fit the 33% Raven L + 67% N660 data and the N660 data has the same form as equation (7.3).

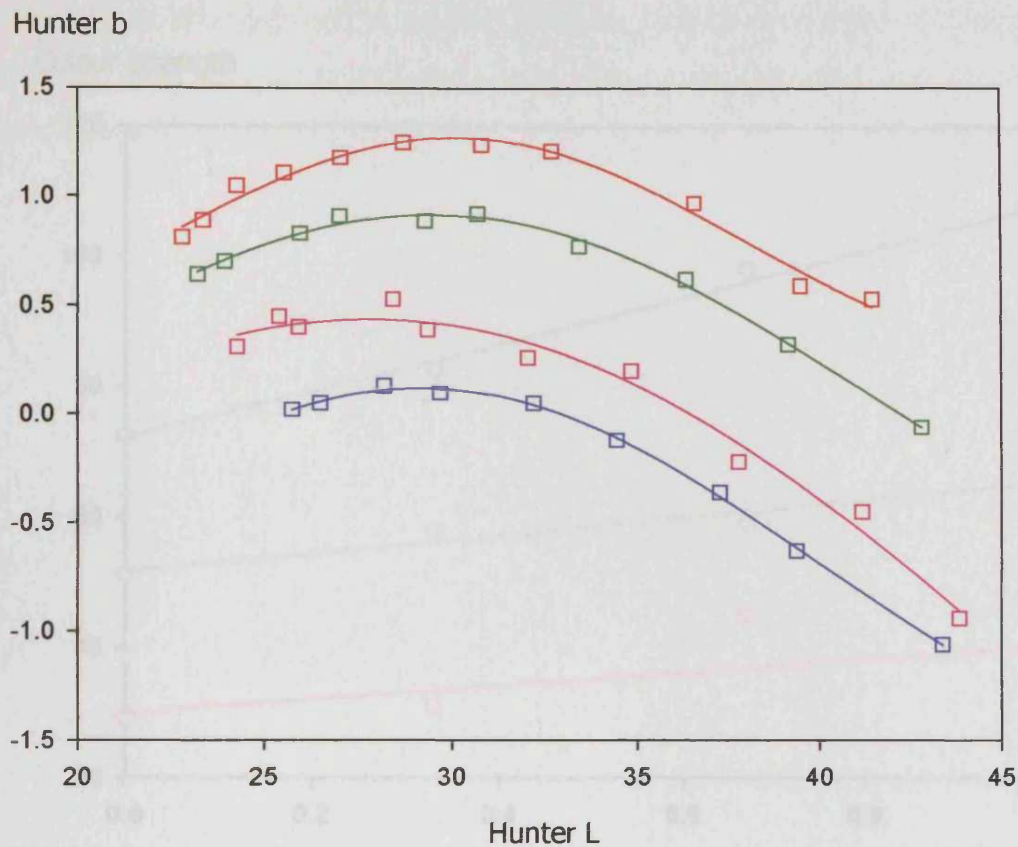


Fig 7.7(d): Hunter b vs Hunter L data for (\square) Raven[®] L, (\square) 67% Raven[®] L + 33% N660, (\square) 33% Raven[®] L + 67% N660 and (\square) N660 carbon black in oil dispersions with $\phi_{particle} = 0.18$. All of the data are fitted to a Gaussian peak.

This graph is in total agreement with the previous graph which shows that the Raven L particle dispersion has a bluer undertone than dispersions containing large amounts of N660 particles.

From these fits, and by using the values Hunter $L = 30, 35$ and 40 the corresponding Hunter b values were calculated. By using these values and the print weights obtained from fig 7.6(b), the colour strength was plotted against Raven L composition as shown in figure 7.7(e).

Colour strength

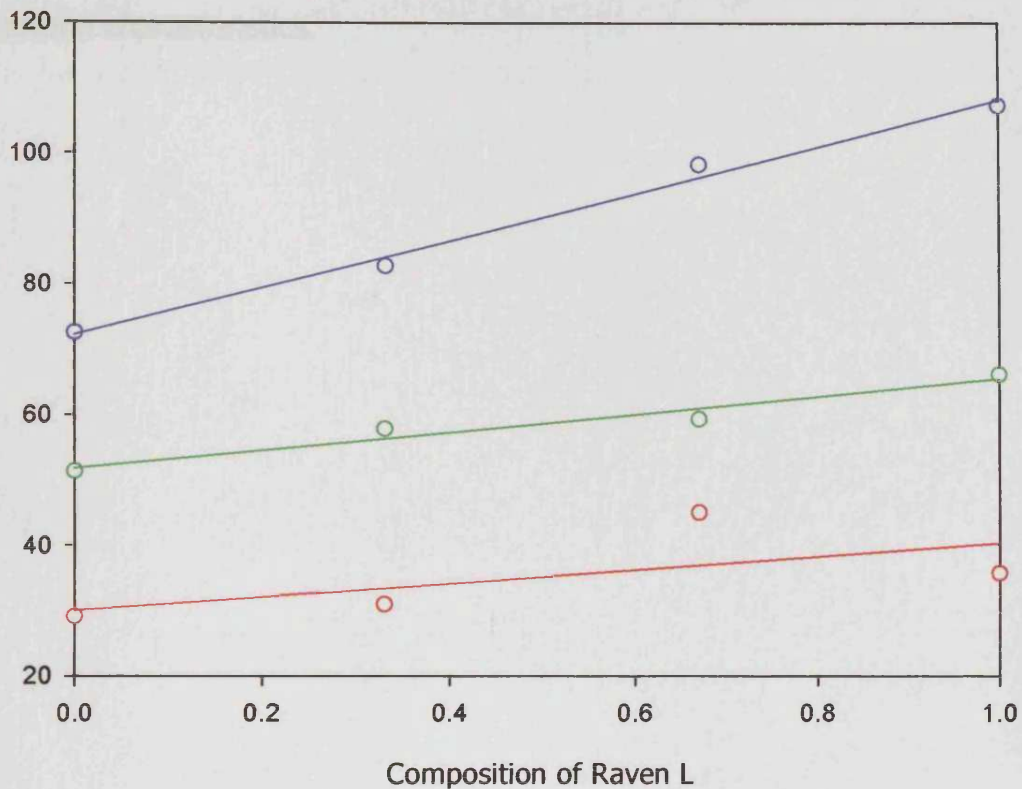


Fig 7.7(e): Colour strength versus Raven L composition data for (○) corresponding Hunter b when Hunter L = 30, (○) corresponding Hunter b when Hunter L = 35 and (○) corresponding Hunter b when Hunter L = 40 for mixed particle carbon black in oil dispersions.

These data were also fitted to a straight line equation.

Ultimately, these results suggest that there is a linear relationship between the colour strength and the composition of Raven L, obtained from both the Hunter L and Hunter b values. Generally, on increasing the amount of pigment that you add to a dispersion a corresponding decrease in Hunter L can be seen. The presence of carbon black is therefore used to achieve a

jetter colour in which the dispersion is darkened or tinted. The level of blackness (jetness) and undertone produced by a carbon black is however affected by several factors related to carbon black properties and dispersion quality, both of which influence light absorption (jetness) and (scattering) undertone characteristics.

References:

- ¹ Barnes, H.A., Hutton, J.F., Walters, K., *An introduction to Rheology*, Elsevier Science, (1989), 125
- ² Nassau, K., *Scientific Am.*, 243, (4), 124, (1980)
- ³ Voet, A., *Rubber Age*, 82, (4), 656, (1958)

CHAPTER 8: RESULTS AND DISCUSSION – MIXED PARTICLE DISPERSIONS

Carbon black particles are polydisperse in terms of particle size and morphology. Comparisons between the two particle types that differ only in the level of structure allow this feature to be explored. The effects of particle size are somewhat more difficult to elucidate without fractionation of the particle size distribution. A simple approach to overcome this is to mix particles. Chapter 8 is therefore principally concerned with dispersions consisting of mixed particles of Raven L, Raven M, N660 and N772 in different combinations.

Table 8.1 gives an average value for the size of aggregates found within each grade of carbon black.

Carbon black grade	Average aggregate diameter / nm
Raven L	87
Raven M	105
N660	215-225
N772	195-205

Table 8.1: *Typical aggregate sizes.*

The following results were obtained on investigating the effect of combining the carbon black grades in different combinations (ratio) and quantities (concentrations). The ratio is referred to as ε and is represented as follows:

$$\varepsilon = \left(\frac{M_A}{M_A + M_B} \right) \quad (8.1)$$

where M_A is the mass of particle type A and M_B is the mass of particle type B.

Therefore, all values of ε lie in the range $0 \leq \varepsilon \leq 1$.

8.1 Aqueous mixed particle dispersions

Only one aqueous mixed particle system was studied. This consisted of both Raven[®] L particles (particle A) and Raven[®] M particles (particle B) in an aqueous polymer solution of J61, where $\varphi_{\text{polymer}} = 0.1575$. Here, a range of samples were studied where the total particle volume fraction $\varphi_{\text{total particle}} = 0.15$, made up by combining the two Raven particles in differing amounts.

The two Raven grades are very similar in properties (e.g. mean particle diameter where the diameter ratio is 1.2) however, there is a difference in the "structure" of the particles. Raven L forms roughly spherical aggregates and has a low to medium structure, whereas Raven M is comprised of slightly larger more fractal aggregates and has a medium to high structure.

On combining two different sized particles to produce a bimodal system, it has been shown, using latex¹ (78nm and 372nm, hence the diameter ratio was 4.76) stabilised with an ABA block copolymer of ethyleneoxide (A) and propyleneoxide (B), that broadening the particle size distribution leads to an increase in the maximum packing fraction, where small particles fit in the gaps between the large particles. Ultimately, polydispersity allows a greater particle loading that does not increase the viscosity above that of the equivalent monodisperse viscosity. Without considering the adsorbed layer thickness a minimum in the relative high shear rate viscosity was found in the range 15-20% by volume of small particles and another minimum was also found at 20% by volume of small particles for the dynamic viscosity measurements. Other research^{2,3} has also confirmed that the extent of the packing depends on the proportions of the two spheres and is a maximum when the smaller constituent is 27% of the total solids volume. Also, for studies on bimodal suspensions consisting of fine and coarse particles^{4,5,6} this minimum low shear viscosity occurs at ~25-35% fine particles.

The aim, therefore, was to contrast these findings using both an aqueous and an oil based bimodal carbon black system that comprised of two particles of different shape and structure in addition to a slightly different size. The results for the aqueous system are shown in figure 8.1(a).

Viscosity / Pa.s

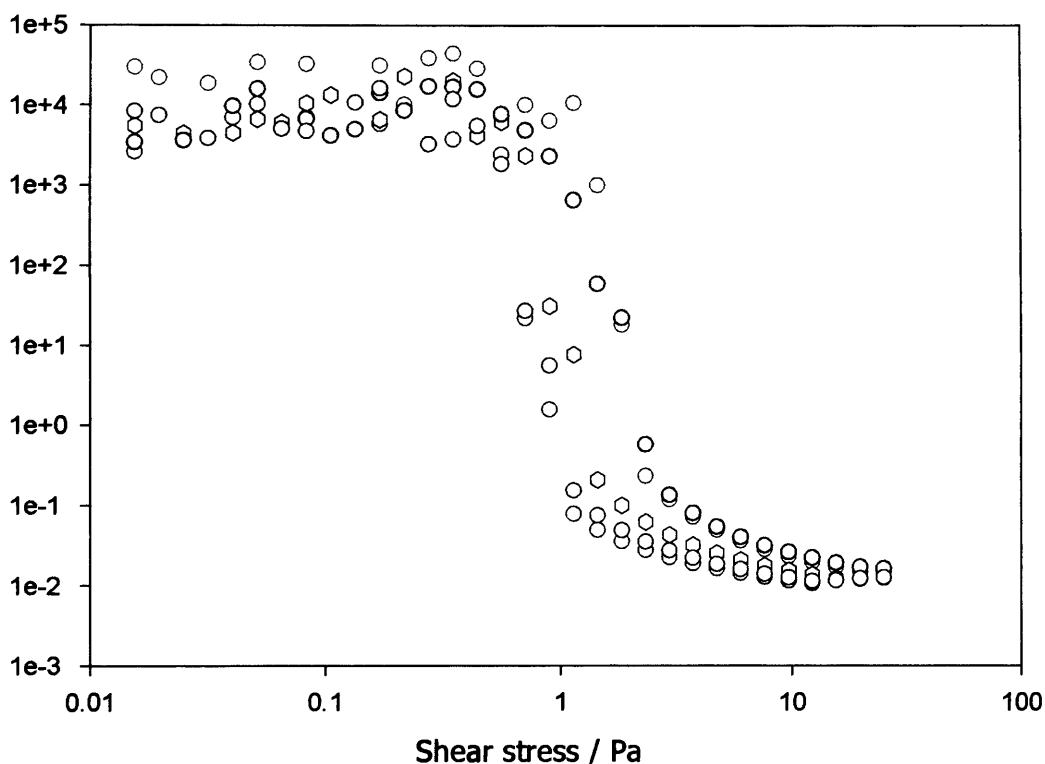


Fig 8.1(a): Typical viscosity-shear stress curves for the "spherical" Raven[®] L carbon black particles, the "fractal" Raven[®] M particles and a mixture of both particles in aqueous polymer solutions where $\phi_{polymer} = 0.1575$; (O) $\varepsilon = 0$, (O) $\varepsilon = 0.25$, (O) $\varepsilon = 0.5$, (O) $\varepsilon = 0.75$ and (O) $\varepsilon = 1$.

In the low shear stress region it was very difficult to distinguish any differences, however at high shear, small differences are apparent. Fig 8.1(b) relates the high shear viscosity to the particle ratio.

High shear viscosity / Pa.s

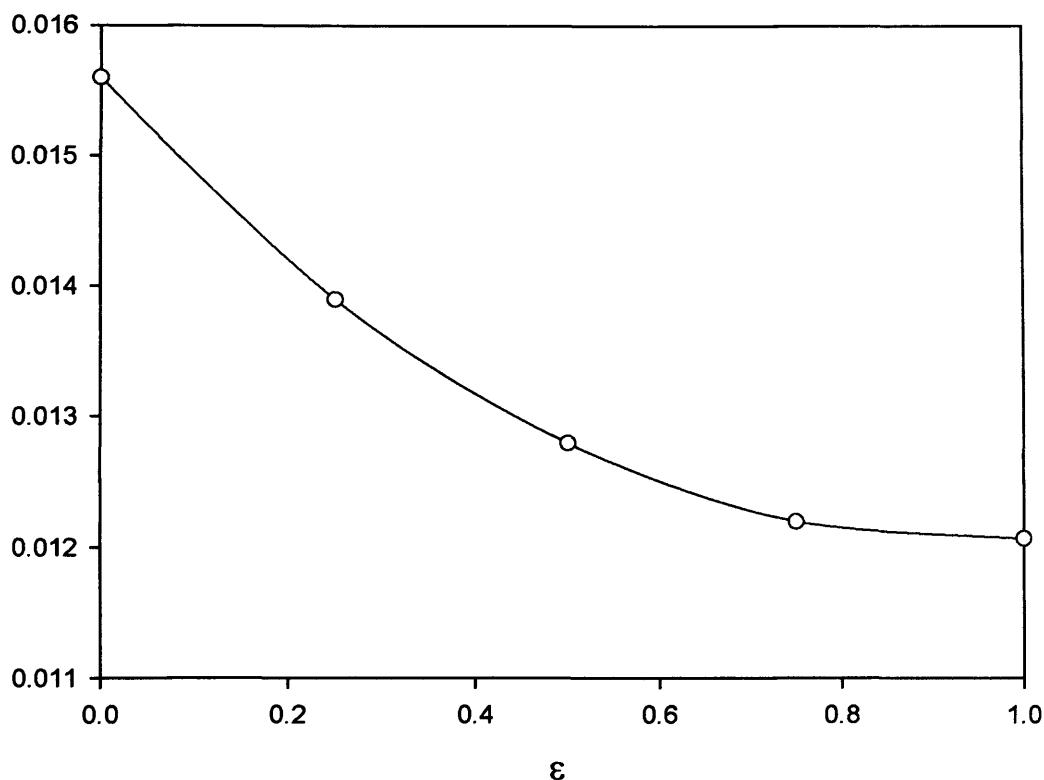


Fig 8.1(b): *High shear viscosity-particle content ratio data for an aqueous mixed particle dispersion containing J61 and both Raven L and Raven M particles. Here $\varphi_{polymer} = 0.1575$ and $\varphi_{particle\ total} = 0.15$. The line is to guide the eye.*

The dispersion that consists entirely of Raven M particles (where $\varepsilon=0$) has the highest value for the high shear viscosity. On incorporation of Raven L particles, the high shear viscosity decreases towards the value obtained for the Raven L particle dispersion. This high shear viscosity behaviour is general for this system, but the relative magnitudes vary as a function of shear stress.

8.2: Mixed particle in oil dispersions

Four different carbon black grades were used here; Raven L, Raven M, N660 and N772. The aim here was to understand how the low shear viscosity, high shear viscosity and yield stress vary as a function of the proportion of either particle. Table 8.2 briefly summarises the properties of the four particles used, namely the differences in the structure and the type of particle hence this table is used, along with table 8.1, in order to assist in the explanation of the results obtained.

Structure	Particle type	
	fine	coarse
Low-medium	Raven L	N772
Medium-high	Raven M	N660

Table 8.2: *Four carbon black particles and their associated properties.*

To begin with only the effect of particle type was investigated so the low-medium structured, fine particle Raven L grade (particle A) was combined with the low-medium structure, coarse particle N772 grade (particle B), shown in fig 8.2(a). Here, the diameter ratio is 2.2-2.4.

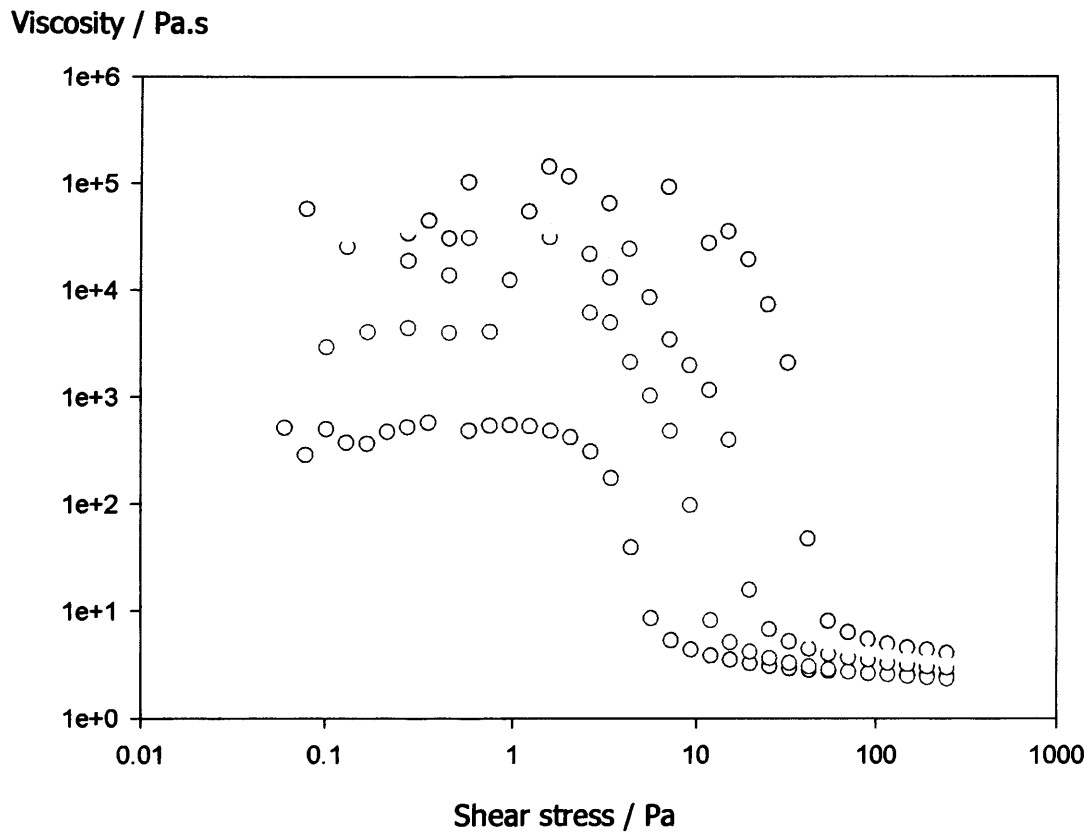


Fig 8.2(a): *Typical viscosity-shear stress curves for a Raven L (particle A) and N772 (particle B) mixed particle system in oil with (○) $\varepsilon = 1$, (◐) $\varepsilon = 0.75$, (◑) $\varepsilon = 0.5$, (◒) $\varepsilon = 0.25$ and (○) $\varepsilon = 0$.*

Fig 8.2(b) shows the results obtained when the stock Raven M (particle A) dispersion was mixed with the stock N660 (particle B) particle dispersion in varying amounts. Remember that, Raven M consists of fine particles with a medium- high structure and N660 consists of coarse particles with medium-high structure and the diameter ratio is 2-2.1.

Viscosity / Pa.s

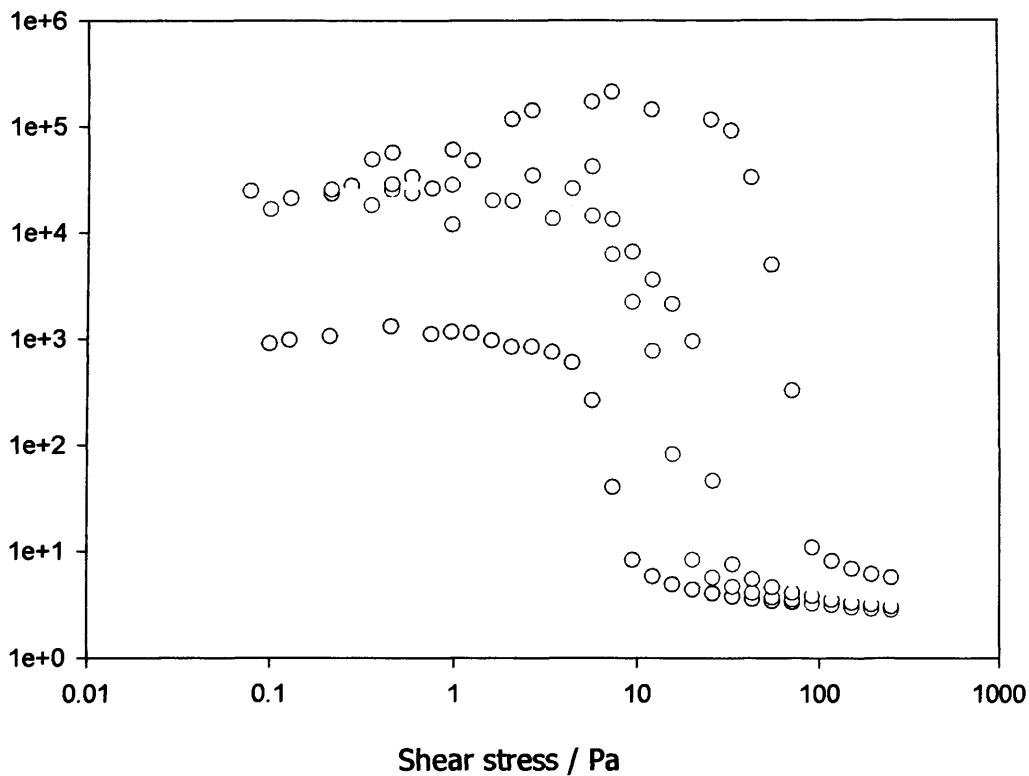


Fig 8.2(b): Typical viscosity-shear stress curves for a Raven M (particle A) and N660 (particle B) mixed particle system in oil with (○) $\varepsilon = 1$, (◐) $\varepsilon = 0.75$, (◑) $\varepsilon = 0.5$, (◒) $\varepsilon = 0.25$ and (○) $\varepsilon = 0$.

The data for dispersions consisting of the low-medium structured Raven L and N772 instead of the medium-high structured Raven M and N660 seem to be "cleaner". The low shear viscosity values are more constant, giving a more definite plateau and there is a clear distinction between the data sets obtained for each ratio measured.

Using figures 8.2(a) and 8.2(b), each curve was generalised using the method adopted for the aqueous system. Therefore values for the low shear viscosity, the high shear (limiting) viscosity and the yield stress were taken and plotted

as a function of the particle ratio. Figures 8.2(c), 8.2(d) and 8.2(e) represent these data respectively.

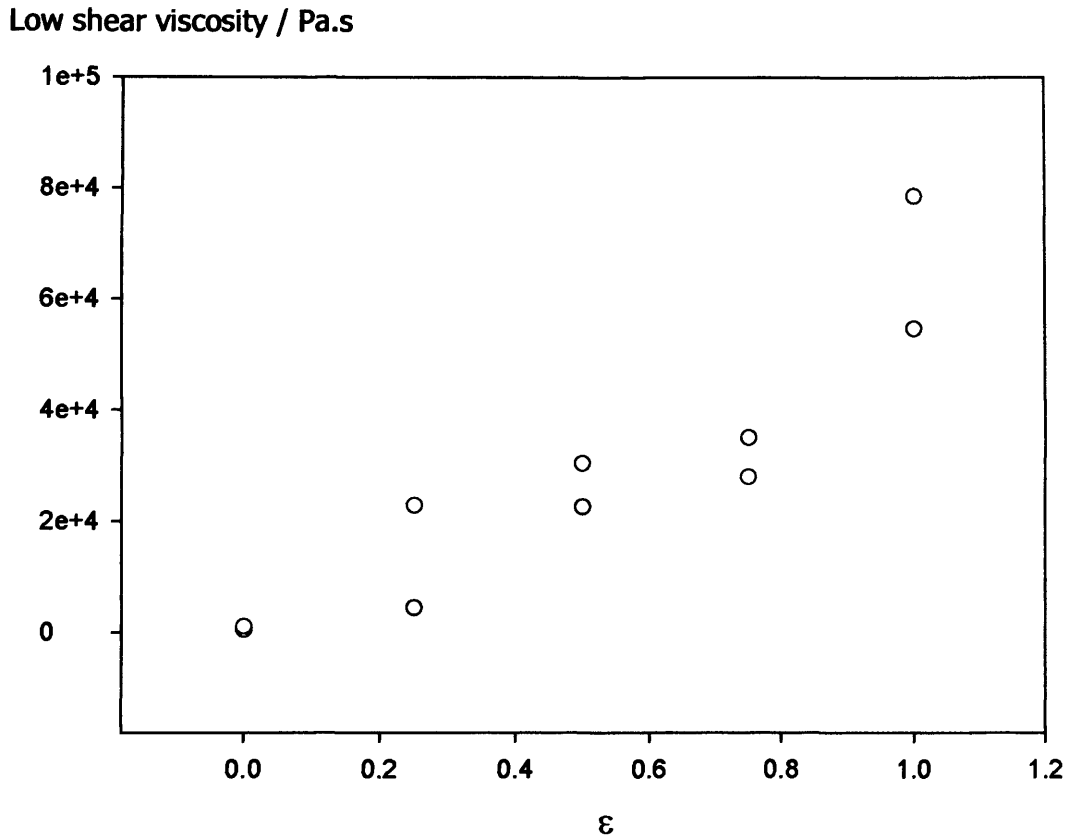


Fig 8.2(c): *Low shear viscosity-particle content ratio data for mixed dispersions of (○) Raven M + N660 and (○) Raven L + N772 carbon black particles in oil.*

The low shear viscosity for dispersions consisting of Raven L and N772 particles does not change much as a function of particle ratio. However, for both systems, the dispersion consisting entirely of the coarse carbon black particles (N772 or N660) has the lowest value for the low shear viscosity plateau. The initial addition of Raven M particles (where $\epsilon=0.25$) to the N660 dispersion was accompanied by a substantial increase in viscosity. Although, following this initial increase, the addition of more Raven M particles (where $\epsilon=0.5$ and 0.75) does not seem to have a huge effect on the viscosity. Here, the viscosity of the dispersion consisting entirely of Raven M particles (where

$\varepsilon=1$) is considerably higher than all of the other dispersions. This is because small particles have a much higher effective volume fraction than the large particles due to the adsorbed polymer layer. In contrast, upon incorporation of Raven L to the N772 dispersion (where $\varepsilon=0.25$) there was little change in the viscosity. However, further addition of Raven L particles (where $\varepsilon=0.5, 0.75$ and 1) steadily increased the low shear viscosity value.

High shear viscosity / Pa.s

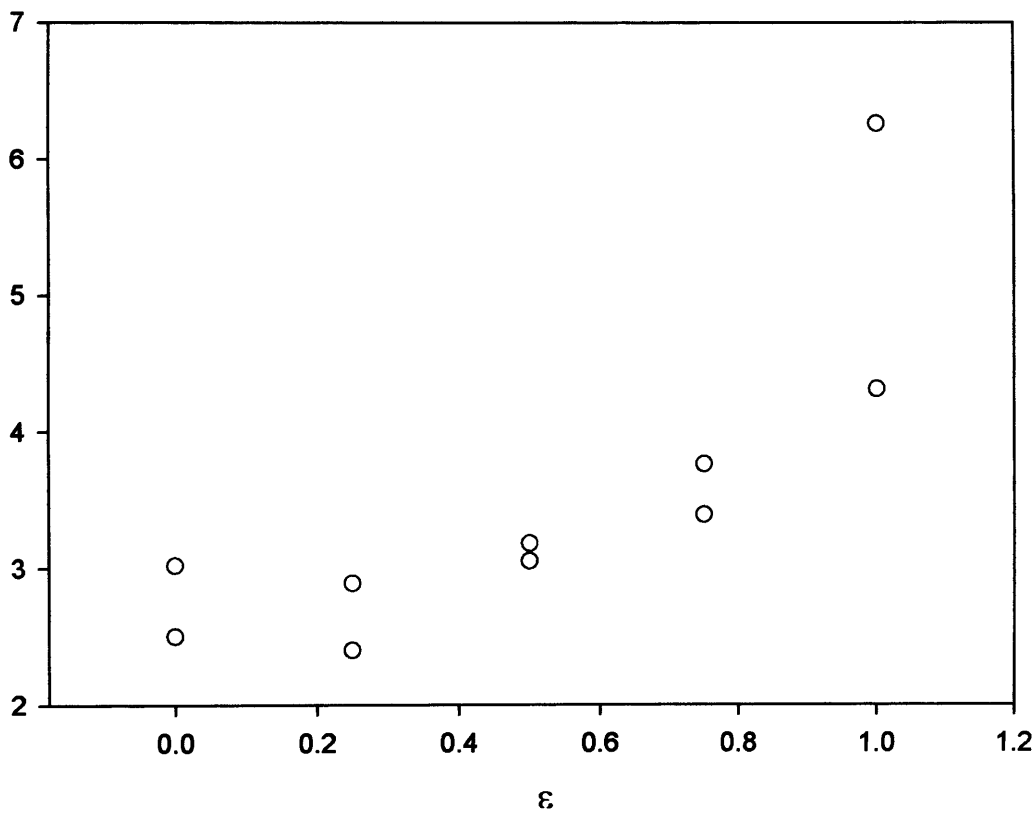


Fig 8.2(d): *High shear viscosity-particle content ratio data for mixed dispersions of (○) Raven M + N660 and (○) Raven L + N772 carbon black particles in oil.*

The errors were calculated for these data, however the error bars obtained were comparable to the size of the data points and have therefore been omitted for clarity.

For both systems, the initial incorporation (where $\varepsilon=0.25$) of fine particles (Raven M or Raven L) to a coarse particle dispersion tends to decrease the high shear viscosity plateau slightly before an increase can be seen with increasing particle ratio. Here, the ϕ of small particles is 25% of the total ϕ of solids. Greenwood, Luckham and Gregory¹ also found a minimum in the high shear viscosity at 15-20% by volume of small particles. However, if the adsorbed layer thickness is taken into account then the minimum is found between 27-36%, which is in good agreement with these results. Johnson and Kelsey⁷ reported a viscosity minimum at 25% small particles by volume after studying mixtures of styrene-butadiene lattices. Further, on studying a binary mixture of polystyrene and silica, Okubo⁸ has also reported a minimum viscosity at 25% small particles.

In the region where $\varepsilon=0.25, 0.5$ and 0.75 , the increase in the high shear (limiting) viscosity is similar for both systems, but Raven M (where $\varepsilon=1$) has a much higher value for the limiting viscosity than Raven L (where $\varepsilon=1$).

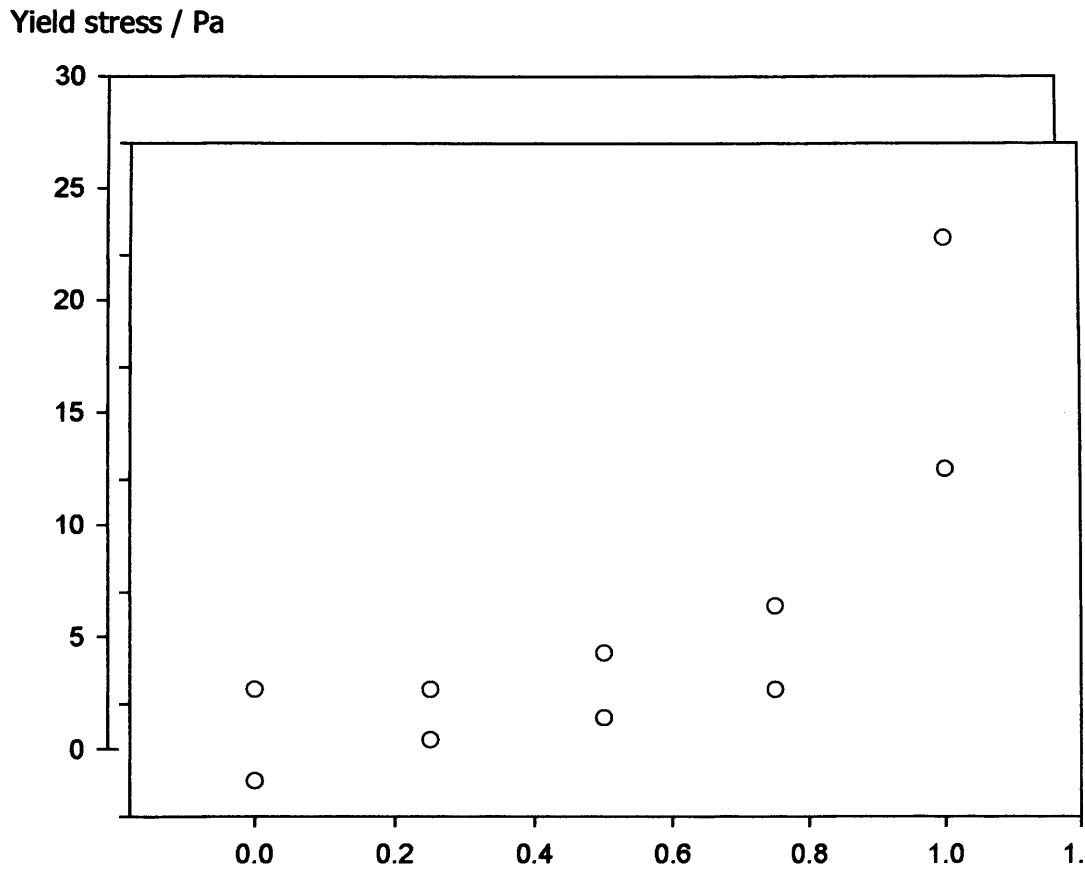


Fig 8.2(e): Yield stress-particle content ratio data for mixed dispersions of (○) Raven M + N660 and (○) Raven L + N772 carbon black particles in oil.

The yield stress data is rather similar for both bimodal systems, however the values are slightly higher for the Raven M and N660 medium-high structured combination.

Following this, the effect of particle structure was investigated along with particle type. Here, the low-medium structured, fine particle Raven L grade (particle A) was combined with the medium-high structure, coarse particle N660 grade (particle B).

Fig 8.2(f) shows the results obtained when the stock Raven L (particle A) dispersion was mixed with the stock N660 (particle B) particle dispersion in varying amounts. Raven L consists of fine particles with a low-medium structure and N660 consists of coarse particles with medium-high structure. Here the particle diameter ratio is 2.5-2.6.

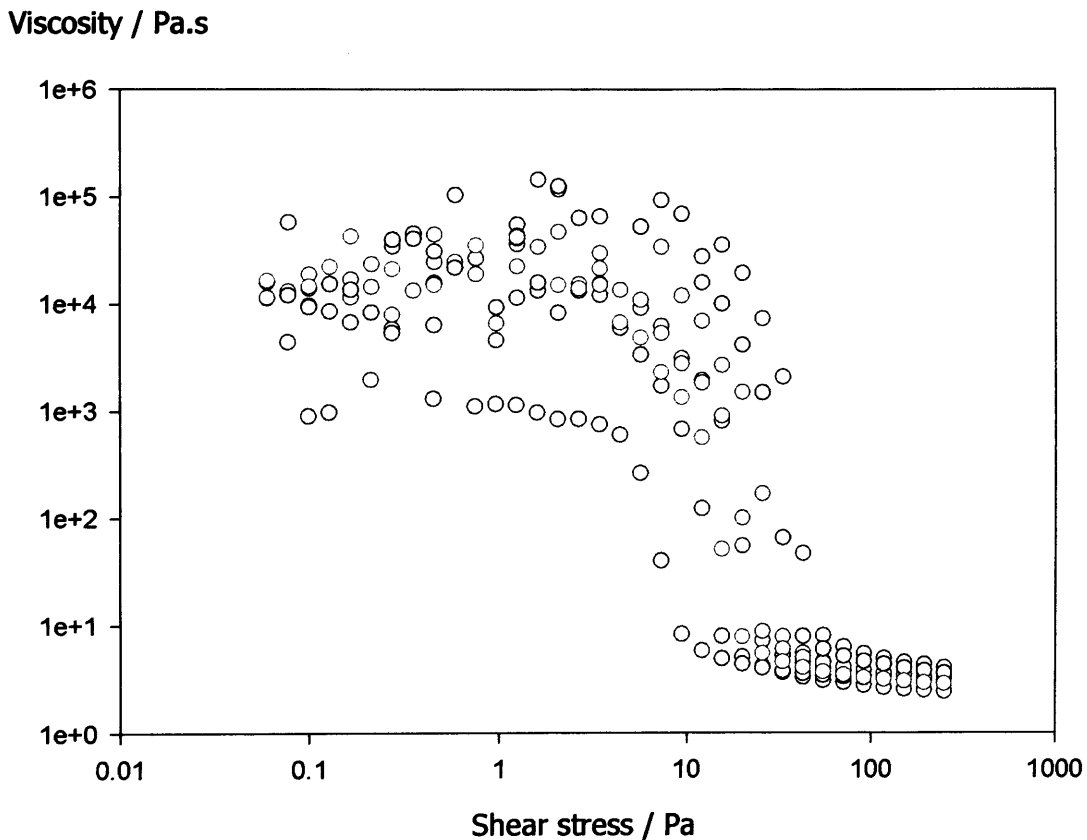


Fig 8.2(f): Typical viscosity-shear stress curves for a Raven L (particle A) and N660 (particle B) mixed particle system in oil with (○) $\epsilon = 1$, (○) $\epsilon = 0.9$, (○) $\epsilon = 0.75$, (○) $\epsilon = 0.6$, (○) $\epsilon = 0.5$, (○) $\epsilon = 0.4$, (○) $\epsilon = 0.25$ and (○) $\epsilon = 0$.

Fig 8.2(g) shows the results obtained when the stock Raven M (particle A) dispersion was mixed with the stock N772 (particle B) particle dispersion in varying amounts. Raven M consists of fine particles with a medium-high structure and N772 consists of coarse particles with low-medium structure. Here the particle diameter ratio is 1.9-2.0.

Viscosity / Pa.s

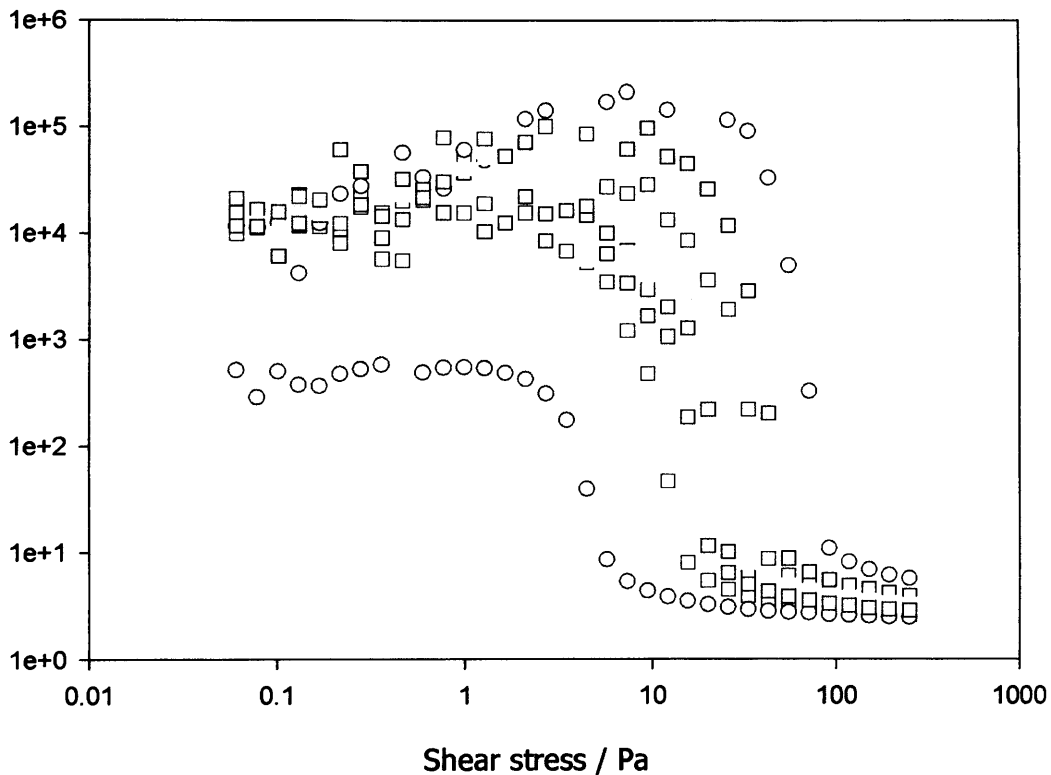


Fig 8.2(g): Typical viscosity-shear stress curves for a Raven M (particle A) and N772 (particle B) mixed particle system in oil with (○) $\varepsilon = 1$, (□) $\varepsilon = 0.9$, (◻) $\varepsilon = 0.75$, (◻) $\varepsilon = 0.6$, (◻) $\varepsilon = 0.5$, (◻) $\varepsilon = 0.4$, (◻) $\varepsilon = 0.25$ and (◻) $\varepsilon = 0$.

As done previously, each curve was generalised using the method adopted for the aqueous system and values for the low shear viscosity, the high shear (limiting) viscosity and the yield stress were taken and plotted as a function of

the particle ratio. Figures 8.2(h), 8.2(i) and 8.2(j) represent these data respectively.

Low shear viscosity / Pa.s

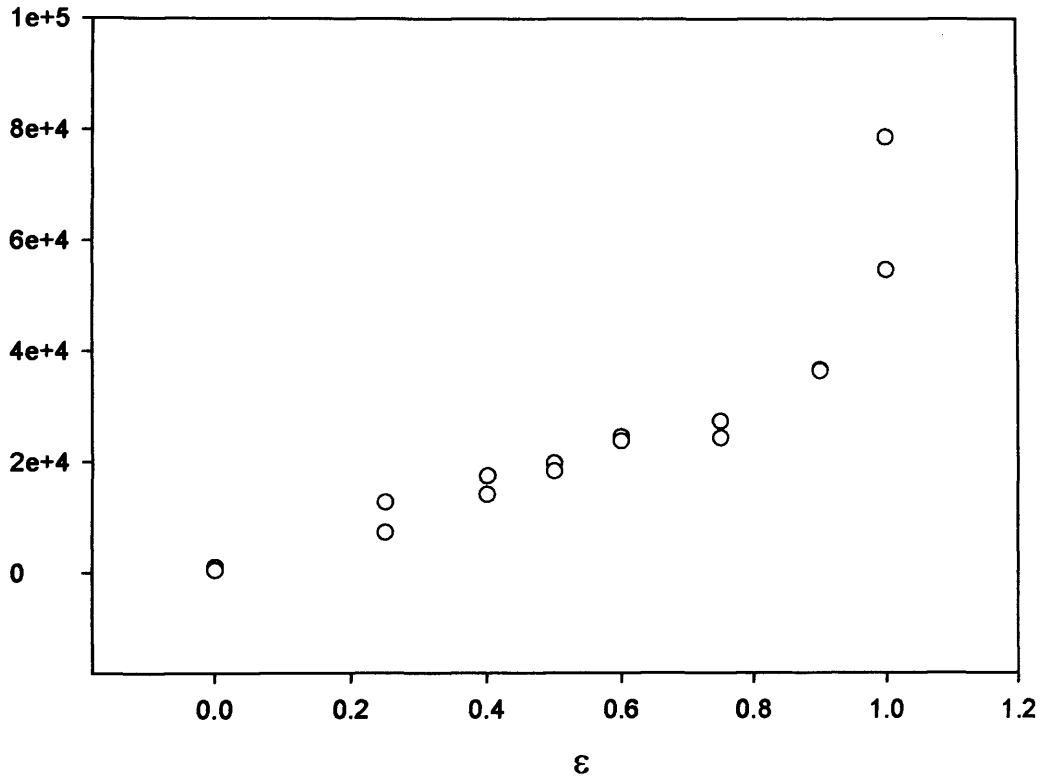


Fig 8.2(h): *Low shear viscosity-particle content ratio data for mixed dispersions of (○) Raven M + N772 and (○) Raven L + N660 carbon black particles in oil.*

The low shear viscosity data is very similar for both bimodal systems, however the low shear viscosity of the monomodal Raven M (where $\epsilon = 1$) system is higher than that of the monomodal Raven L system.

High shear viscosity / Pa.s

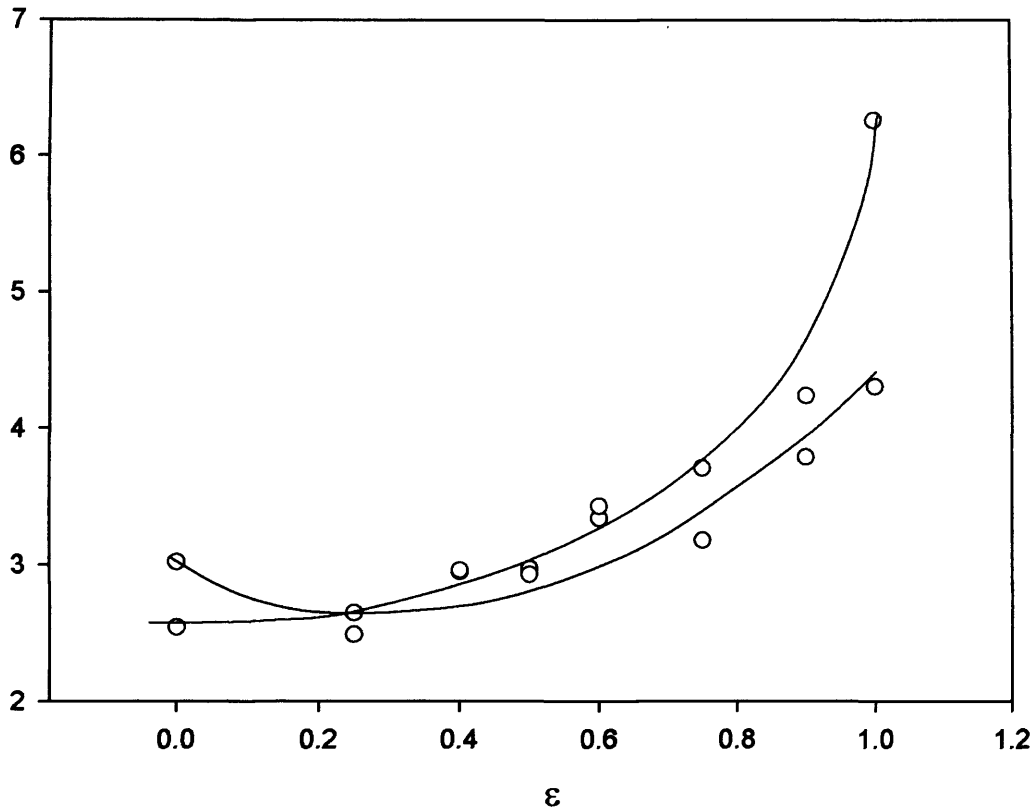


Fig 8.2(i): *High shear viscosity-particle content ratio data for mixed dispersions of (○) Raven M + N772 and (○) Raven L + N660 carbon black particles in oil. The lines are best fit lines and act as a guide to the eye.*

For the Raven M and N772 bimodal dispersion, the high shear limiting viscosity increases gradually with increasing particle ratio. On the other hand, for the Raven L and N660 bimodal dispersion, there is a minimum in the high shear viscosity at $\epsilon = 0.25$. This was found for both the Raven M/N660 and Raven L/N772 bimodal dispersions (fig 8.2(d)) and is in good agreement with previous studies¹⁻⁸.

Yield stress / Pa

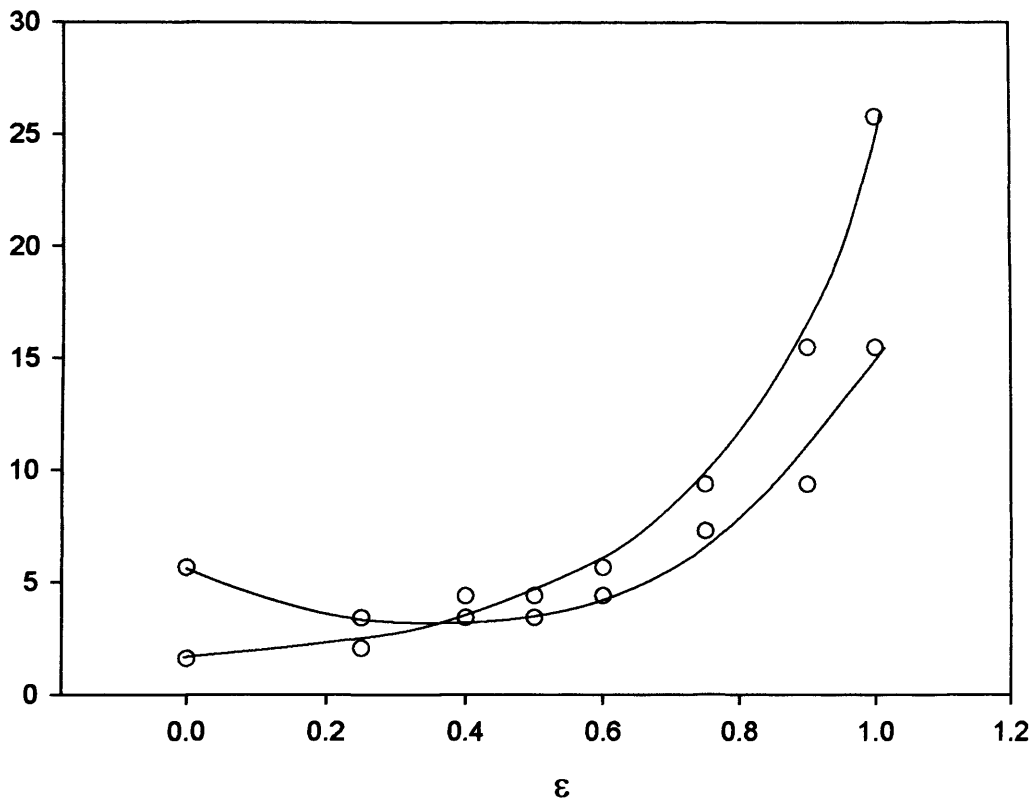


Fig 8.2(j): Yield stress-particle content ratio data for mixed dispersions of (○) Raven M + N772 and (○) Raven L + N660 carbon black particles in oil. The lines are best fit lines and are to guide the eye only.

For the Raven M and N772 bimodal dispersion, the yield stress increases gradually with increasing particle ratio. On the other hand, for the Raven L and N660 bimodal dispersion, there is a smooth decrease in the yield stress point and it's not until $\epsilon = 0.5$ that a noticeable increase is apparent.

Summary:

The low shear viscosity is very similar for the Raven L/N772 and Raven L/N660 dispersions and also for the Raven M/N660 and Raven M/N772. Therefore, the particle structure of the larger particle, when combined with Raven L, appears to have little effect. However, the low shear viscosity of the Raven M/N660 combinations at $\varepsilon = 0.25, 0.5$ and 0.75 are higher than the low shear viscosity of the Raven M/N772 system. The low shear viscosity of the Raven L/N772 system at $\varepsilon = 0.5$ and 0.75 is higher than the low shear viscosity of Raven L/N660 but at $\varepsilon = 0.25$ this is reversed.

For the high shear viscosity, when Raven M/N660 and Raven L/N772 are combined, a slight minimum is observed for both systems at $\varepsilon = 0.25 (\pm 0.05)$. However, when Raven M/N772 and Raven L/N660 are combined, only the Raven L/N660 bimodal system show a minimum high shear viscosity at $\varepsilon = 0.25$. There is no evidence of a minimum in the high shear viscosity for the Raven M/N772 system.

On investigating the yield stress for Raven M/N660 and Raven L/N772, the data are very similar, although the values for the Raven M/N660 dispersion are slightly higher. There seems to be an abrupt increase in the yield stress point from $\varepsilon = 0.75$ to $\varepsilon = 1$. On combining Raven M/N772 and Raven L/N660 the increase in the yield stress is gradual for the Raven M/N772 system whereas the Raven L/N660 system actually passes through a minimum value between $\varepsilon = 0.25$ and $\varepsilon = 0.5$.

For the bimodal aqueous system of Raven L/Raven M, the low shear viscosity and the high shear viscosity do not appear to change a great deal with ε . However, the oil based systems show a variety of behaviour.

References

- 1 Greenwood, R., Luckham, P.F., Gregory, T., *Coll. Surf. A: Physicochemical and Engineering Aspects*, 144, (1998), 139-147
- 2 Furnas, C.C., *Ind. Eng. Chem.*, 23, (1931), 1052
- 3 Fraser, R., *J. Geol.*, 43, (1935), 910
- 4 Chong, J.S., Christiansen, E.B., Baer, A.D., *J. Appl. Poly. Sci.*, (1971), 15, 2007
- 5 Pal, R., *AIChE J.*, (1996), 42, 3181
- 6 Parkinson, C., Matsumoto, S., Sherman, P., *J. Colloid Interface Sci.*, (1970), 33, 150
- 7 Johnson, P., Kelsey, R., *Rubber World*, 138, (1958), 877
- 8 Okubo, T., *J. Phys. Chem.*, 94, (1962), 1990

CHAPTER 9: CONCLUSION OF RESULTS

In industry the control of a materials flow properties plays an extremely important role for the development of new printing inks and paints. Inks and paints are essentially aqueous or oil based colloidal dispersions that have been stabilised using a polymeric material. However, the flow properties are highly dependent on the nature of the stabiliser.

The aim of this thesis was to study the rheological behaviour of carbon black dispersions with a variety of different particle types, adsorbents and dispersion media

9.1: AQUEOUS DISPERSIONS

Firstly, the interaction of carbon black with an acrylic resin (J61) was investigated by rheology. Two carbon blacks, Raven L and Raven M, with similar particle size (87nm for Raven L and 105nm for Raven M) and surface characteristics but with different particle morphologies were examined. On attempting to characterise the particles, the results shown by small-angle neutron scattering (SANS) and ultrasonic spectroscopy showed subtle differences. Thus it is from these data that the Raven L and Raven M particles are arbitrarily denoted as "spherical" and "fractal" respectively. The transmission electron micrographs (TEM) further support this distinction that the Raven M (fractal) particle has a more open structure.

In the absence of polymer, stable aqueous dispersions could not be obtained. Stable dispersions could be obtained however upon the addition of polymer to a level corresponding to a ratio of 50mg of polymer per $13\text{m}^2(\pm 1)$ of surface area (i.e. 15wt% particles). These stable dispersions exhibit flow typical of concentrated dispersions - Newtonian behaviour up to some apparent "yield" or critical value. Above this value pronounced shear thinning is observed. This critical stress increases with increasing polymer concentration. When a significant amount of non-adsorbed polymer is also present, superimposed on the shear thinning behaviour is a second Newtonian plateau. This feature is

observed for both particle types but is more pronounced for the fractal particle.

When there is little or no non-adsorbed polymer, the viscosity of the fractal particle dispersion (~ 10 Pa.s) is greater than the viscosity of the spherical particle dispersion (~ 0.45 Pa.s). This is in excellent agreement with the, albeit rather limited, ultrasonic spectroscopy studies. In addition, the fractal particle dispersions undergo shear thinning at a higher shear stress (~ 0.08 Pa) than the spherical particles (~ 0.04 Pa). The limiting high shear viscosity is similar for both particles at ~ 0.004 Pa.s.

When there is a significant amount of non-adsorbed "free" polymer in the solution, the low shear stress is increased further. However, further addition of polymer, to an already highly concentrated system, appears to have little effect on the low shear viscosity but an increase of about an order of magnitude can be seen in the high shear viscosity.

The increase in the low shear viscosity with an increasing polymer concentration above the coverage can be explained as being due to the polymer in solution, with the particles forming a network. The "dilution experiments" in which the ratio ϕ_{particle} to ϕ_{polymer} was held constant, were conducted to further understand the role of the interaction between the polymer layer and the polymer in the continuous phase. Similar viscosity-shear stress behaviours were observed for all systems and of particular interest was an intermediate Newtonian plateau. On dilution, the viscosity at low shear rates decreases significantly, an effect that is more pronounced for the Raven L (spherical) particle.

Oscillation experiments were undertaken on these samples and it was found that at low polymer concentrations, the dispersions are predominantly viscous at low shear stresses, as illustrated by the Lissajous plots. The phase angle decreases significantly over a narrow shear stress range and the rheology

tends to more elastic behaviour. At higher shear stresses, the dependence on particle morphology is weak.

At low shear rates/frequencies, the carbon black and polymer form an extended network of high viscosity, which responds to oscillation in a predominantly viscous manner. Above some characteristic relaxation time, the network breaks and there is a reduction in viscosity, the phase angle decreases and the response becomes more elastic. An intermediate (Newtonian) region is observed which reflects the interaction between the polymer layer and the polymer matrix. This is probably the viscous drag between polymer chains adsorbed on the particles with the polymer in solution.

An experiment was conducted to study the effect of changing the dispersion pH on the rheology of the aqueous carbon black/J61 system. Altering the pH of the system from 8 to 12 has a relatively small effect on the rheology of the carbon black dispersions. However, the small differences can be explained by the increase of the negative charge on the surface, which results in an increase in the attraction of polymer to the surface. This ultimately leads to an "enlargement" of the particle and an increase in the viscosity.

The nature of the adsorbent has proven to be a very important factor that is able to alter the rheology of the resulting dispersion. On changing the acrylic resin polymer (J61) for a styrene acrylic resin (JHPD-96 E) at the same ϕ_{polymer} the typical behaviour associated with concentrated dispersions is not observed, rather the behaviour has a much lower viscosity and is Newtonian. However, for a system comprising of PEG-PPG-PEG adsorbed onto carbon black, the rheological behaviour is similar to that of the J61/carbon black system.

Most carbon blacks are hydrophobic, but the level of hydrophobicity can be reduced by the presence of chemisorbed oxygen and certain other functional groups. By studying the rheology of two very similar carbon blacks (the only difference being that one had been subjected to ozonolysis) subtle differences

were apparent. The particle with the extended built up layer of chemisorbed oxygen displays a slightly higher viscosity. This results from the increased surface activity, the adsorbed layer thickness and hence the effective size of the particles.

9.2: OIL DISPERSIONS

As well as being used extensively in waterborne inks and coatings, carbon black is also used as a pigment in oil based inks. Here, the colloidal particles are stabilised by bitumen, which is a very long chain petroleum hydrocarbon.

In addition to the fine particles, Raven L and Raven M, the colour properties and the rheology of two coarse carbon blacks (N660 and N772) were also investigated. The typical rheological behaviour that is associated with concentrated dispersions was observed for all of the systems studied.

Common observations included:

- On decreasing the particle concentration, the overall viscosity was reduced.
- The lower the particle concentration, the lower is the value of the low shear viscosity. Hence the shear-thinning region is not so pronounced.
- The high shear (limiting) viscosity for all dispersions, regardless of particle content, tends to a common value (that of the oil).
- Decreasing the particle concentration results in a reduction of the yield stress point.

On comparing the particle types it became apparent that the low shear viscosity, the high shear (limiting) viscosity and the yield stress values decreased in the order, Raven M → Raven L → N660 → N772. The fine particles having much higher viscosities than the coarse particles, although there is also a noticeable dependence on the structure of the particles. The Raven M and N660 having a medium-high structure and the Raven L and N772 having a low-medium structure.

Further, the high shear viscosity data was fitted using the Krieger-Dougherty equation and it was found that all particle types displayed a low maximum packing fraction—a consequence of the non-spherical nature. Also, there was a

decrease in the value obtained for the intrinsic viscosity in the same order as before: Raven M→ Raven L→N660→N772.

The use of carbon black in plastics and inks is common for two colour applications. Firstly, it is simply used to make black products and secondly to modify the colour imparted by other pigments present. The colour properties however are highly dependent on the particle size, aggregate size, size distribution and structure of the carbon black used. In essence, the results show that small, fine particle blacks produce dispersions that are "blacker" and they also suggest that there is a linear relationship between the colour strength and the composition of fine particles within a dispersion.

9.3: MIXED PARTICLE DISPERSIONS

Previous studies (see chapter 8 references 1-8) have shown that combining particles of different sizes within a suspension can act to reduce the viscosity without there being any change in the total particle concentration. In other words, a bimodal system can have a greater particle loading with the same viscosity as a monomodal system. In industry, this finding has proved useful because pumping costs can be minimised and also more environmentally sensitive products with less polluting solvent can be produced.

For aqueous bimodal systems consisting of similar sized particles with a different structure, there is not a great deal of change in the viscosity compared to the monomodal systems. The dispersion consisting entirely of the medium-high structured particle has a slightly higher viscosity, which decreases upon the continuous addition of the low-medium structured particle.

The oil based dispersions consisted of either:

- 1) Two different sized particles, where one is coarse and the other is fine or
- 2) Two different sized particles, where one is coarse and one is fine, but with a differing structure.

Similar results were obtained for the low shear viscosity regardless of structure. For example, the low shear viscosity of the Raven L/N772 system is

very similar to that of the Raven L/N660 and the Raven M/N660 has a similar viscosity to the Raven M/N772.

For the high shear viscosity, a minimum is observed at $\varepsilon = 0.25$ (25% of small particles) for both Raven M/N660 and Raven L/N772. This is in excellent agreement with previous studies (see chapter 8 for references 1-8).

Also, for these systems the yield stress data is very similar but with the Raven M/N660 system having slightly higher values.

More noticeable effects may have arisen if the difference in particle size was larger. A theoretical prediction by McGeary¹ states that, if the large particles form a randomly packed array then the limiting factor to allow smaller particles into the interstices is the triangular pore size. If the small particles are smaller than the pore size they are free to move through the lattice created by the larger particles. Here, the particle diameter ratio is small.

From this research, it is evident that the rheology is a very important factor for the production of painting inks and paints. However in order to understand the rheology it is essential to firstly understand the interactions that occur within a colloidal system and to experiment with conditions/variables that may affect these interactions.

Due to the colour and opacity of the systems studied, many problems were encountered whilst attempting to obtain data related to the polymer adsorption e.g. isotherm, layer thickness. However, characterisation of this system is possible using the ultrasonic spectroscopy technique. This recently developed technique allows the direct probing of intermolecular forces within most materials, including opaque carbon black samples!

References:

- ¹ McGeary, R.K., *J. Am. Ceram. Soc.*, 44, (1961), 513.

APPENDIX

APPENDIX ONE:

List of rheological symbols

SYMBOL	NAME	CSG UNITS	SI UNITS
σ	Shear stress	dynes / cm ²	Pascals
γ	Shear strain	dimensionless	
$\dot{\gamma}$	Shear rate	1/sec	1/sec
f	Frequency	Hertz	Hertz
ω	Radian Frequency	rad/sec	rad/sec
η	Viscosity	Poise	Pascal / sec
η^*	Complex viscosity	Poise	Pascal / sec
G'	Storage Modulus	dynes/cm ²	Pascals
G''	Loss Modulus	dynes/cm ²	Pascals
δ	Phase Angle	radians	radians
De	Deborah number	dimensionless	
Pe	Péclet number	dimensionless	

Conversion factors:

1 Pascal = 10 dynes / cm²

1 Pascal / second = 10 Poise

APPENDIX TWO:

Publication



Rheology of aqueous carbon black dispersions

C.L. Barrie,^a P.C. Griffiths,^{a,*} R.J. Abbott,^b I. Grillo,^c E. Kudryashov,^d and C. Smyth^e

^a School of Chemistry, Cardiff University, P.O. Box 912, Cardiff CF10 3TB, UK

^b European Central Laboratory, Columbian Chemical Company, Avonmouth Road, Bristol BS11 0YL, UK

^c Institut Laue-Langevin, 6 rue Jules Horowitz, Grenoble Cedex 9, France

^d Department of Chemistry, University College Dublin, Belfield, Dublin 4, Ireland

^e Ultrasonic Scientific Ltd, Unit 1, Richview Office Park, Clonsilla, Dublin 14, Ireland

Received 20 November 2002; accepted 2 December 2003

Abstract

The interaction of carbon black with an acrylic resin has been investigated by rheology. Two carbon blacks, with similar particle size and surface characteristics but quite different particle morphologies, have been examined. These are somewhat arbitrarily denoted as “spherical” and “fractal” as shown by small-angle neutron scattering (SANS) and ultrasonic spectroscopy studies. In the absence of polymer, stable aqueous dispersions could not be obtained. Stable dispersions could be obtained, however, upon addition of polymer to a level corresponding to a ratio of 50 mg of polymer per 13 m² (± 1 m²) of surface area (i.e., 15 wt% particles). These stable dispersions exhibit flow typical of concentrated dispersions—Newtonian behavior up to some apparent “yield” or critical value, above which pronounced shear thinning is observed. The critical stress increases with increasing polymer concentration. When a significant amount of nonadsorbed polymer is also present, a second Newtonian plateau is superimposed on the shear-thinning behavior. This feature is observed for both particle types but is more pronounced for the fractal particle. When there is little or no nonadsorbed polymer, the viscosity of the fractal particle dispersions is greater than the viscosity of the spherical particle dispersions. At low polymer concentrations, the dispersions are predominantly viscous at low shear stresses. The phase angle decreases significantly over a narrow shear stress range and the rheology tends to more elastic behavior. At higher shear stresses, the dependence on particle morphology is weak.

© 2003 Elsevier Inc. All rights reserved.

Keywords: Carbon black; Fractal; Spherical; Concentrated dispersions; Rheology; Oscillation; Lissajous plots; Ultrasonic spectroscopy

1. Introduction

Carbon black is an intensely black, finely divided powdered form of highly dispersed elemental carbon manufactured by the controlled vapor phase pyrolysis of hydrocarbons [1]. Its principal use is as a reinforcing agent in automobile tires and other rubber products, but it is also used as an extremely black pigment with high hiding power suitable for use in printing inks, paints, and carbon paper. The blackness and tint properties of such ink coatings are all highly dependent on the particle size distribution, morphology, and structure. Carbon black particles are usually spherical in shape and less crystalline than graphite [2]. The precise structure is intermediate between those of graphite and a truly amorphous material—small crystallites made up of paral-

lel graphitic layers 0.35–0.38 nm apart. The formation of carbon black involves three important stages: Nucleation of soot precursors produces a particulate system from a molecular system; the precursors subsequently agglomerate to form particles with typical dimension 1–2 nm. The final step involves the association of these particles to form roughly spherical, primary particles. Aggregation of these primary particles thus determines the ultimate morphology of carbon black aggregates, henceforth termed fractal or spherical particles. Average aggregate diameters range from 0.1 to 0.8 μ m.

In the manufacture of inks, carbon black is often used in conjunction with waterborne acrylic resins. The resins act as a cross-linking polymer network. Although the printing process involves many high-shear interactions, understanding the low-shear behavior of the ink is more relevant to the ink's properties (tack, transference, cohesion, and drying).

The rheological properties of concentrated dispersions are of great importance in many other technological appli-

* Corresponding author.

E-mail address: griffithspc@cardiff.ac.uk (P.C. Griffiths).

cations, such as food concentrates and pharmaceuticals [3]. Polymer dispersions exhibit a complete spectrum of rheological behavior from pure viscosity to dominating elasticity [4]. Many factors contribute to the flow behavior of the system, but most importantly, the size, shape, and concentration of the dispersed particles, coupled to the dispersion stability, are known to be the flow-determining factors. Experiments conducted with spherical particles, sterically stabilized with grafted polymers, have shown that large particles behave similarly to hard spheres [5–8]. Through optical and rheological measurements on near hard-sphere suspensions of silica particles, it was concluded that the characteristic shear thinning in concentrated dispersions is due to changes in the thermodynamic contribution to the stress tensor while the hydrodynamic contribution remains relatively constant [9]. However, shear thickening was attributed to increased hydrodynamic interactions and is therefore a result of strong lubrication forces generated by the formation of nonpermanent clusters. Further studies on the effects of added polymer on the stability of fumed silica particles [10] state that after being fumed and dispersed in *trans*-decalin, the resulting suspensions showed strong elastic responses due to the formation of gel-like materials.

Nonspherical particles such as montmorillonite clay are often stabilized by surfactants and/or polymers [11]. Investigation shows that the flow curves (curves relating stress to rate of shear) for the suspensions at maximum coverage of adsorbing species exhibited more pronounced shear-thinning behavior than those with lower surfactant concentrations. It was also noticed that, with increasing the clay content (>3%), an apparent deviation from Newtonian behavior was observed and the shear-thinning behavior of the suspension was enhanced. Flocculation of the suspension (attributed to the bridging of micelles between the particles) occurs below the maximum surfactant coverage and occurs to a greater extent at approximately 50% coverage.

In studying the rheology of dispersed furnace carbon black particles, it is impossible to avoid taking the flocculated structures present into account because it is these structures that introduce properties such as shear thinning/thickening and yield stress. For 10–15 wt% carbon black particles suspended in a low-molecular-weight silicone oil [12], it was found that structural breakdown is observed at low shear rates, but this is reversed at higher shear rates. The values of G' and G'' (~ 3000 and ~ 200 Pa, respectively) obtained for a 12.5 wt% carbon black suspension in oil from this same experiment, indicate solidlike viscoelastic behavior for all carbon black suspensions.

The rheology resulting from the adsorption of poly(ethylene oxide)–poly(propylene oxide) ABA block copolymers on carbon black has also been studied [13]. The results showed a decrease in the amount of adsorption with an increase in the ethylene oxide (EO) chain length and it was therefore concluded that the adsorption is governed by the size of the PEO chain. Incorporating the results from their previous studies, Miano et al. deduced that the ABA block

copolymers were not as effective in stabilizing carbon black dispersions as ABC surfactants containing a nonylphenyl group in addition to the PPO chain. The results indicated that anchoring of the chain to the carbon black surface is enhanced in the presence of the nonylphenyl group.

Recently, Aoki et al. have studied the rheology of carbon black dispersed in various media [14,15]—an alkyd resin (AR), a modified phenol resin (PR), and a polystyrene/dibutyl phthalate solution (PS/DBP). Three different types of rheological behavior were observed, depending on the affinity of the suspending media for the particles. When the medium has a poor affinity for the particles (PS/DBP), the rheology was characterized by a network of agglomerates, i.e., it was “highly nonlinear elastoplastic.” With moderate affinity (PR), the suspension showed a sol–gel transition with increasing particle concentration. This behavior suggested the formation of a self-similar fractal agglomerate. Further, with increasing affinity of the suspending media for the particles (AR), the particles become more evenly dispersed, forming no agglomerates.

This paper describes the rheology of carbon black dispersions stabilized by a synthetic homopolymer in aqueous solution. Of key interest here is the impact of particle morphology, which has been characterized by small-angle neutron scattering (SANS) and ultrasonic spectroscopy.

2. Experimental

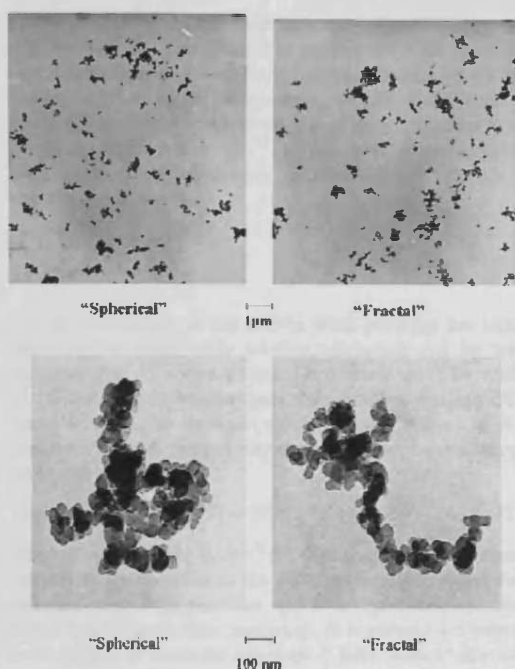
2.1. Materials

“Structure” is the term used to express the size and bulkiness of the aggregates and agglomerates. Low-structure carbon blacks consist of small, spherically shaped aggregates, whereas high-structure carbon blacks consist of larger, more bulky, nonspherical aggregates. Two particle morphologies were studied: spherical or “low-structure” particles and fractal or “high-structure” particles. The characteristics of the particles are presented in Table 1 and the corresponding transmission electron micrographs can be seen in Scheme 1. The actual morphology is not as different as this nomenclature may suggest. The average aggregate diameters are 87 and 105 nm for the spherical particle and the fractal particle, respectively [2].

The polymer solution used in this study is a varnish comprising a low-molecular-weight (wt. av. ~ 8500) poly(acrylate) (Johnson Polymer), a product that is extensively

Table 1
Characterization of carbon black particles

	“Spherical”	“Fractal”
Structure	medium–low	medium–high
Carbon content (%) of a typical ink	16–20	10–13
Mean particle diameter (nm)	30.0	31.4
Particle surface area (m^2/g)	91.4	85.9
Dry state aggregate diameter (nm)	86.8	104.5



Scheme 1. Transmission electron micrographs of the "spherical" and "fractal" carbon black particles.

used in the printing industries. It has a pH of 8.3 and a density of 1.07 g/cm^3 at 25°C and is formulated as an ammoniacal solution with $\varphi_{\text{polymer}} = 0.35$ with the following solvent composition by weight: ammonia (25% solution) 9.5%, isopropanol 3.0%, propylene glycol 1.5%, and water 51.0%.

2.2. Sample preparation

Initially, dispersions were prepared using a paint shaker. A concentrated stock carbon black dispersion was prepared by shaking the desired amount of carbon black with steel ball bearings for 30 min. This stock was then diluted to the desired carbon black loading ($\sim 15 \text{ wt}\%$) and then further shaken for 15 min to ensure even dispersion. It was found subsequently that a normal high-shear mixer was sufficient to disperse the desired amount of carbon black directly into the polymeric vehicle. Using the high-shear mixer, samples were stirred for 24 h, left to equilibrate overnight, and then analyzed. For example, a typical sample would comprise 15 wt% particles and 60 wt% polymer resin (of which 21 wt% is polymer and 39 wt% solvent), the remainder (25 wt%) being water—this is denoted as $\varphi_{\text{particles}} = 0.15$, $\varphi_{\text{polymer}} = 0.21$.

During this equilibration period, the IPA evaporates. No attempt is made to counter this and NMR is used to check that there is no substantial difference between the polymer

solutions. Such NMR studies have not been applied to the carbon black systems, but we assume they would be no different from the simple polymer solutions. Indeed, duplicate rheological measurements performed upwards of a week later show that no discernible differences in the observed behavior. This criterion is how we arrive at the distinction of "stable" or "unstable" and hence, the adsorbed amount of 50 mg of polymer per 13 m^2 (± 1) of particle surface area.

2.3. Equipment

The controlled-stress rheology measurements were performed on a Bohlin CS10 rheometer employing a double gap geometry (the diameters of the inner and outer cylinders being 24 and 27 mm, respectively). This geometry allows us to facilitate accurate measurements of low-viscosity samples, while the shear rate sweep and oscillatory shear stress sweep measurements were conducted on a StressTech (ReoLogica Instruments AB) with a cone and plate geometry (the cone has a diameter of 40 mm and an angle of 4°).

2.4. Small-angle neutron scattering studies

SANS measurements were performed on the D22 diffractometer at the ILL, Grenoble. Neutron wavelengths of 8 Å were taken with three instrument configurations to span a Q-range of approximately 0.002 to 0.4 \AA^{-1} .

The samples were contained in 2-mm pathlength UV-spectrophotometer-grade quartz cuvettes (Hellma) mounted in aluminum holders on top of an enclosed computer-controlled sample changer. Sample volumes were approximately 0.4 cm^3 . All scattering data were (a) normalized for the sample transmission, (b) background-corrected using an empty quartz cell (this also removes the inherent instrumental background arising from vacuum windows, etc.), and (c) corrected for the linearity and efficiency of the detector response. The data were put onto an absolute scale by reference to a flat scatterer such as water.

2.5. High-resolution ultrasonic measurements

The velocity (u) and attenuation coefficient (α) of longitudinal ultrasonic waves in carbon black dispersions were measured with a HR-US 102 high-resolution ultrasonic spectrometer (Ultrasonic Scientific, Dublin). The limiting resolution of the spectrometer is $10^{-5}\%$ for ultrasonic velocity and better than 0.2% for ultrasonic attenuation. Two identical cells of volume 1 cm^3 are used; the measuring cell was filled with a sample of carbon black dispersion, while the reference cell was filled with water. Ultrasonic velocity and attenuation in the sample and reference solution were measured at frequencies between 2 and 15 MHz at 25°C . The particle sizes of the carbon black particles in the dispersion were analyzed using the HR-US 102 particle size software module, based on the scattering the-

ory described by Allegra and Hawley [16] and Waterman and Truell [17]. The following parameters were used in the calculations: aqueous phase (volume fraction of 0.925, density = 1049 kg/m³, ultrasonic velocity = 1574 m/s, intrinsic attenuation coefficient normalized per square of frequency $\alpha/f^2 = 4 \times 10^{-13}$ s²/m), solid particles (volume fraction = 0.08, density = 2600 kg/m³, ultrasonic velocity = 4600 m/s).

3. Results and discussion

The morphology of the carbon black particles has been examined by small-angle neutron scattering and by microscopy. Fig. 1a shows a typical scattering curve for each of the two particles studied here. Many materials show different structural levels when examined over a range of dimensions [18]. A general representation for the scattering on a particular level is

$$I(q) \cong G \exp(-q^2 R_g^2/3) + B(1/q^*)^P, \quad (1)$$

where $q^* = q/[\text{erf}(kq R_g/6^{1/2})]^3$, G is the Guinier prefactor defined by the specifics of the particle composition and the concentration of the particles, and B is a prefactor specific to the type of power-law scattering. B is defined according to the regime in which the exponent P falls. Such a behavior is particularly true here given the nature of the carbon blacks studied, viz., particles with characteristic size 1–2 nm that form aggregates of dimension 87 and 105 nm. Since each of these structural levels can be described by a Guinier term that accounts for the average dimension and a power law term that corresponds to the mass- or surface-fractal character of the scatterer, a double logarithmic plot such as Fig. 1a, will exhibit a “knee” tending toward a limiting linear slope at high Q . The two particles have very similar limiting slopes, with a power law $P = -3.6$. This value of P corresponds to a surface fractal. At low Q , P decreases toward the behavior expected from a mass fractal, i.e., -2.5 . However, this slope is simply a tangent and the exponent will decrease further. A difference in the scattering from the two particles is only observed at low Q , corresponding to larger dimensions, with the particle denoted “fractal” showing a slope slightly greater than that of the particle denoted “spherical.” These results are in good agreement with those of Lin et al. [19] and Gerspacher and O’Farrell [20], who found that the fractal dimension was nearly constant for 15 different carbon black grades. The SANS results presented here confirm the TEM results that the fractal particle has a more open structure.

Two samples comprising $\phi_{\text{spherical particles}} = 0.15$, $\phi_{\text{polymer}} = 0.11$, and $\phi_{\text{fractal particles}} = 0.15$, $\phi_{\text{polymer}} = 0.11$ can be easily differentiated by their ultrasonic parameters, as shown in Fig. 1b. Both the ultrasonic velocity and the attenuation in the dispersion of “fractal” particles are higher than those in samples with “spherical” particles. The differences in ultrasonic velocity and attenuation between the two

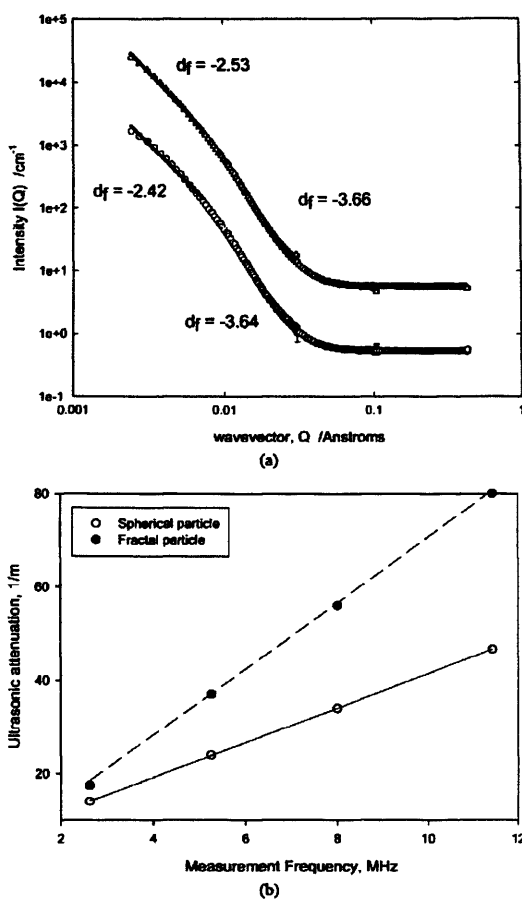


Fig. 1. (a) Particle characterization by SANS. Small-angle neutron scattering data for 0.5 wt% carbon black particles dispersed in water with 0.18 wt% polymer. The polymer is “invisible” in this experiment due to the low contrast. (b) Frequency dependence of ultrasonic attenuation in carbon black dispersions in water: (O) $\phi_{\text{spherical particle}} = 0.15$ and $\phi_{\text{polymer}} = 0.11$, and (●) $\phi_{\text{fractal particle}} = 0.15$ and $\phi_{\text{polymer}} = 0.11$.

samples are 7 m/s and 25.7 m⁻¹, respectively, at a frequency around 8 MHz. Fig. 1b shows the difference in ultrasonic attenuation in the two suspensions as a function of frequency. This difference in attenuation can be attributed to the scattering contribution to ultrasonic attenuation, which depends on the particle size. The second line in the Fig. 1b shows the calculated (via the HR-US 102 particle size software module) difference in ultrasonic attenuation based on the best-fit average sizes of particles in both suspensions, 0.8 and 1.1 μm . As can be seen from the figure, the attenuation data are well described by the scattering of ultrasonic waves due to particles of different sizes. Further, the sizes of the particles are in good agreement with the (dry state) aggregate diameters determined by microscopy (Table 1).

The difference in ultrasonic velocity between two samples cannot be explained just by the relative sizes of the particles in two suspensions. The calculated (HR-US 102 particle size software module) scattering contribution to the ultrasonic velocity for the above particle sizes is about 0.3 m/s; this is significantly less than the measured difference in ultrasonic velocity between the two samples (12 m/s). The large variation in ultrasonic velocity can be attributed to different internal compressibility of particles (i.e., inaccessibility to solvent). Ultrasonic velocity in liquids is determined by the density ρ and adiabatic compressibility β of the liquid, $u = (\rho\beta)^{-0.5}$. Therefore, the greater ultrasonic velocity is attributed to lower compressibility of the particles. The relative compressibilities can be attributed to the different packing of the elementary carbon particles within “fractal” particle aggregates. It could be expected that the internal core of “fractal” particles would be less compressible than that of “spherical” particles, thus resulting in higher velocity values.

However, another factor that could be responsible for these differences in ultrasonic velocity is the interaction of polymer with the particles. Adsorption of polymer onto the surface of a particle will be accompanied by solvation effects, which in turn affect the compressibility of the suspension [21,22].

Figs. 2a and 2b show a series of typical viscosity vs shear stress behaviors for both particle types with fixed particle volume fraction $\varphi_{\text{particle}} = 0.15$ and a range of polymer volume fractions: $\varphi_{\text{polymer}} = 0.053, 0.11,$ and 0.21 . All the dispersions show, in essence, similar behavior—a Newtonian region at low shear stresses (rates), which shear thin above some critical shear stress. Sometimes a slight upturn in viscosity with increasing shear stress at high shear stress is present. This is an experimental artefact and is not shown in these data; hence the data cease at different shear stresses.

Dispersions with $\varphi_{\text{polymer}} < 0.053$ were unstable. Hence, we conclude that $\varphi_{\text{polymer}} = 0.053$ corresponds to sufficient polymer to stabilize the particles. Therefore, for $\varphi_{\text{polymer}} > 0.053$, excess nonadsorbed polymer will be present in the solution. This is a realistic representation of many industrial situations.

The effects of nonadsorbed polymer on the dispersion viscosity are then apparent. Consider the $\varphi_{\text{particle}} = 0.15/\varphi_{\text{polymer}} = 0.053$ system, i.e., where there is little or no free polymer. At low shear stresses the fractal particle (Fig. 2b) has a much higher viscosity of ~ 10 Pa s compared to a viscosity of ~ 0.45 Pa s for the spherical particle (Fig. 2a). This is in excellent agreement with the rather limited ultrasonic spectroscopy studies. In addition, the fractal particle dispersions undergo shear thinning at a higher shear stress (~ 0.08 Pa) than the spherical particle (~ 0.04 Pa). The limiting high-shear viscosity is similar for both particles at ~ 0.004 Pa s. For the dispersions with $\varphi_{\text{particle}} = 0.15/\varphi_{\text{polymer}} = 0.11$, there is significant free polymer in solution—the low-shear-stress viscosity increases accordingly, some four orders of magnitude compared to the

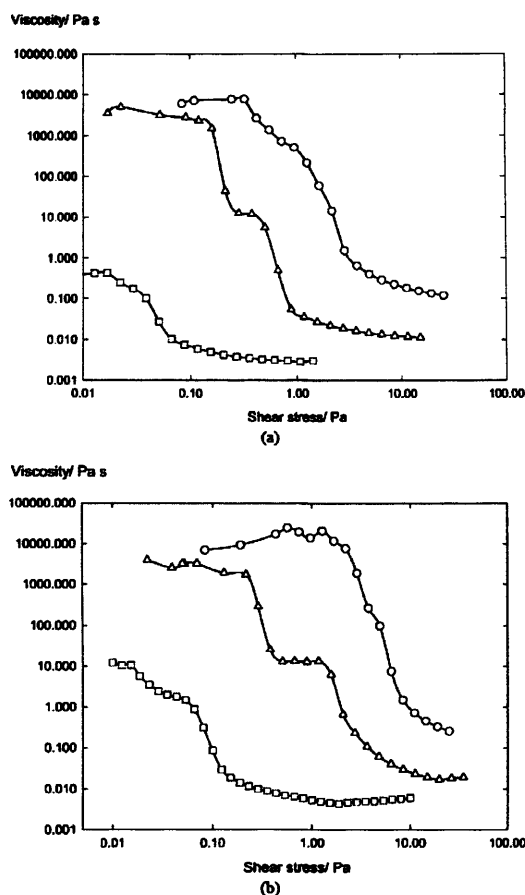


Fig. 2. Typical viscosity–shear stress curves for (a) spherical and (b) fractal carbon black particles in aqueous polymer solutions with $\varphi_{\text{particle}} = 0.15$ and \square $\varphi_{\text{polymer}} = 0.053$, Δ $\varphi_{\text{polymer}} = 0.11$, and \circ $\varphi_{\text{polymer}} = 0.21$.

$\varphi_{\text{polymer}} = 0.053$ case. Further increases in φ_{polymer} , i.e., $\varphi_{\text{particle}} = 0.15/\varphi_{\text{polymer}} = 0.21$, have a far less pronounced effect on the low-shear-stress viscosity. However, the viscosity at higher stresses increases by about an order of magnitude and indeed the particle morphology has a negligible effect on the rheology under these conditions. However, there is a distinct difference in the yield stress vs φ_{polymer} behavior for the two particle types.

To explain the details in the shear stress behavior, we should therefore examine the rheology of the simple polymer solutions. For all concentrations, the response is largely Newtonian (to a first approximation at least) over the majority of the shear stress range, Fig. 3a, and the viscosity increases with concentration, Fig. 3b. The viscosity–concentration scaling behavior increases around $\varphi_{\text{polymer}} = 0.03$, indicating interaction of the polymer molecules, such as the formation of a weak polymer network or aggrega-

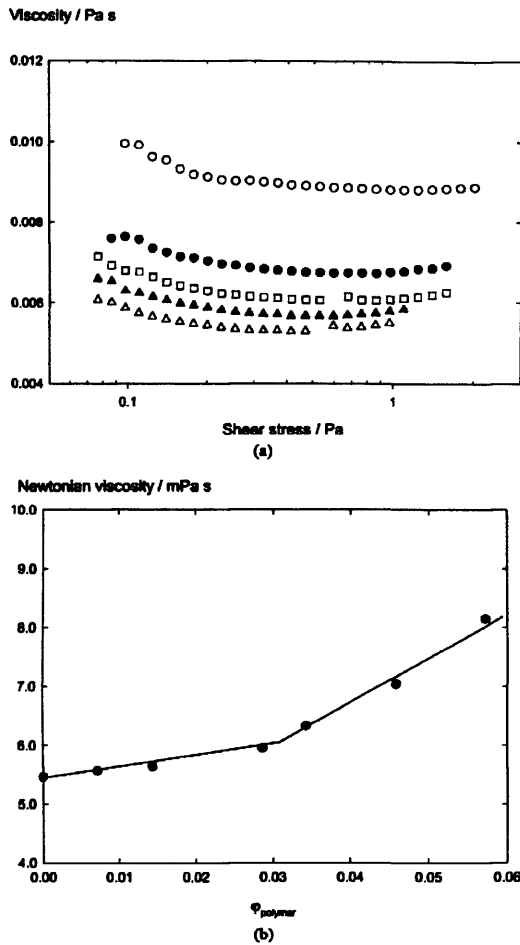


Fig. 3. (a) A series of viscosity–shear stress curves for a series of different concentration aqueous polymer solutions: (Δ) $\phi_{\text{polymer}} = 0.04$, (\blacktriangle) $\phi_{\text{polymer}} = 0.09$, (\square) $\phi_{\text{polymer}} = 0.11$, (\bullet) $\phi_{\text{polymer}} = 0.14$, and (\circ) $\phi_{\text{polymer}} = 0.18$. (b) Viscosity–polymer volume fraction behavior for aqueous poly(acrylamide) solutions.

tion. Accordingly, the data presented in Figs. 2a and 2b correspond to one system with little or no free polymer and two where sufficient excess polymer is present so that the continuous phase is a reasonably concentrated polymer solution. The substantially greater low-shear viscosity in the $\phi_{\text{particle}} = 0.15/\phi_{\text{polymer}} = 0.11$ and $\phi_{\text{particle}} = 0.15/\phi_{\text{polymer}} = 0.21$ cases is therefore due to polymer in solution, with the particles forming a network.

To understand further the role of interaction between the polymer layer and the polymer in the continuous phase, “dilution experiments” were undertaken, in which the ratio ϕ_{particle} to ϕ_{polymer} was held constant, but ϕ_{particle} and therefore ϕ_{polymer} decreases. Of particular interest was the

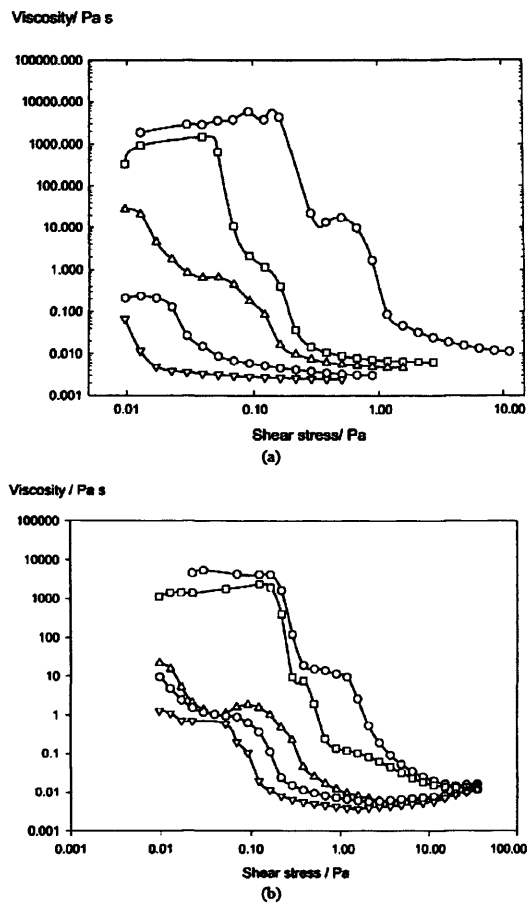


Fig. 4. (a) Typical viscosity–shear stress curves for (a) spherical carbon black particles in aqueous polymer solutions at a fixed (polymer)/(particle) as a function of ϕ_{particle} : (\circ) $\phi_{\text{particle}} = 0.15$, (\square) $\phi_{\text{particle}} = 0.118$, (Δ) $\phi_{\text{particle}} = 0.107$, (\circ) $\phi_{\text{particle}} = 0.093$, and (∇) $\phi_{\text{particle}} = 0.081$. (b) Typical viscosity–shear stress curves for fractal carbon black particles in aqueous polymer solutions at a fixed (polymer)/(particle) as a function of ϕ_{particle} : (\circ) $\phi_{\text{particle}} = 0.15$, (\square) $\phi_{\text{particle}} = 0.128$, (Δ) $\phi_{\text{particle}} = 0.114$, (\circ) $\phi_{\text{particle}} = 0.10$, and (∇) $\phi_{\text{particle}} = 0.092$.

intermediate Newtonian plateau observed in the $\phi_{\text{particle}} = 0.15$, $\phi_{\text{polymer}} = 0.11$ system, i.e., where $\phi_{\text{particle}}/\phi_{\text{polymer}} = 1.4$. Typical viscosity vs shear stress plots are shown in Figs. 4a and 4b for dispersions with $\phi_{\text{particle}}/\phi_{\text{polymer}} = 1.4$ as a function of ϕ_{particle} . Similar viscosity–shear stress behavior is observed for all systems: a Newtonian region that shear thins above a critical point, passing through some intermediate plateau before approaching a common viscosity at high shear stresses. On dilution, the viscosity at low shear rates decreases significantly, an effect that is more pronounced for the spherical particle (Fig. 4a). Note also that as the particle concentration is decreased, the intermediate

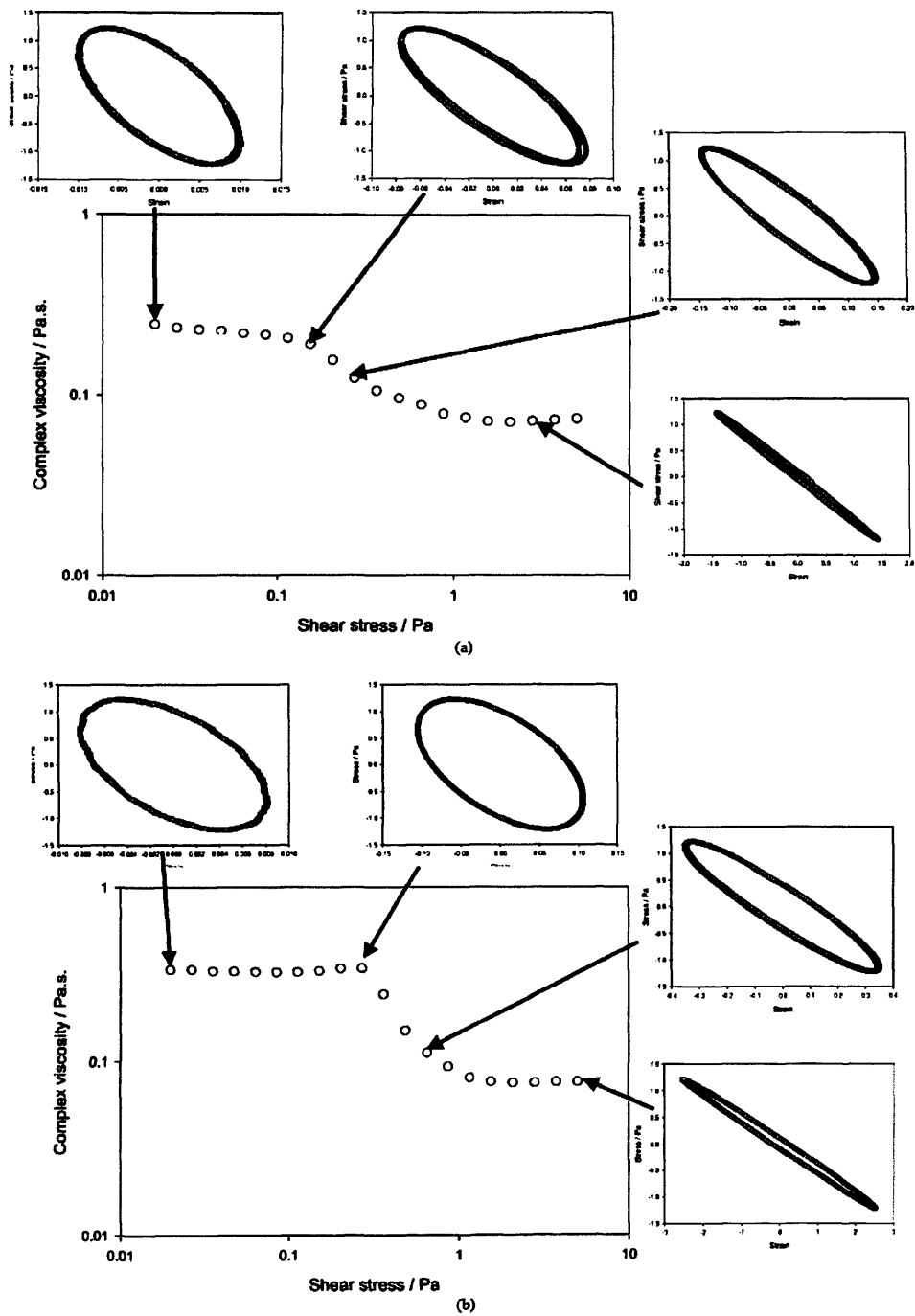


Fig. 5. (a) Typical shear stress sweep data and associated Lissajous plots at 1 Hz for a dispersion of (a) spherical and (b) fractal particles, $\phi_{\text{particle}} = 0.15$, $\phi_{\text{polymer}} = 0.053$.

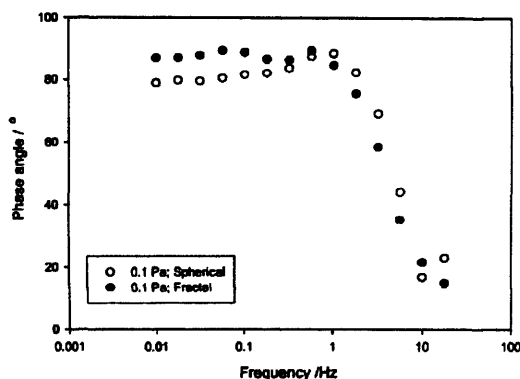


Fig. 6. Frequency sweep/phase angle data at 0.1 Pa for both the spherical particle dispersion (O), where $\varphi_{\text{particle}} = 0.15$, $\varphi_{\text{polymer}} = 0.053$, and the fractal particle dispersion (●), where $\varphi_{\text{particle}} = 0.15$, $\varphi_{\text{polymer}} = 0.053$.

Newtonian plateau shifts to lower shear rates until around $\varphi_{\text{particle}} \approx 0.10$, it cannot be distinguished.

Oscillation experiments were undertaken on these samples at various oscillation frequencies and amplitudes. The shear stress sweep experiments, Figs. 5a and 5b showed that the linear viscoelastic regions extend only over a very narrow range of shear stress. The complex viscosity of the fractal particle (Fig. 5b) is slightly higher and the shear thinning more pronounced than that of the spherical particle (Fig. 5a). Also, the apparent “yield” of the fractal particle is slightly higher than the spherical one, but otherwise the two behaviors are rather similar. As illustrated by the oval Lissajous plots, both systems are viscous at low shear stresses (a purely viscous response would be spherical, whereas an elastic response would be a diagonal line) but become elastic at higher shear stresses.

The frequency response is presented in Fig. 6 for the $\varphi_{\text{particle}} = 0.15$, $\varphi_{\text{polymer}} = 0.053$ spherical and fractal dispersions at a shear stress of 0.1 Pa—toward the end of the Newtonian plateau. This representation concurs with the Lissajous data, namely that the response to deformation is viscous at low shear stresses/frequencies, but becomes more elastic with increasing shear.

4. Conclusions

At low shear rates/frequencies, the carbon black and polymer form an extended network of high viscosity, which

responds to oscillation in a predominantly viscous manner. Above some characteristic relaxation time, the network breaks and there is a reduction in viscosity, the phase angle decreases, and the response becomes more elastic. An intermediate (Newtonian) region is observed which reflects the interaction between the polymer layer and the polymer matrix, probably viscous drag between polymer chains adsorbed on the particles with the polymer in solution.

Acknowledgments

C.B. acknowledges the financial support of Columbian Chemicals for a studentship, and EPSRC/ILL for provision of beamtime. Alison Paul and Mike Turner are thanked for their help with the SANS and TEM measurements, respectively.

References

- [1] J. Donnet, R. Bansal, M. Wang, Carbon Black, second ed., 1993, pp. 1–66.
- [2] J. Donnet, R. Bansal, M. Wang, Carbon Black, second ed., 1993, pp. 89–163.
- [3] P.F. Luckham, M.A. Ukeje, J. Colloid Interface Sci. 220 (1999) 347–356.
- [4] T.F. Tadros, Progr. Colloid Polym. Sci. 79 (1989) 120.
- [5] A.A. Zaman, M. Bjelopavlic, B.M. Moudgil, J. Colloid Interface Sci. 226 (2000) 290–298.
- [6] E. Kilbmann, T.H. Wild, N. Gutling, H. Maier, Colloids Surf. 18 (1986) 241.
- [7] P.N. Pusey, W. van Meegen, P. Bartlett, B.J. Ackerson, J.G. Rarity, J.M. Underwood, Phys. Rev. Lett. 63 (1989) 2753.
- [8] H.N.W. Lekkerkerker, in: S.H. Chen, J.S. Huang, P. Tartaglia (Eds.), Structure and Dynamics of Strongly Interacting Colloids and Supramolecular Aggregates in Solution, Kluwer Academic, Dordrecht, 1992, p. 97.
- [9] Bender, Wagner, J. Colloid Interface Sci. 172 (1995) 171–184.
- [10] M. Kawaguchi, A. Mizutani, Y. Matsushita, T. Kato, Langmuir 13 (1997) 6339–6341.
- [11] S. Rossi, P.F. Luckham, T.F. Tadros, Colloids Surf. 201 (2002) 85–100.
- [12] M. Kawaguchi, M. Okuno, T. Kato, Langmuir 17 (2001) 6041–6044.
- [13] F. Miano, A. Bailey, P.F. Luckham, T.F. Tadros, Colloids Surf. 68 (1992) 9–16.
- [14] Y. Aoki, A. Hatano, H. Watanabe, Rheol. Acta 42 (2003) 209–216.
- [15] Y. Aoki, A. Hatano, H. Watanabe, Rheol. Acta 42 (2003) 321–325.
- [16] J.R. Allegra, S.A. Hawley, J. Acoust. Soc. Am. 51 (1972) 545.
- [17] P.C. Waterman, R. Truell, J. Math. Phys. 2 (1961) 512.
- [18] G. Deaucage, J. Appl. Crystallogr. 29 (1996) 134–146.
- [19] Y. Lin, T.W. Smith, P. Alexandridis, Langmuir 18 (2002) 6147–6158.
- [20] M. Gerspacher, C.P. O’Farrell, Elastomerics 123 (4) (1991) 35–39.
- [21] V.A. Buckin, C. Smyth, Sem. Food Anal. 4 (2) (1999) 89–105.
- [22] V.A. Buckin, B.I. Kankiya, D. Rentzeperis, L. Marky, J. Am. Chem. Soc. 116 (1994) 9423–9429.

